NUREG/CR-0105
ORNL/NUREG-45

PWR Blowdown Heat Transfer Separate-Effects Program Data Evaluation Report—Heat Transfer for THTF Test Series 100

W. G. Craddick
C. R. Hyman
C. B. Mullins
R. A. Hedrick
K. G. Turnage

Prepared for the U.S. Nuclear Regulatory Commission
Office of Nuclear Regulatory Research
Under Interagency Agreements DOE 40-551-75 and 40-552-75

OAK RIDGE NATIONAL LABORATORY
OPERATED BY UNION CARBIDE CORPORATION · FOR THE DEPARTMENT OF ENERGY

Printed in the United States of America. Available from
National Technical Information Service
U.S. Department of Commerce
5285 Port Royal Road, Springfield, Virginia 22161

NUREG/CR-0105
ORNL/NUREG-45
Dist. Category R2

Contract No. W-7405-eng-26

Engineering Technology Division

PWR BLOWDOWN HEAT TRANSFER SEPARATE-EFFECTS PROGRAM DATA EVALUATION REPORT — HEAT TRANSFER FOR THTF TEST SERIES 100

W. G. Craddick
C. R. Hyman R. A. Hedrick
C. B. Mullins K. G. Turnage

Manuscript Completed — August 31, 1978
Date Published — September 1978

Prepared for the
U.S. Nuclear Regulatory Commission
Office of Nuclear Regulatory Research
Washington, D.C. 20555
Under Interagency Agreements DOE 40-551-75 and 40-552-75

NRC FIN No. B-0125

Prepared by the
OAK RIDGE NATIONAL LABORATORY
Oak Ridge, Tennessee 37830
operated by
UNION CARBIDE CORPORATION
for the
DEPARTMENT OF ENERGY

CONTENTS

LIST OF FIGURES

LIST OF TABLES

ACKNOWLEDGMENTS

In the conduct of a large experimental and analytical program, there are always a great many individuals whose contributions should be recognized. The dedicated efforts of the entire Blowdown Heat Transfer Program staff are reflected in this report. The authors express their appreciation to the following persons:

M. C. Adair
M. E. Bagwell
J. L. Bartley
R. E. Bohanan
V. D. Clemons
S. B. Cliff
S. K. Combs
R. D. Dabbs
C. E. Davis
E. D. Drennen
R. M. Flanders
D. J. Fraysier
C. A. Gifford
R. H. Greene
R. C. Hagar
P. A. Jallouk
A. F. Johnson
D. M. Leon
R. W. McCulloch
G. S. Massengill
G. M. Maxwell
F. R. Mynatt
L. J. Ott
H. R. Payne
W. Ragan, Jr.
J. L. Redford
M. J. Roberts
L. I. Schlemper
A. N. Smith
R. D. Stulting
R. E. Textor
D. G. Thomas
H. E. Trammell
B. J. Veazie
J. D. White
M. D. White
J. E. Wolfe

PWR BLOWDOWN HEAT TRANSFER SEPARATE-EFFECTS PROGRAM DATA EVALUATION REPORT — HEAT TRANSFER FOR THTF TEST SERIES 100

W. G. Craddick
C. R. Hyman R. A. Hedrick
C. B. Mullins K. G. Turnage

ABSTRACT

Heat transfer phenomena are analyzed for test series 100 of the Thermal-Hydraulic Test Facility, part of the Pressurized-Water Reactor Blowdown Heat Transfer Separate-Effects Program. Heater rod surface temperatures are found to be sensitive to relatively small variations in flow. The mechanisms causing departure from nucleate boiling and rewetting are analyzed.

Comparisons are made between heater rod surface temperatures calculated from thermocouple responses and surface temperatures produced by the thermal-hydraulic transient simulator RELAP4/MOD5 (update 2). The code's predictions are relatively accurate in the lower region of the test section and considerably high in the upper region. The procedures in the code which produce these results are discussed in detail.

I. INTRODUCTION

This report is an analysis of the heat transfer phenomena observed in test series 100 of the Thermal-Hydraulic Test Facility (THTF), part of the ORNL Pressurized-Water Reactor (PWR) Blowdown Heat Transfer (BDHT) Program. The program, which is sponsored by the Nuclear Regulatory Commission, was established to obtain information for use in developing models that can be used to determine the margin of safety extant in the design of PWRs. Hence the program's primary objectives are (1) the determination of time to critical heat flux (CHF), surface heat fluxes, surface temperatures, local fluid properties, and heat transfer coefficients during a blowdown transient and (2) the evaluation of the ability of existing computer codes to predict the transient behavior of the THTF. The primary source of data to meet these objectives is the THTF, a nonnuclear pressurized-water loop containing 49 full-length,* electrically

*Full length refers to the 3.66-m (12-ft) heated length. For a description of the THTF, see Ref. 1.

heated rods arranged in a 7 × 7 bundle (Fig. I.1). Test series 100 consisted of six tests conducted from April 23 to August 19, 1976 (Table I.1). The overall system response of the THTF in test series 100 was analyzed in a previous report.[2]

Table I.1. ORNL BDHT Separate-Effects Program test matrix — first 49-rod bundle

Variable	Test No.					
	100[a]	101	102	104	103	105
Rod power, kW/rod	0	30.5	122	122	122	122
Unpowered rods	0	0	0	0	0	0
Coolant mass flow rate						
$kg\ m^{-2}\ hr^{-1} \times 10^{-6}$	12.7	12.3	12.1	12.3	12.3	12.2
$lb_m\ hr^{-1}\ ft^{-2} \times 10^{-6}$	2.60	2.51	2.48	2.51	2.51	2.50
Break location (and area ratio where applicable)	In (0.5A) Out (0.5A)	Out	In (0.5A) Out (0.5A)	In (0.5A) Out (0.5A)	In (0.4A) Out (0.6A)	In (0.4A) Out (0.6A)
Nominal break size,[b] %	200	100	200	200	200	200
Time heater rod power on after blowdown initiation, sec		0	0	2	2	2 + power decay[c]
Coolant inlet temperature						
K	560	558	558	560	558	558
°F	549	545	545	548	545	545
Coolant outlet temperature						
K	559	573	608	607	607	607
°F	547	571	633	632	632	632
System pressure						
MPa	15.6	15.5	15.7	15.6	15.8	15.5
psig	2263	2245	2271	2263	2284	2253
Pump condition during blowdown	Off	Off	Off	Off	Off	Off
Sheath thermocouple upper set point						
Steady state		T_{max} + 50°F or 28 K ——————————>				
Transient		T_{max} + 50°F or 28 K		1350°F 1005 K	1350°F 1005 K	1450°F 1061 K
Schedule	4/23/76	5/27/76	6/18/76	7/8/76	8/4/76	8/19/76

[a] Isothermal test.

[b] A 200% break has a total break area A of 12.5 cm^2 (0.0135 ft^2).

[c] Heater rod power decayed with a 0.45-sec time constant for a total of eight time constants.

In this report the test section heat transfer is considered in detail. Since an understanding of the observed heat transfer phenomena is impossible without familiarity with the hydrodynamic response of the system, the reader is urged to read Appendix A prior to reading the main text. Test series 100 was the first series conducted in the THTF with the electric rods in place. The first three tests of the series were designed to

obtain baseline hydraulic information and did not have sufficient power to produce a significant number of departures from nucleate boiling (DNB). Therefore, only the last three tests of the series — 103, 104, and 105 — will be considered here. Each of these tests began with the THTF near 15.5 MN/m^2 (2250 psig) and with 5.978 MW being supplied to the rods. The system was then allowed to blow down into a large cavity at near atmospheric pressure through two simultaneous breaks.

The heat transfer effects produced by these tests are analyzed both qualitatively and quantitatively. An explanation of the phenomenological sequence, with emphasis on the causes of CHF and subsequent rewetting, is presented first. In this discussion, we use rod surface temperatures and fluxes calculated from rod power and thermocouple responses. Fluid conditions have been inferred from measurements of volumetric flow, pressure, density, and fluid temperature. Although THTF behavior is not claimed to model a PWR undergoing a hypothetical loss-of-coolant accident (LOCA), this section identifies areas deserving particular attention by those attempting to develop accurate thermal-hydraulic codes for margin-of-safety calculations.

Two important reasons exist for computer code verification work in the BDHT Program. First, the thermal-hydraulic environment of the THTF is in the range of operating conditions of a PWR. Thus the successes or failures of a code in predicting the transient behavior of the THTF can provide direct guidance in choosing calculational methods for future code development. Second, calculation of local fluid conditions, such as quality and mass flow, for use in heat transfer coefficient correlations requires the accurate "extrapolation" of fluid measurements outside the test section to specific locations within the rod bundle. An accurate thermal-hydraulic code is therefore a necessity. This report evaluates the ability of RELAP4/MOD5 (update 2) (or RELAP4/M5U2)[3] to predict THTF behavior and to function as an "extrapolator" for experimental boundary conditions. This version of RELAP is the most recent one in general use. Although RELAP4/MOD6 has been developed, it is currently available for CDC computers only and thus is unavailable for general use.

Following the discussion of RELAP are the results of heat transfer coefficient calculations. These results are both tentative and limited

because of our current inability to achieve the accurate local fluid conditions mentioned in the preceding paragraph. We were able to calculate fairly extensively the ratio of the surface flux to the difference of surface temperature and fluid saturation temperature, but we are unable to evaluate, for comparison, current correlations that require mass flux, quality, or similar variables, except in a very restricted period.

Finally, a summary of the most important points of our analysis is presented. We believe that these results can make a significant contribution in defining areas most in need of attention in the development of codes for determination of the margin of safety for PWRs.

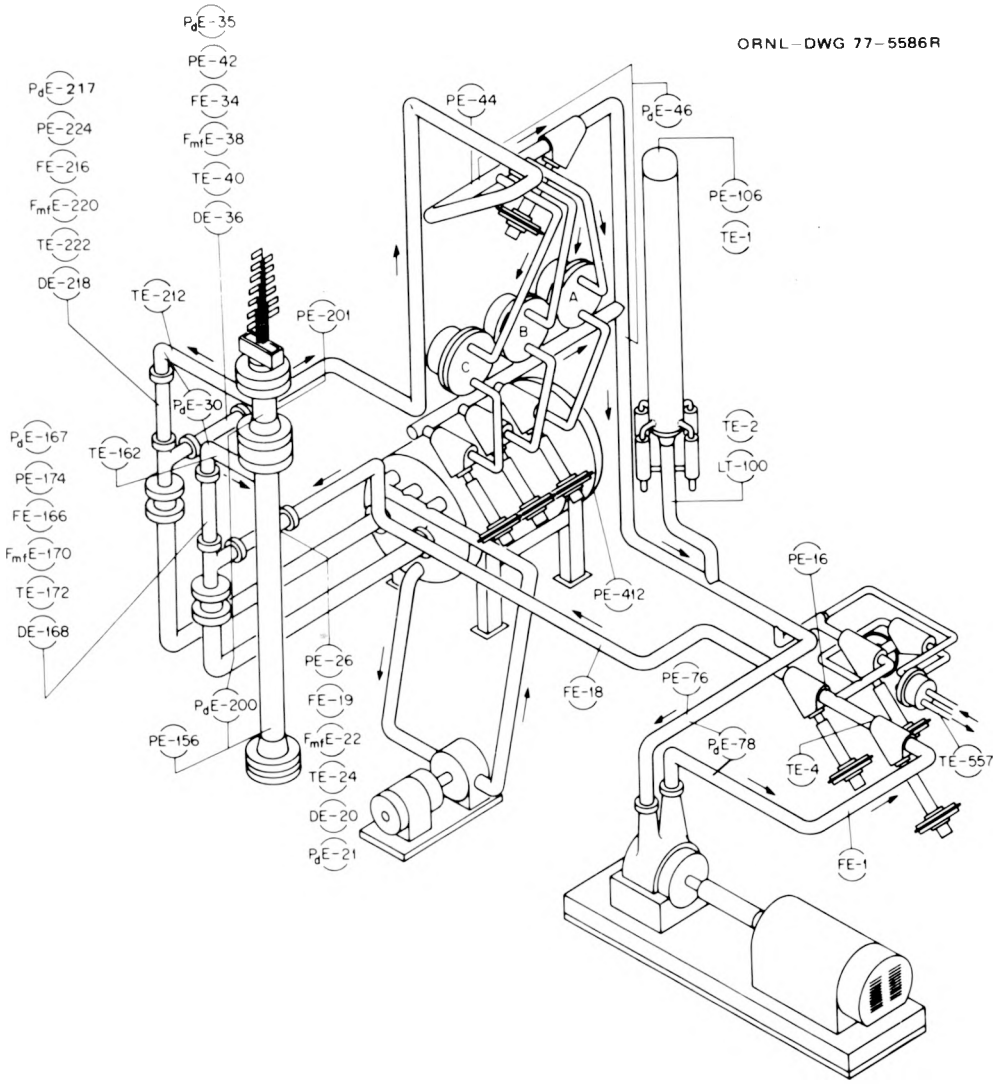

Fig. I.1. Thermal-Hydraulic Test Facility (THTF).

II. PHENOMENOLOGICAL ANALYSIS

II.1 Discussion of Experimental Data

Any analysis of experimental results must include consideration of measurement error associated with the data acquisition and reduction process. Therefore a brief discussion of measurement error in the THTF will precede the description of tests 103 to 105. Several facets of this discussion will be of considerable importance in Chapters III and IV as well as later in this section.

The instrumentation in the THTF is described in Tables II.1 and II.2 and can be located using Figs. I.1 and II.1. Tables II.3 and II.4 present the precision of the recorded signals. The steady-state pressure difference across the THTF test section is approximately 0.207 MN/m^2 (30 psi) and is even smaller throughout most of the transient. Thus the standard deviation of the absolute pressure measurement [0.185 MN/m^2 (26.8 psi)] makes it impossible to accurately determine the pressure difference across the core by subtracting absolute pressures on each end. Since the pressure difference instruments across the test section suffer from excessive "ringing" in their output signals, accurate pressure differences across the test section in the transient are not currently available. However, absolute pressures and temperatures are measured fairly well. Unfortunately, the same cannot be said for the volumetric flow measurements (Table II.4). Rather than accepting the manufacturer's quoted errors in precision, BDHT Program personnel are verifying the precision of all THTF instrumentation. Such efforts have led to the discovery of a large possible error in the turbine meter output.[4] Although these errors cause us to be suspicious of the magnitude of the output signal at any given time, we believe that the fluctuations in the signal usually represent actual fluctuations in the volumetric flow. Even this statement must be qualified by the fact that changes in rod bundle power or mechanical vibrations were apparently the cause of occasional reverses in polarity in the turbine meter signals, thereby reversing the algebraic sign of their output. Further, the THTF drag disks were sized to measure the violent initial shock of blowdown, thereby causing output signals for

Table II.1. Data sensor locations and systems characteristics

Location and measurement	Instrument application No.[a]	Sensor designation[b]
Main pump		
Inlet pressure	PE-76	P1
Inlet fluid temperature	TE-74	TF3
Differential pressure	P_dE-78	DP1
Pump flow	FE-1	F2
Discharge fluid temperature	TE-4B, TE-568	TF2
Pressurizer		
Vapor space pressure	PE-106	P1
Vapor space pressure	PT-102	P3
Vapor space temperature	TE-1	TF4
Vapor space temperature	TE-101	TF2
Bottom outlet liquid temperature	TE-3	TF4
Liquid level	LT-100	L
Pump bypass heat exchanger		
Secondary outlet temperature	TE-13, TE-557	TF2
Secondary flow	FE-550	F1
Primary outlet temperature	TE-5B	TF3
Three main heat exchangers		
Primary upstream pressure of all	PE-44	P1
Primary ΔP of all	P_dE-46	DP1
Primary ΔP of each	P_dT-48	DP2
Primary outlet temperature	TE-30B, TE-32B, TE-34B	TF3
Secondary outlet temperature	TE-52/-525, TE-54/-627, TE-56/-727	TF2
Secondary flow of each	FE-522A, FE-620, FE-720	F1
Primary downstream temperature of all	TE-28B	TF3
Test section		
Test bundle inlet pressure	PE-156	P1
Test bundle outlet pressure	PE-201	P1
Test bundle ΔP	P_dE-200	DP1
Miscellaneous bundle ΔP[c]	P_dT-199	DP2
Fuel pin temperatures	TE-301–TE-349 (460 max)[d]	TP
Inlet line fluid temperature	TE-162	TF4
Inlet line fluid temperature	TE-160	TF2
Outlet line fluid temperature	TE-212	TF4
Outlet line fluid temperature	TE-210A, TE-210B	TF2
Bundle inlet temperature	TE-150–153	TF4
Inlet to outlet fluid ΔP	P_dT-30	DP2
Voltage across bundle		E
Individual rod current	(49 max)[d]	I
Outlet subchannel fluid temperature	(64 max)[d]	TF1
Miscellaneous fluid temperature	(36 max)[d]	TF4
Outlet line pressure	PT-32	P3
Individual generator currents	(4 max)[d]	I

Table II.1 (continued)

Location and measurement	Instrument application No.[a]	Sensor designation[b]
Inlet line spool pieces[e]		
Fluid density	DE-20, DE-168	D
Pressure	PE-26, PE-174	P1
Fluid temperature	TE-24, TE-172	TF4
Momentum flux	F_{mf}E-22, F_{mf}E-170	MF
Velocity	FE-19, FE-166	V
Outlet line spool pieces		
Fluid density	DE-36, DE-218	D
Pressure	PE-42, PE-224	P1
Fluid temperature	TE-40, TE-222	TF4
Momentum flux	F_{mf}E-38, F_{mf}E-220	MF
Velocity	FE-34, FE-216	V
Pressure-suppression system		
Receiver pressure	PE-412	P1
Recirculating water temperature	TE-408B	TF3
Recirculating water flow	FT-406	F3
Blowdown lines		
Initiation of blowdown	XE-420–XE-423	BW
Rupture disk buffer pressure	PE-979, PE-989	P2

[a] Many of the symbols on the figures in this report refer to the instrument application numbers given in this column.

[b] See Table II.2.

[c] Three different measurements possible; only one monitored at any one time.

[d] Numbers in parentheses indicate quantity of sensors for the measurement.

[e] There are two spool pieces in the test section inlet line and two in the test section outlet line, with the blowdown lines connected between the spool piece in each line.

most of the transient, when momentum flux is much smaller, to be of the same order as the instrument uncertainty. Efforts to improve THTF instrumentation are under way.

When analyzing three-dimensional phenomena, it is important to remember the distinction between quantities measured directly and quantities calculated from direct measurements. This is particularly important for transient three-dimensional phenomena. Determination of rod surface

Table II.2. Sensor description

Measurement	Designation	Type
Fluid temperature	TF1	Chromel/Alumel, 0.090-in.-OD metal-sheathed thermocouple
	TF2	Platinum RTD
	TF3	Chromel/Alumel, 0.125-in.-OD
	TF4	Fast-response, exposed-junction Chromel/Alumel thermocouple
Fuel pin simulator	TP	Chromel/Alumel, 0.020-in.-OD metal-sheathed, insulated-junction thermocouple
Pressure	P1	Strain gage
	P2	Bourdon tube gage
	P3	Force balance pressure transmitter
Differential pressure	DP1	Strain gage
	DP2	Force balance DP cell
Fluid flow	F1	Turbine meter
	F2	Orifice
	F3	Pipe elbow taps
Momentum flux	MF	Strain gage cantilever beam (drag disk), bidirectional
Density	D	Gamma attenuation/photomultiplier tube
Voltage	E	Voltage divider
Current	I	Shunt
Initiation of blowdown	BW	To detect when rupture disks have broken (blowdown initiated)
Liquid level	L	Force balance DP cell
Velocity	V	Turbine meter, bidirectional

Table II.3. Precision of experimental measurements in the THTF for test series 100

System	Standard deviation
Pressure measurement, MN/m^2 (psig)	
Computer-Controlled Data Acquisition System (CCDAS)	0.185 (26.8)
Analog tape system	0.197 (28.5)
Pressure difference measurement	
CCDAS, MN/m^2 (psid)	
6.89-MN/m^2 (1000-psid) span	0.025 (3.6)
1.38-MN/m^2 (200-psid) span	0.005 (0.72)
0.34-MN/m^2 (50-psid) span	0.001 (0.18)
Analog tape system, MN/m^2 (psid)	
6.89-MN/m^2 (1000-psid) span	0.033 (4.8)
1.38-MN/m^2 (200-psid) span	0.007 (0.95)
0.34-MN/m^2 (50-psid) span	0.002 (0.24)
Temperature measurement, K (°F)	2.4 (4.3)
Electric core power measurement	
Rod current, A	0.877
Rod voltage, V	0.304
Momentum flux measurement, $kg/m\text{-}s^2$ ($lb_m/ft\text{-}sec^2$)	
CCDAS	2264 (1522)
Analog tape system	2554 (1716)
Density measurement at 961 kg/m^3 (60 lb_m/ft^3), kg/m^3 (lb_m/ft^3)	12.9 (0.81)

Table II.4. Precision of flow measurements in the THTF for test series 100

Measurement system	Standard deviation [m^3/s (gpm)]	
	Forward	Reverse
	All tests except test 101	
FE-19	+0.0009 (+13.97) −0.0002 (−2.90)	+0.0011 (+16.77) −0.0004 (−5.70)
FE-166	+0.0012 (+18.74) −0.0005 (−7.68)	+0.0010 (+16.15) −0.0003 (−5.09)
FE-216	+0.0048 (+75.59) −0.0041 (−64.52)	+0.0020 (+31.79) −0.0013 (−20.72)
FE-34	+0.0021 (+33.39) −0.0007 (−11.26)	+0.0124 (+197.11) −0.0110 (−174.97)
	Test 101	
FE-19	+0.0018 (+28.59) −0.0004 (−6.45)	+0.0022 (34.15) −0.0008 (−12.02)
FE-166	+0.0051 (+81.55) −0.0037 (−59.41)	+0.0034 (+53.43) −0.0020 (−31.29)
FE-216	+0.0101 (+159.35) −0.0087 (−137.21)	+0.0040 (63.35) −0.0026 (−41.21)
FE-34	+0.0021 (+33.39) −0.0007 (−11.26)	+0.0124 (+197.11) −0.0110 (−174.97)

temperatures, rod surface heat fluxes, local heat transfer coefficients, and mass flows requires the use of calculational procedures to derive these quantities from measured properties. In the literature, errors quoted for such quantities are usually derived by assuming the method of calculation to be exact and simply computing the propagation of the errors in the direct measurements. Since there is seldom any way to quantify the error inherent in the calculational method, there is little else one can do. However, this implies that adoption of a crude but simple calculational procedure will make error calculations quick and easy and may produce small computed error in the result. A more sophisticated and rigorous calculational method may result in error calculations becoming quite

difficult and in the ultimate production of larger quoted errors. Even though this latter method appears to require greater effort and to give a poorer result, it is frequently superior to the former. Data analysis is commonly performed using crude calculational models that produce cosmetically superior results without consideration of the possible errors introduced by these models. The BDHT Program personnel have resisted this temptation and are attempting to use calculational procedures that are as accurate as possible for each computed quantity.

Design of the heater rods in the THTF was motivated by a desire to simulate the thermal-hydraulic response of nuclear fuel pins. The resulting complex design (Fig. II.2) has produced considerable problems in the calculation of surface temperatures and fluxes. Notable among these problems have been imperfectly crushed MgO and BN within the rods, which makes it impossible to use tabulated values for their thermal properties, and the presence of a gap near the thermocouple groove between the two steel sheaths, which introduces a large step in the radial rod temperature profile. A major effort is being made to properly account for the effects of these factors since ignoring them would introduce considerable error in the calculated surface conditions. The code ORINC[5] was developed to perform these calculations in one dimension. All surface temperatures and fluxes described as experimental in this report have been calculated by ORINC from direct measurements. Because of ORINC's complexity, the calculation of error propagation is difficult and has not been completed.[6] Work is currently under way to develop a code that will perform three-dimensional calculations of rod surface conditions, thus evaluating azimuthal variations due to the thermocouple grooves, off-center heating elements, and similar factors.[7]

Mass flows must also be calculated from direct measurements. A common method of calculation is to multiply measured density and measured volumetric flow. This method, however, ignores the slip that is present in most two-phase flow. A method has been devised to calculate mass flows accounting for slip by combining momentum flux measurements with density and volumetric flow measurements.[8] Unfortunately, neither of these schemes has been executed satisfactorily for the THTF because of the previously described large errors in the primary instruments. Mass flows

have been calculated,[9] but their accuracy is highly suspect. No calculations have been performed which propagate the errors in the instruments through the calculational procedure.

Axial locations of thermocouples along the heated rod length are referred to as levels and are designated by the letters D to N, as shown in Fig. II.3. The heated region of the rod bundle will be referred to as the core. The individual rods are assigned numbers (1 to 49) and are grouped in regions, as shown in Fig. II.4. This discussion will describe the behavior of rods at each level as a group, since radial effects within the bundle are small for most of the transient. Typical radial effects within the bundle will be described in Chapter III. Calculated rod surface temperatures for each level of each test are presented in Figs. II.5 to II.38 (see Table II.5 for key to the symbols used on these and other figures in this report). The temperatures shown are for all rods in the center region that had thermocouples. The intermediate region for level F in test 104 (Fig. II.13) is also shown since two of the six center rods behaved atypically at that level in that test. So few rods had thermocouples at levels M and N that they are all shown.

The reader will notice that the calculations for rod 25 for all levels above level H (TE-325 I—N in Figs. II.21 to II.38) produce markedly higher temperatures than those for immediately adjacent rods. Manufacture of the heater rods resulted in static torsional stresses in the two outer stainless steel sheaths (Fig. II.2). Since the width of the air gap between the sheaths is a function of rod temperature and its gradient, a model is required to predict such variations for use in extrapolation of sheath thermocouple temperatures to surface temperatures. During numerous calibration experiments, several rods at various levels exhibited changes in gap sizes which do not conform to that expected on the basis of thermal expansion and rod geometry. We are currently unable to model these unusual changes, which may be due to relative azimuthal rotation of the sheaths produced by the interaction of thermal expansion and static torsional stresses produced during manufacture. Surface-temperature calculations for rods with deviant gap-size fluctuations are made by using an average gap size held constant throughout the transient. This procedure has generally worked well for most rods

Table II.5. Key to symbols used on figures[a]

ORINC Rod Surface Temperatures

ORINC rod surface temperatures are designated by the particular sheath thermocouples used in the calculation of those temperatures according to the following scheme:

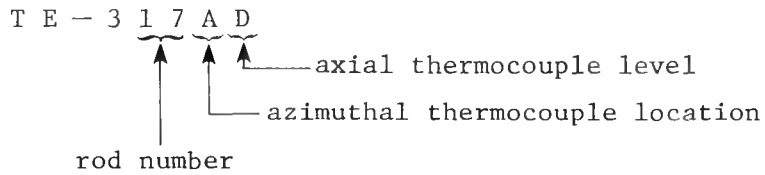

Thus this designation refers to the sheath thermocouple in rod 17 at level D. (Rod numbers are shown in Fig. II.4.)

Quantities Calculated by RELAP

Quantities calculated by RELAP are designated according to the following scheme:

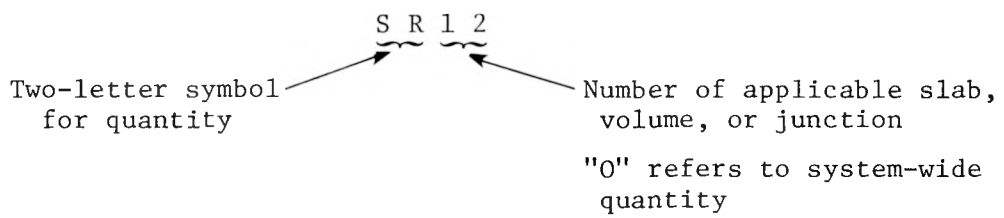

The two-letter symbols used are:

AP — Average pressure
AT — Average temperature
AR — Average density
AX — Average quality
WV — Volume average mass flow
JF — Junction volumetric flow
SR — Slab surface temperature
FR — Slab surface heat flux
KR — Slab surface heat transfer mode
DR — Slab critical heat flux
LE — Total energy leaked from system
LM — Total mass leaked from system
CR — Slab surface heat transfer coefficient

[a]Additional instrument designations (e.g., DE-36) used in the figures are listed in Table II.1.

with unusual gap behavior, judging by the similarity of calculated temperatures to those of adjacent rods with more predictable gap variations. The exception is rod 25 above level H. However, steady-state data for rod 25 above level H indicate that its gaps are dramatically larger than those for any levels of any other rods. The unusual results of the transient surface temperature calculations for rod 25 above level H cause us to suspect that a large, unusual gap-size change occurs in rod 25 at these levels. The calculated surface temperatures for rod 25 at these levels are considered to be extremely inaccurate.

II.2 Phenomenological Sequence

Tests 103, 104, and 105 will now be considered in detail. The reader is once again urged to read Appendix A to familiarize himself with the key hydrodynamic features of these tests. The following description will compare the three tests, proceeding chronologically from break initiation. "Positive flow" refers to flow in the same direction as in steady state: through the inlet spool pieces, down the downcomer, through the lower plenum, up the core, through the upper plenum, and through the outlet spool pieces (Fig. II.39). Note that positive flow at the vertical inlet spool piece (VI) and negative flow at the vertical outlet spool piece (VO) will indicate flow into the test section. Tests 103 and 105 had a total break area of 12.5 cm^2 (0.0135 ft^2), divided 60% at the outlet and 40% at the inlet. Test 104 had the same total break area, evenly divided between inlet and outlet. Tests 103 and 104 had full power (5.968 MW — 122 kW/rod) supplied until 2 sec after rupture, when power was cut off. Test 105 had the same power until 2 sec, after which power was decayed exponentially with a 0.45-sec time constant until 5.8 sec and was then cut off.

The transient is initiated by simultaneous opening of inlet and outlet break orifices. Flow reverses immediately at the VI and reverses at the VO before 1 sec. Thus a flow stagnation point is created at the VI and moves through the core, eventually reaching the VO. During the initial pressure drop, the pressure becomes low enough that fluid near level M would be expected to saturate, based on the initial temperature distribution. Since movement of a flow stagnation point through

subcooled water must be extremely rapid, the stagnation point is expected to reach the top of the core almost immediately. This causes the relatively hot fluid in the upper core to pass back down through the core, thereby increasing its enthalpy. The passage of high-enthalpy fluid causes uniform DNB at approximately 0.6 sec at level H and below in tests 103 and 105 (Figs. II.5, .7, .8, .10, .11, .14, .15, .17, .18, and .20). Levels D and E are at lower power than F, G, and H, but fluid reaching D and E has increased further in enthalpy; so general CHF still occurs at this time. Levels I and J (Figs. II.21, .23, .24, and .26) are at the same power as level E, but the fluid at I and J has had too little increase in enthalpy for widespread DNB. Some rods at these levels show brief temperature excursions, around 0.6 sec, presumably due to temporary local variations in fluid conditions. Test 104, with its smaller outlet and larger inlet break sizes, experiences much stronger negative flow through the core than tests 103 and 105. One would expect the stronger flow to reduce the enthalpy of fluid reaching the lower core (smaller transit time), promote better heat transfer, and, perhaps, make it more difficult for steam formed on the rod surfaces to coalesce into a film. Less CHF is observed in test 104. Level H, in spite of its high power, does not have fluid enthalpies high enough for CHF to occur for all rods (Fig. II.19). Level H in test 104 behaves like levels I and J in tests 103 and 105, while levels I and J in test 104 (Figs. II.22 and .25) show no CHF at all until well after 0.6 sec. Note that in the lower core, some rods at level F (Figs. II.12 and .13) and some at level E (Fig. II.9) do not have DNB at this time, while levels G (Fig. II.16) and D (Fig. II.6), which surround E and F, show general CHF. We currently have no explanation for this.

Between 1 and 3 sec, flow at the VO becomes positive again, and flow from both vertical spool pieces is toward the breaks. In tests 103 and 105, flow at the VI is much greater than at the VO, with flow at the VO reaching 0.013 m^3/s (200 gpm) slightly before 2 sec and remaining near this value for over 1 sec (Figs. II.40 and .41; note time scale). From this we infer that the flow stagnation point has moved from the VO down into the core and resides within the core for this period. Between 1.8 and 2.5 sec, there is a general occurrence of DNB at levels I, J, and K

in tests 103 and 105 (Figs. II.21, .23, .24, .26, .27, and .29). The stagnation point is probably in the upper core and the associated low flow causes the CHF. Levels I and J are in the same power zone, but J shows lower temperatures resulting from the 2-sec CHF than does I. Level L (Figs. II.30 and .32) is in the same power zone as K, but some rods at L do not undergo CHF at this time. This could be explained if the stagnation point is assumed to be at or below level I, which would cause flow at J to be greater than at I and flow at L to be greater than at K. Alternatively, since levels K and I are very near spacer grids, their higher temperatures may be the result of flow effects produced by the spacer grids. A third possible cause of the lower temperatures at J and L is axial conduction; the thermocouples at J and L are only 2.54 cm (1 in.) from the next lower power zones. In test 104, flow at the VO (Fig. II.42) is positive for a much shorter period and reaches 0.013 m^3/s (200 gpm) for only a brief moment, rather than remaining near that value for a second as in tests 103 and 105. Thus the stagnation point is in the core for a shorter period of time, and the VO flow data suggest that it may move more rapidly while inside. In test 104, DNB is observed in the upper core at this time (Figs. II.19, .22, .25, .28, .31, .34, and .37), but the temperature excursions are much smaller than in tests 103 and 105. This may be due to more rapid entrance and exit of the stagnation point or to the removal of more energy from the rods by the stronger early negative flow of test 104. The rods at levels E and F (Fig. II.9, .12, and .13) that had not had large temperature excursions with the rest of the lower core at 0.6 sec have DNB at this time. The movement of the flow stagnation point into the upper core probably reduces flow in the lower core, which may cause these excursions at levels E and F.

Between approximately 3 and 5 sec, arrival of low-quality fluid at the horizontal outlet spool piece (HO) causes flow out of the test section at the VO to decrease. During this period, all three tests exhibit rewetting between the levels at the top of the core and various lower levels. Test 105 shows complete rewetting down to level K, with some rods rewetting at I and J. Test 103 shows rewetting completely from the top to level I and some effects at level H. Test 104 shows rewetting

completely through level G and considerable rewetting at F and E. Test 104, which shows the most rewetting, also shows the greatest decrease in flow at the VO; test 105 shows the least rewetting and the smallest decrease in VO flow. Test 103 falls between the other two tests in both extent of rewetting and VO flow decrease.

Although these rewets are considered to be triggered by the change in flow, the precise mechanism of the phenomena is uncertain. In test 104, VO flow first becomes negative at 3.1 sec and oscillates about zero until 4.4 sec, when it moves more negative, reaching -0.008 m^3/s (-120 gpm) at 4.9 sec (Fig. II.42). During this period the VO densitometer (Fig. II.43) signal stops falling, begins fluctuating at about 240 kg/m^3 (15 lb_m/ft^3), and surges to 560 kg/m^3 (34 lb_m/ft^3) coincident with the negative surge in the VO flow. The flow stagnation point has moved out of the test section and into the VO. The instrument readings imply that low-quality fluid from the HO has entered the vertical piping leading to the test section. This suggests that the low-quality fluid from the HO may be the source of the core rewets. However, in test 103, the VO densitometer (Fig. II.44) shows a much smaller increase between 3 and 5 sec, and VO flow (Fig. II.40) fluctuates about zero but never becomes lower than -0.003 m^3/s (-50 gpm). Much less low-quality fluid appears to have penetrated the test section; yet sharp rewets are seen as low as level I. In test 105, the VO turbine meter signal (Fig. II.41) drops to 0.007 m^3/s (100 gpm) from 3.4 to 4.2 sec, after which it drops to zero but never becomes negative. A small but distinct density increase is seen at the VO from 3.4 to 5 sec (Fig. II.45). The occurrence of this density increase while the turbine meter still shows flow toward the break suggests countercurrent flow, but one must keep in mind the large possible errors in the flow measurements (Table II.4). The lack of precision in the turbine meters prevents us from knowing with certainty whether flow was negative during the 3- to 5-sec period in these tests. Thus, penetration of the test section by low-quality fluid from the HO remains a possible cause of the observed rewets.

In all three tests, from 3 to 5 sec, flow at the VO toward the outlet break drops or reverses, and flow at the VI almost doubles toward the inlet break. This implies that the flow stagnation point has moved toward

the outlet and that flow through most or all of the core is negative and increasing in magnitude. A second possible explanation for the observed rewets is that the increased flow cools the upper rod surfaces below their Leidenfrost temperature, allowing liquid phase already extant in the core to rewet those surfaces. If this explanation were correct, one would expect test 104 to show the greatest rewetting because in this test core flow is largest from 3 to 5 sec and rod surface temperatures are lowest at 3 sec. Similar reasoning would lead one to expect the least rewetting for test 105, as observed. Rod surfaces in the lower core may fail to rewet because of a combination of increasing quality or superheating of the fluid as it flows down through the core and the higher temperatures of the lower surfaces from the earlier CHF. Some of the four fluid thermocouples located in the base of the lower plenum show the existence of superheated fluid during this period for all three tests, with 105 showing the most and 104 the least. Thus, cooling below the Leidenfrost temperature due to increased flow is also a possible explanation for the observed rewets from 3 to 5 sec.

In addition, the possible existence of liquid phase caught or entrained in the upper plenum may contribute to the rewetting. The rods enter a guide box as they pass through the upper plenum. The fluid in the upper portion of this box cools the upper plenum pressure seals and is at a temperature >56 K (100°F) below that of the rest of the upper plenum. The box has holes in its sides near the bottom, allowing flow into the upper plenum. The fluid in this box which has not been swept to the outlet from 1 to 3 sec might be liquid phase and able to penetrate the core from 3 to 5 sec. The complex geometry of the upper plenum may allow liquid phase in flow from the core to be deentrained and subsequently to fall back into the core during the flow change from 3 to 5 sec. Of course, the observed rod surface temperature behavior may be due to the combined effect of all of the possibilities previously discussed.

At approximately 5 sec, the last of the low-quality fluid from the HO is expelled through the outlet break, and the increased volumetric flow at the outlet break produces the second complete reversal of flow in the core. Flow toward the break in the VO increases dramatically

(Figs. II.40 to .42), and flow toward the break at the VI begins to decrease, culminating in flow toward the test section by 7 sec. Thus the flow stagnation point moves completely through the test section from outlet to inlet. As mentioned previously, fluid thermocouples in the lower plenum indicate the presence of superheated fluid during the negative core flow from 3 to 5 sec. The flow reversal sweeps this superheated steam back up the core, where its passage is recorded by fluid thermocouples located just above the heated zone in the subchannels between rods (Figs. II.46 to .48). The passage of this steam produces temperature excursions at all levels. The excursions are smallest for test 104, whose subchannel thermocouple signals show very little superheated steam, and largest for test 105, whose subchannel thermocouple signals show the most. The subchannel thermocouples indicate that the steam has collected in the center of the bundle, with little or no superheat being shown by the instruments near the corners and walls. This explains why the corner and wall rods for levels M and N (Figs. II.33 to .38) show little or no temperature excursion. The temperature increases are smaller and of shorter duration in the upper core, where the stored energy remaining in the rods is lower. Test 104, which has little superheat, has only small temperature excursions at all levels except level F.

Once the flow stagnation point reaches the inlet break plenum and flow at the VI reverses, fluid from the horizontal inlet spool piece (HI) passes through the VI toward the test section. At approximately 7 sec the system pressure has reached the saturation pressure of the relatively cool fluid in the HI. Thus the fluid entering the VI is saturated but is of low quality, as indicated by the VI densitometer (Figs. II.49 to .51). Positive flow in the VI and its penetration by low-quality fluid produce the rewet at level D at approximately 8 sec (Figs. II.5 to .7). The fluid that actually rewets the rods may be liquid phase which has collected in the lower plenum in the previous few seconds. Note that while the VI density for test 104 shows a single narrow peak at 8 sec (Fig. II.49), test 105 has a second smaller surge at 11 sec (Fig. II.51), and test 103 has low quality from 8 to 11 sec (Fig. II.50). Both tests 105 and 103 have a second positive surge in the VI flow. The higher temperatures of test 105 coupled with the very small decrease in quality of this second

surge prevent the rewetting of any more levels, while in test 103 the second surge is able to produce rewetting of level E from 10 to 11 sec. In both tests the cooling effect is apparent at all levels from the dip in rod surface temperatures at this time. The flow pattern is apparently annular in the upper core since the cooling effect at the top three levels is seen in the center rods (Figs. II.30 and .32) but not in rods near the corners or walls (Figs. II.33, .35, .36, and .38 contain corner and wall rods).

Starting at approximately 9 sec, evidence of a general lack of liquid phase in the upper core is observed in tests 103 and 105. Those rods that were not already at temperatures well above the fluid temperature (levels L and above in test 105 and J and above in test 103) begin temperature excursions. Dryout is not seen in the lower levels (D in test 105 and D and E in test 103) until 12 sec or later. In test 104, dryout is seen between 10 and 12 sec. Those rods already at elevated temperatures slow or halt the gradual cooling they had been exhibiting. Beyond 11 sec, dryout is interrupted at times by penetration of the core by low-quality fluid from the HO. This fluid probably originates in the main heat exchangers. These "slugs" of low-quality fluid appear at different times in each test and cause the observed dips in rod temperatures.

II.3 Conclusions

Before some general conclusions are drawn, the preceding discussion will be summarized. The initial flow reversal causes a quality increase in the middle and lower core which is sufficient to produce early CHF there (at approximately 0.6 sec). Low flow in the upper bundle produces CHF in the upper core at approximately 2 sec. Superheated steam, generated by negative flow through the core, is swept up the core by the 5- to 7-sec flow reversal and causes a second occurrence of DNB in those rods that had rewet. The major rewets are caused by flow bringing lower quality fluid into the core or by increased cooling due to increased flow.

A general comparison of the rod surface temperatures and flows of the three tests leads to an important conclusion. Comparing the temperature behavior in general, test 104 shows considerably smaller temperature

excursions than tests 103 or 105, most notably in the upper core. Tests 103 and 105 are relatively similar, even though 22% more energy was added to the core during the transient in test 105. The flow patterns of tests 103 and 105, both of which have 60% to 40% break area ratios, are almost identical (see Appendix A). Test 104, with its 50% to 50% ratio, has a flow pattern that still contains all the major features of the flows of tests 103 and 105, although different in magnitude in some places. Yet this somewhat different flow pattern produced a much larger variation in rod temperature behavior than the addition of more energy. Thus we conclude that rod temperature behavior in the THTF is sensitive to flow and density variations but that the flow itself is not as sensitive to the addition of energy through the core. It is clear that accurate prediction of rod surface temperatures in the THTF would require extremely accurate predictions of fluid flow and density variations. We believe it possible that reactor cladding surface temperatures might exhibit a similar sensitivity to flow and therefore that a code for margin-of-safety calculations must show considerable success in predicting the hydrodynamic response of pertinent systems.

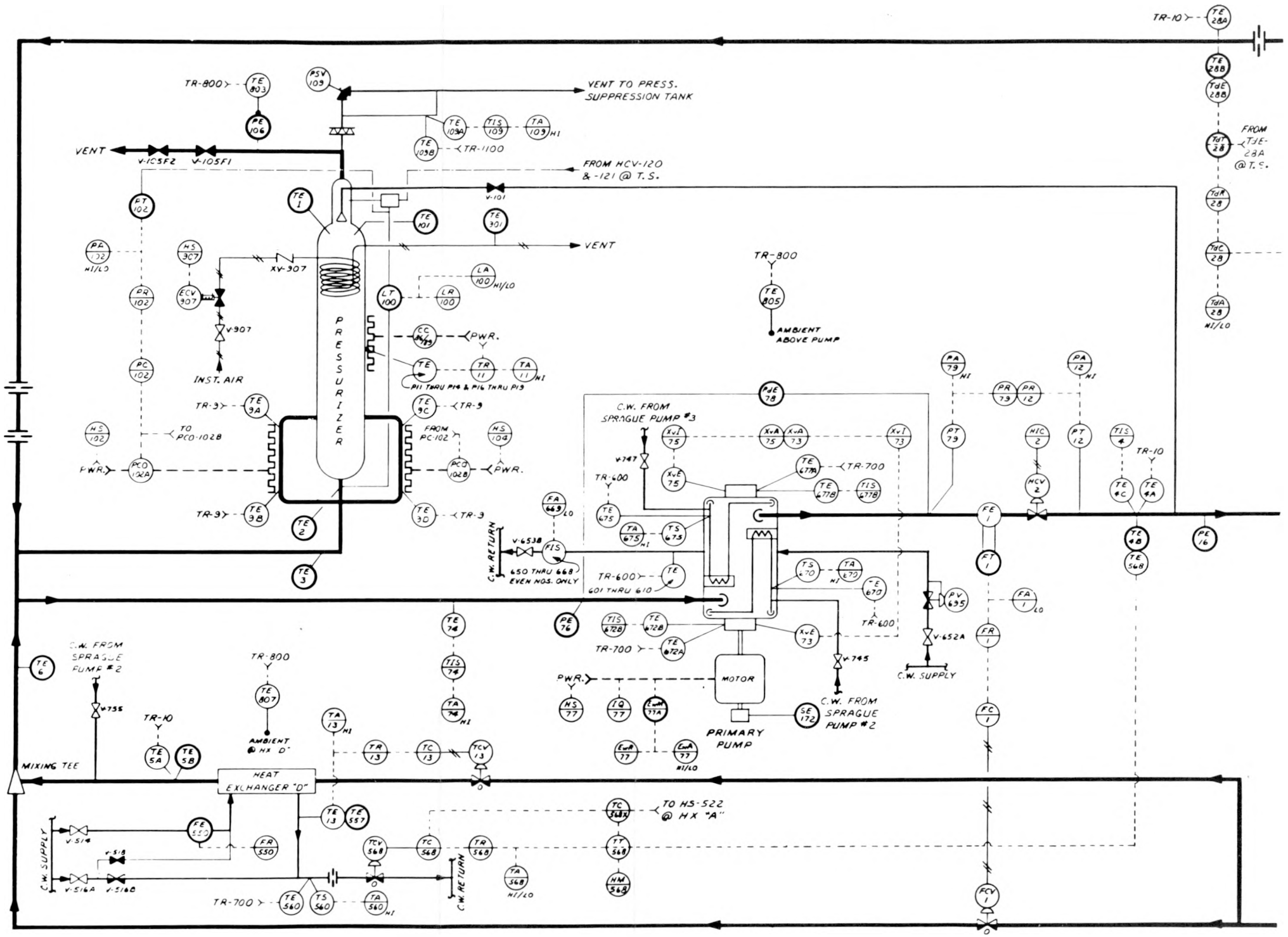

Fig. II.1. THTF instrumentation diagram.

ORNL -DWG 77-12968

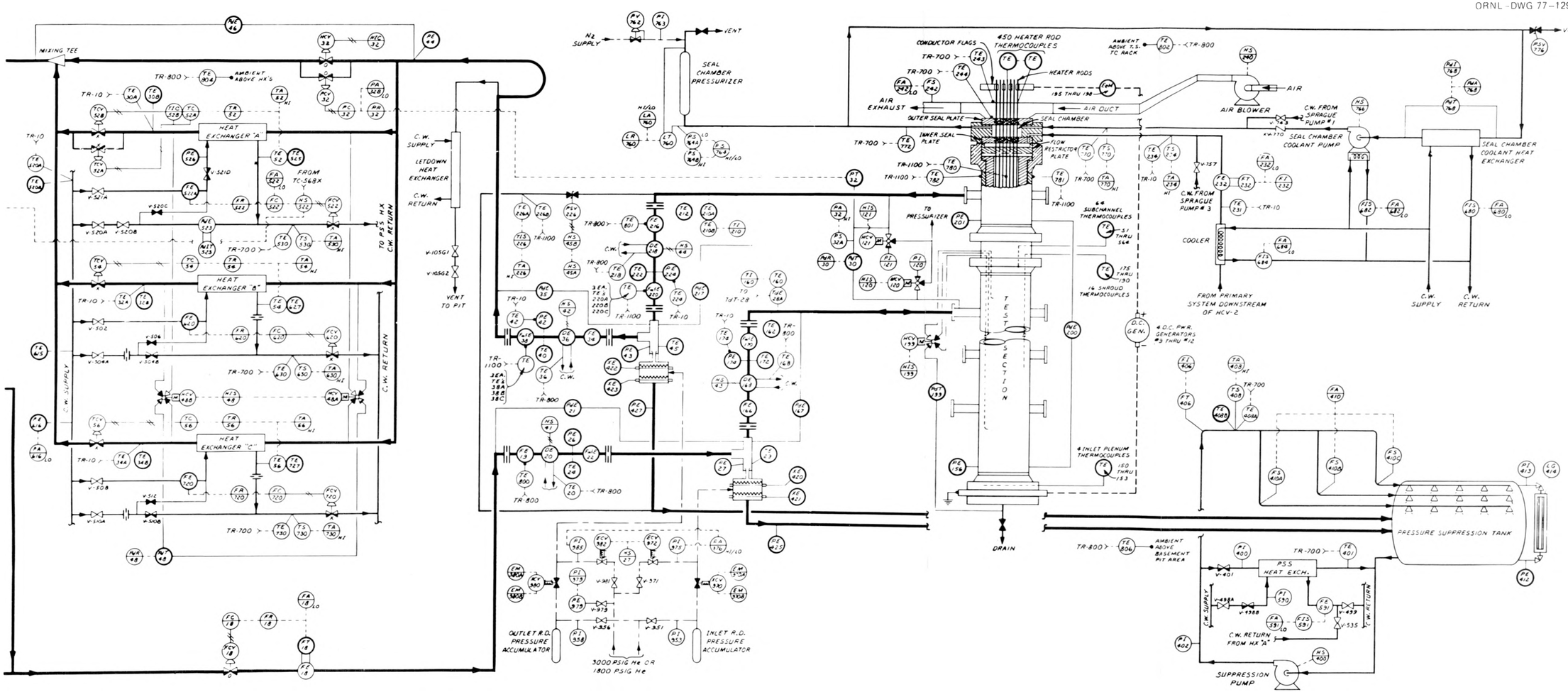

Fig. II.1 (continued)

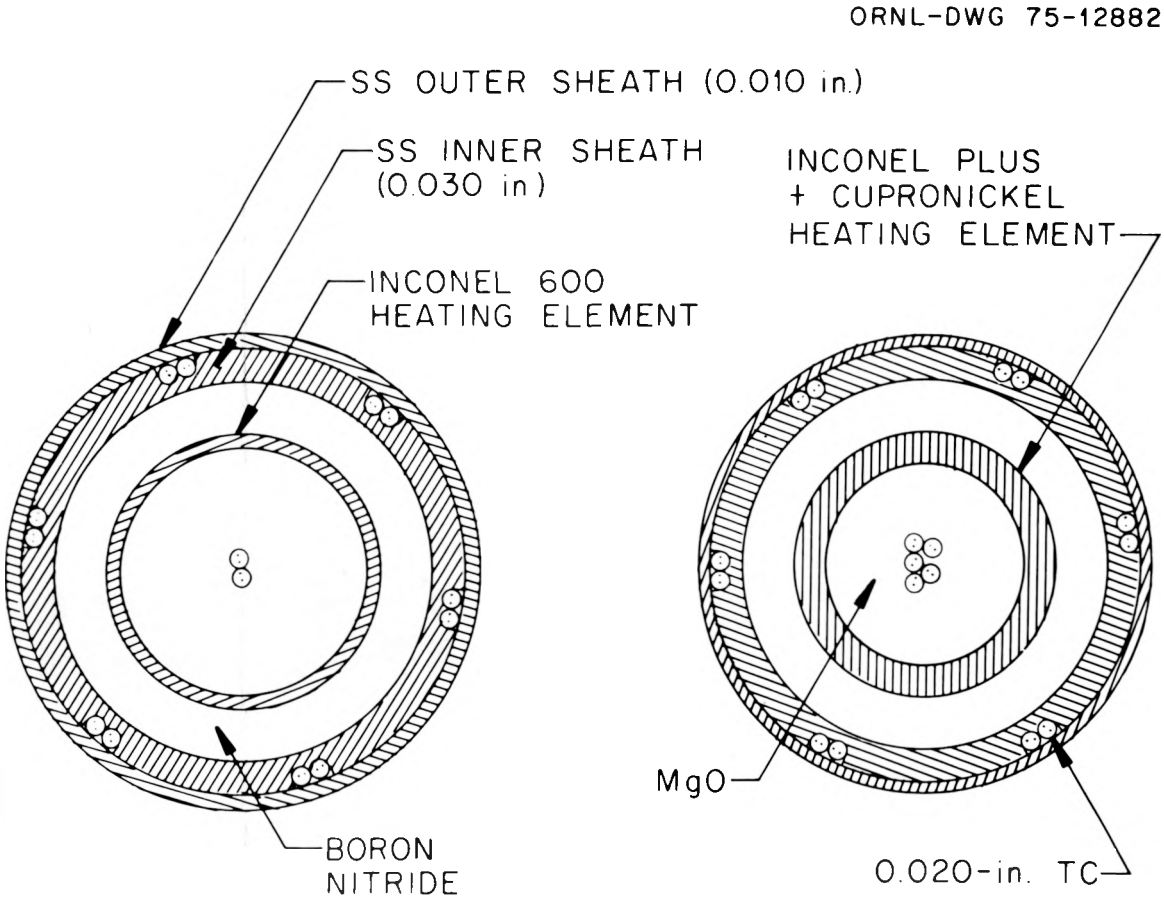

Fig. II.2. Heater rod cross sections (0.442-in. diam) (2.54 cm = 1 in.).

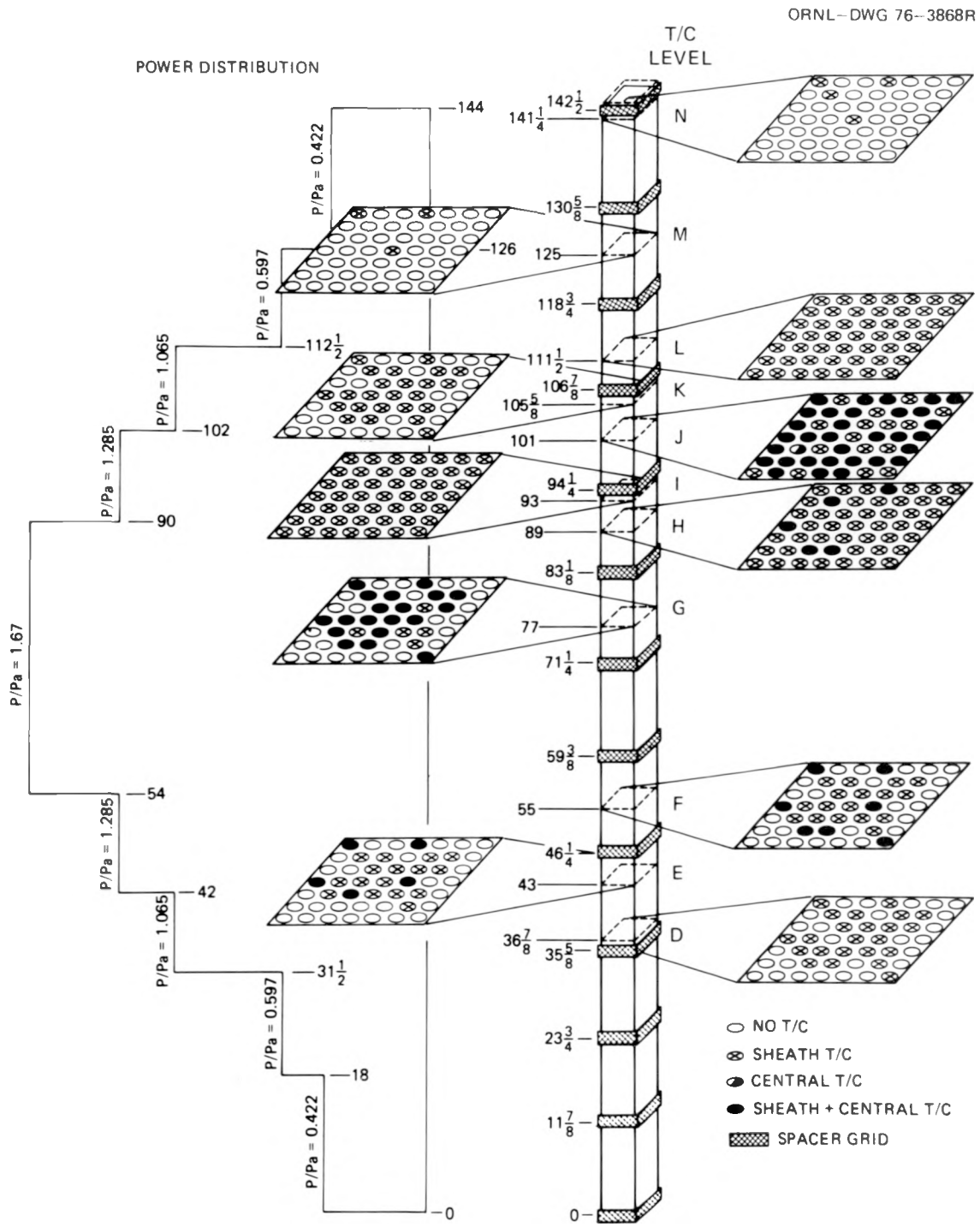

Fig. II.3. Location of thermocouples in THTF bundle 1. (For the convenience of the reader, a foldout of this figure appears on p. 185.)

ORNL–DWG 78–13207

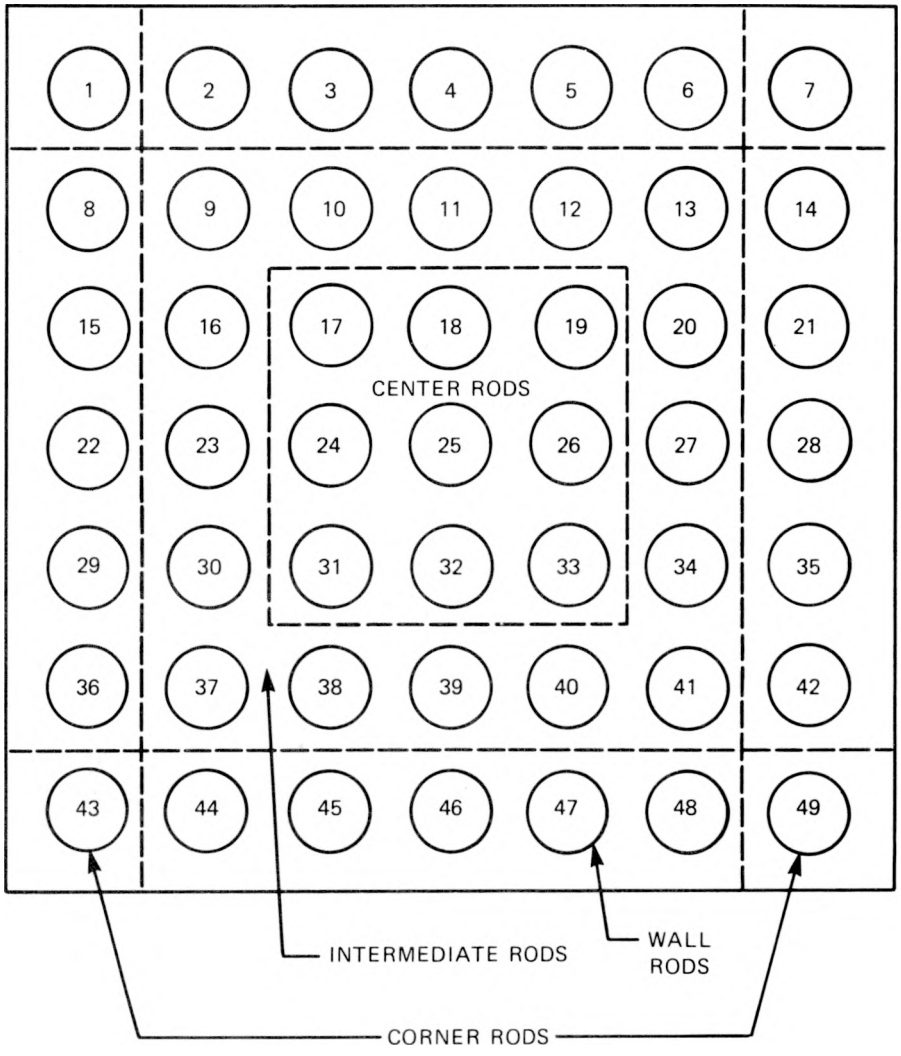

Fig. II.4. THTF numerical rod designations and radial regions.

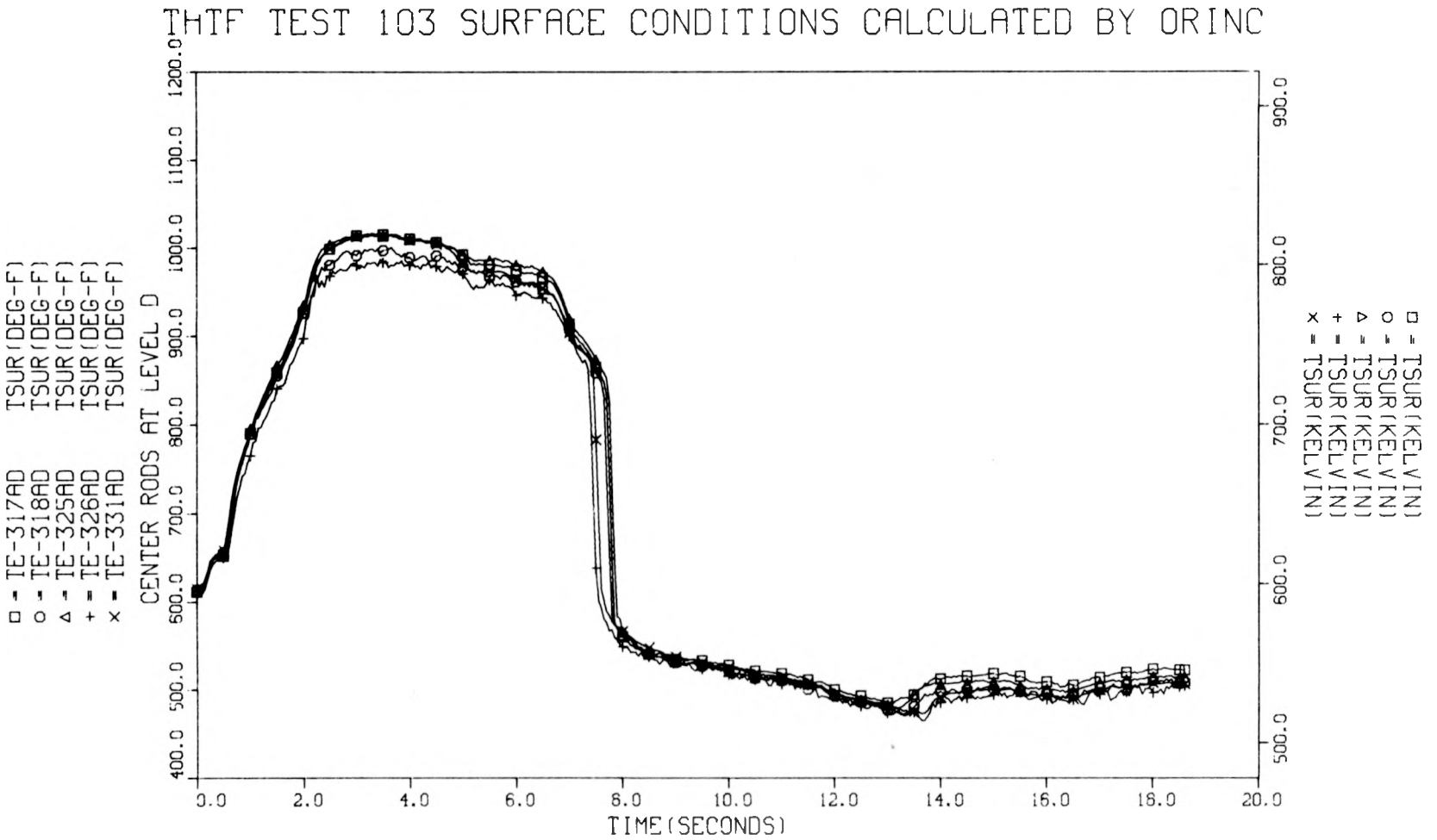

Fig. II.5. Test 103 center rod ORINC surface temperatures — level D.

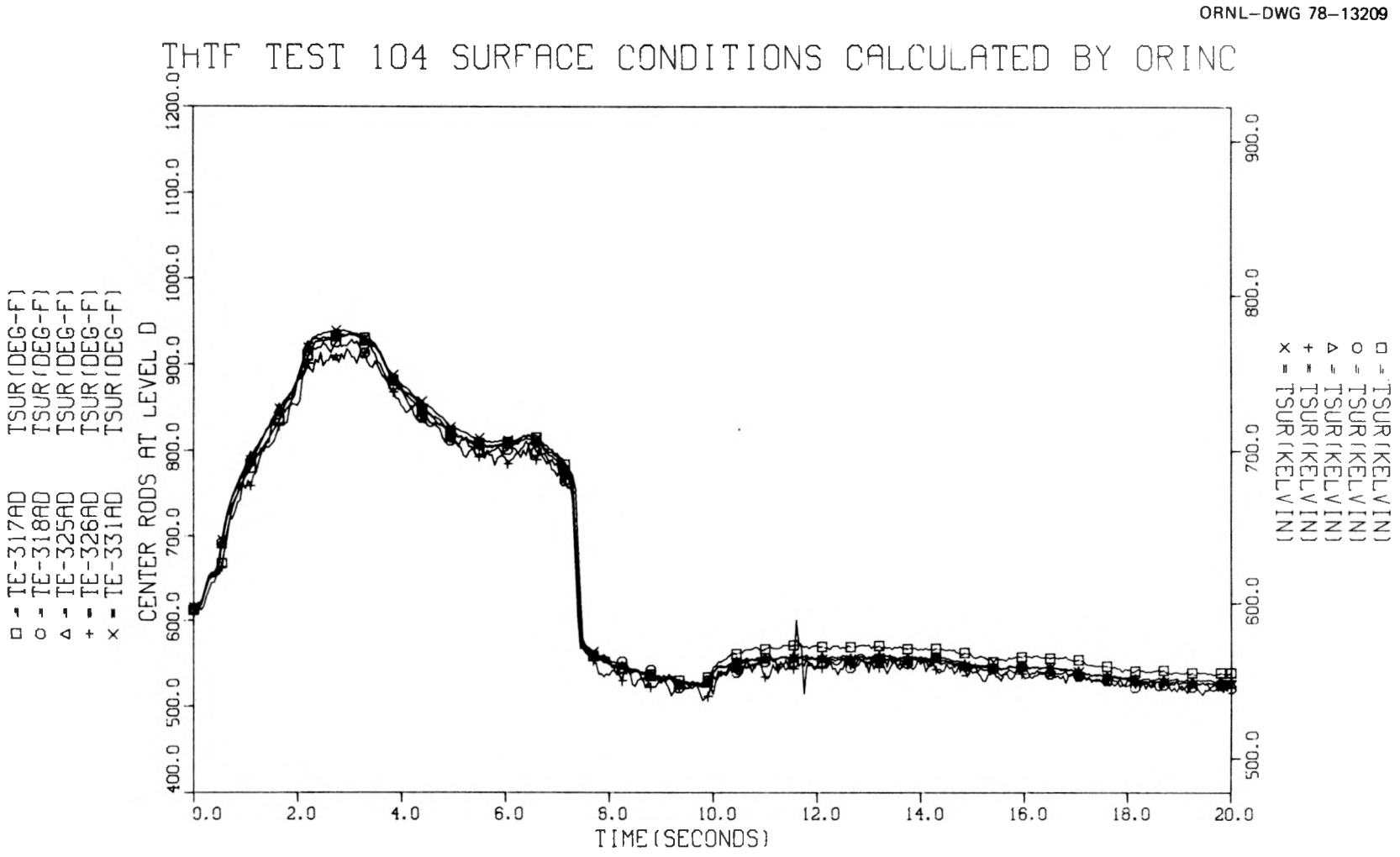

Fig. II.6. Test 104 center rod ORINC surface temperatures — level D.

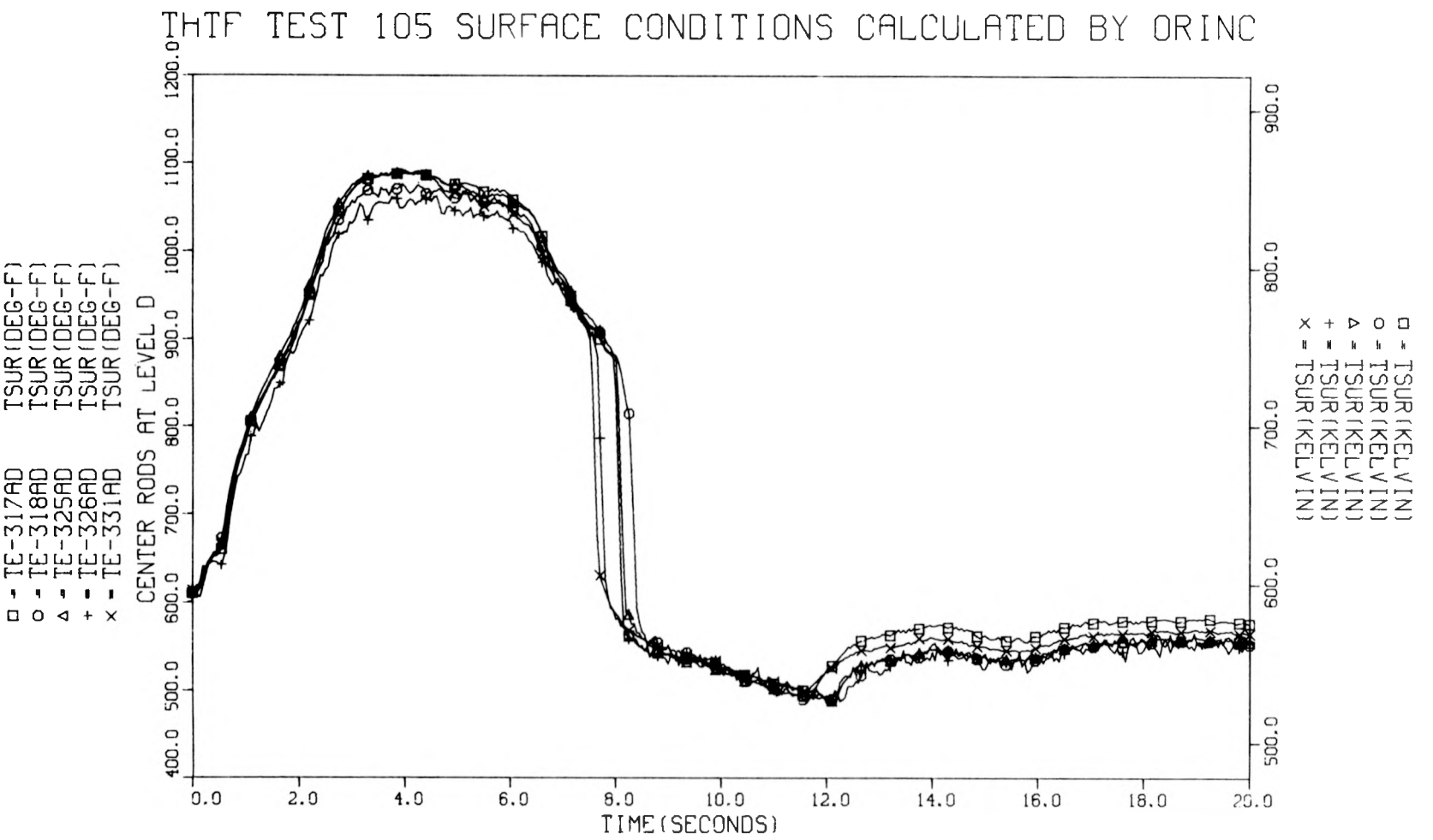

Fig. II.7. Test 105 center rod ORINC surface temperatures — level D.

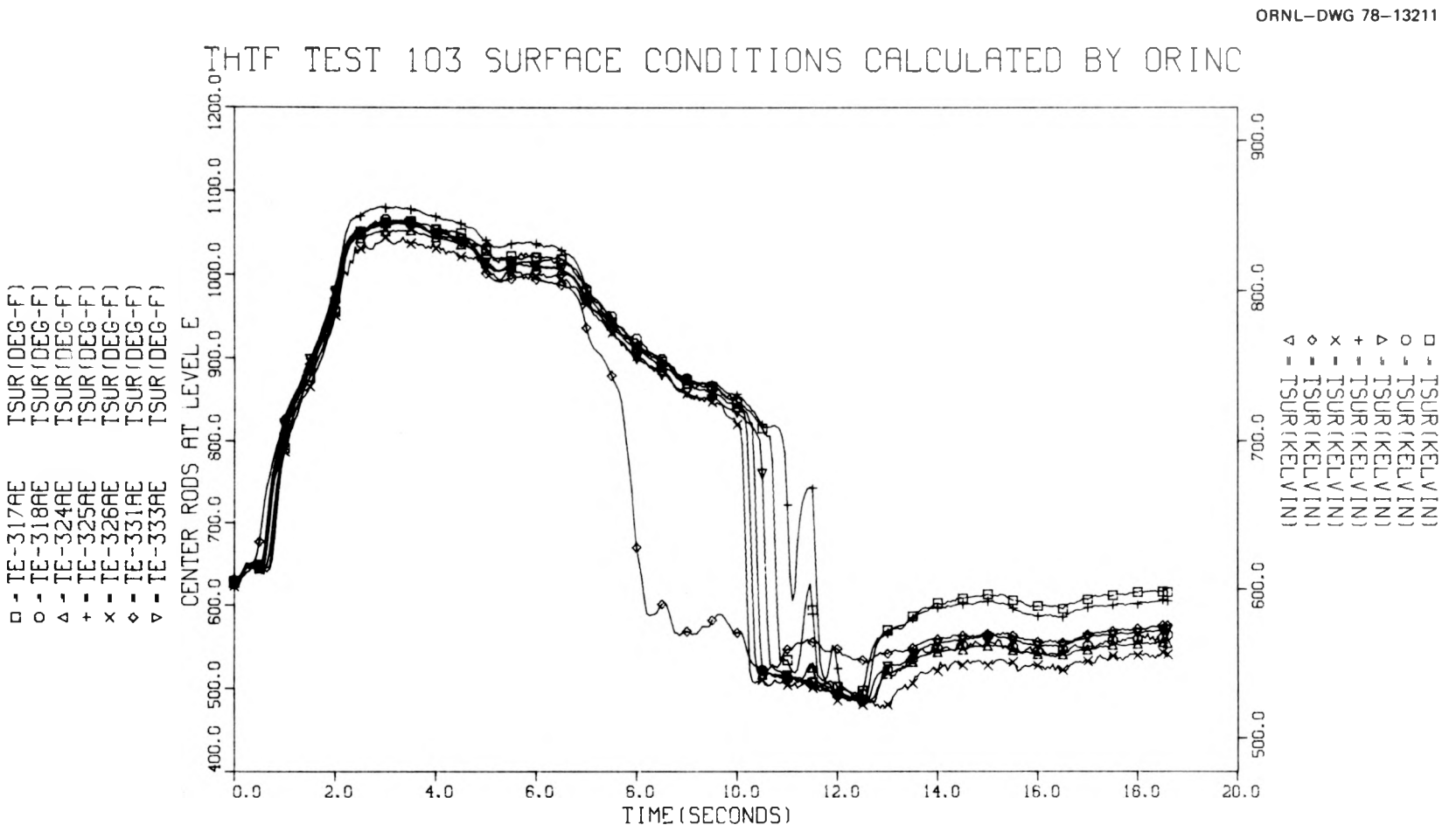

Fig. II.8. Test 103 center rod ORINC surface temperatures — level E.

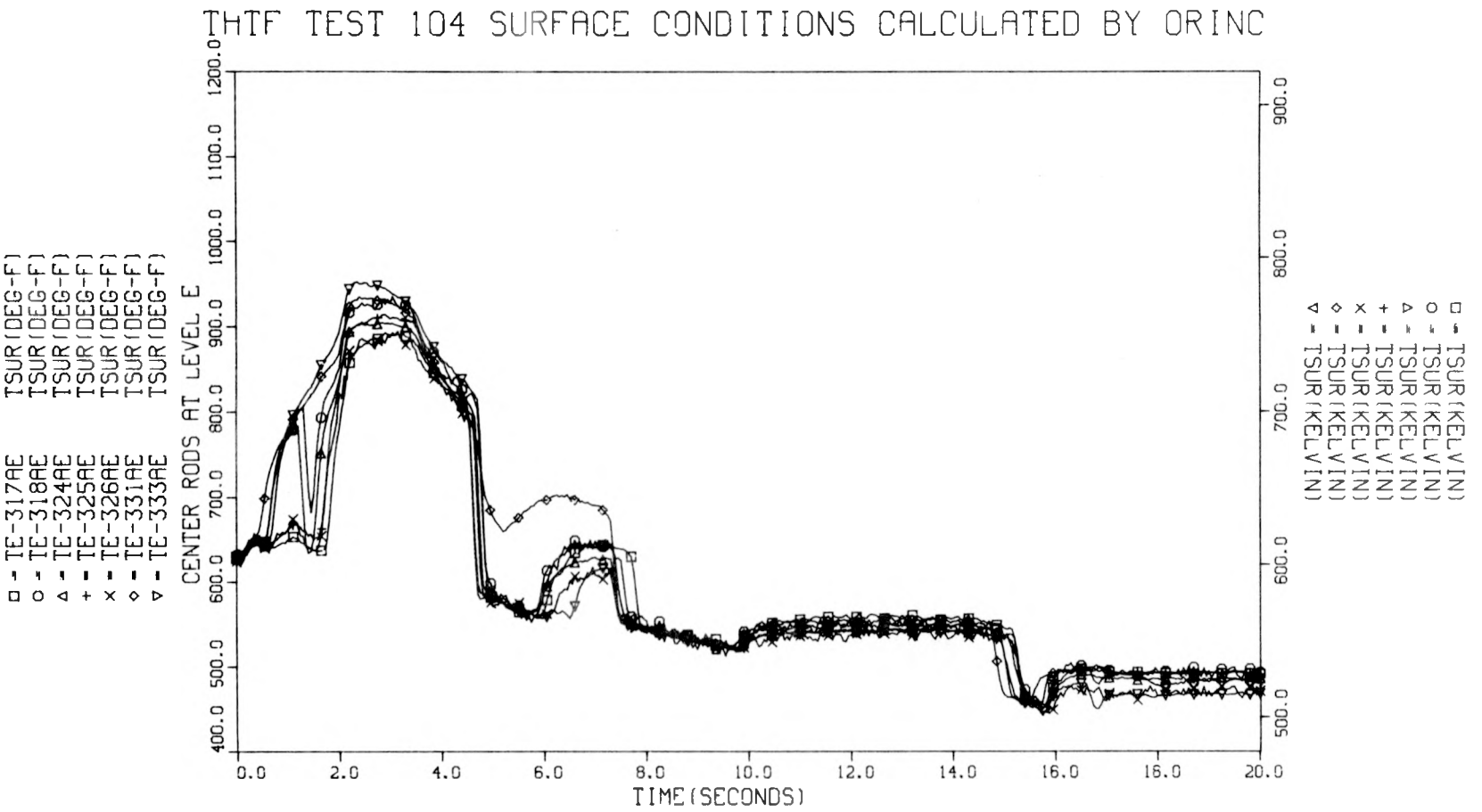

Fig. II.9. Test 104 center rod ORINC surface temperatures — level E.

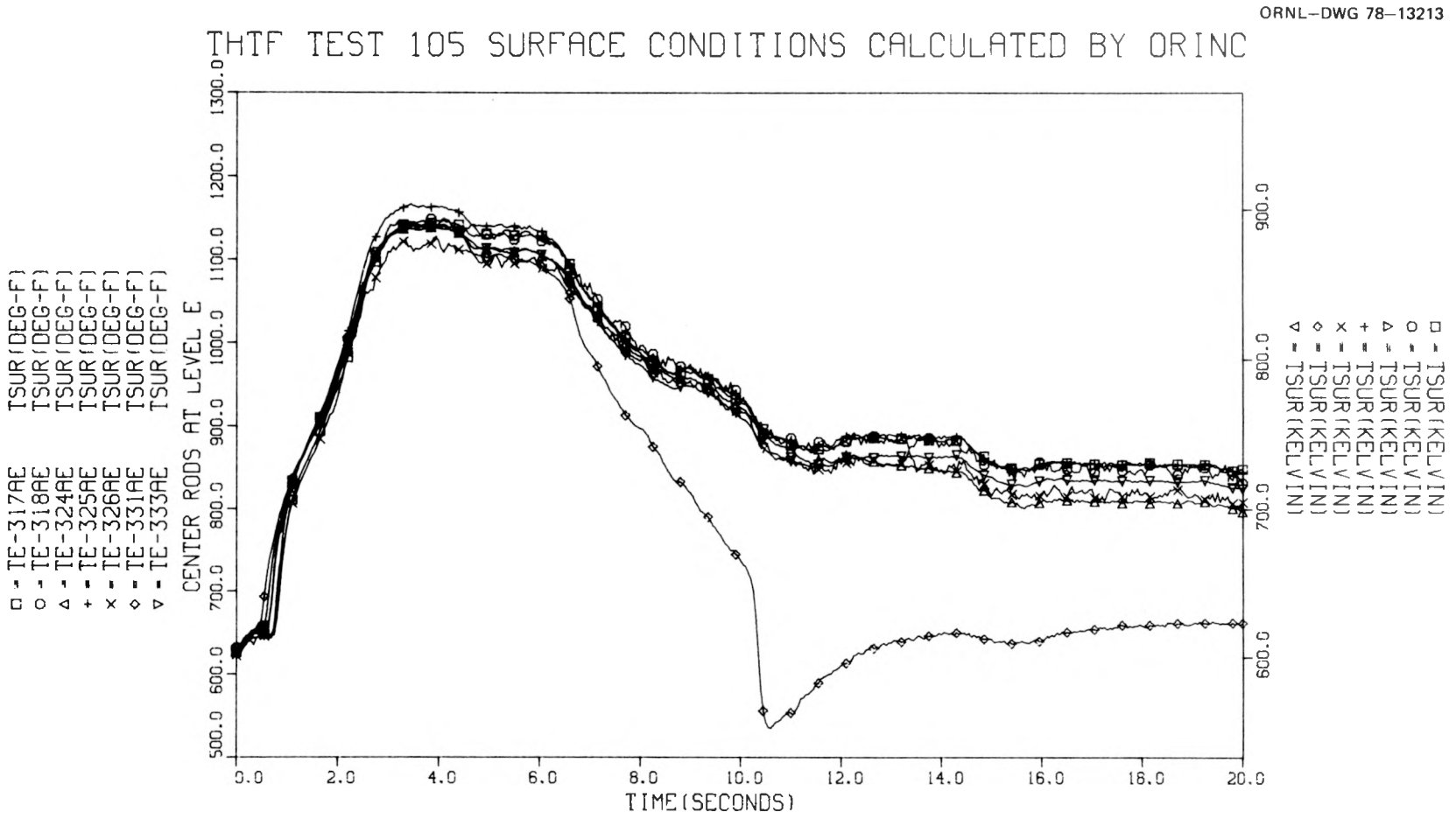

Fig. II.10. Test 105 center rod ORINC surface temperatures — level E.

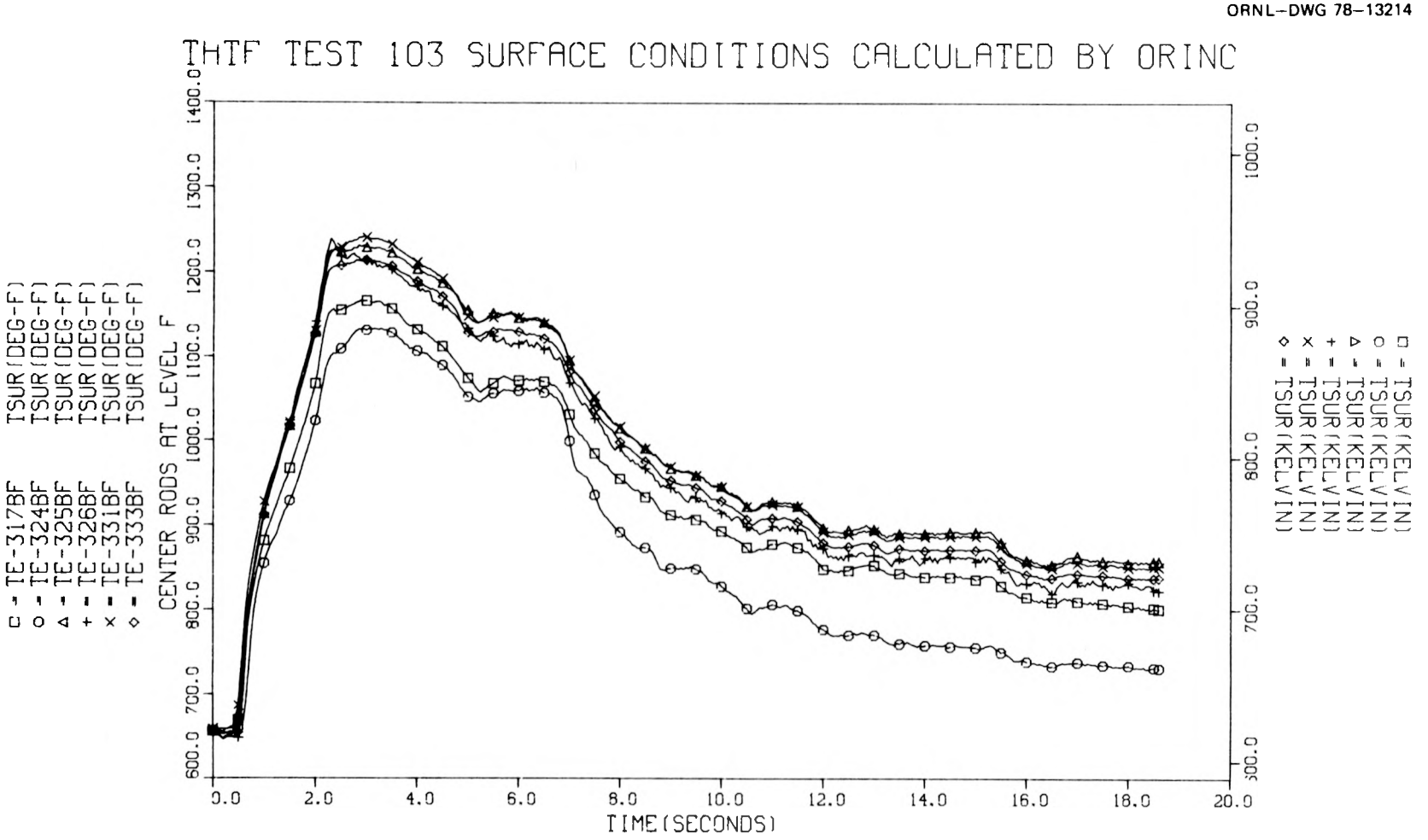

Fig. II.11. Test 103 center rod ORINC surface temperatures — level F.

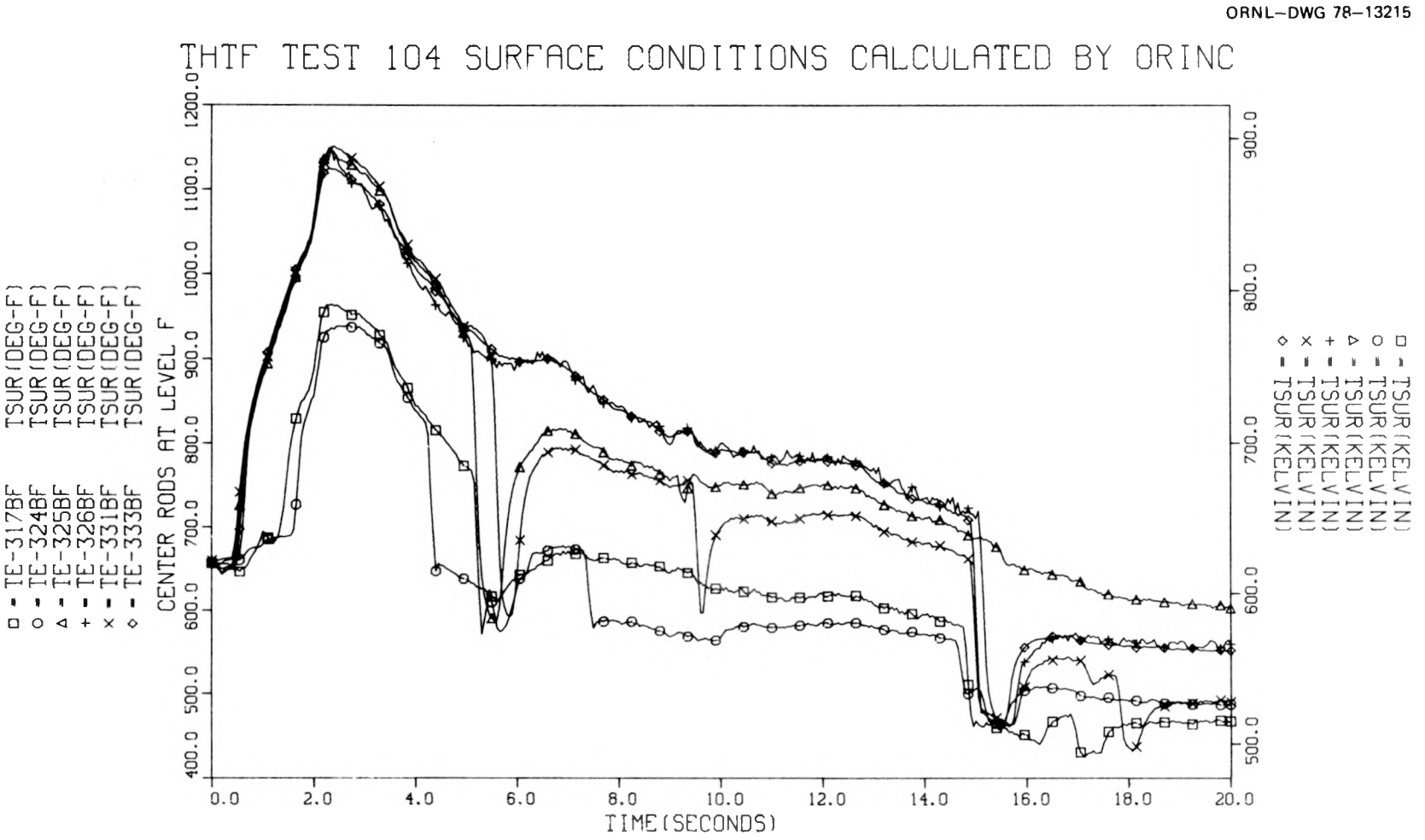

Fig. II.12. Test 104 center rod ORINC surface temperatures — level F.

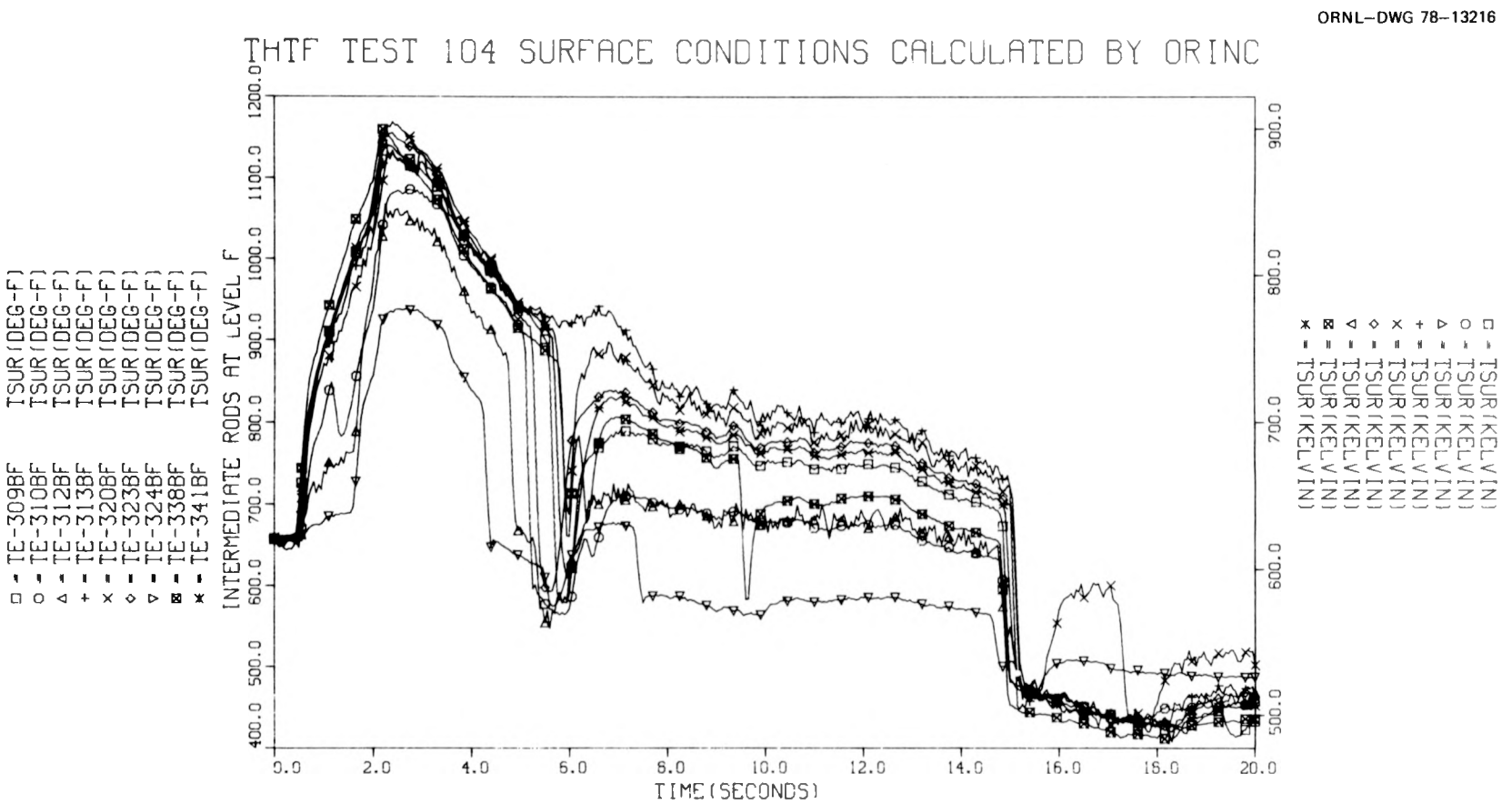

Fig. II.13. Test 104 intermediate rod ORINC surface temperatures — level F.

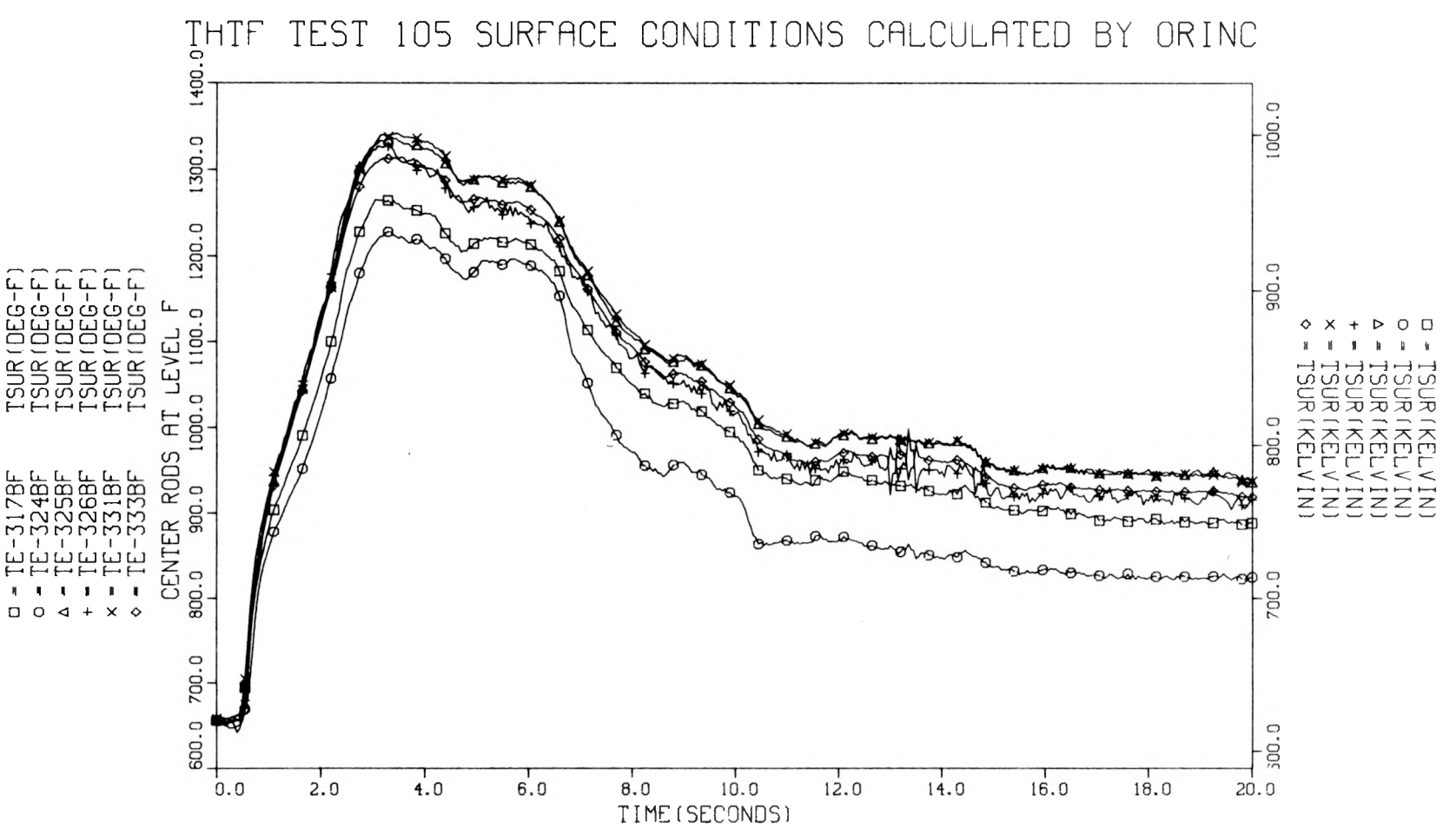

Fig. II.14. Test 105 center rod ORINC surface temperatures — level F.

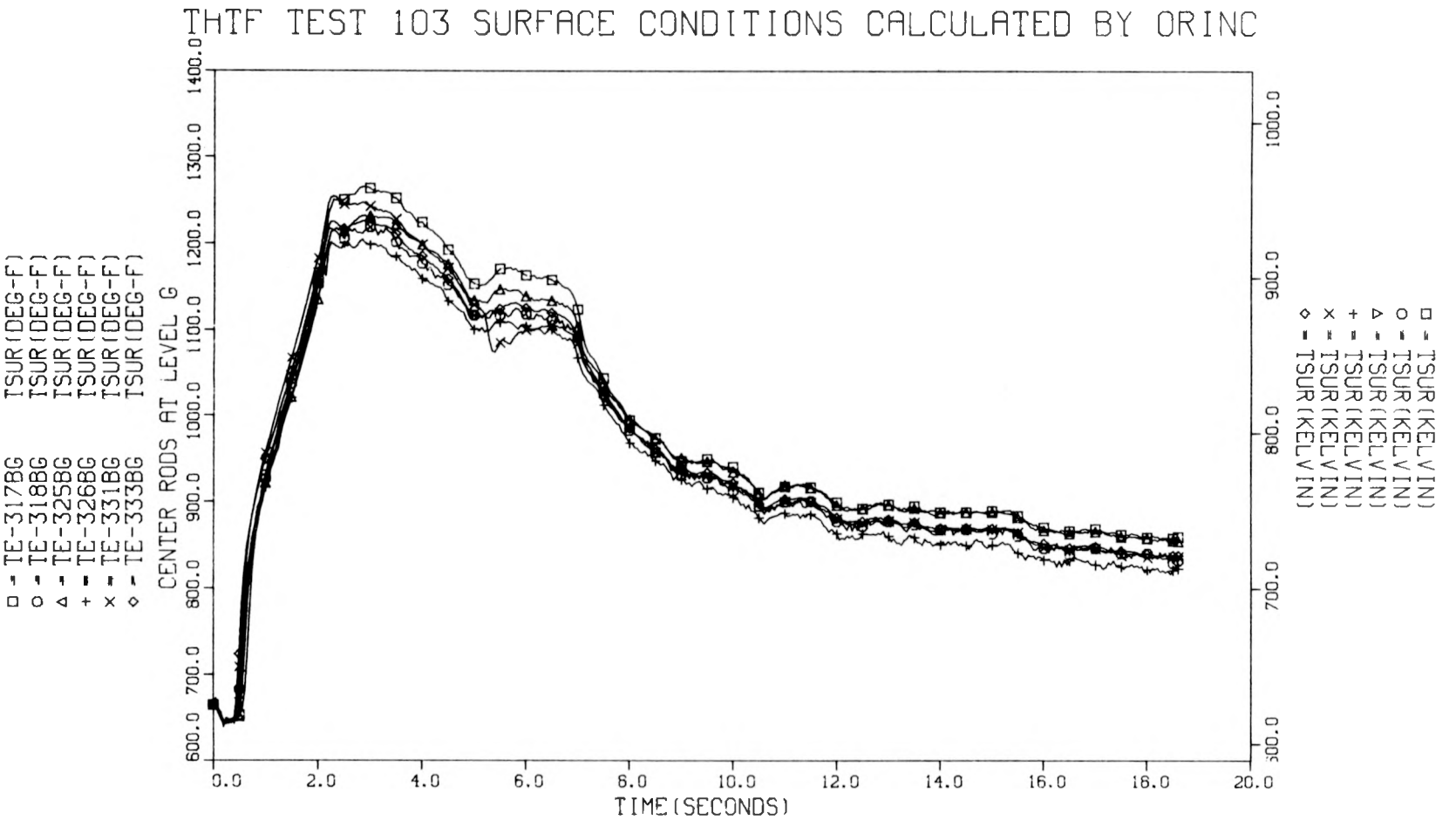

Fig. II.15. Test 103 center rod ORINC surface temperatures — level G.

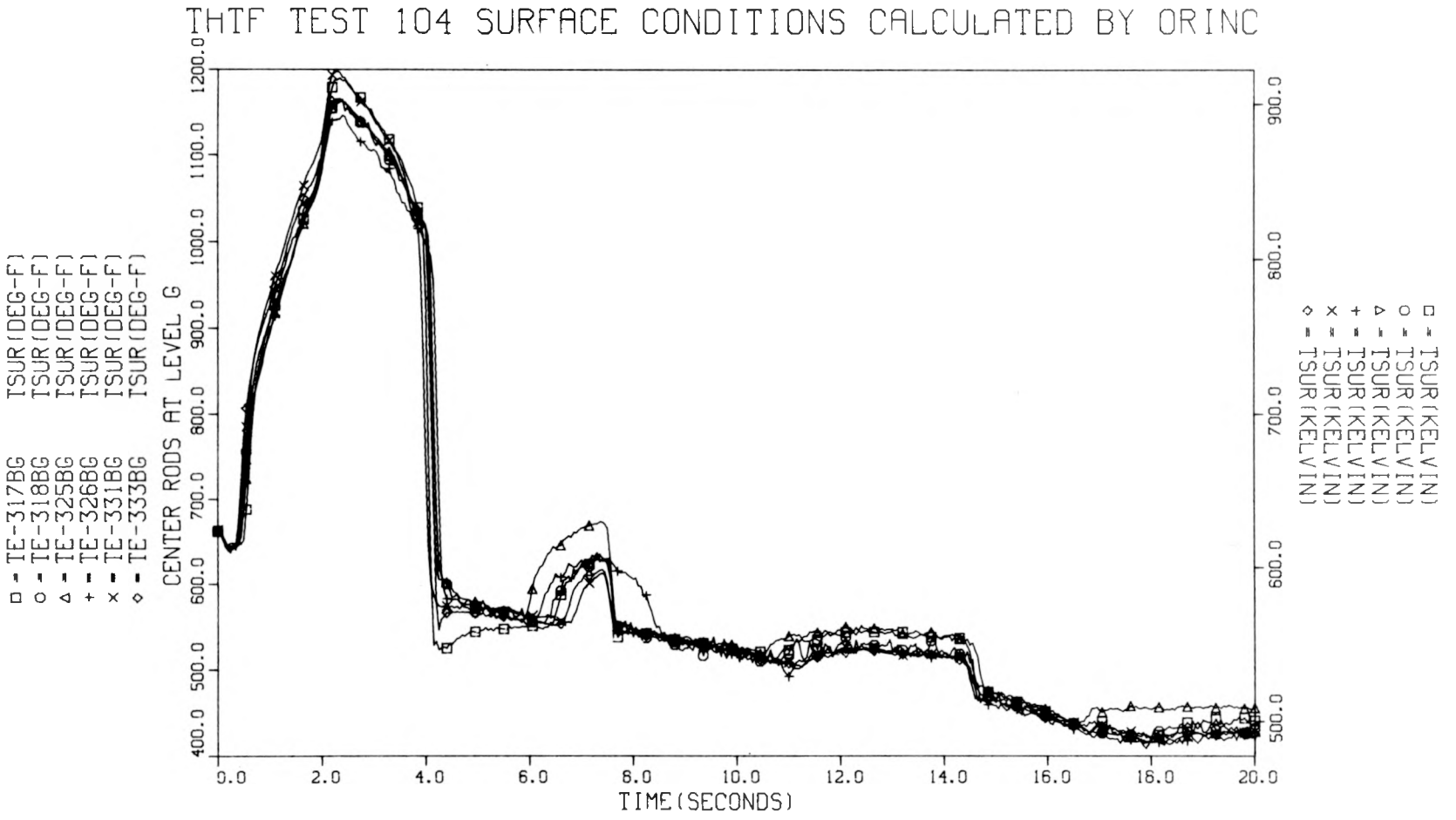

Fig. II.16. Test 104 center rod ORINC surface temperatures — level G.

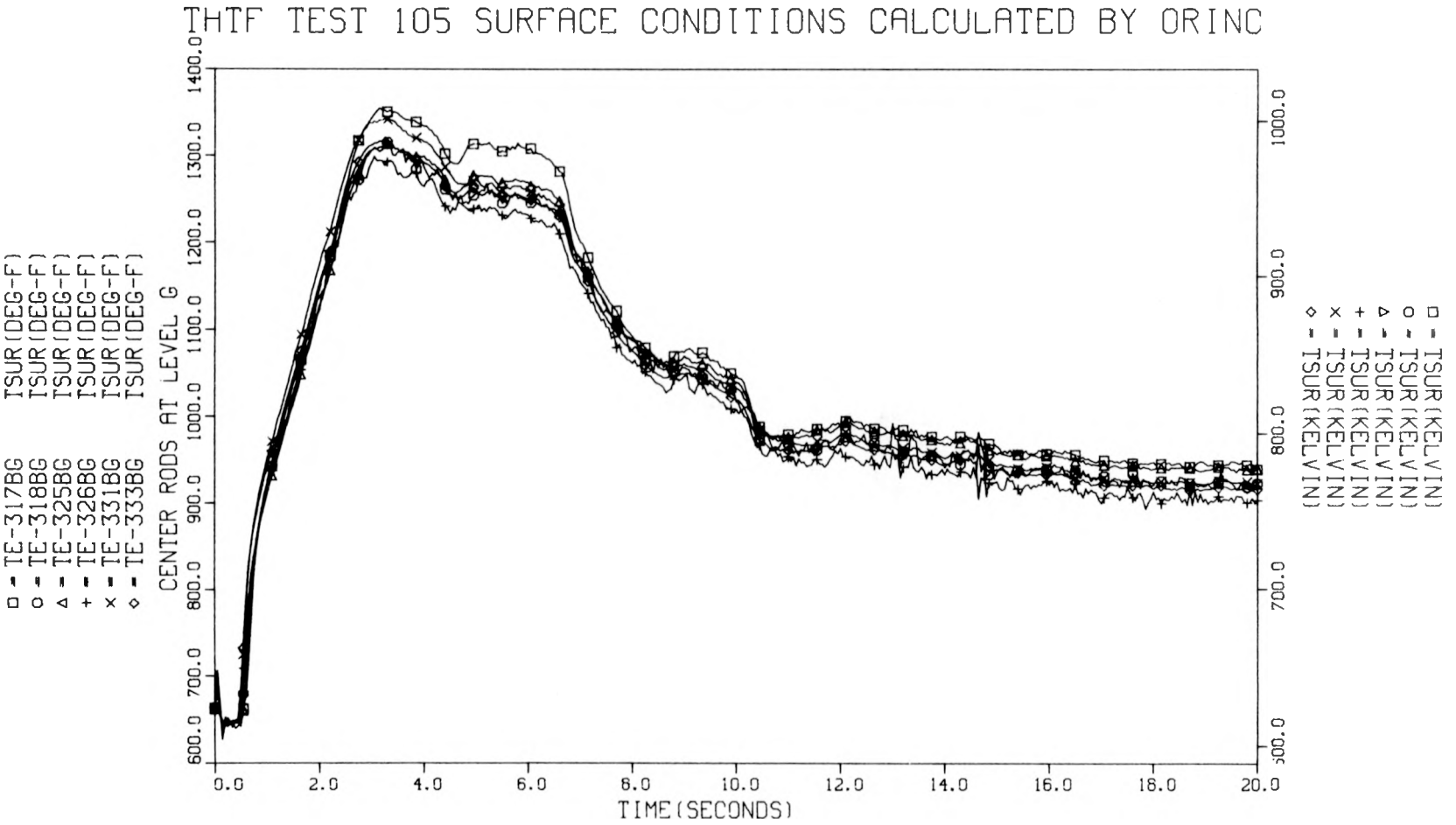

Fig. II.17. Test 105 center rod ORINC surface temperatures — level G.

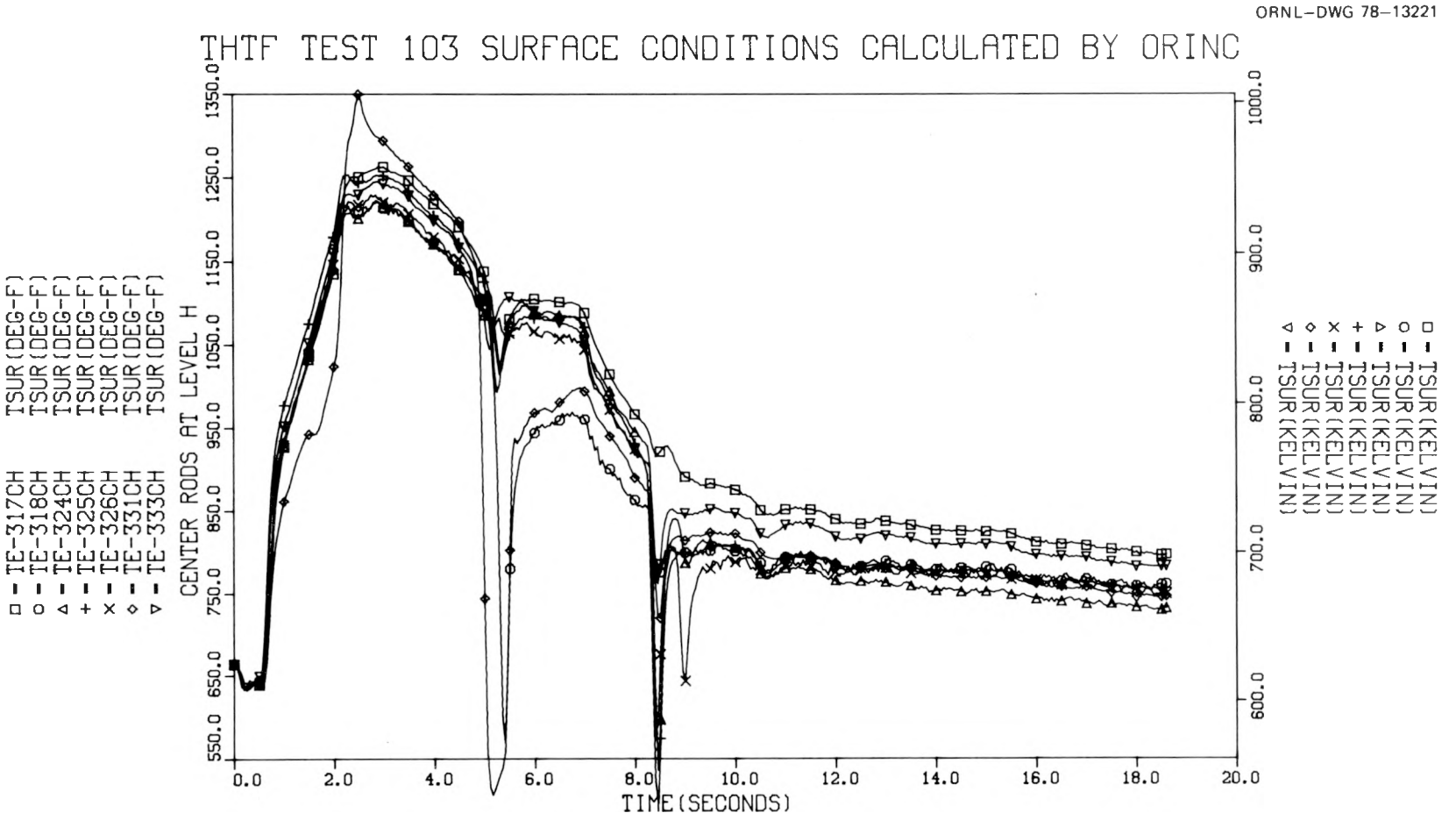

Fig. II.18. Test 103 center rod ORINC surface temperatures — level H.

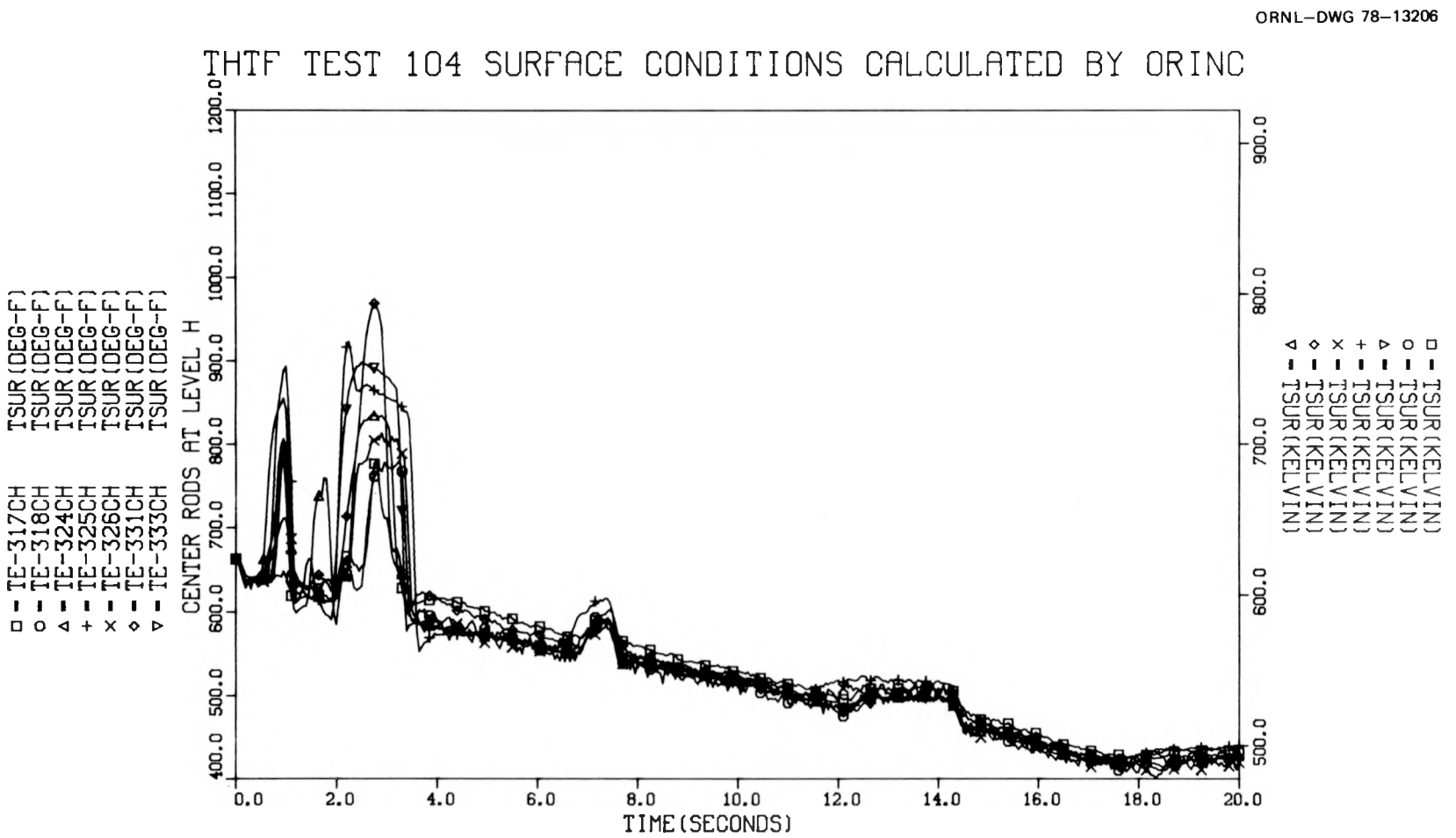

Fig. II.19. Test 104 center rod ORINC surface temperatures — level H.

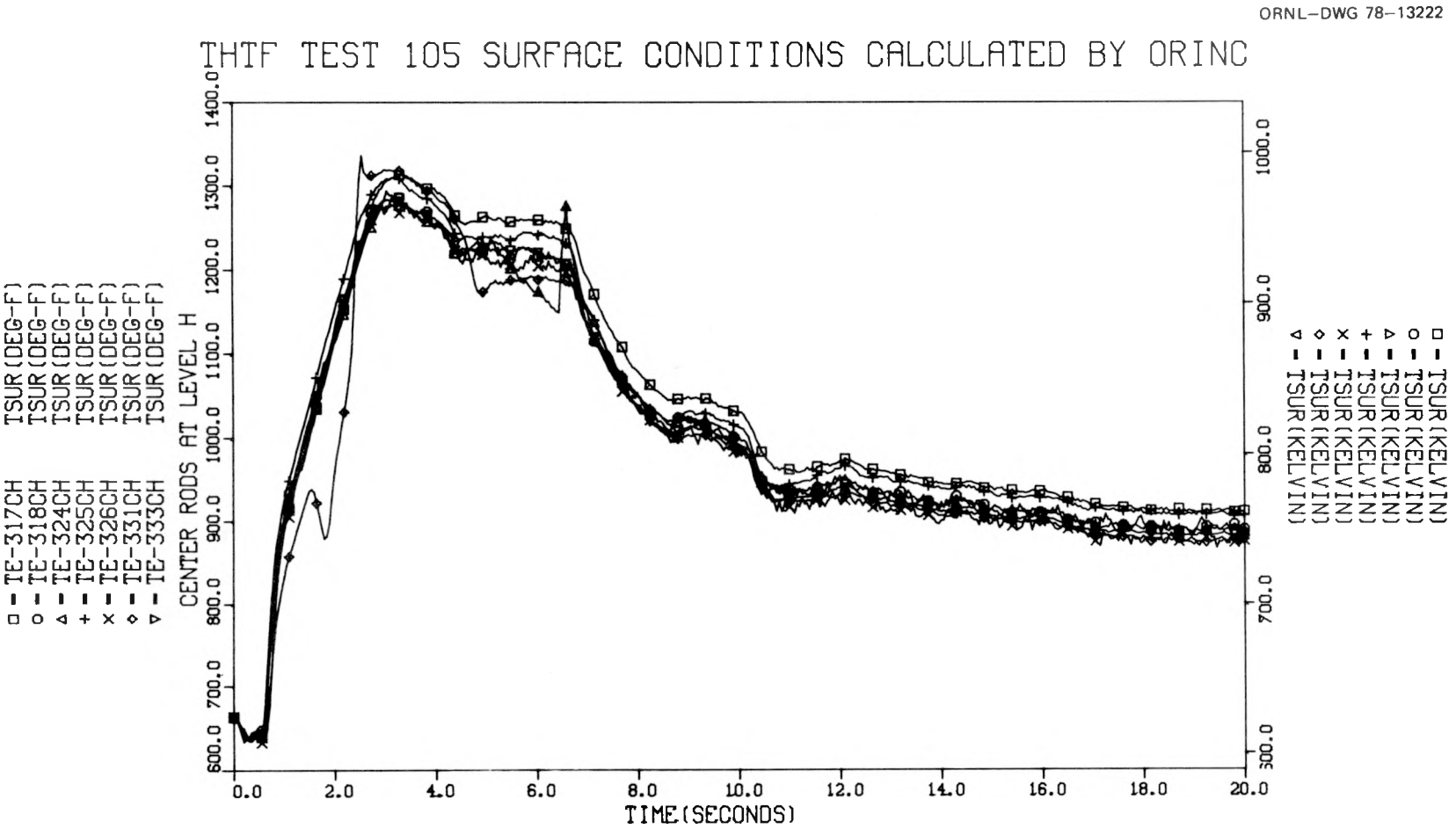

Fig. II.20. Test 105 center rod ORINC surface temperatures — level H.

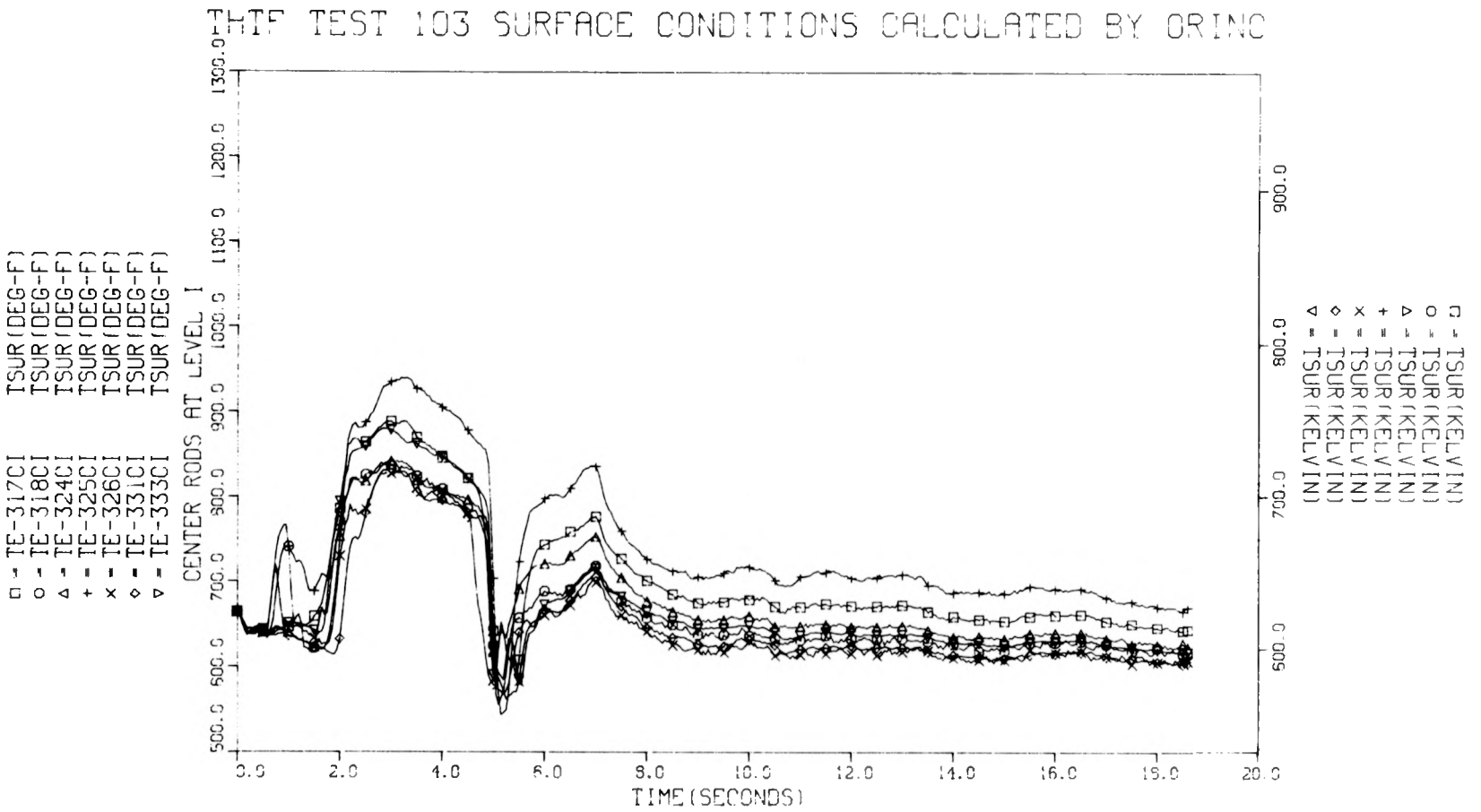

Fig. II.21. Test 103 center rod ORINC surface temperatures — level I.

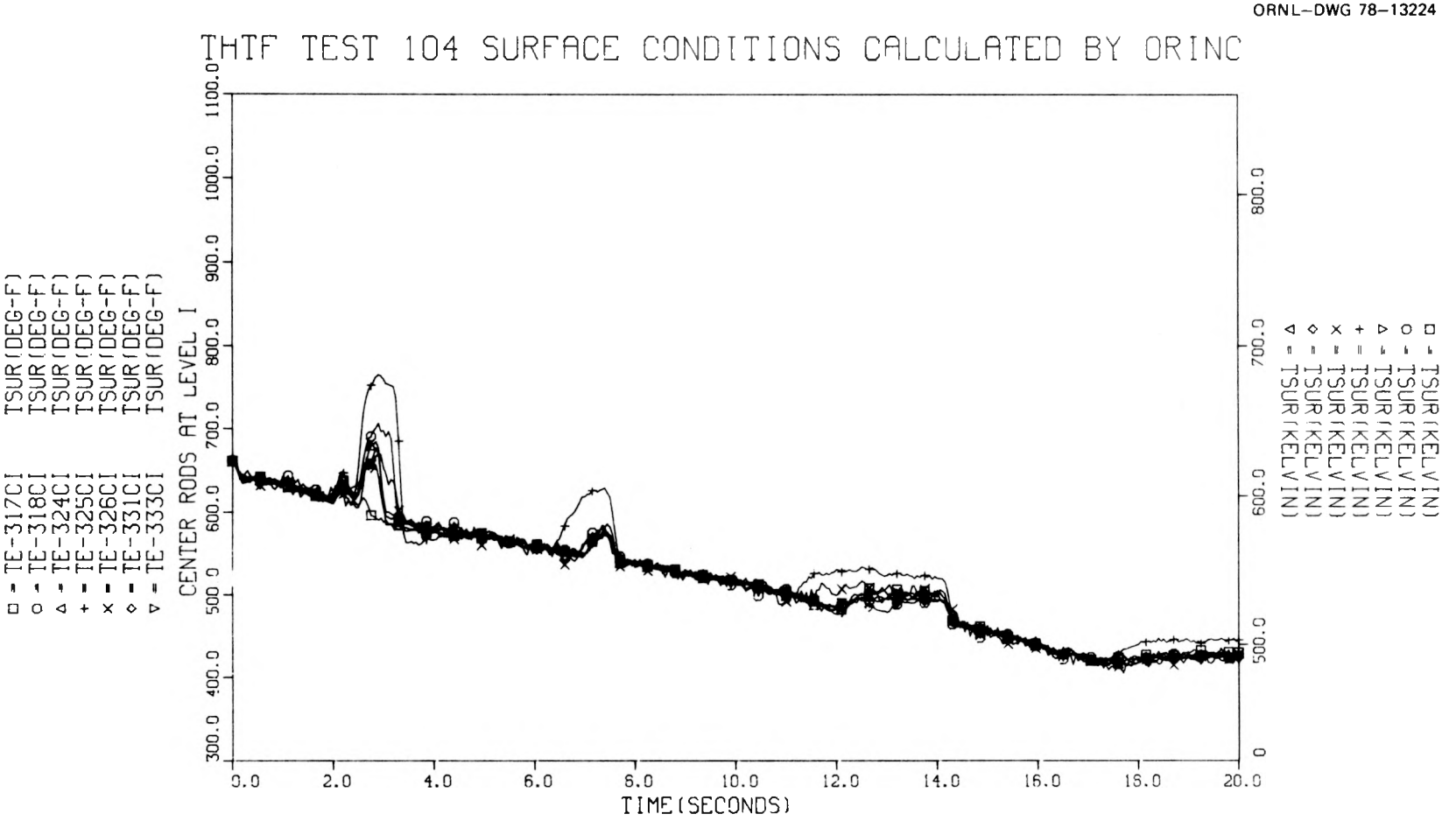

Fig. II.22. Test 104 center rod ORINC surface temperatures — level I.

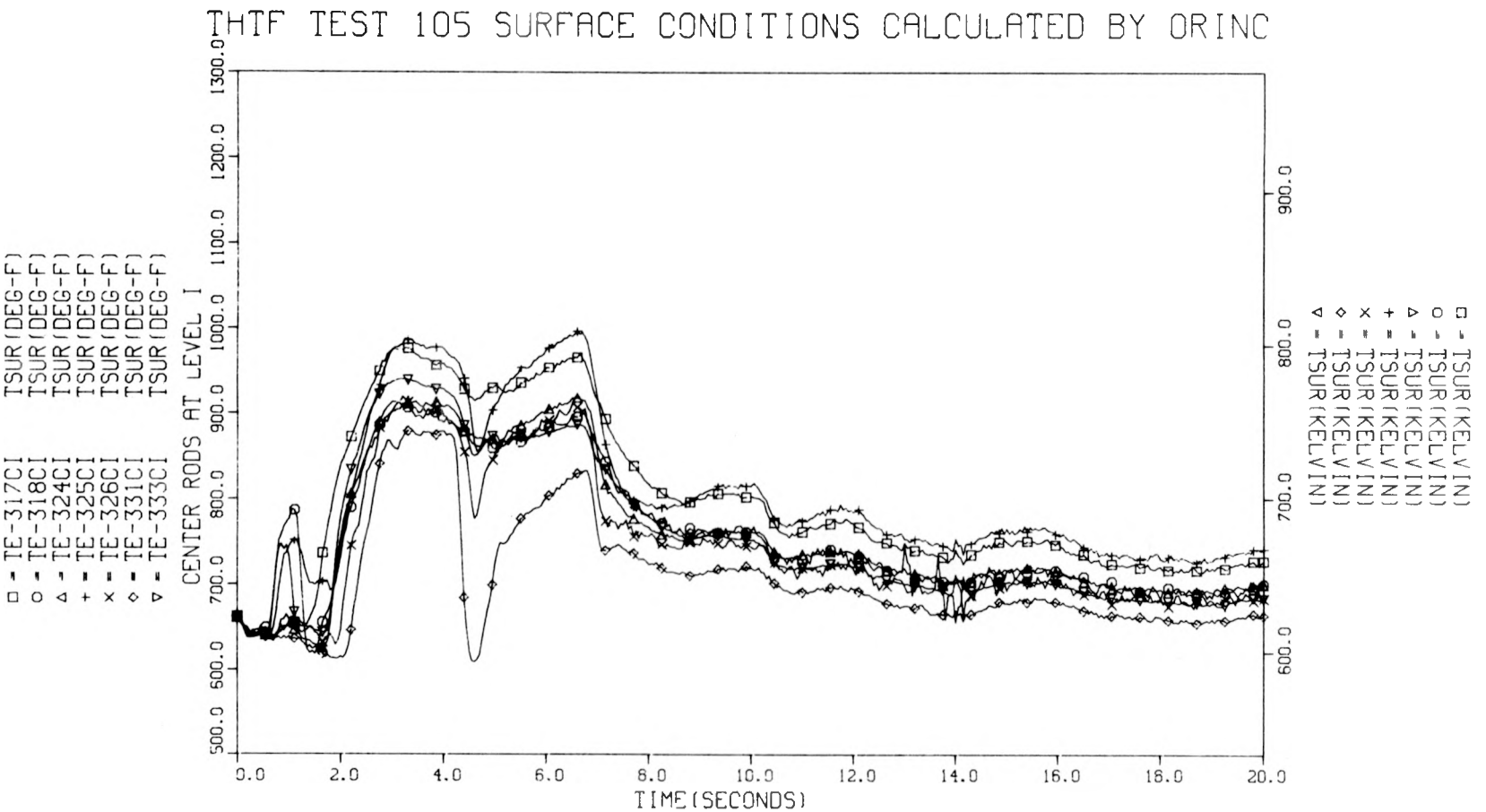

Fig. II.23. Test 105 center rod ORINC surface temperatures — level I.

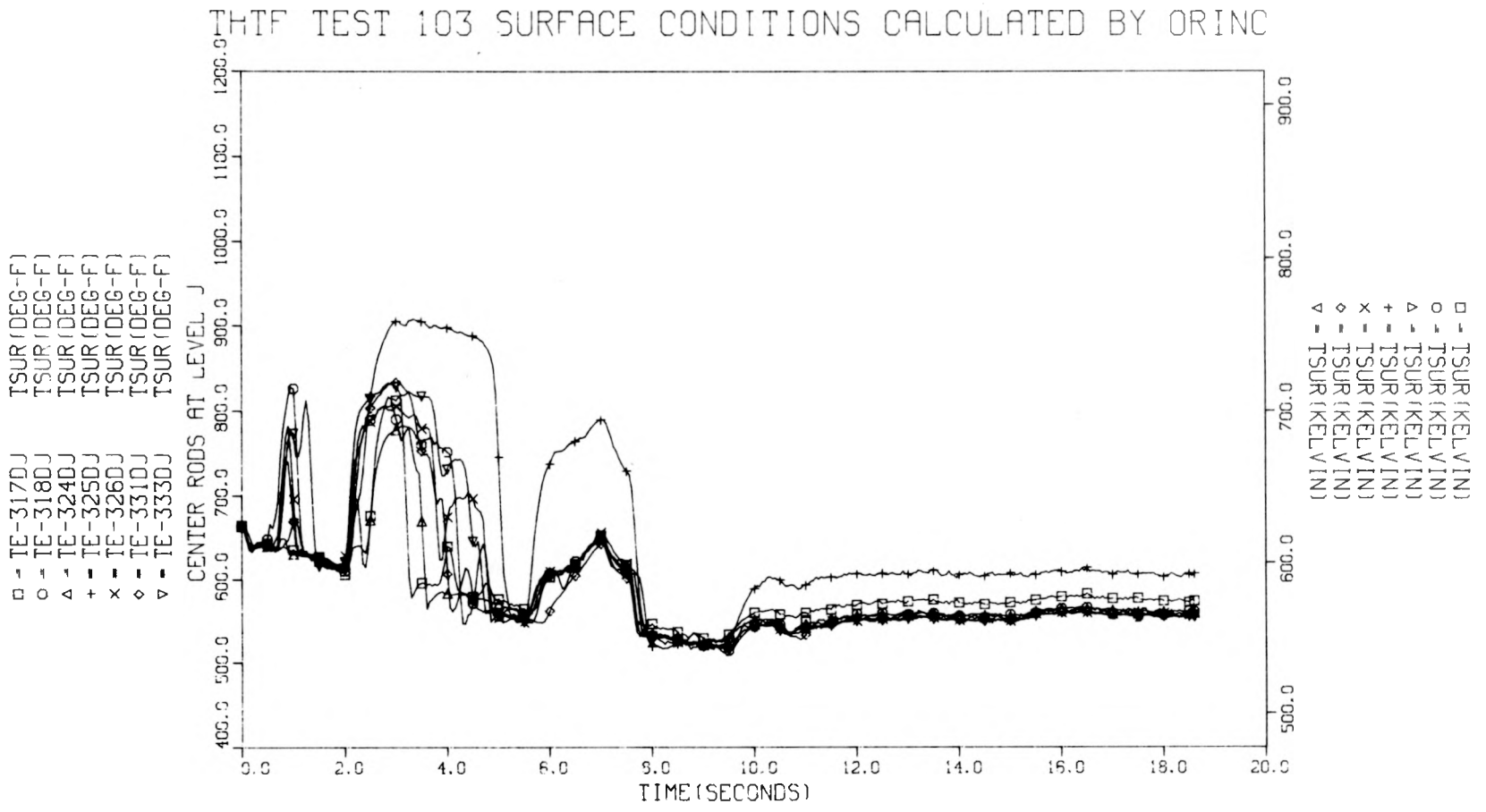

Fig. II.24. Test 103 center rod ORINC surface temperatures — level J.

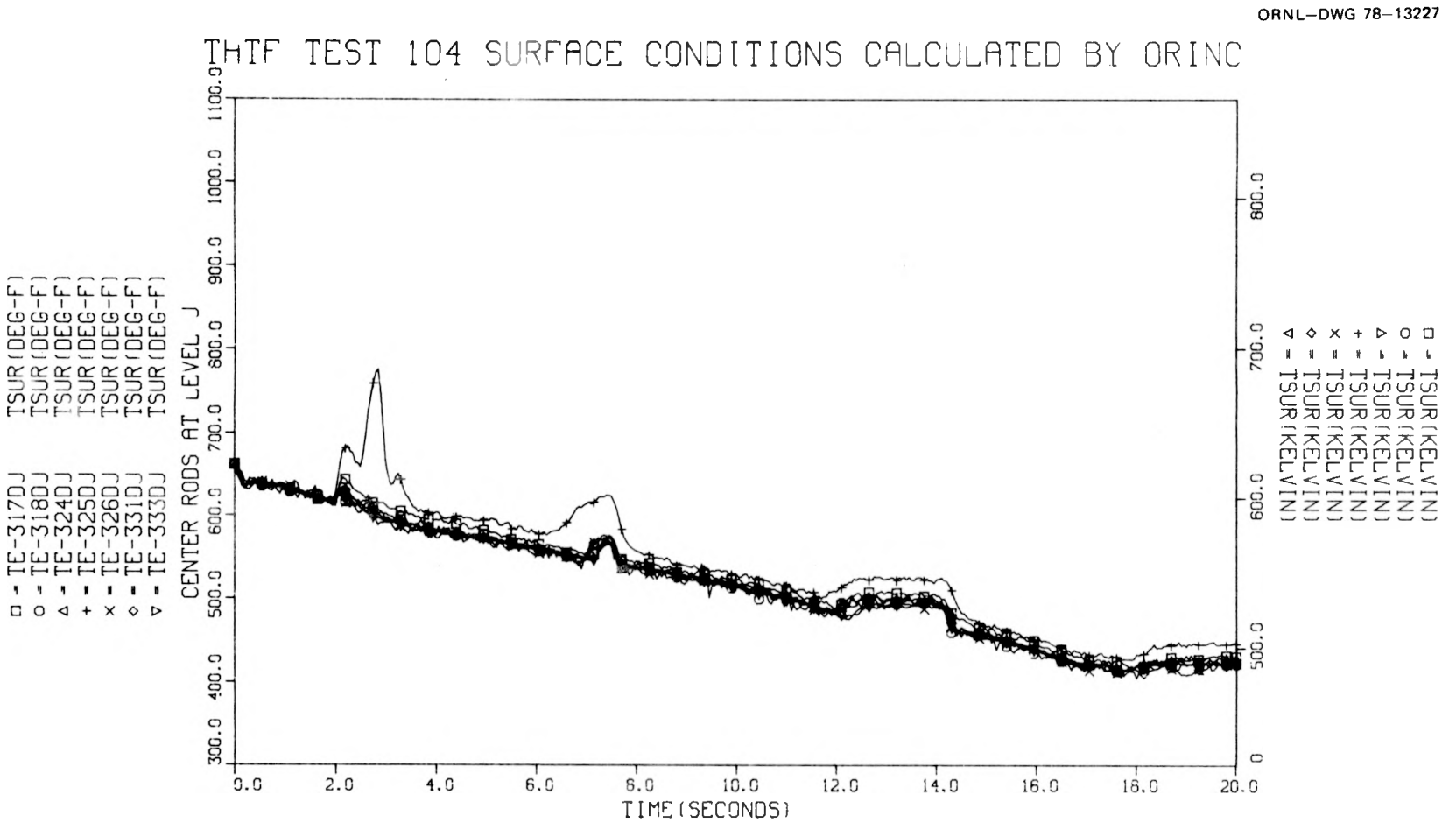

Fig. II.25. Test 104 center rod ORINC surface temperatures — level J.

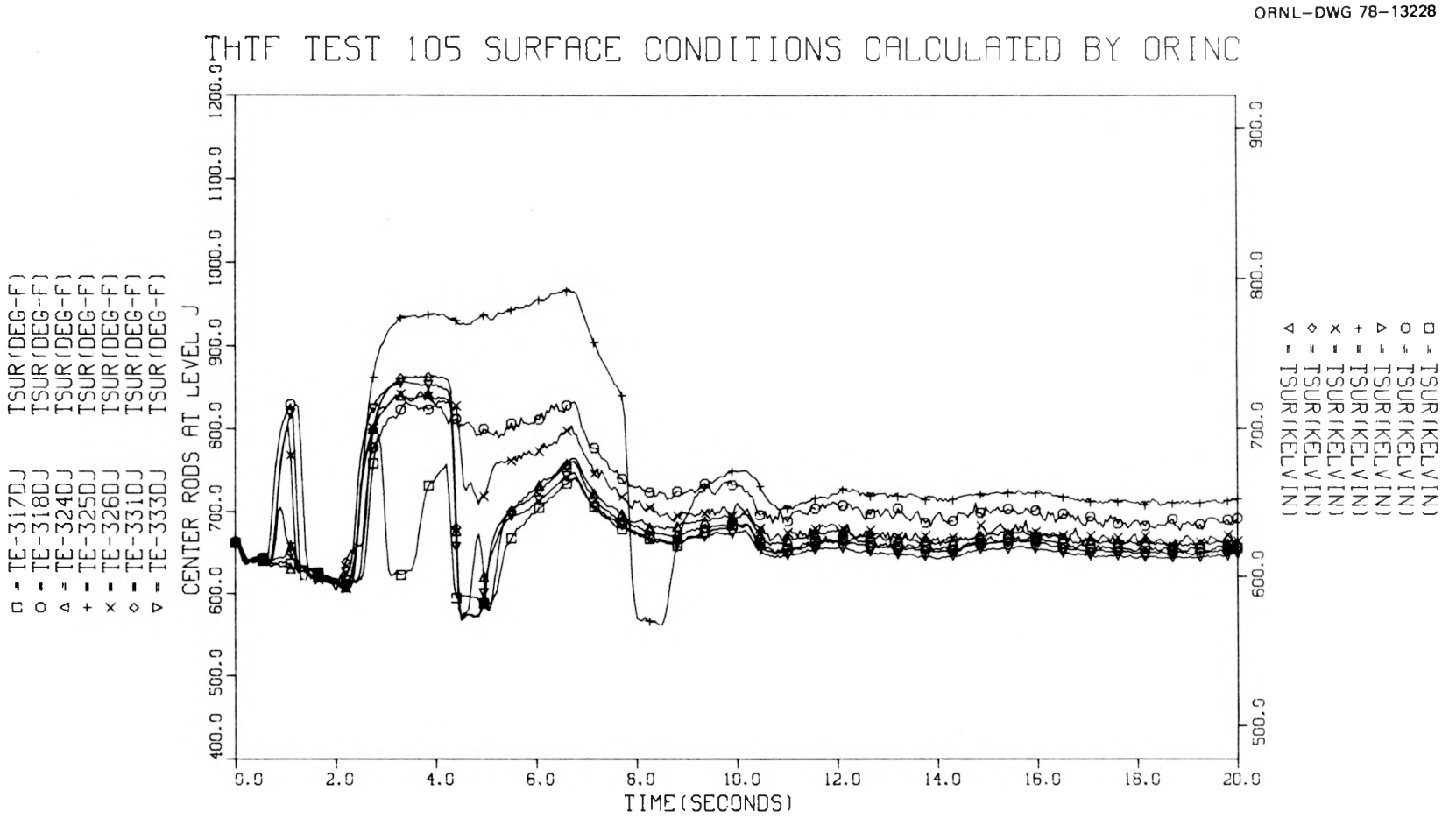

Fig. II.26. Test 105 center rod ORINC surface temperatures — level J.

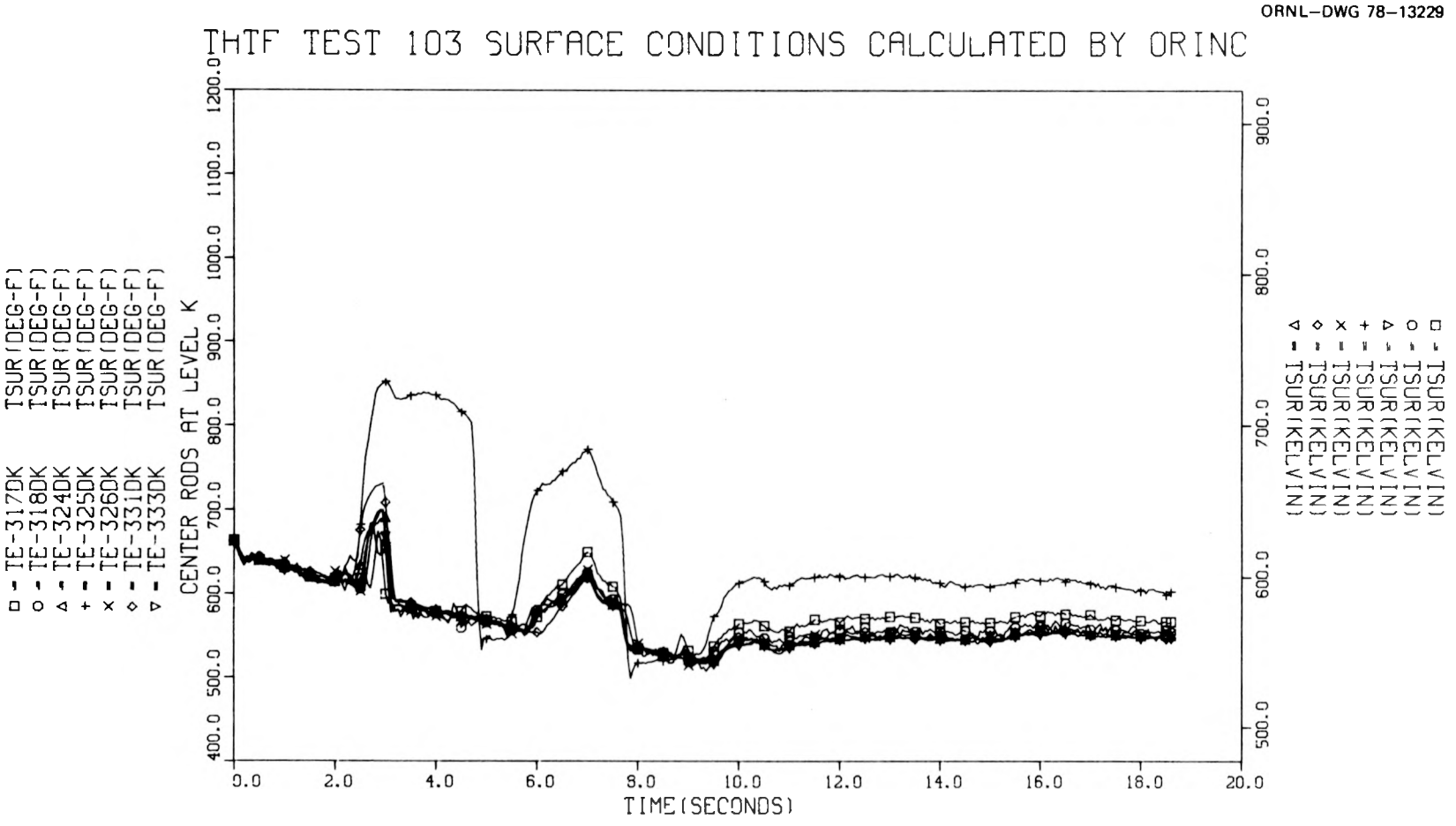

Fig. II.27. Test 103 center rod ORINC surface temperatures — level K.

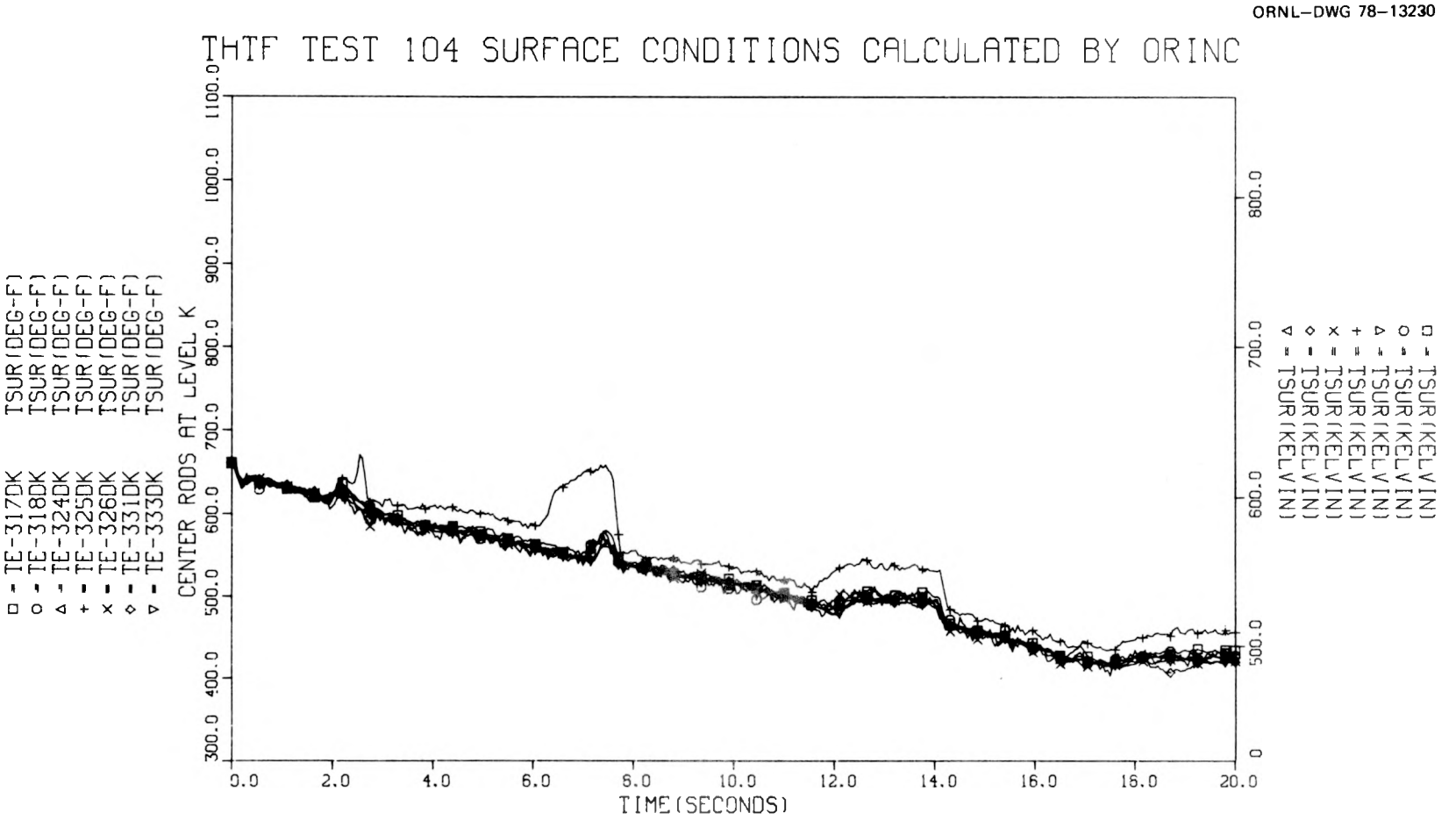

Fig. II.28. Test 104 center rod ORINC surface temperatures — level K.

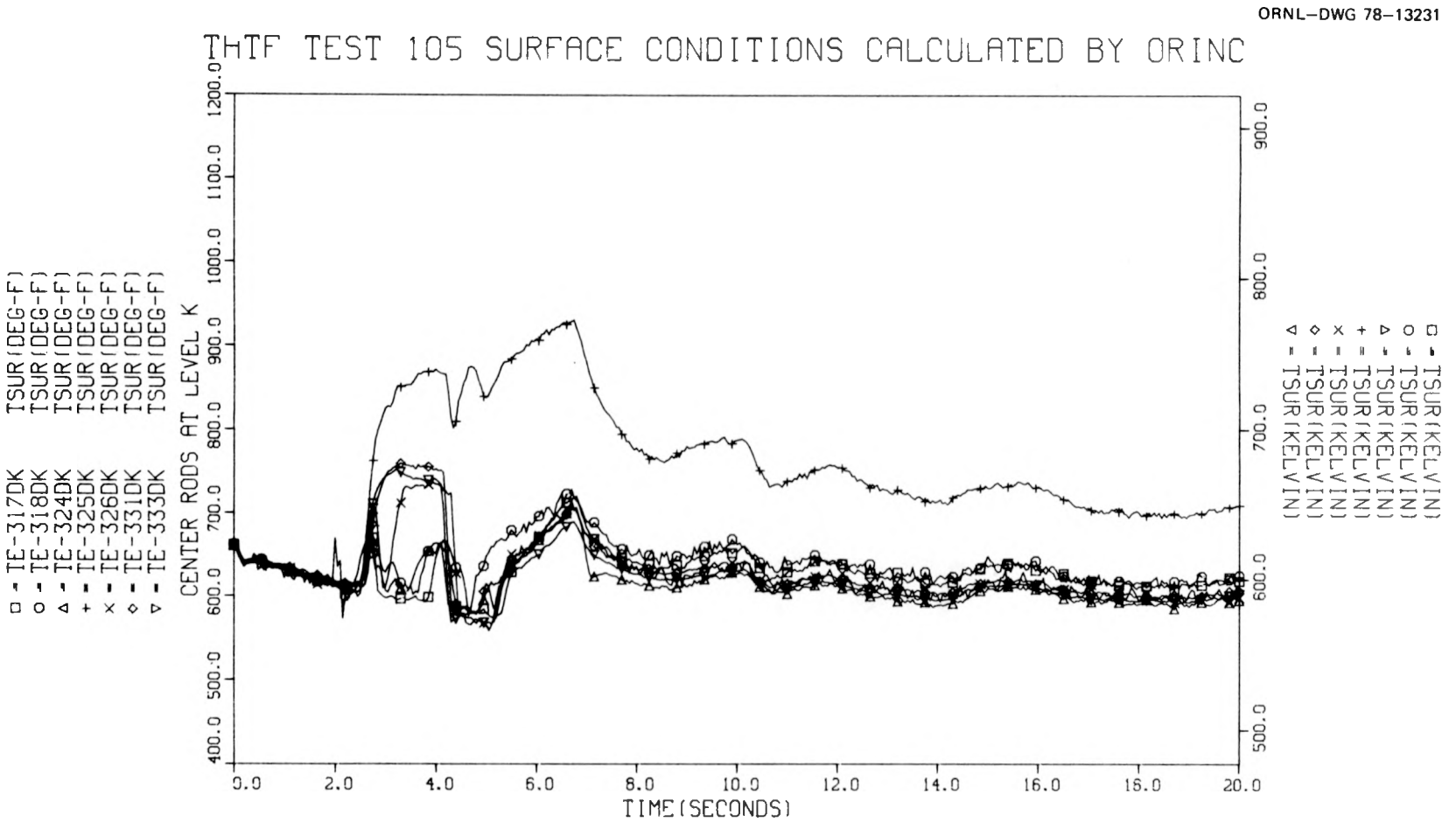

Fig. II.29. Test 105 center rod ORINC surface temperatures — level K.

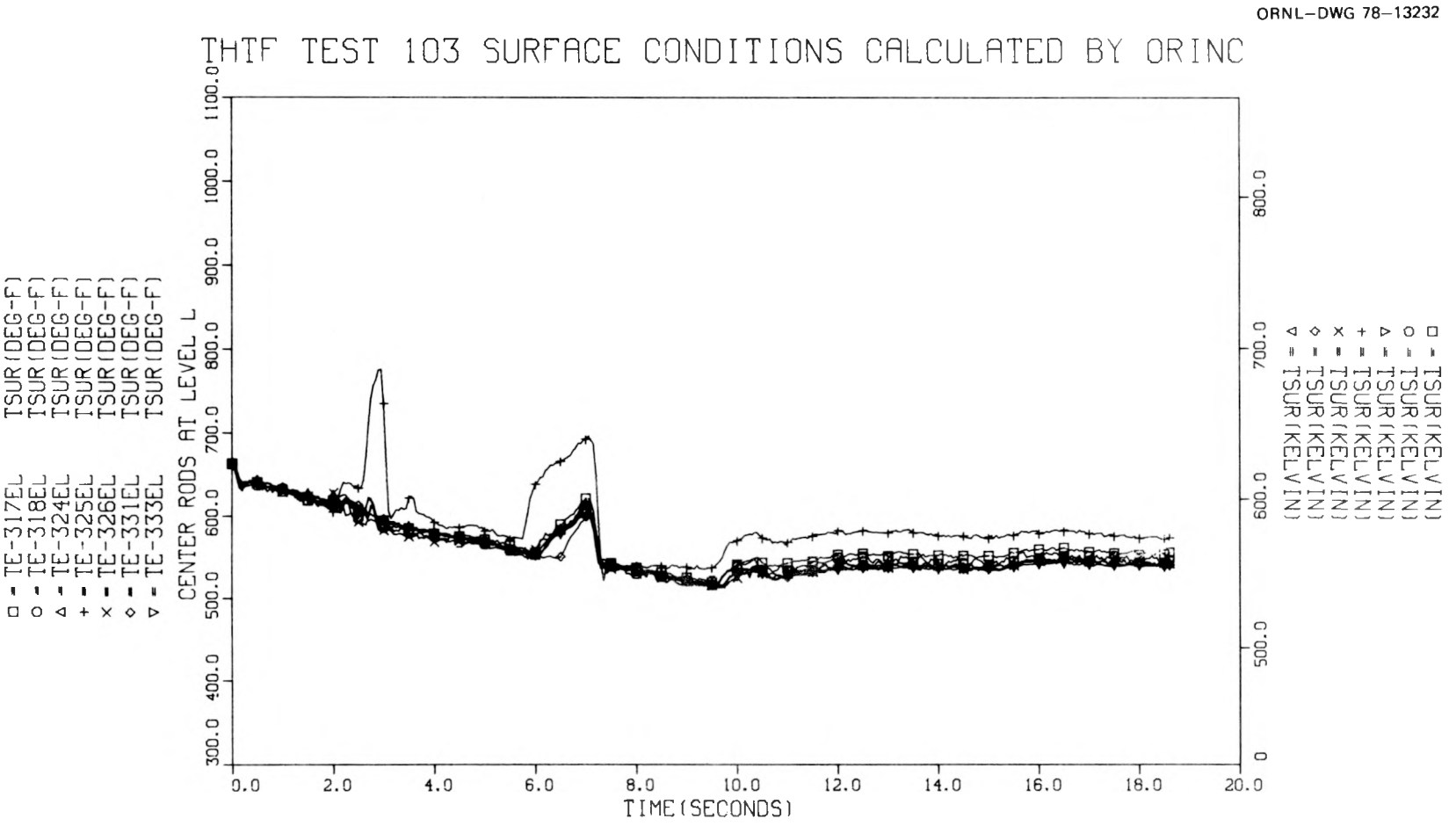

Fig. II.30. Test 103 center rod ORINC surface temperatures — level L.

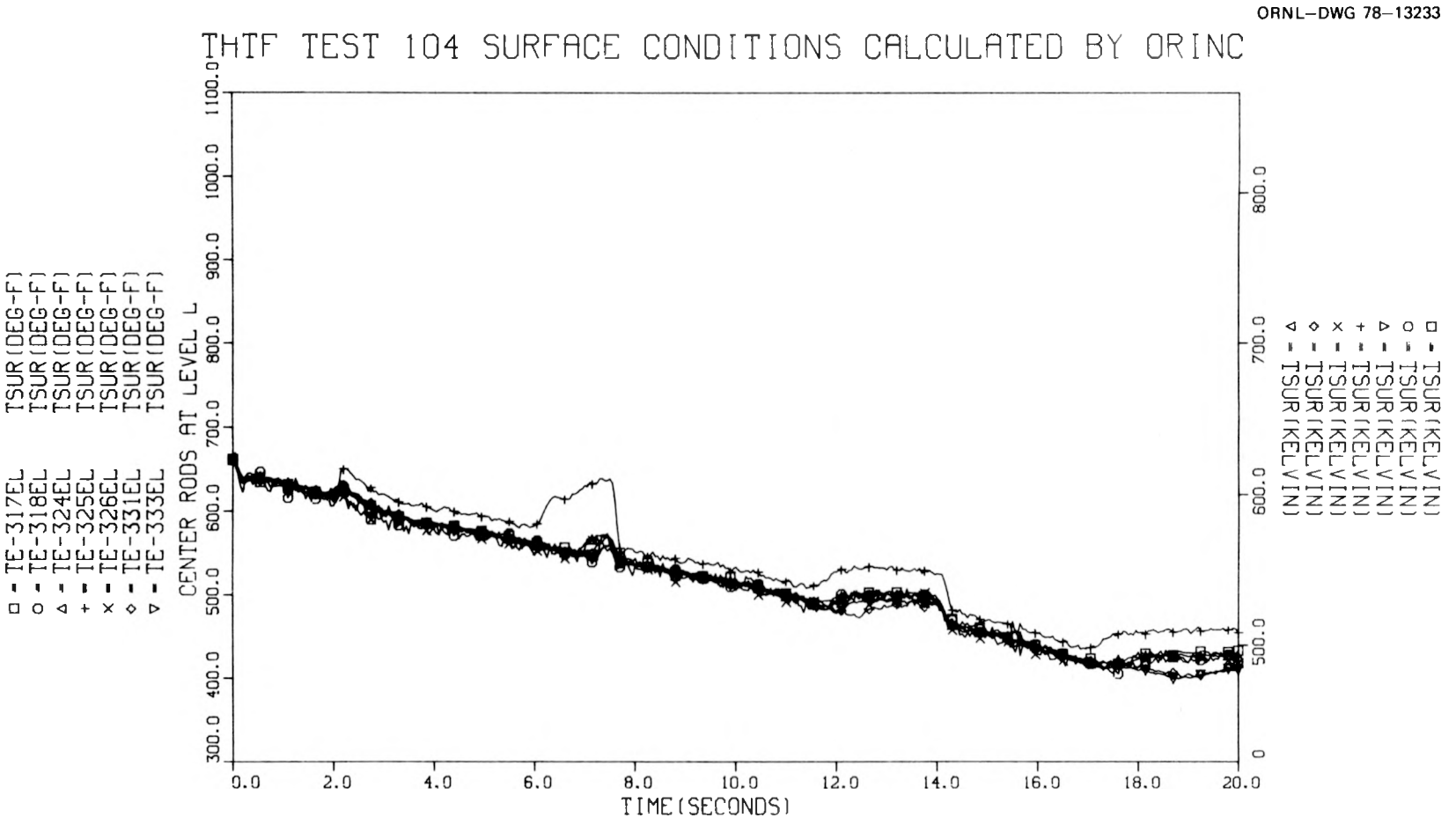

Fig. II.31. Test 104 center rod ORINC surface temperatures — level L.

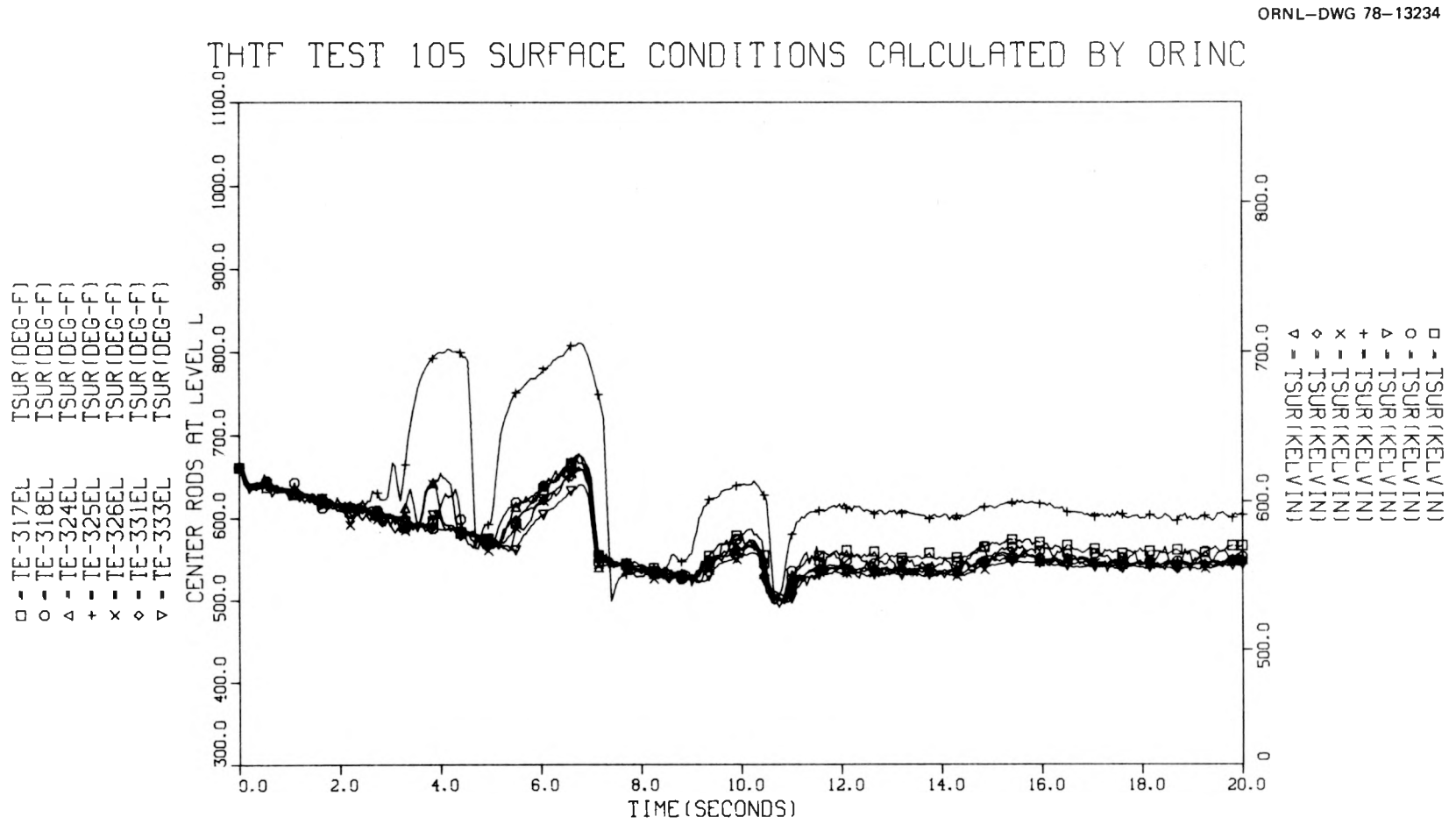

Fig. II.32. Test 105 center rod ORINC surface temperatures — level L.

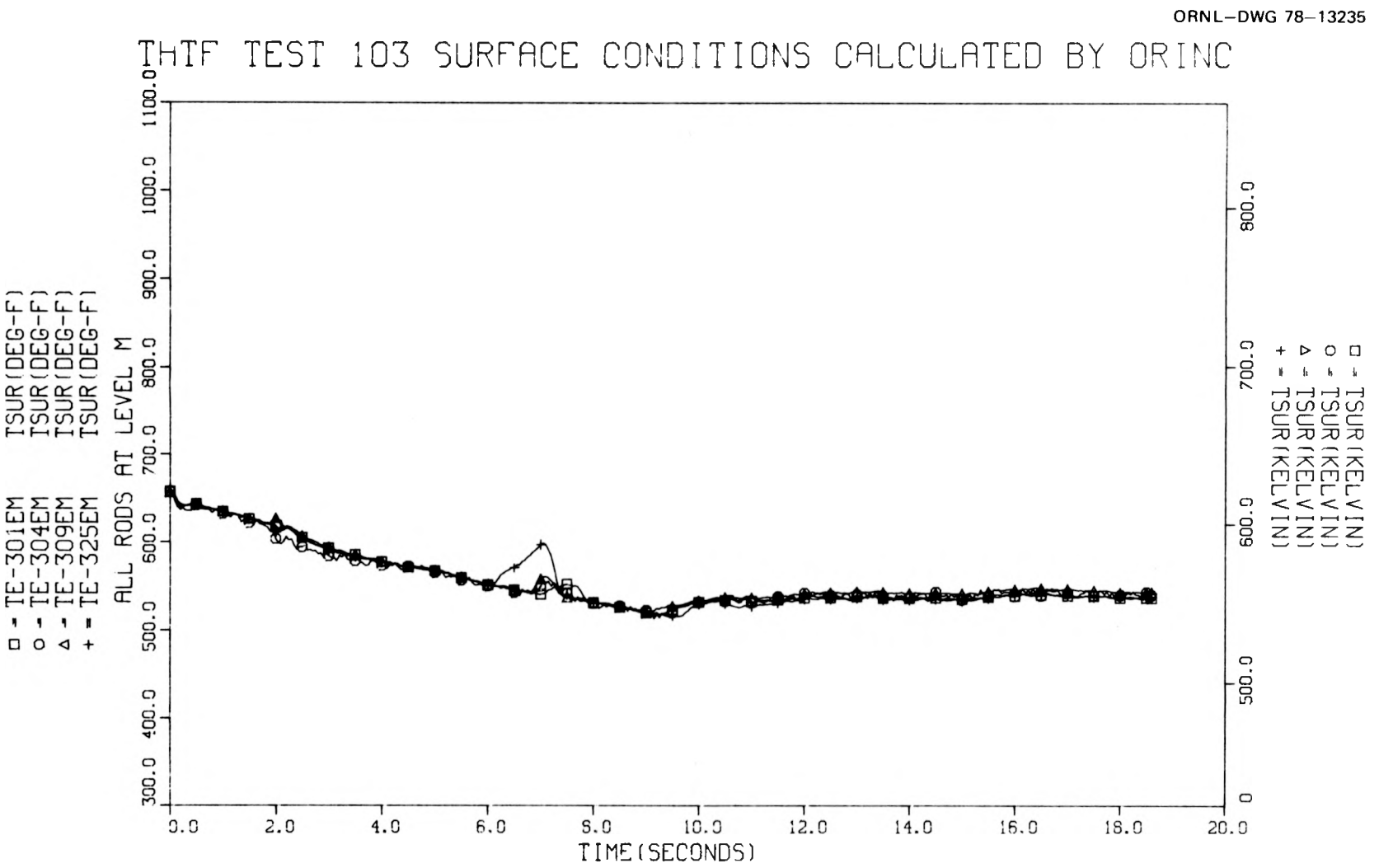

Fig. II.33. Test 103 rod ORINC surface temperatures — level M.

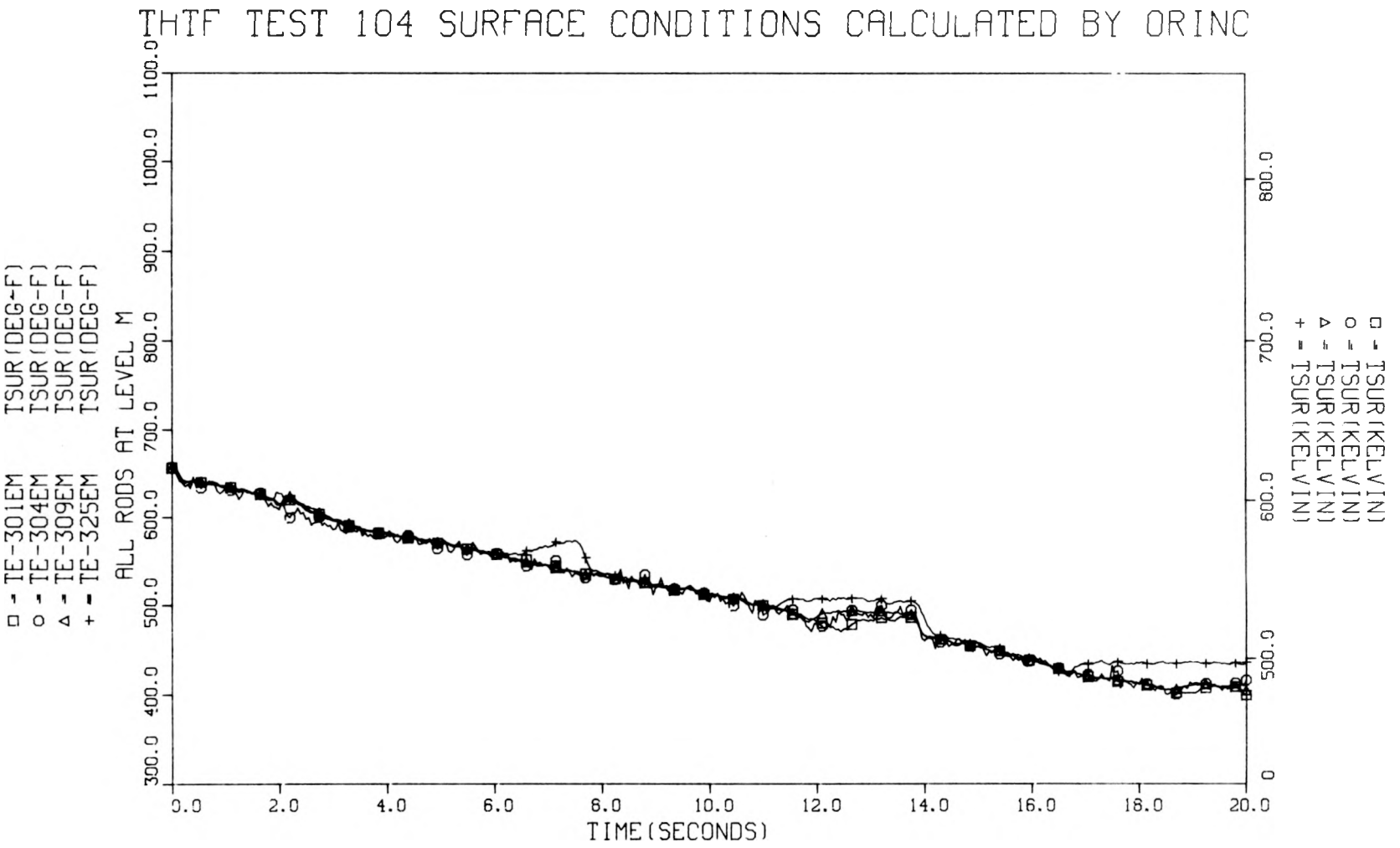

Fig. II.34. Test 104 rod ORINC surface temperatures — level M.

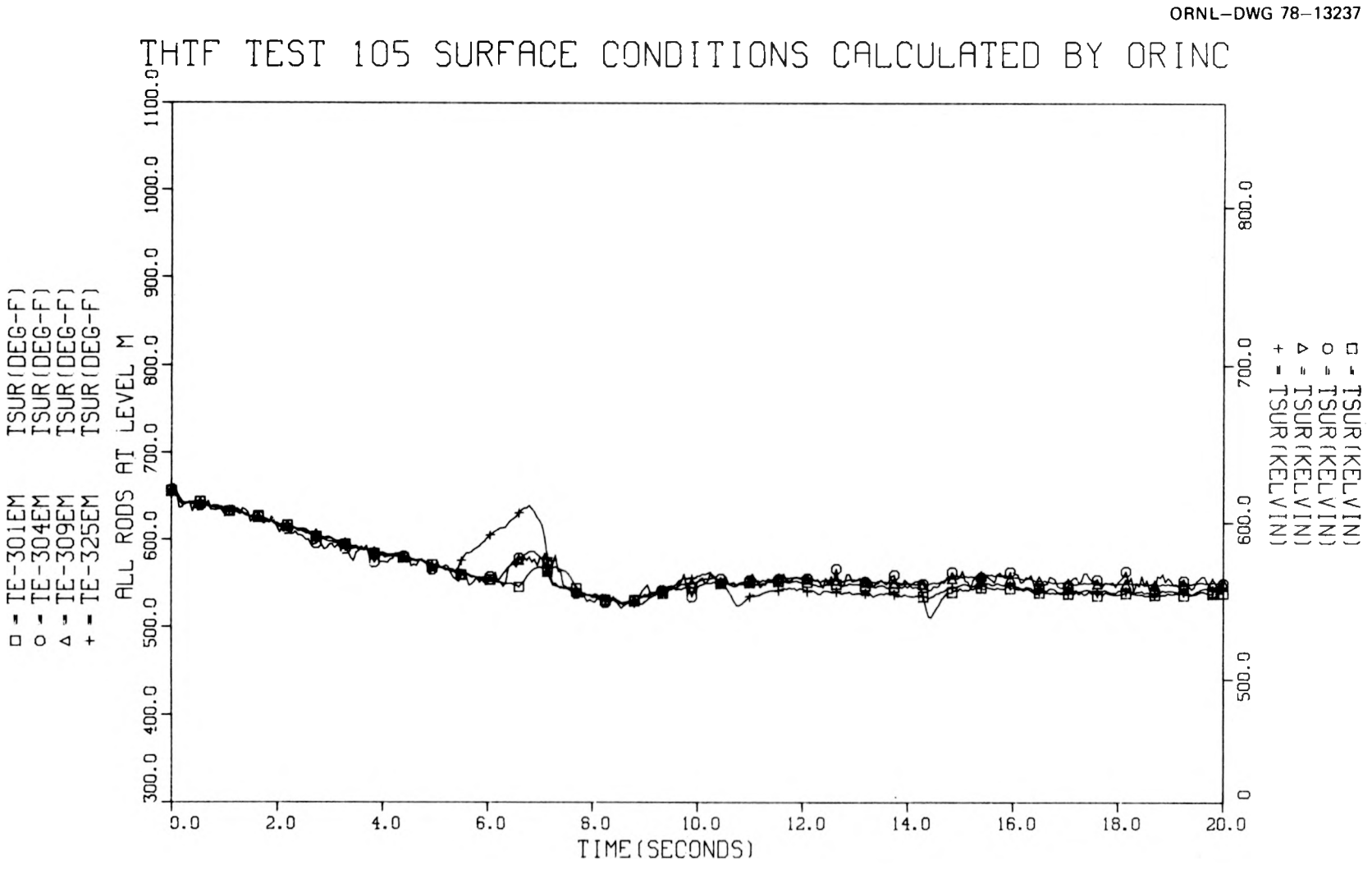

Fig. II.35. Test 105 rod ORINC surface temperatures — level M.

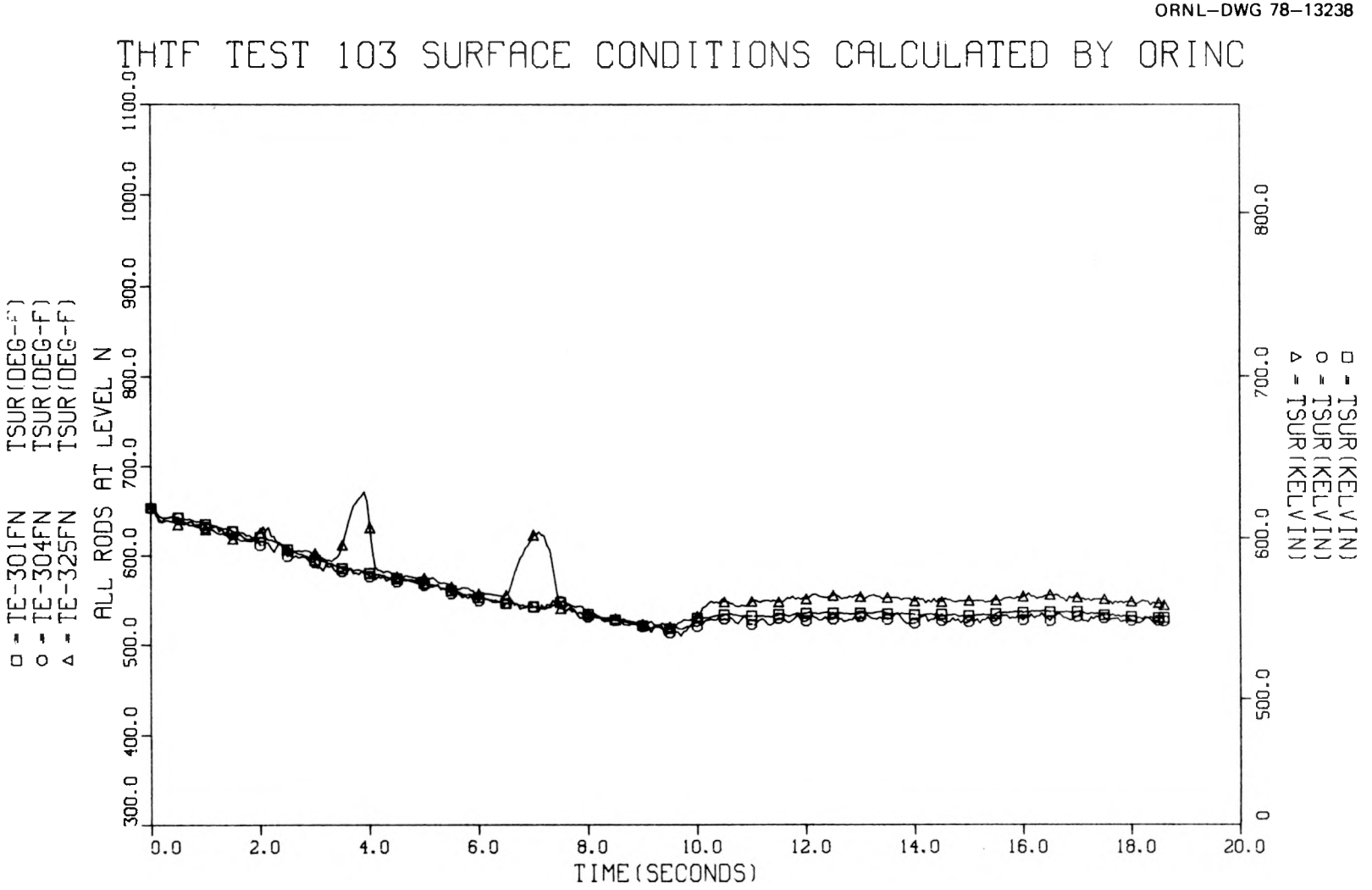

Fig. II.36. Test 103 rod ORINC surface temperatures — level N.

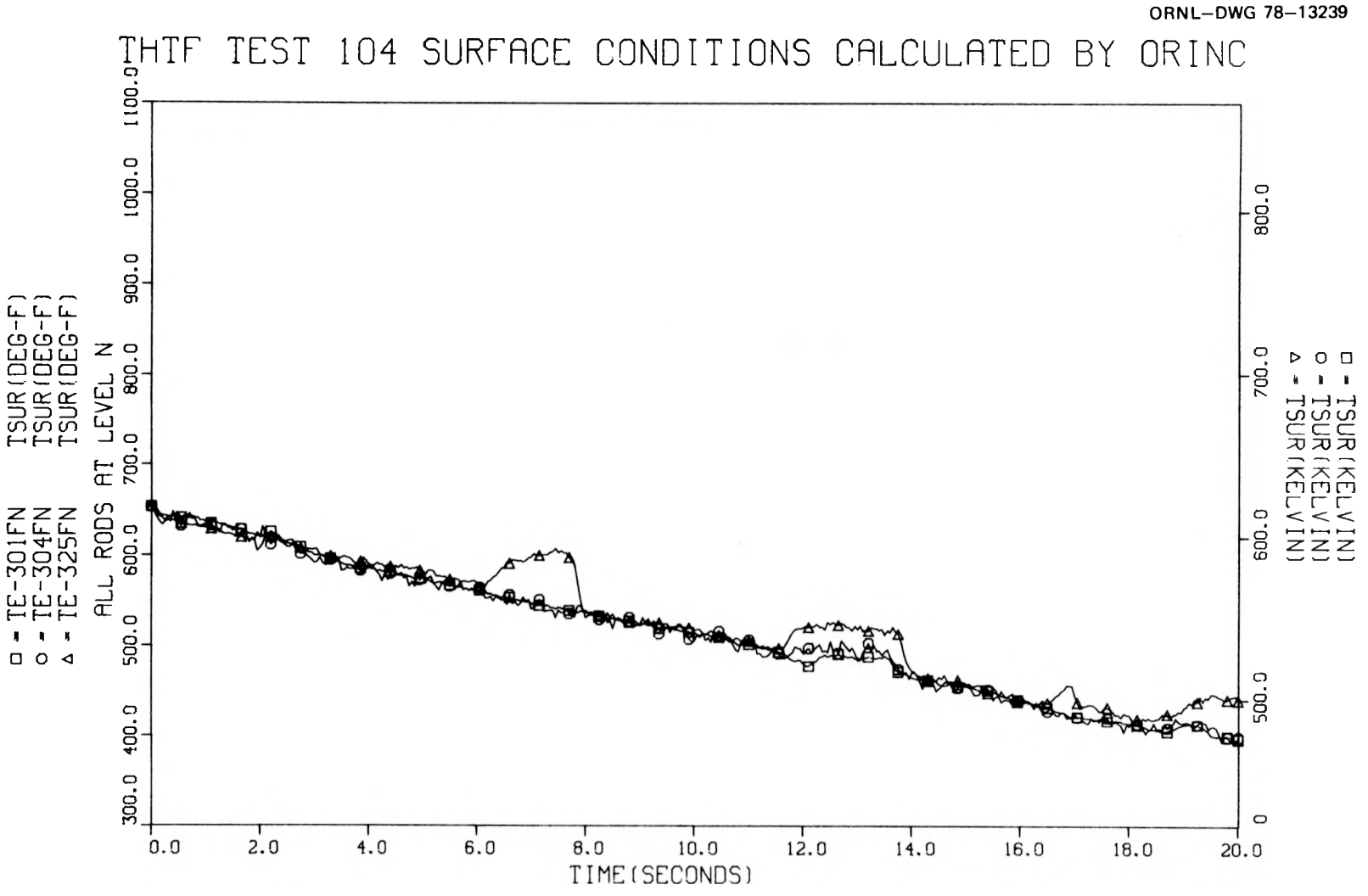

Fig. II.37. Test 104 rod ORINC surface temperatures — level N.

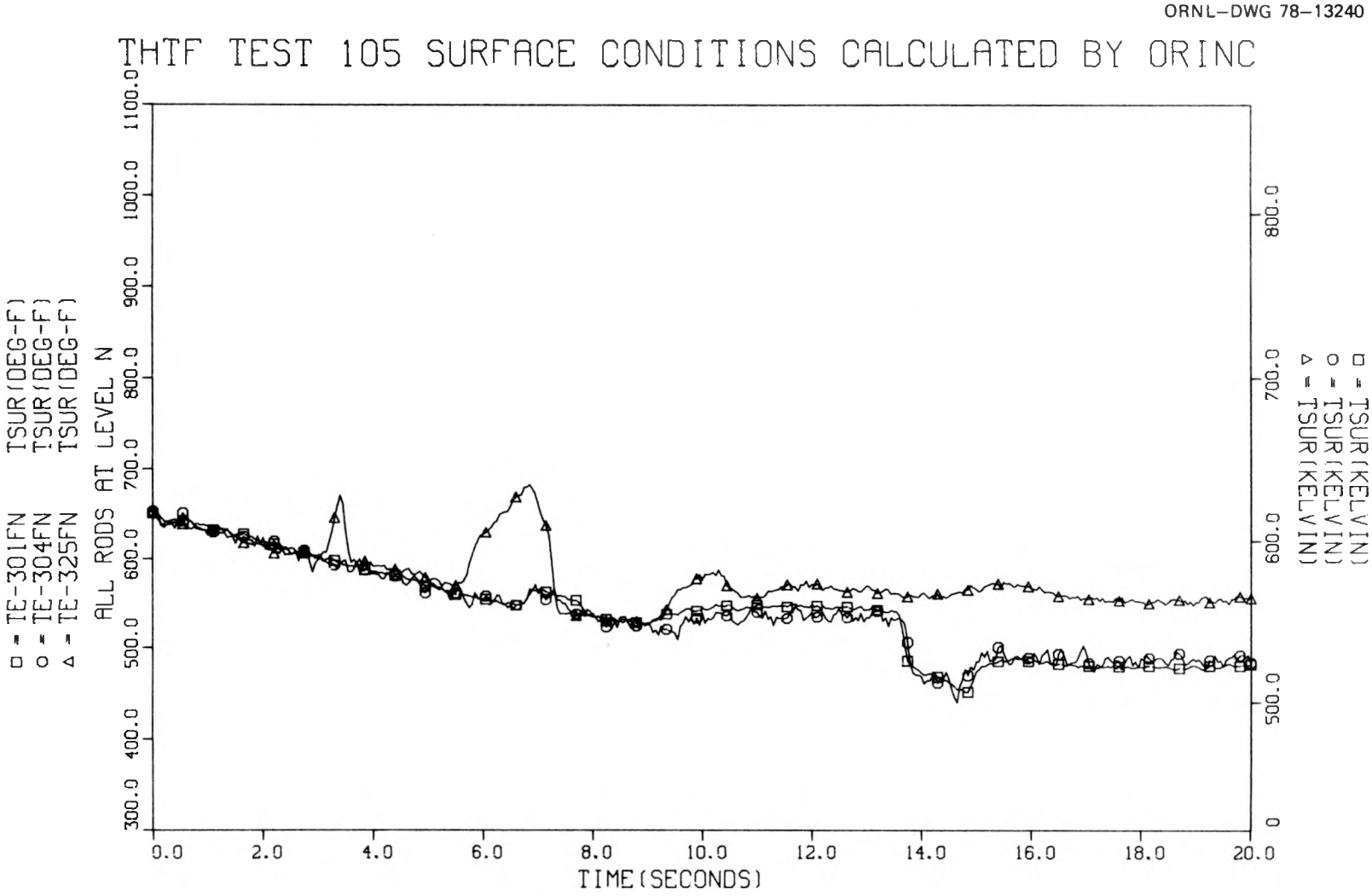

Fig. II.38. Test 105 rod ORINC surface temperatures — level N.

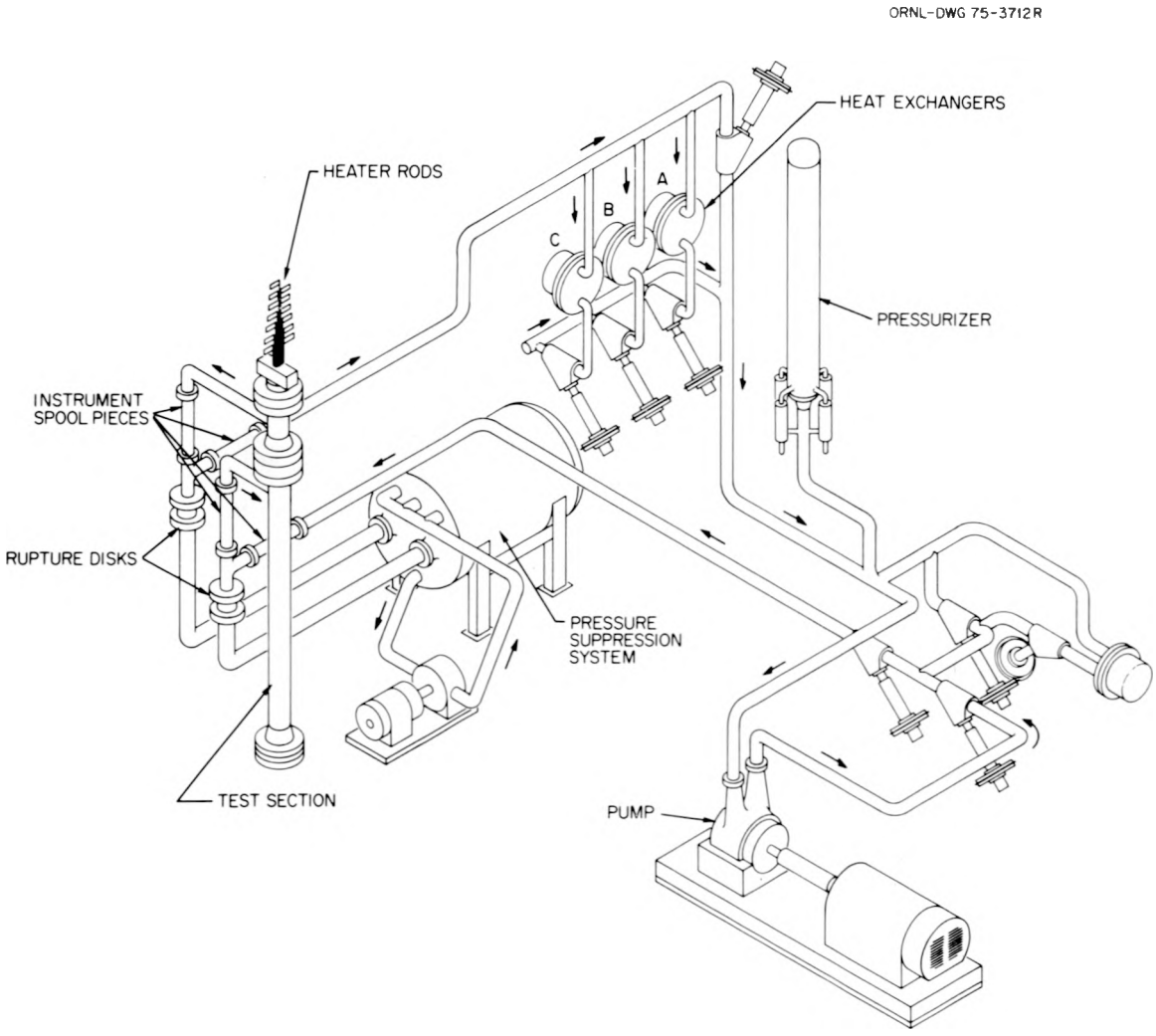

Fig. II.39. Thermal-Hydraulic Test Facility.

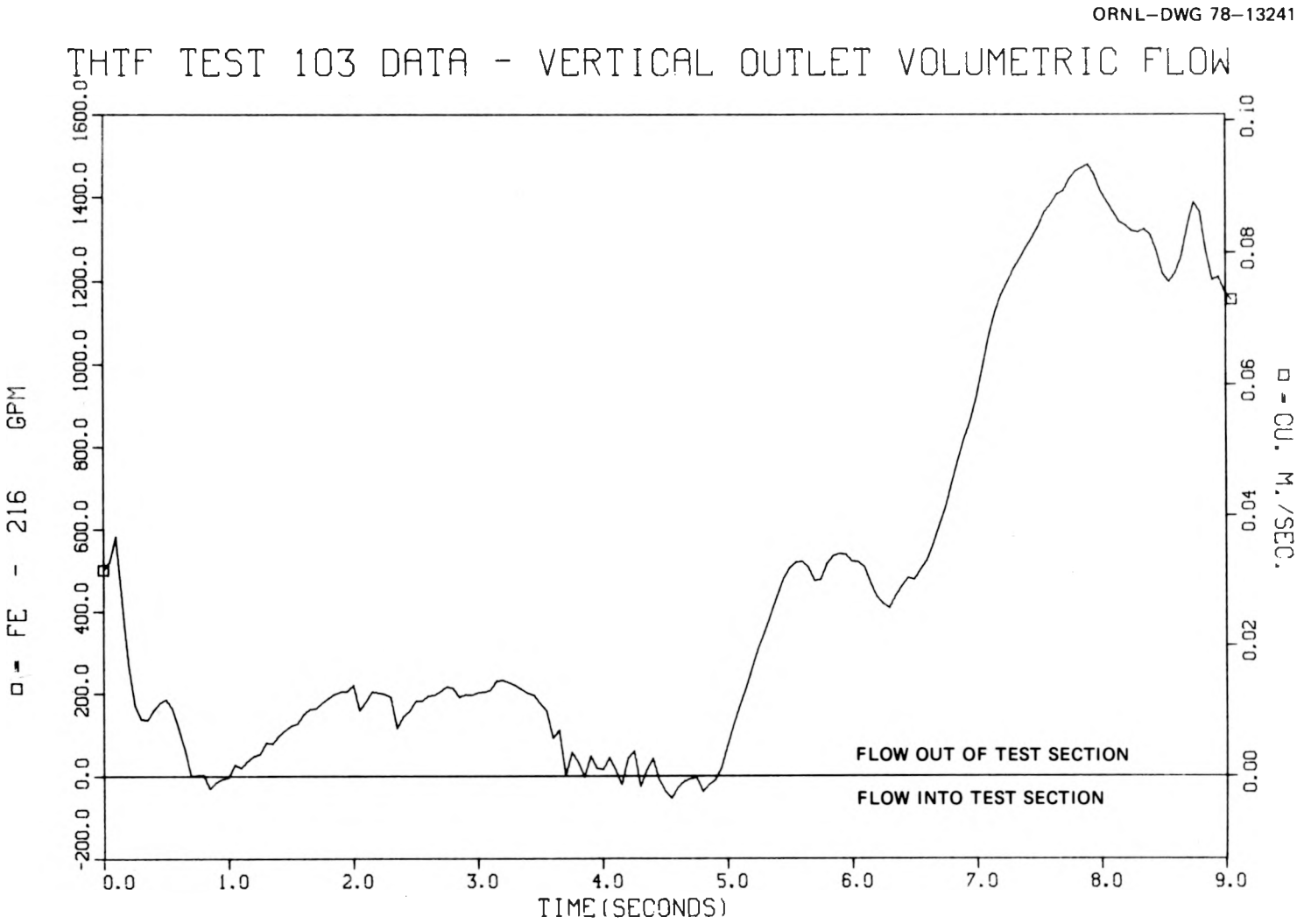

Fig. II.40. Test 103 vertical outlet volumetric flow.

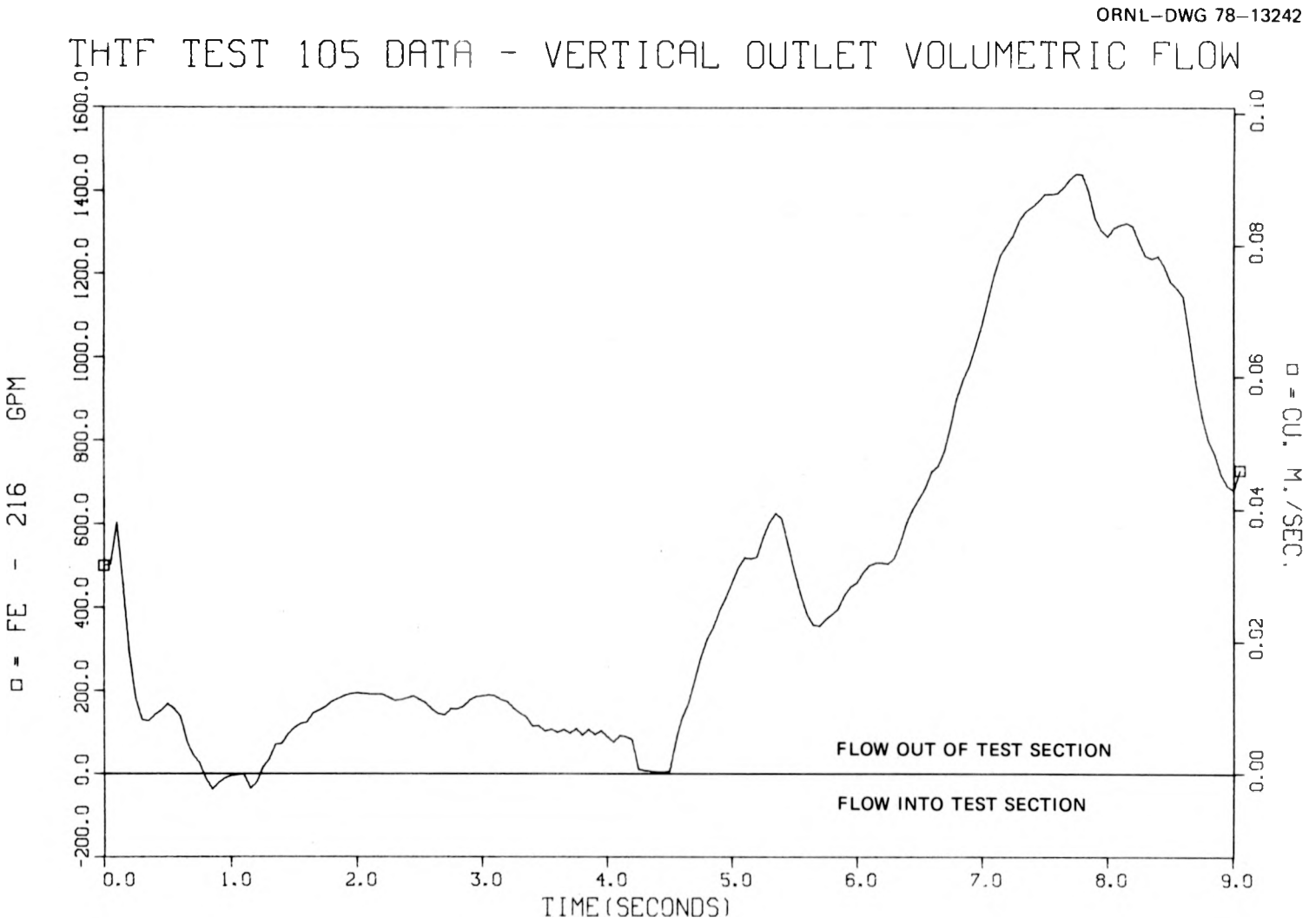

Fig. II.41. Test 105 vertical outlet volumetric flow.

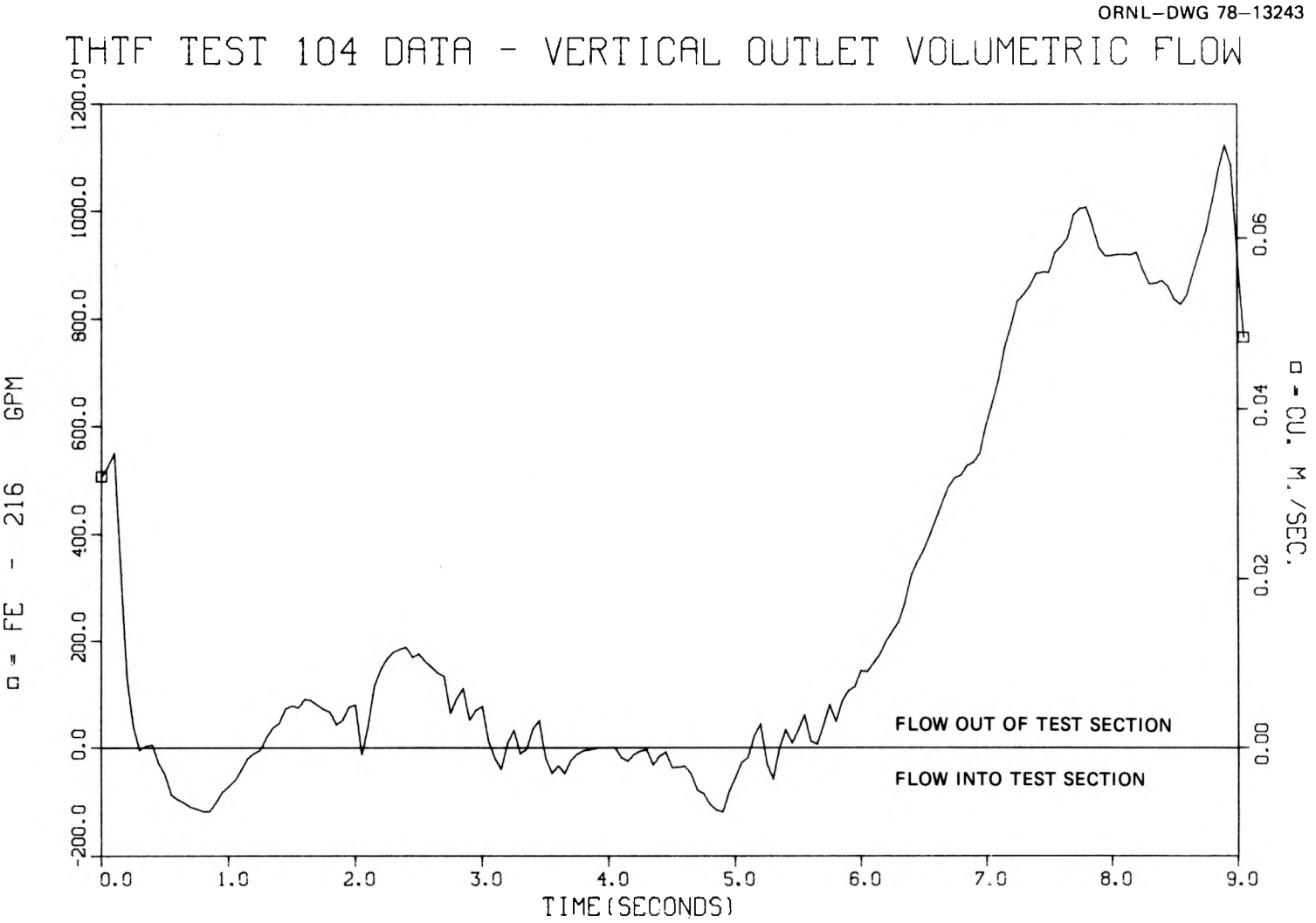

Fig. II.42. Test 104 vertical outlet volumetric flow.

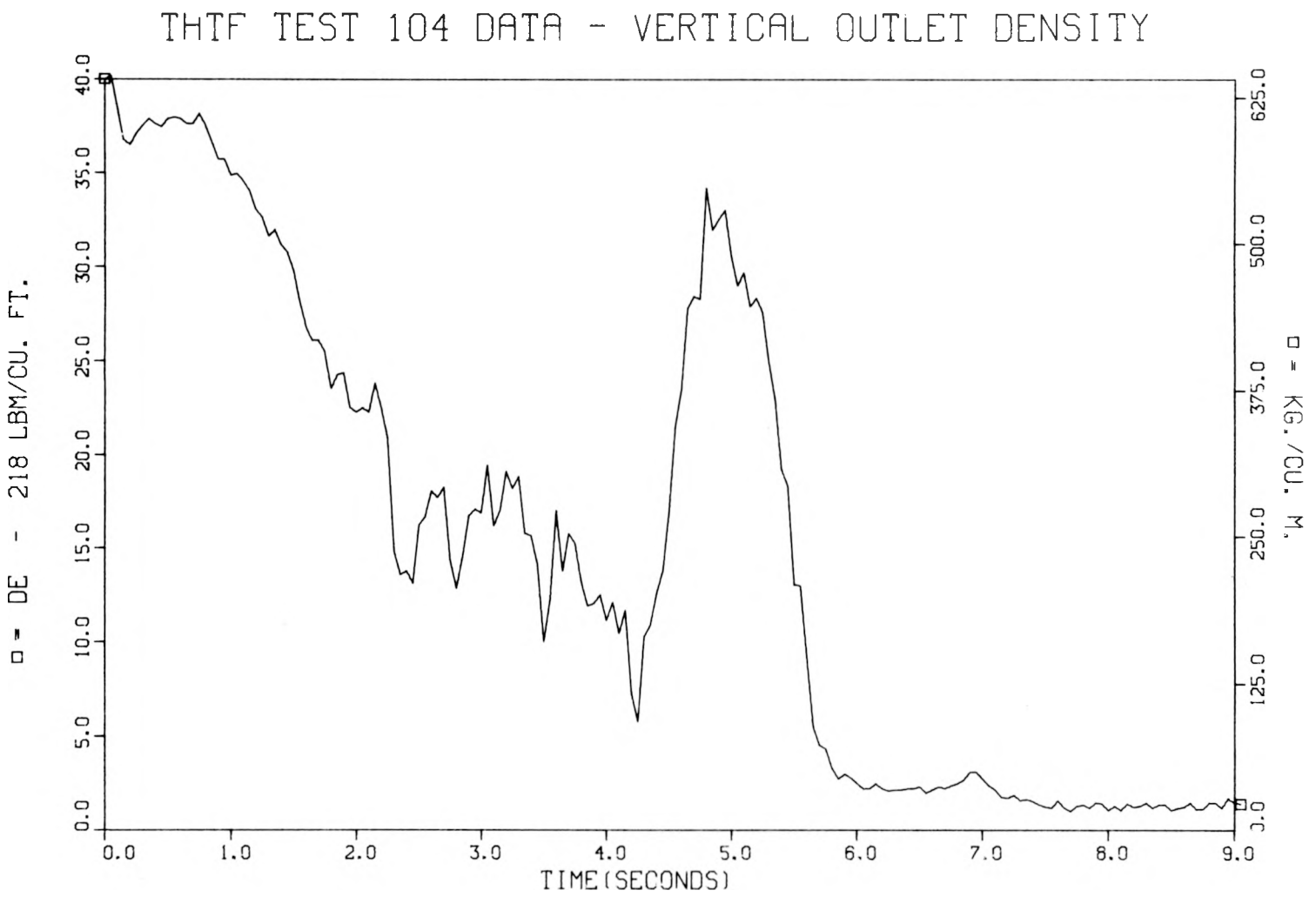

Fig. II.43. Test 104 vertical outlet density.

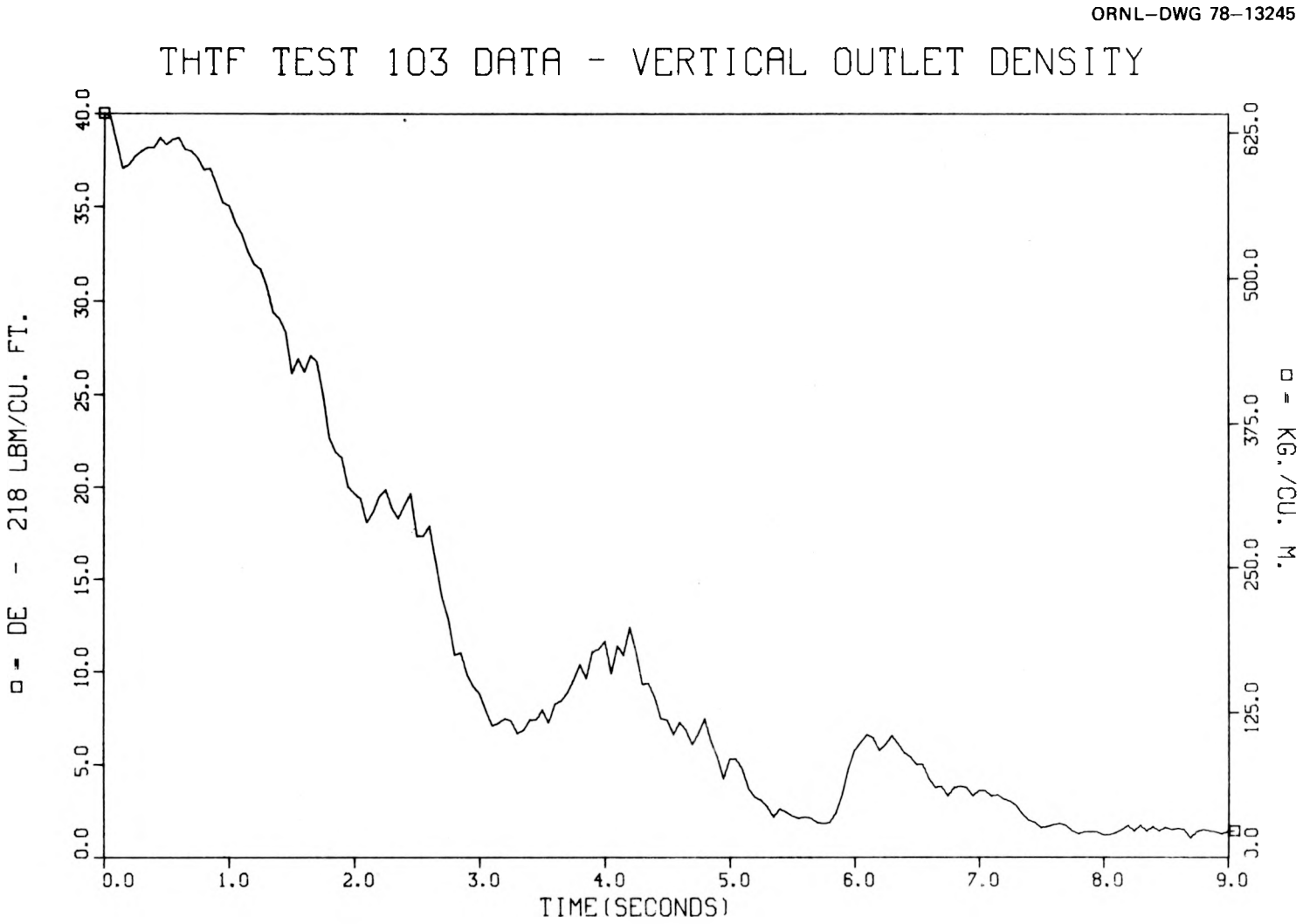

Fig. II.44. Test 103 vertical outlet density.

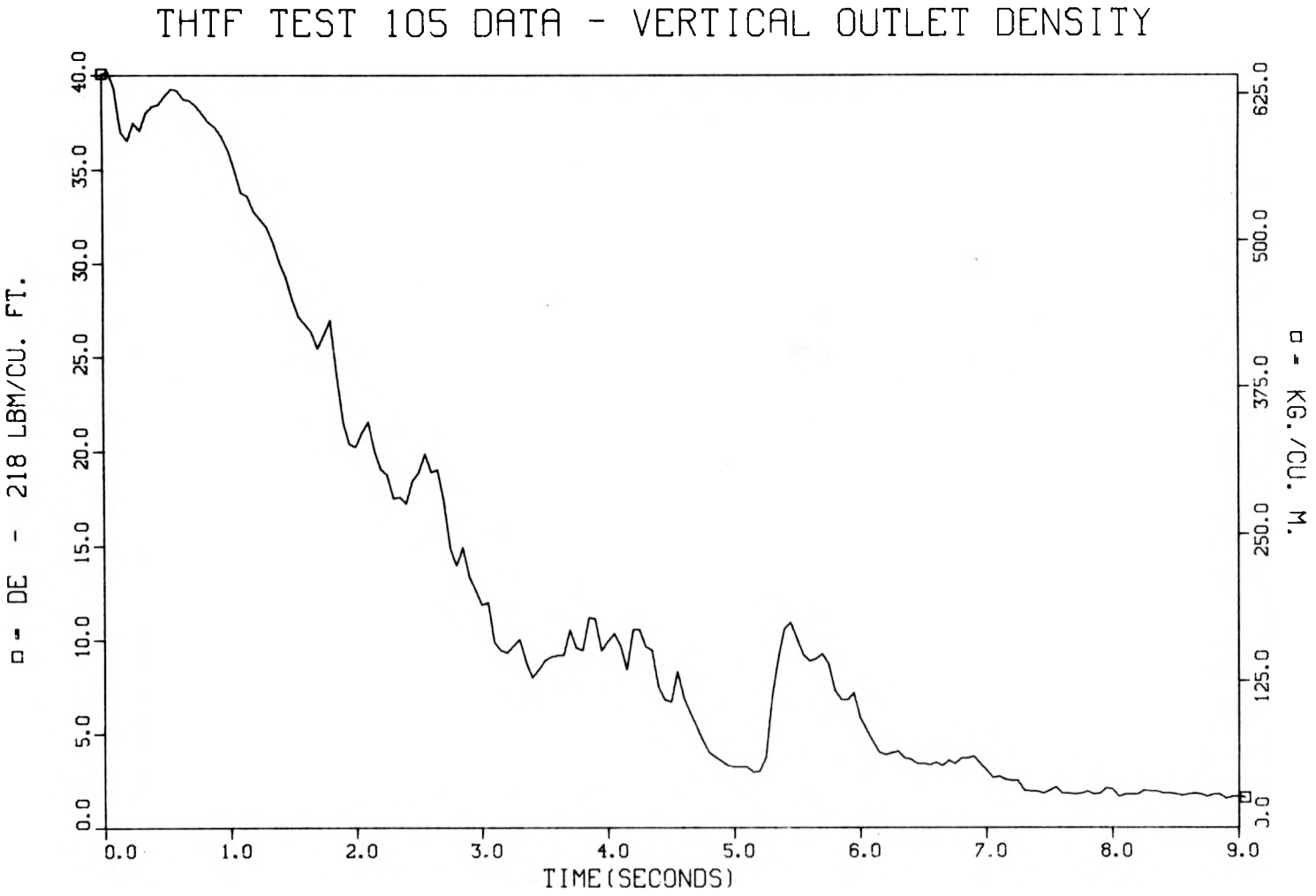

Fig. II.45. Test 105 vertical outlet density.

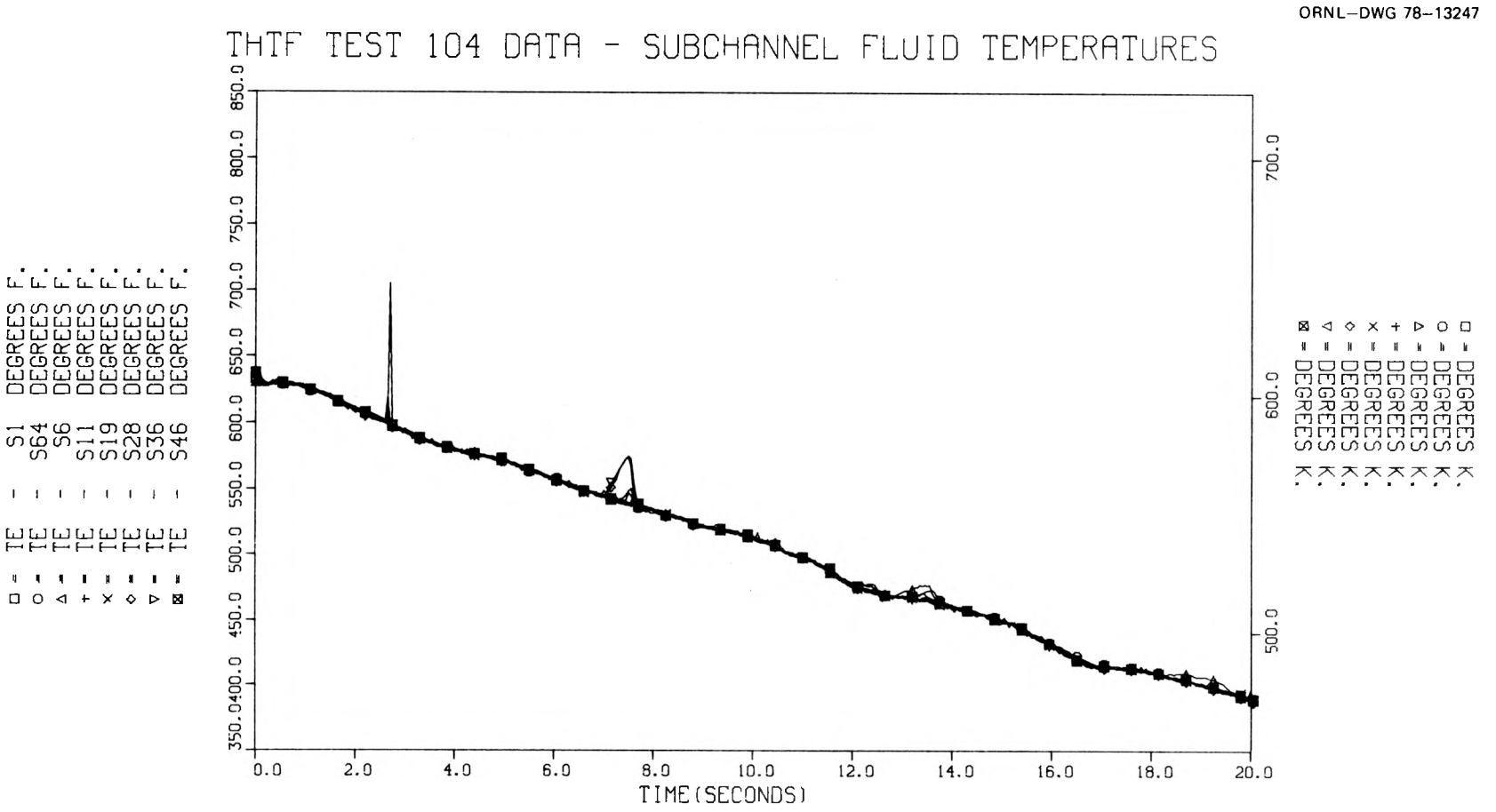

Fig. II.46. Test 104 subchannel thermocouple temperatures.

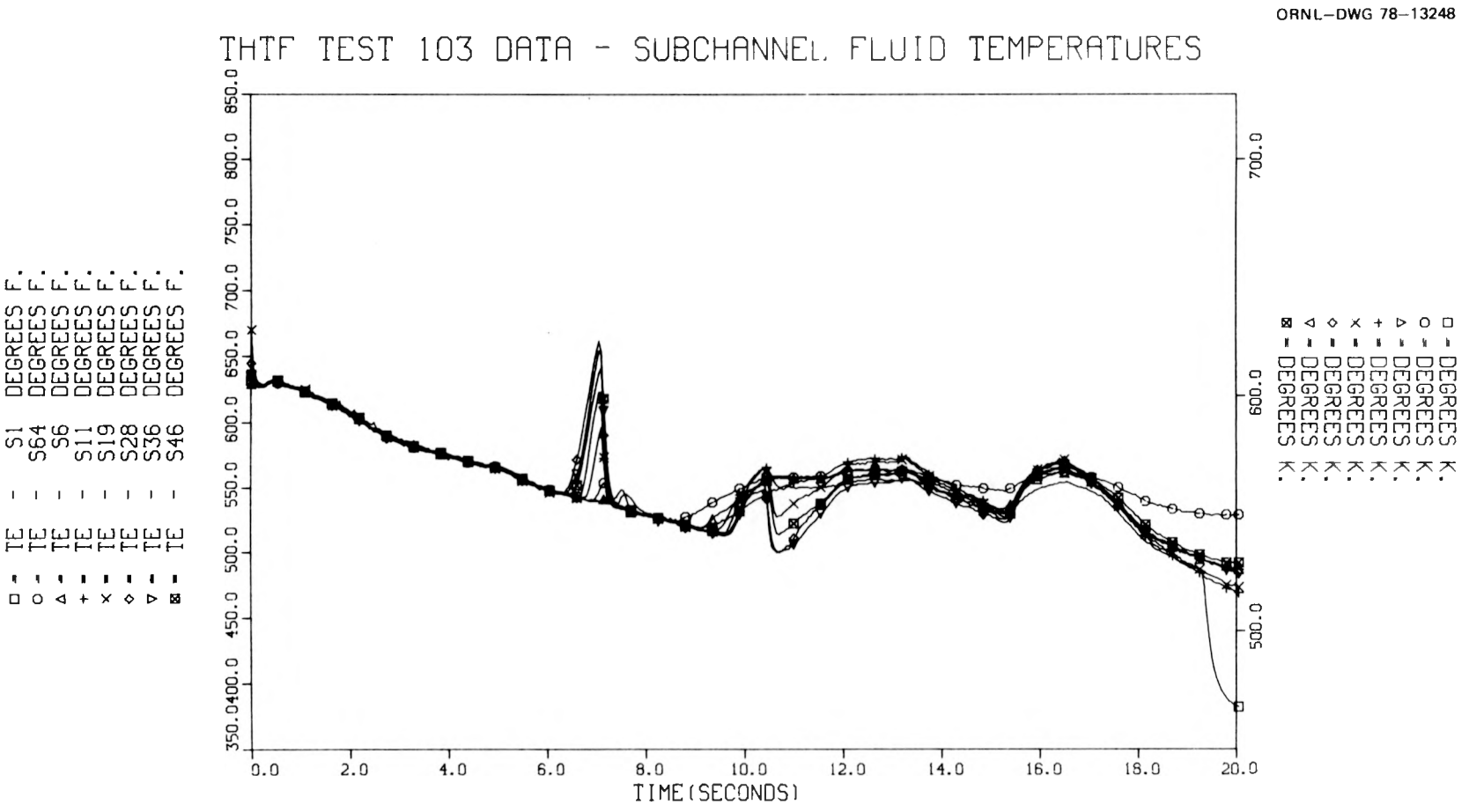

Fig. II.47. Test 103 subchannel thermocouple temperatures.

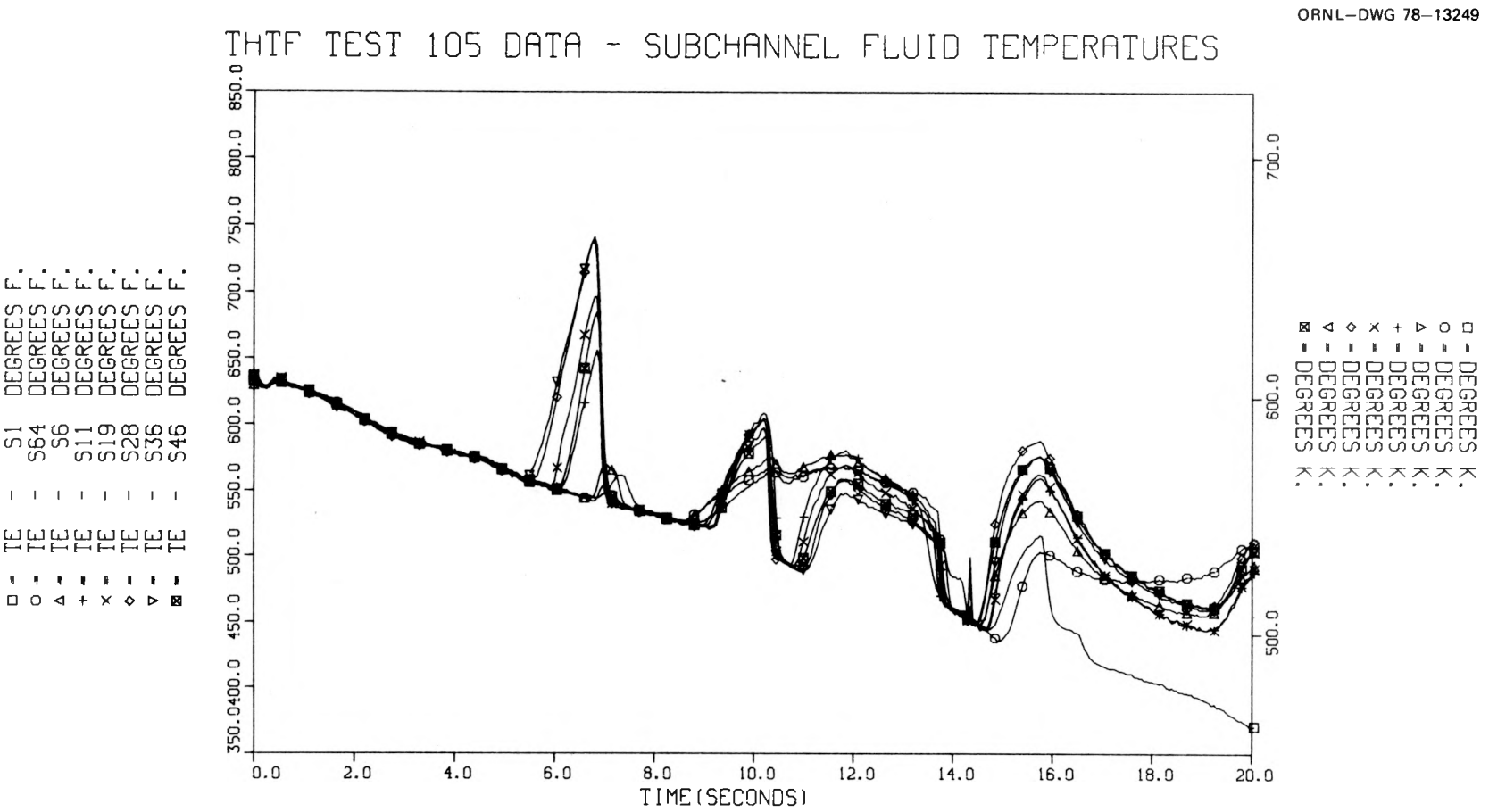

Fig. II.48. Test 105 subchannel thermocouple temperatures.

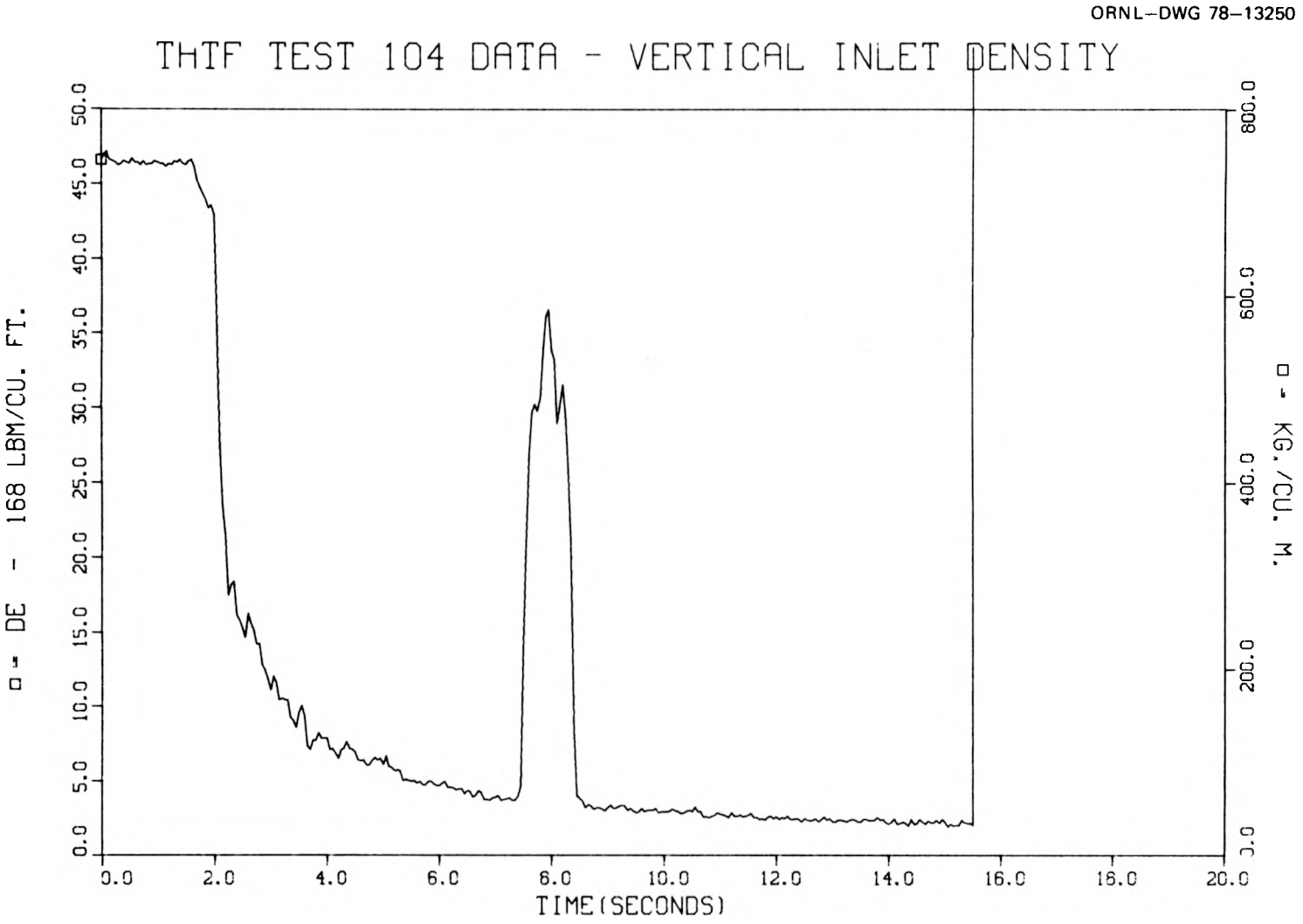

Fig. II.49. Test 104 vertical inlet density.

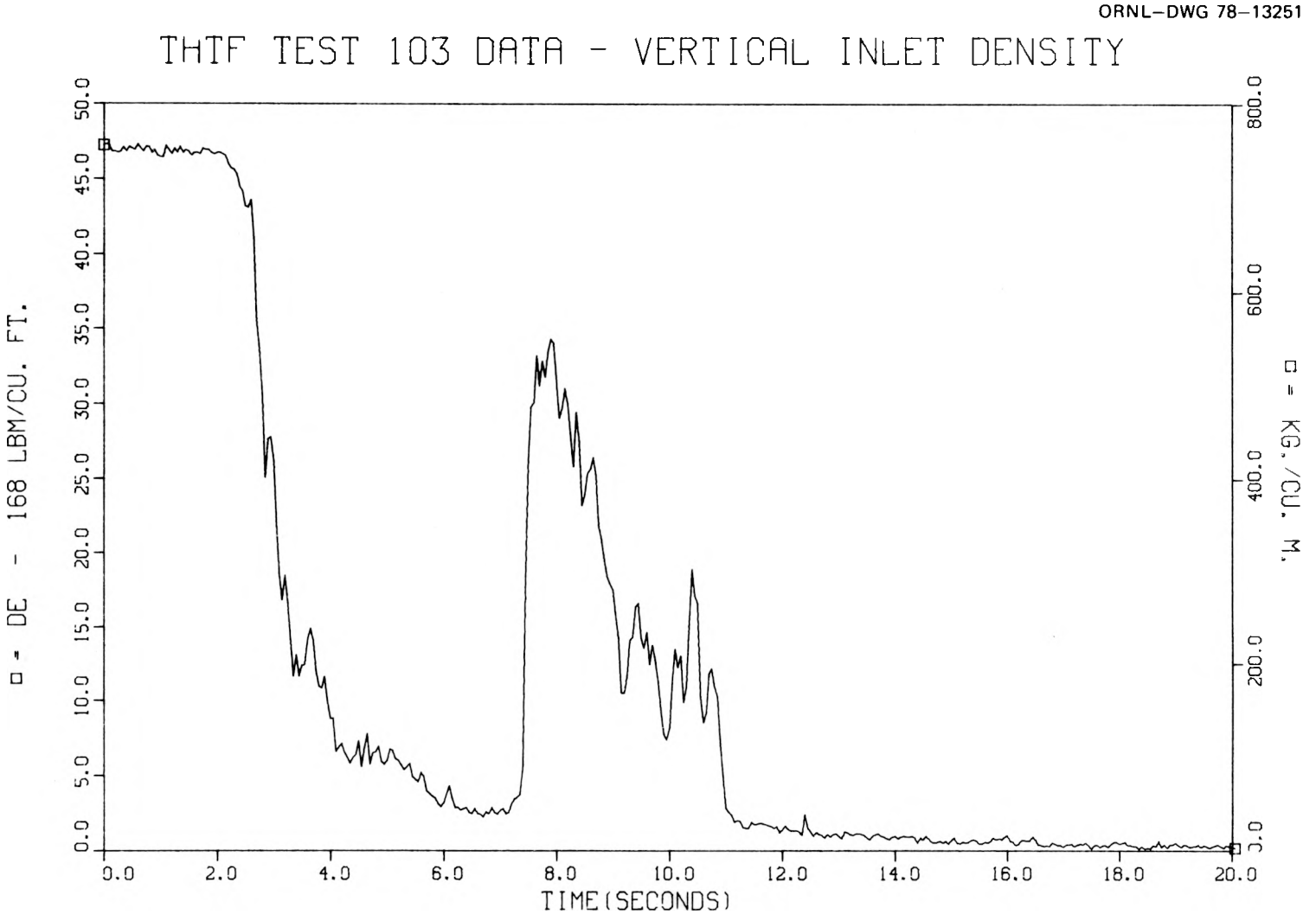

Fig. II.50. Test 103 vertical inlet density.

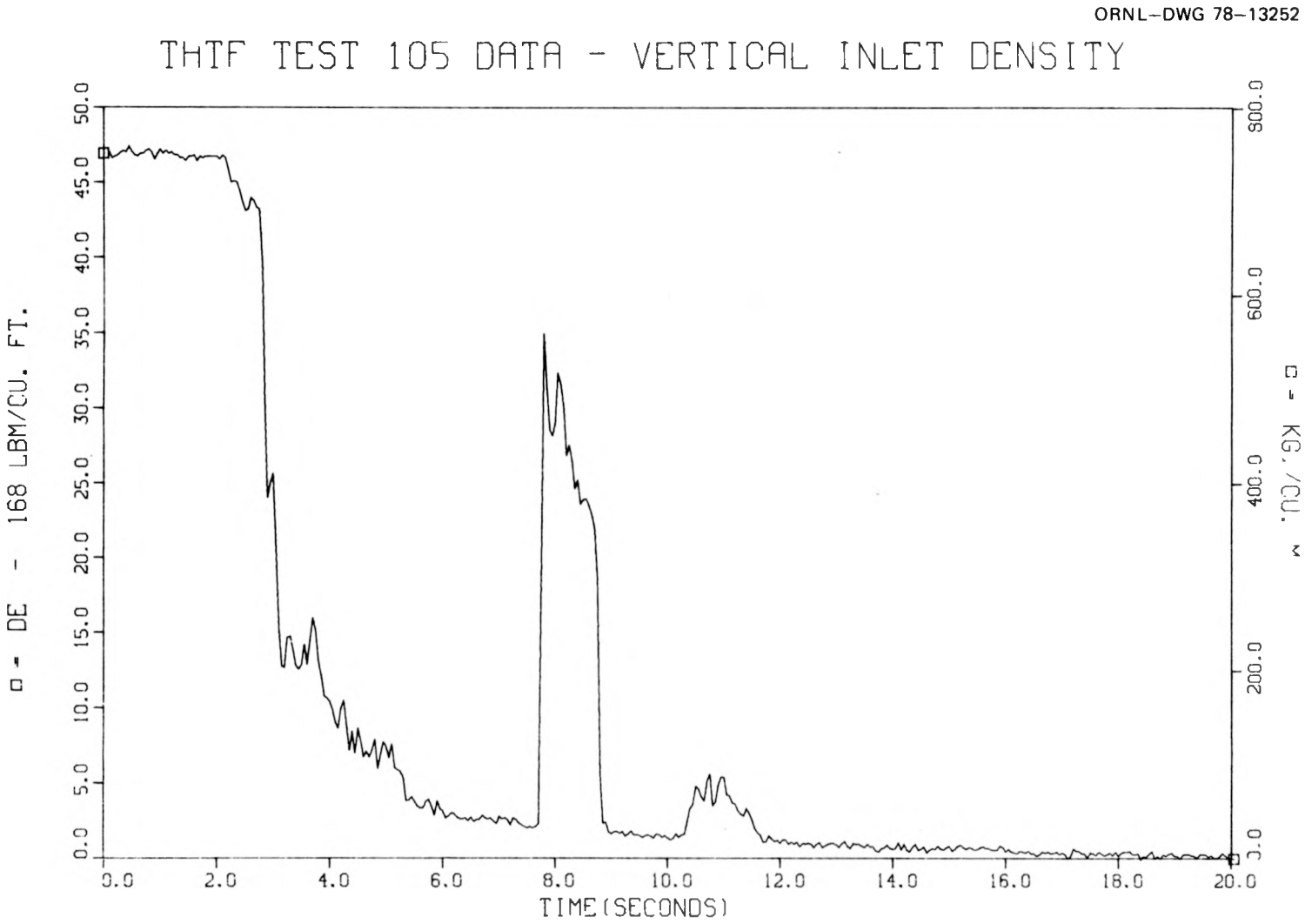

Fig. II.51. Test 105 vertical inlet density.

III. RELAP CODE VERIFICATION

III.1 Background

An analysis of existing light-water reactor transient thermal-hydraulic codes to determine which features are successful or unsuccessful in predicting experimental results can provide guidance in the development of codes for margin-of-safety calculations. Within the PWR-BDHT Program, the code RELAP4/M5U2 is undergoing analysis.[3] This section presents the results of this analysis to date and will concentrate on RELAP's heat transfer calculations and those parameters which most directly affect heat transfer.

RELAP's ability to predict the hydrodynamic response of the THTF for test series 100 was analyzed in a previous report.[2] One of the major conclusions of that report was that RELAP's assumption of homogeneous thermodynamic equilibrium in each control volume at each time step caused the code to predict low pressures and gradual density changes when, in reality, large and abrupt changes in density occurred. These factors then combine to cause markedly incorrect predictions for saturation times, fluid temperature increases, and flow reversals. Errors in the prediction of density changes and flow reversals are of particular significance when one considers the sensitivity of surface temperatures in the THTF to flow and density variations.

The configuration of RELAP used in reactor licensing, called the Evaluation Model, was not used because its restrictive assumptions are not appropriate for code verification utilizing the THTF. Rather, RELAP in its configuration with minimum controls was used in order to allow maximum freedom in obtaining the most accurate calculations possible.

In this section, two applications for the code are investigated. First, RELAP's ability as a pure predictor of THTF transients was studied. Second, RELAP was provided with experimental boundary conditions outside the test section and was used to "extrapolate" these conditions into the core. Since flow and density measurements are not available within the THTF core, some calculational procedure is required if correlations requiring these or related parameters are to be evaluated or developed.

For predicting THTF behavior, a system model was used to provide calculated boundary conditions to a more detailed test section model. For "extrapolation," experimental boundary conditions were supplied to the detailed test section model.

III.2 THTF System Model

The system model used for this report is a refinement of the models discussed in the data evaluation report for system response in test series 100.[2] When the strengths and weaknesses of a code are analyzed, every effort must be made to ensure that inaccuracies in the predictions reflect inaccuracies in the code itself and not poor modeling by the code user. Several improvements to the system model have been made, and although no significant difference in RELAP's predictions resulted, these changes add confidence that we are not attributing errors to RELAP which are the results of deficiencies in the model. A nodalization diagram of the system model used in this report is presented in Fig. III.1, and a system model listing is given in Appendix C. Since the heat transfer from system piping was found to have a significant effect on system pressure late in the transient, the test section is noded fairly simply to free as many heat slabs as possible while providing a heat slab for each volume.

Although flow in the secondary side of the main heat exchangers is stopped during the transient, flow in the secondary side of heat exchanger D (a small heat exchanger near the pump) is left on. Thus the main heat exchangers have modeled secondary sides, while heat exchanger D is modeled as a constant temperature heat sink. The new model includes a small line [approximately 0.8 cm (0.3 in.) in diameter] which leads from piping near the pump to the top of the upper plenum. In steady-state operation, the fluid in this line is cooled to 450 K (350°F) by a small heat exchanger that is inoperative during the transient. The fluid is then used to cool pressure seals around the rods in the upper plenum. After passing through a flow restricting plate, referred to as the baffle outlet zone orifice (BOZO), the cool fluid enters the upper plenum in a rectangular skirt (surrounding the upper parts of the rods) which has holes in the sides. The volume inside the skirt has been modeled as a separate volume at a

temperature below that of the upper plenum. The THTF shroud box extends beyond the heated length at both the top and bottom of the core. These unheated fluid volumes had previously been modeled as part of the lower and upper plenums but have now been included in the adjacent heated volumes. This change was made to more correctly model the hydraulic resistances and geometry for this fluid. In addition, revised estimates of hydraulic diameters and form loss coefficients have been included throughout the core and plenums. As mentioned previously, no significant differences resulted from these changes.

III.3 THTF Test Section Models

Three different test section models were studied to determine whether multiple-channel models of the THTF core would allow RELAP to predict radial surface temperature effects within the bundle or would improve its surface temperature predictions in general. Actual radial variation in surface temperature in the THTF is not large through most of the transient. Surface temperatures calculated by ORINC[5] for each radial region (Fig. II.4) for level G, test 103 (Figs. II.15 and III.2 to .4) show as much radial variation as has been seen in the test series. The RELAP models considered had three channels (Figs. III.5 and .6), two channels (Fig. III.7) and one channel (Fig. III.8), respectively, within the core. The two-channel model is basically the model developed at the Idaho National Engineering Laboratory (INEL) for the THTF.[10] The internal rod geometry, material properties, and some correlation choices were altered so that the three RELAP models would differ only in their channel geometries. All models had the same axial divisions in the noding of the heated length, and all were supplied with the same experimentally determined boundary conditions for these comparisons. Neither of the multiple-channel models had junctions laterally connecting the parallel core channels (i.e., no cross flow).

At each axial level, the rod surface temperature predictions of the one-channel model and of both wall and center nodes of the two-channel model were virtually identical. Further, rod surface temperatures predicted by the three-channel model for its wall and center nodes matched

those of the other models. The predictions of the three-channel model for its corner channel were several hundred degrees below those for the center and wall channels. Lateral connections between channels were then added to the three-channel model to determine whether the code's calculation of cross flow might ameliorate the radial effects predicted for the corner channel. Cross flow had little or no effect. Therefore, we conclude that the two-channel model provides no improvement over the one-channel model and that the three-channel model grossly exaggerates radial effects in the corners. Since the one-channel model uses fewer heat slabs per level, considerably more axial detail could be included in the model within RELAP's limit of 50 slabs. Therefore, a more detailed single-channel model was created (Fig. III.9) and is used as the test section model in the rest of this report. C. B. Davis of INEL, while making RELAP calculations of THTF behavior,[10] found that some unrealistic flow surges predicted by RELAP resulted from flashing of downcomer volumes and that this effect could be minimized by fine downcomer nodalization. The current single-channel test section model, therefore, has detailed axial divisions in the downcomer as well as in the core.

III.4 Experimental Boundary Conditions

As mentioned previously, RELAP is being used to "extrapolate" experimental conditions into the core, thus providing estimates of local flow and quality. RELAP calculations can be bounded by specifying mass flux and enthalpy at a junction (fill table) or by specifying time-dependent fluid conditions in a volume (TDV). The instruments in the THTF provide various means of calculating either of these boundary conditions for the vertical spool pieces. The use of calculated mass fluxes as fill tables simultaneously at both the inlet and outlet of the test section model resulted in RELAP calculations of pressure considerably below the measured pressure. This discrepancy may be due to our current inability to correctly calculate mass flows and may not reflect calculational error by RELAP. A TDV in RELAP can act as an infinite flow source or sink, the calculated flow being dictated by the specified pressure in the TDV. Use of a TDV in RELAP calculations of the THTF causes RELAP's calculated

pressures throughout the test section to be reasonably close to the measured pressures. However, RELAP calculations made with a TDV specified at both inlet and outlet did not produce calculated volumetric or mass flows close to the experimental flows. Since the steady-state pressure difference across the core is approximately 0.207 MN/m^2 (30 psid) and the absolute pressure measurements have a standard deviation of 0.185 MN/m^2 (26.8 psig), this is not surprising. Calculating a value for the pressure at one end of the test section from an absolute pressure measurement at the other end and a pressure difference measurement produced no better results from RELAP, probably because of the "ringing" in the pressure difference instruments.

The best combination of flows and pressures was calculated by RELAP when the test section model was bounded by a fill table at one end and a TDV at the other. RELAP's calculated flows at the spool piece used as the TDV were still not good enough to suggest that accurate "extrapolation" of the experimental conditions was being achieved. Whether RELAP could provide accurate extrapolation if it were provided with more accurate mass flows or an accurate transient measurement of the core pressure difference remains unknown. Improvement in the boundary conditions will probably require work in the following areas: (1) improvement of current spool piece instruments; (2) addition of measuring stations in closer proximity to the phenomena of interest; (3) new measurement concepts; and (4) new data reduction and utilization techniques.

Although RELAP's calculations of flows and other fluid quantities using the test section model bounded by a TDV and a fill table are poor, they are still the best we can presently obtain. They are an improvement over fluid conditions predicted by RELAP when the test section model is bounded by RELAP's predictions using the system model. Therefore, in an analysis of RELAP's heat transfer procedures, a study of their response to the more correct fluid conditions produced by experimental bounding is useful. In the remainder of this report, experimentally or hydraulically bounded RELAP calculations will refer to the test section model bounded by a fill table and a TDV. Specifically, the vertical inlet spool piece (volume 1, Fig. III.9) was used as the TDV, and one end of the vertical outlet spool piece (junction 36, Fig. III.9) was bounded

by a fill table. Note that this test section model requires a boundary condition at the BOZO (junction 37, Fig. III.9) as well as at the inlet and outlet. No data were recorded for conditions in the line leading to the BOZO for these tests, but sensitivity studies were made to determine the effect of variations in the BOZO boundary condition on RELAP predictions. Variation of flow over extremely wide ranges had virtually no effect on RELAP calculations of core conditions. A RELAP system model was used to calculate a best-estimate flow for the BOZO, and this data is supplied as a boundary condition fill table to all the hydraulically bounded RELAP test section model calculations in this report.

III.5 Analysis of RELAP4 Heat Transfer Calculations

Rod surface temperatures predicted by RELAP using the test section model bounded by the system model predictions represent the response of RELAP's heat transfer logic and correlations to its predicted fluid conditions. The results produced by RELAP's heat transfer routines in response to the somewhat better fluid conditions provided by the test section model bounded by experimental conditions are of equal interest. The following discussion will analyze both cases for test 105, RELAP's calculations for that test being representative of those for the other tests.

First, consider RELAP's predictions for the test section model bounded by the system model. An estimate of the extent of error in the core fluid conditions can be gained from a comparison of the fluid conditions predicted for the inlet and outlet spool pieces and the experimental data (Figs. III.10 to .15; see key to symbols in Table II.5). In particular, note that the predicted volumetric flows in the first 3 sec oscillate about the measured data and the size of the oscillations is often larger than the magnitude of the observed flow (Figs. III.12 and .14). RELAP's predicted rod surface temperatures are relatively good in the lower core (Figs. III.16 to .20) but are considerably high in the upper core (Figs. III.21 to .24).

In estimating the probable extent of error in the core fluid conditions for the experimentally bounded RELAP calculations, volumetric

flow at the inlet (bounded by TDV) and pressure and density at the outlet (bounded by a fill table) are the relevant quantities (Figs. III.25 to .27). A comparison of the relative error in calculated fluid temperatures at the subchannel fluid thermocouples in the upper core (of Figs. III.15 and .28) indicates an improvement in fluid conditions calculated by the experimentally bounded RELAP. However, note that the calculated volumetric flow in the first 3 sec still has oscillations of a magnitude comparable to the absolute magnitude of the experimental data. This suggests that the calculated core fluid conditions, particularly flow, may still be in substantial error. The calculated rod surface temperatures from the experimentally bound RELAP model are similar to the "pure" RELAP predictions; the calculated temperatures in the lower core are "good" (Figs. III.29 to .33), while those in the upper core are "bad" (Figs. III.34 to .37).

The question that naturally arises from the preceding comparisons is "What causes predictions in the upper core to be poor, while those in the lower core are relatively good?" To answer this question, RELAP's heat transfer correlations and logic must be presented. For the purposes of this discussion, we will assume that RELAP solves the rod heat conduction equation correctly if it can obtain the correct surface boundary condition. Thus the subject of our analysis will be RELAP's correlations for surface heat flux, heat transfer coefficient, and critical heat flux and the logic which determines its choice of correlations. Table III.1, which is taken from the RELAP4/M5 Users' Manual,[3] lists the correlations (modes) RELAP may use to provide the surface boundary condition to the conduction equation. Figure III.38, a more detailed version of a similar figure in the RELAP4/M5 Users' Manual, depicts the logic by which RELAP chooses the heat transfer mode. This logic is used to make a mode selection for every heat slab surface at every time step.

A value for the critical heat flux (q_{CHF}) is needed for comparison with fluxes calculated for some modes. The correlations used in RELAP for q_{CHF} are listed in detail in Appendix B. Unless the user specifies otherwise, RELAP uses a Babcock & Wilcox correlation, B&W-2, for pressures above 10.34 MN/m^2 (1500 psia), the Barnett correlation from 8.96 to 6.89 MN/m^2 (1300–1000 psia), and a modified Barnett correlation below

Table III.1. List of heat transfer correlations and associated symbol definitions used in RELAP4/MOD5[a,b]

Mode 1 Subcooled Liquid Forced Convection: Dittus and Boelter[19]

$$h = 0.023 \frac{k}{D_e} Pr^{0.4} Re^{0.8}$$

Mode 2 Nucleate Boiling: Thom[18]

$$q = \left[\frac{\Delta T_{sat} \exp (P/1260)}{0.072}\right]^2$$

Mode 3 Forced Convection Vaporization: Schrock and Grossman[20]

$$h = (2.5)\ (0.023) \frac{k_f}{D_e} Pr_f^{0.4} [Re_f\ (1 - X)]^{0.8}$$

$$\times \left[\left(\frac{X}{1 - X}\right)^{0.9} \left(\frac{\mu_g}{\mu_f}\right)^{0.1} \left(\frac{\rho_f}{\rho_g}\right)^{0.5}\right]^{0.75}$$

Mode 4 Transition Boiling: McDonough, Milich, and King[21]

$$q = q_{CHF} - C(P)\ (T_w - T_{w,CHF})$$

Pressure, psi	C(P)
2000	979.2
1200	1180.8
800	1501.2

Mode 5 Stable Film Boiling: Groeneveld[22]

$$h = a \frac{k_g}{D_e} Pr_w^c \left\{Re_g \left[X + \frac{\rho_g}{\rho_f} (1 - X)\right]\right\}^b$$

$$\times \left[1.0 - 0.1\ (1 - X)^{0.4} \left(\frac{\rho_f}{\rho_g} - 1\right)^{0.4}\right]^d$$

Table III.1 (continued)

	Groeneveld Equation (5.9)	Groeneveld Equation (5.7)
	IMCL (or IMCR) = 0	IMCL (or IMCR) = 1
a.	0.00327	0.052
b.	0.901	0.688
c.	1.32	1.26
d.	−1.50	−1.06

Mode 6 Low-Flow Film Boiling: Modified Bromley

$$h = 0.62 \left[\frac{k_g^3 \, h_{fg} \, \rho_g \, g(\rho_f - \rho_g)}{\mu_g \, L \, \Delta T_{sat}} \right]^{0.25}$$

$$L = 2\pi \sqrt{\frac{g_c \sigma}{g(\rho_f - \rho_g)}}$$

Mode 7 Free Convection plus Radiation

$$h = h_c + h_r$$

$$h_c = 0.4 \, (Gr \, Pr_f)^{0.2}$$

$$Gr = \frac{L_g^3 \, \beta_g \, \rho_g^2 \, \Delta T_{sat}}{\mu_g^2}$$

$$L = \frac{D_e}{2}$$

$$h_r = 0.23 \, \frac{1.714(10^{-9}) \, (T_w^4 - T_{sat}^4)}{\Delta T_{sat}}$$

Mode 8 Superheated Vapor Forced Convection: Dittus and Boelter[19]

$$h = 0.023 \, \frac{k}{D_e} \, Pr^{0.4} \, Re^{0.8}$$

Table III.1 (continued)

Mode 9 Low-Pressure Flow Film Boiling: Dougall and Rohsenow[23]

$$h = 0.023 \frac{k_g}{D_e} Pr_g^{0.4} \left\{ Re_g \left[X + \frac{\rho_g}{\rho_f} (1 - X) \right] \right\}^{0.8}$$

Definition of Symbols

C_p = specific heat, Btu/lb_m-°F
D_e = equivalent diameter, ft
g = local acceleration due to gravity, ft/sec^2
g_c = gravitational constant, ft-lb_m/lb_f-sec^2
h = heat transfer coefficient, Btu/ft^2-hr-°F
k = thermal conductivity, Btu/ft-hr-°F
L = channel length, in.
P = pressure, psia
Pr = Prandtl number, $C_p\mu/k$
q = heat flux, Btu/ft^2-hr
Re = Reynolds number, GD_e/μ
T_{sat} = saturation temperature, °F
T_w = wall temperature, °F
$\Delta T_{sat} = T_w - T_{sat}$, °F
X = quality
β = coefficient of thermal expansion, 1/°F
ρ = density, lb_m/ft^3
μ = viscosity, lb_m/ft-hr
σ = surface tension, lb_f/ft

Subscripts:

f = saturated liquid conditions
g = saturated vapor conditions
v = superheated vapor conditions
w = wall

[a]Source: *RELAP4/MOD5: A Computer Program for Transient Thermal-Hydraulic Analysis of Nuclear Reactors and Related Systems Users' Manual*, ANCR/NUREG/1335, Vol. 1 (September 1976).

[b]Superscript numbers in brackets refer to references in Vol. 1 of the RELAP4/MOD5 Users' Manual.

5.00 MN/m^2 (725 psia). RELAP interpolates on pressure between 10.34 and 8.96 MN/m^2 (1500–1300 psia) and between 6.89 and 5.00 MN/m^2 (1000–725 psia). The following analysis will be confined to the early transient, during which RELAP predicts DNB for all rods, and therefore will require only B&W-2. RELAP will never use a value for q_{CHF} below 283.72 kW/m^2 (90,000 Btu/ft^2-hr) regardless of the correlation's predicted value. If the predicted mass flux falls below 271.10 kg/m^2-s (200,000 lb_m/ft^2-hr), RELAP interpolates on mass flux between an assumed q_{CHF} of 283.72 kW/m^2 (90,000 Btu/ft^2-hr) for zero flow and the value produced by the correlation using 271.10 kg/m^2-s (200,000 lb_m/ft^2-hr). The B&W-2 correlation is a function of pressure, quality, and mass flux (Figs. III.39 and .40), and its behavior will play a key role in the following discussion.

A detailed analysis of two heat slabs that represent heater rods in the test section model (Fig. III.9) will be presented. The chosen slabs are slab 3 in the lower core, which encompasses thermocouple level D, and slab 9 in the upper core, which encompasses thermocouple levels K and L. Although RELAP's calculations are different for every slab, calculations for slab 3 are very similar to those for all lower core slabs, and slab 9 is representative of the upper core slabs. Each slab will be analyzed for two test section model calculations, one bounded by the system model predictions and one by experimental data. The two calculations for each slab are so similar that they will be discussed simultaneously, beginning with slab 3.

Slab 3 is judged by RELAP to be in mode 1 (Dittus-Boelter for subcooled forced convection) at steady state. Upon initiation of the transient, flow in the adjacent volume is calculated to reverse (Figs. III.41 and .42), crossing zero at approximately 0.1 sec, and pressure begins to fall (Figs. III.43 and .44). When the pressure has dropped enough to lower the fluid saturation temperature to the wall surface temperature, RELAP begins to compare mode 1, Dittus-Boelter, and mode 2, Thom's nucleate boiling (Fig. III.38), and will choose the mode producing the larger heat flux. The decreasing flow reduces the flux predicted by mode 1 below that predicted by mode 2, and mode 2 is selected in both calculations (Figs. III.45 and .46). As flow approaches zero, the calculated value for q_{CHF} will drop sharply (Figs. III.47 and .48) as RELAP

interpolates between the minimum value of 283.72 kW/m^2 and that produced by B&W-2. The flow is near zero only briefly for the hydraulically bounded calculation (Fig. III.41); so the calculated q_{CHF} does not drop below that predicted by mode 2 at 0.1 sec (Fig. III.47). As flow increases, the flux predicted by mode 1 increases, and it is selected over mode 2 (Fig. III.45).

In the calculation bounded by the system model, the flow remains near zero somewhat longer (Fig. III.42), causing the calculated q_{CHF} to drop below the flux predicted by mode 2 and thus causing RELAP to select transition boiling, mode 4 (Fig. III.48 and .46). Increasing flow then drives q_{CHF} back up, and the calculation returns to a pre-CHF mode, mode 2. By 0.2 sec, flow in both calculations is negative and of such magnitude that mode 2 is chosen rather than mode 1. Both calculations remain in mode 2 through 0.55 sec. However, between 0.4 and 0.6 sec, q_{CHF} falls dramatically (Figs. III.47 and .48) because of increasing quality (Fig. III.40), causing RELAP to switch to mode 4 at 0.6 sec. While decreasing flows between 0.15 sec and 0.35 sec in the experimentally bound calculation cause a decrease in q_{CHF} during that period, the dominant effect in both cases is the increasing quality.

In mode 4 the heat transfer coefficient is much lower than the pre-CHF coefficients, causing the beginning of the surface temperature excursion (Figs. III.47 and .48). As surface temperature increases, the flux predicted by mode 4 will decrease (Table III.1) and rapidly fall below that predicted by the film boiling correlation. RELAP compares the fluxes predicted by the transition and film boiling correlations and chooses the larger (Fig. III.38). Thus RELAP switches from mode 4 to the user's selected film boiling correlation (in this case, mode 9) at 0.7 sec. The increasing surface temperatures and the low value of q_{CHF} keep the flux predicted by mode 4 low enough that RELAP continues to select mode 9 until very high quality causes a switch to forced convection to steam, mode 8, at approximately 2 sec. The key factor in RELAP's calculation of DNB for slab 3 is the sharp drop in q_{CHF} produced by the increase in quality. In the experiment, initial negative flow through the core causes increasing quality in the lower core, which, in turn, produces the observed temperature excursion.

We now consider slab 9 in the upper core, where RELAP also predicts an early DNB but where no significant temperature excursion is seen in the experiment. Slab 9 begins the transient in mode 2 and remains there for 0.4 sec. Flow in the adjacent volume (Fig. III.49) in the system model bounded calculation decreases but does not reach zero during this period. Flow in the experimentally bounded calculation (Fig. III.50) crosses zero twice in the first 0.4 sec, but in neither instance does it remain near zero long enough to decrease the calculated q_{CHF} substantially (Fig. III.52). Note, however, that in both calculations increasing quality (Figs. III.53 and .54) is producing a steady decrease in q_{CHF} (Figs. III.51 and .52). At 0.45 sec in the experimentally bounded case and at 0.5 sec in the system model bounded case, flow drops to very near zero (Figs. III.49 and .50), and the resulting interpolation produces a q_{CHF} close to the minimum of 283.72 kW/m^2. Since the flux predicted by mode 2 now exceeds q_{CHF}, RELAP selects mode 4. Although the DNB was initiated by the flow decrease, the increasing quality would probably have produced a switch to mode 4 within a few tenths of a second even if flow had remained high. The switch to mode 4 yields a much lower heat transfer coefficient and thus initiates the temperature excursion (Figs. III.51 and .52).

The mode selection after the initial switch to mode 4 is characterized by frequent switching between modes 4 and 9 with an occasional choice of mode 7. All these modes have relatively low heat transfer coefficients, and the temperature excursion continues. In general, the switching between modes 4 and 9 in the experimentally bounded calculation is due to flow effects. As q_{CHF} increases, the predicted flux for mode 4 increases (Table III.1), and for qualities of 0.2 or higher, the decreasing flow will increase q_{CHF} (Fig. III.57) provided the flow is not low enough to enter the interpolation region for q_{CHF}. Thus, as flow decreases, the predicted flux increases for mode 4 and decreases for mode 9 (Table III.1). The oscillations in flow (Fig. III.50) thus produce the alternate choices of modes 4 and 9 (Fig. III.54).

Since the flux for mode 4 rises and falls with q_{CHF} (which, in turn, also depends on quality), rapid quality changes can lead to mode switches. In the system model bounded calculation, the fairly high quality from 0.8

to 1.0 sec reduces the mode 4 flux sufficiently to cause RELAP to choose mode 9 (Fig. III.53). The reverse is true from 1.1 to 1.5 sec, when dropping quality causes mode 4 to be chosen most of the time. Beyond 1.8 sec, the high quality in both cases causes RELAP to choose mode 9. The occasional switches to mode 7 in both cases are the result of low flow, causing RELAP to evaluate and compare the predicted flux of mode 7 to the higher of the fluxes of modes 4 and 9 (Fig. III.38) and to choose the maximum. It should be noted that RELAP will compare the predicted surface flux for modes 2 or 3 to q_{CHF} whenever the chosen mode for the previous time step is mode 4, the quality is below 0.999, and the surface temperature is greater than or equal to the fluid saturation temperature. In both calculations, these conditions are met several times after the initial switch to mode 4. However, no return to pre-CHF modes is calculated because high quality holds q_{CHF} low and because high rod surface temperatures produce high flux predictions for mode 2. In summary, both calculations produce initial DNB due to low flow, but both would probably have produced DNB due to rising quality within a short period, and high quality and high surface temperatures maintain the temperature excursion.

Although we have described the mechanism leading to the erroneous upper core surface temperature predictions, we cannot yet allocate the error to any specific correlation or step. Since we are not satisfied with the accuracy of the core fluid conditions produced by the experimentally bounded test section model, we cannot rule out the possibility that RELAP's heat transfer routines would produce highly accurate results if they were provided the correct fluid conditions. Similarly, we cannot be certain that the success of RELAP's lower core predictions is not the result of erroneous heat transfer calculations compensating for erroneous fluid conditions. Although we cannot judge the merits of the heat transfer correlations and logic with the certainty that might be possible with accurate fluid conditions, certain points are suggestive. RELAP predicts DNB when the flux predicted by its pre-CHF modes exceeds its predicted q_{CHF}. In the calculations analyzed, the flux from the pre-CHF modes showed little variation compared with the drastic drop in

q_{CHF}. The correlation used in these calculations, B&W-2, was developed using data from water flow in rod bundles with the following ranges:

Equivalent diameter	0.51—1.27 cm (0.2—0.5 in.)
Bundle length	1.83 m (72 in.)
Pressure	13.79—16.55 MN/m^2 (2000—2400 psi)
Mass flux	1017—5422 kg/m^2-s ($0.75—4.0 \times 10^6$ lb_m/ft^2-hr)
Burnout quality	(—0.03)—(0.2)

When the erroneous DNB in the upper core is predicted, the pressure and flow ranges over which B&W-2 was developed have been exceeded and quality is at the extreme limit of 0.2. Further, RELAP interpolates on mass flux between the B&W-2 prediction and a minimum value of 283.72 kW/m^2 when flow drops below 271.10 kg/m^2-s (200,000 lb_m/ft^2-hr). The sudden, large drop in q_{CHF} which this interpolation procedure produces may be unrealistic. We recommend that additional work be performed to obtain data for critical heat flux under a wider range of conditions, particularly at higher qualities and lower flows.

III.6 Effects of Slip Model

The effect of the vertical slip model available in RELAP on RELAP's calculations was investigated. (RELAP has a horizontal slip model, but it is designed for stratified flow and is not applicable to these tests.) The vertical slip model considers slip due to gravity only. The RELAP Users' Manual describes its vertical slip model as being "postulated on the assumption that gravity forces govern the slip between phases and therefore the model is especially applicable during relatively slow transients when inertia effects are negligible."[3] Transients in the THTF are relatively rapid and inertia effects may be quite significant, particularly in the heated section with its comparatively small flow area. The downcomer flow area is approximately three times larger than that of the core, suggesting that slower velocities in the downcomer would lead to reduced inertia effects. RELAP's slip model was not based on data for core conditions but does reflect high void fraction data from the downcomer in Semiscale Emergency Core Coolant (ECC) penetration

experiments.[10] Thus, as modelers making judgments on which options to use without the benefit of having the experimental results in advance, we would be inclined to use slip in the downcomer but not in the core. These are the choices used in most of the RELAP calculations described in this report.

Additional RELAP calculations were made using slip in the core as well as in the downcomer and not using slip at all. Calculations were made for the system model and for the test section model, both experimentally bounded and bounded by the system model. Our primary interest was in whether use of the slip model would affect RELAP's calculated fluid conditions enough to alter its calculations of surface temperatures. The addition of slip to the downcomer had little effect on surface temperatures, whereas the addition of slip to the core caused a general lowering of predicted temperatures (Figs. III.58 and .59). Peak temperatures were lowered approximately 28 K (50°F), a small amount compared to the extent of overprediction in the upper core. However, RELAP's slip model affects only the fluid energy equation and does not alter the homogeneous mass and momentum equations. If slip were accurately taken into account in all three equations, a substantial change in the predicted rod surface temperatures might result. Davis[10] noted that considerable inaccuracy may exist in RELAP's slip model and pointed out the need for a slip model based on core flow measurements. We concur in these observations with the additional recommendation that an effort be made to incorporate slip into the mass and momentum equations.

One cannot judge a slip model by the effect it has in a complex, integrated code such as RELAP. An erroneous model may improve RELAP's predictions by compensating for other errors the code may make, such as those introduced by the homogeneous equilibrium assumption. The danger in such a situation is that errors which compensate in one situation may reinforce each other in another. The ability to accurately predict thermal-hydraulic transient behavior in situations where measurements are not available is the primary requirement for a code to be used for margin-of-safety calculations. This ability cannot be inferred from successful predictions of experimental facilities such as the THTF unless that success stems from the accurate evaluation and coupling of all

significant physical effects and not from the fortuitous compensation of erroneous models. Future slip models should be based on, and verified against, relative phase velocities calculated from direct measurements in pertinent geometries over a wide range of conditions. They may require construction of specific facilities for measurement of slip, but the effort would be justified because of the importance of accurate prediction of local fluid properties for accurate surface temperature predictions.

III.7 Effect of Alternate Film Boiling Correlation

In all the RELAP calculations described thus far, the Dougall-Rohsenow (DR) correlation has been used as the film boiling correlation, that is, mode 9 instead of mode 5 (Table III.1). RELAP affords the user two other choices for a film boiling correlation, Groeneveld equations 5.9 (G59) and 5.7 (G57). RELAP predictions using the system model for test 105 were made using G59 and were compared with predictions using DR. Above level H the predictions were virtually identical. Some differences were observed in the middle and bottom of the cores, levels D (Fig. III.60) and H (Fig. III.61) being typical. Although DR appears to produce somewhat better predictions than G59, the reader is reminded that these results represent the responses of the correlations to relatively inaccurate fluid conditions and therefore are not valid grounds for comparison. A meaningful comparison of these correlations will be made as soon as we are able to provide reasonably accurate fluid conditions.

III.8 Effect of Alternate CHF Correlation

RELAP also provides alternatives to the standard CHF correlations described earlier. The user may select a combination of two General Electric correlations (GE) to replace B&W-2, Barnett and modified Barnett (see Appendix B). The GE correlations minimize the effects of flow and depend primarily on quality, CHF being proportional to either 0.8 minus quality or 0.84 minus quality. Thus, increasing quality will produce decreasing values for CHF. RELAP predictions for test 105 using

the system model and the GE CHF correlations have been produced and compared with calculations using the standard CHF correlations. There was little difference in the predictions below level I. In the upper core the use of GE produced lower predicted peak temperatures and higher temperature predictions late in the transient (Fig. III.62). With GE correlations, RELAP switches out of pre-CHF modes later than with the standard correlations. (The flow dependence which produced the early mode switch in the upper core with the standard correlations is not present with GE.) The use of GE correlations delays the mode switch until the predicted quality sustains an appreciable increase in the upper core, thereby lowering the CHF. Further, a decrease in predicted quality causes RELAP to switch back to a pre-CHF mode briefly just after 1 sec. The delayed initial switch, coupled with the brief return to pre-CHF modes, removes sufficient energy from the rods to cause RELAP to predict lower peak temperatures. When GE is used, quality increase becomes the cause of DNB for the upper core as it was in the lower core when the standard CHF correlations were used. The reasons for the higher temperatures late in the transient when GE is used have not been investigated to date. Once again, no valid basis exists for declaring one set of correlations to be superior to the other since both are being applied with relatively inaccurate fluid conditions.

III.9 Conclusions

Summarizing the preceding discussion, RELAP predicts rod surface temperatures in the lower core of the THTF for test series 100 fairly well. RELAP predicts DNB in the lower core when rising quality reduces the predicted value of CHF, and this coincides with the experimentally observed occurrence of DNB. In the upper core, RELAP predicts a similarly early DNB, producing surface temperatures far above those actually observed. The use of the "minimum controls" configuration of RELAP has not enabled us to escape all the conservatism present in the Evaluation Model. When RELAP is used to "extrapolate" experimental data, better local fluid conditions are calculated than when RELAP is used as a predictor, but the calculation of excessively high upper core surface

temperatures persists. If the "extrapolated" local fluid conditions were of high accuracy, this fact would have considerable significance. Since they are not, we do not currently have a valid basis upon which to judge either RELAP's heat transfer correlations or its switching logic. RELAP might be capable of producing the accurate local fluid conditions essential to such judgments if it were supplied with better experimental boundary conditions. The development of a slip model verified by comparison to direct measurement of relative phase velocities may be of substantial assistance to RELAP in calculating fluid conditions. It is clear that the primary hindrance to further analysis of RELAP's heat transfer capabilities within the PWR-BDHT Program is our lack of accurate measurement of transient core pressure differences and those quantities needed for accurate mass flow calculations. Considerable effort is currently being expended to remedy these deficiencies.

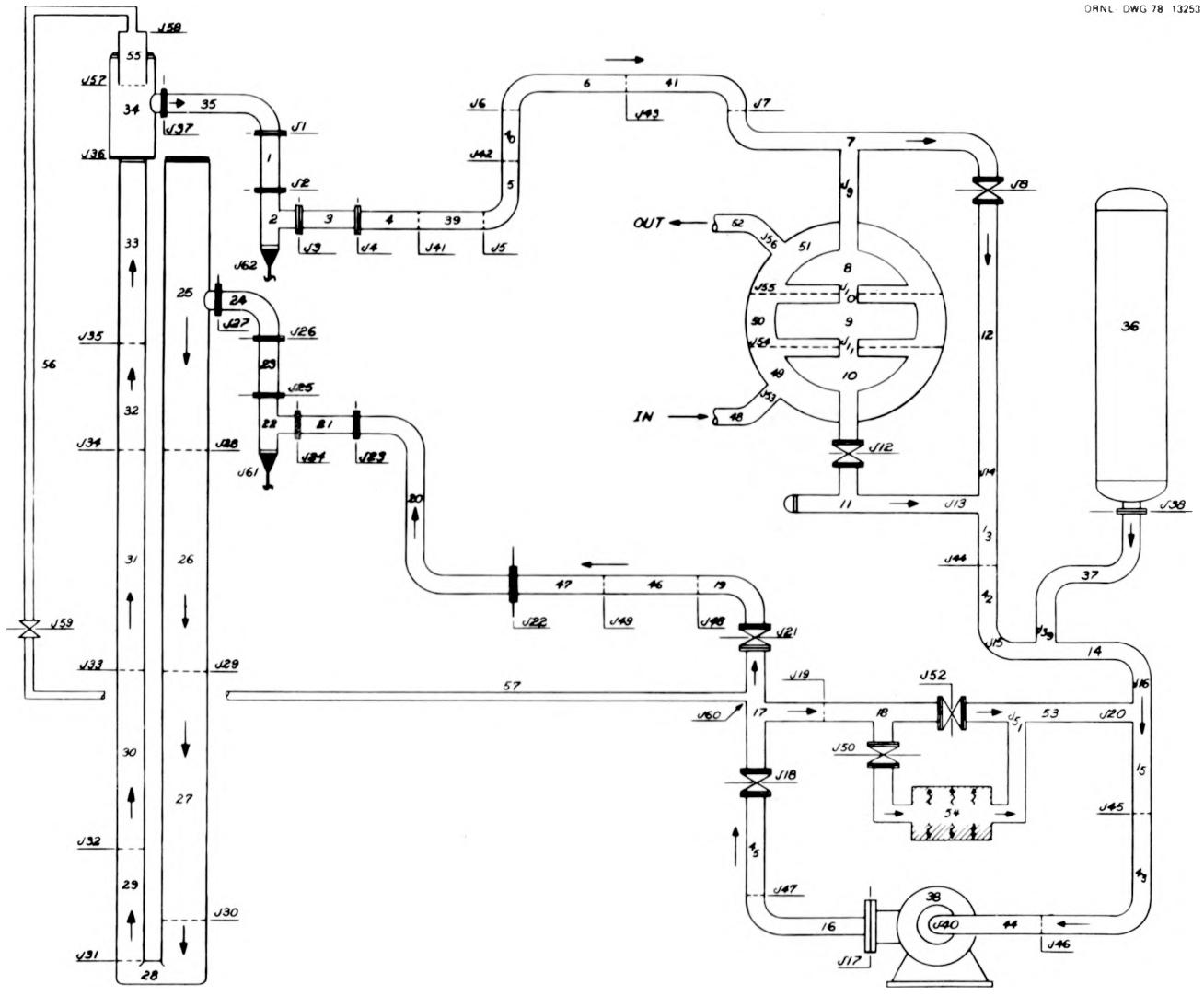

Fig. III.1. RELAP THTF system model.

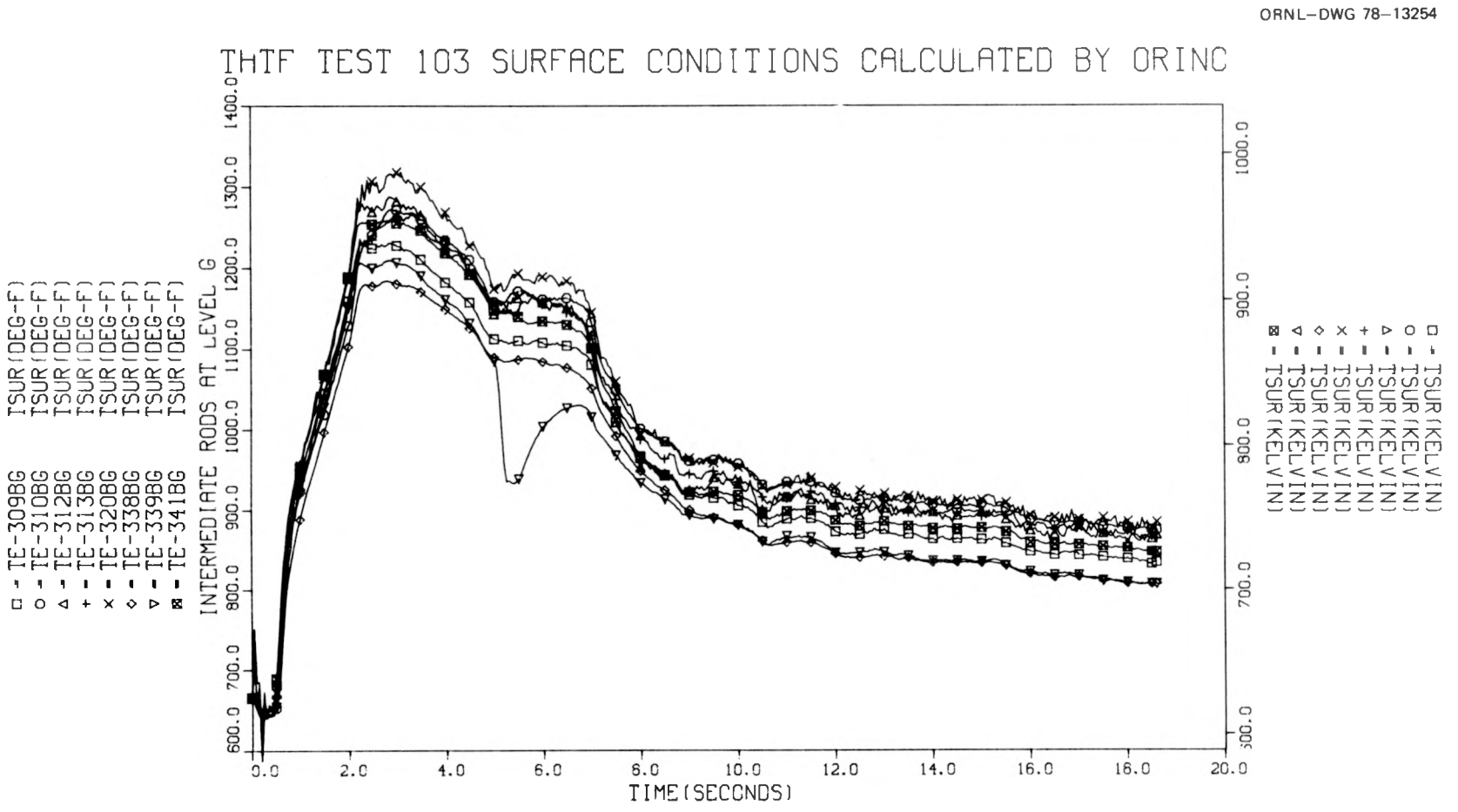

Fig. III.2. Test 103 intermediate rod ORINC surface temperatures — level G.

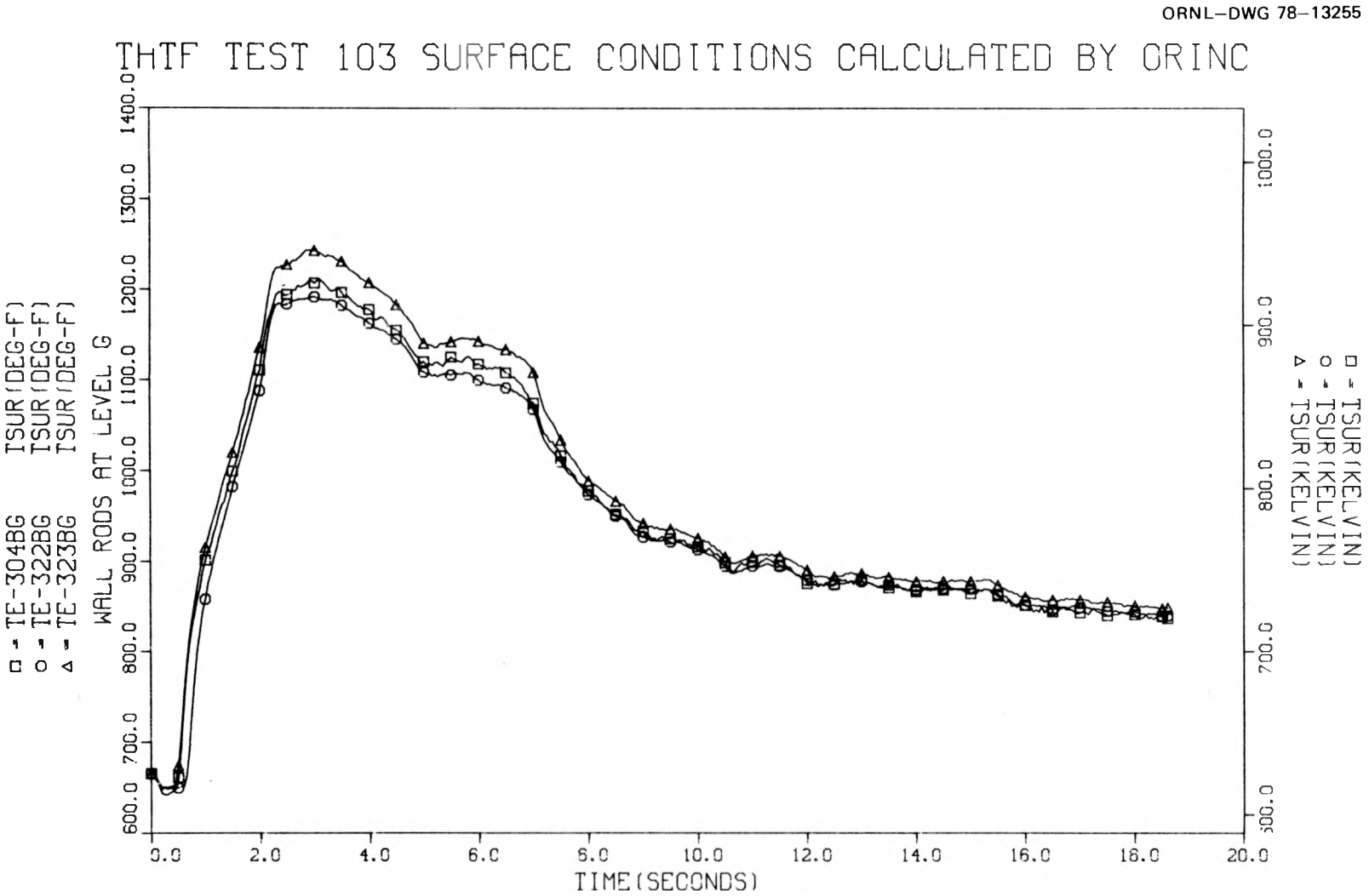

Fig. III.3. Test 103 wall rod ORINC surface temperatures — level G.

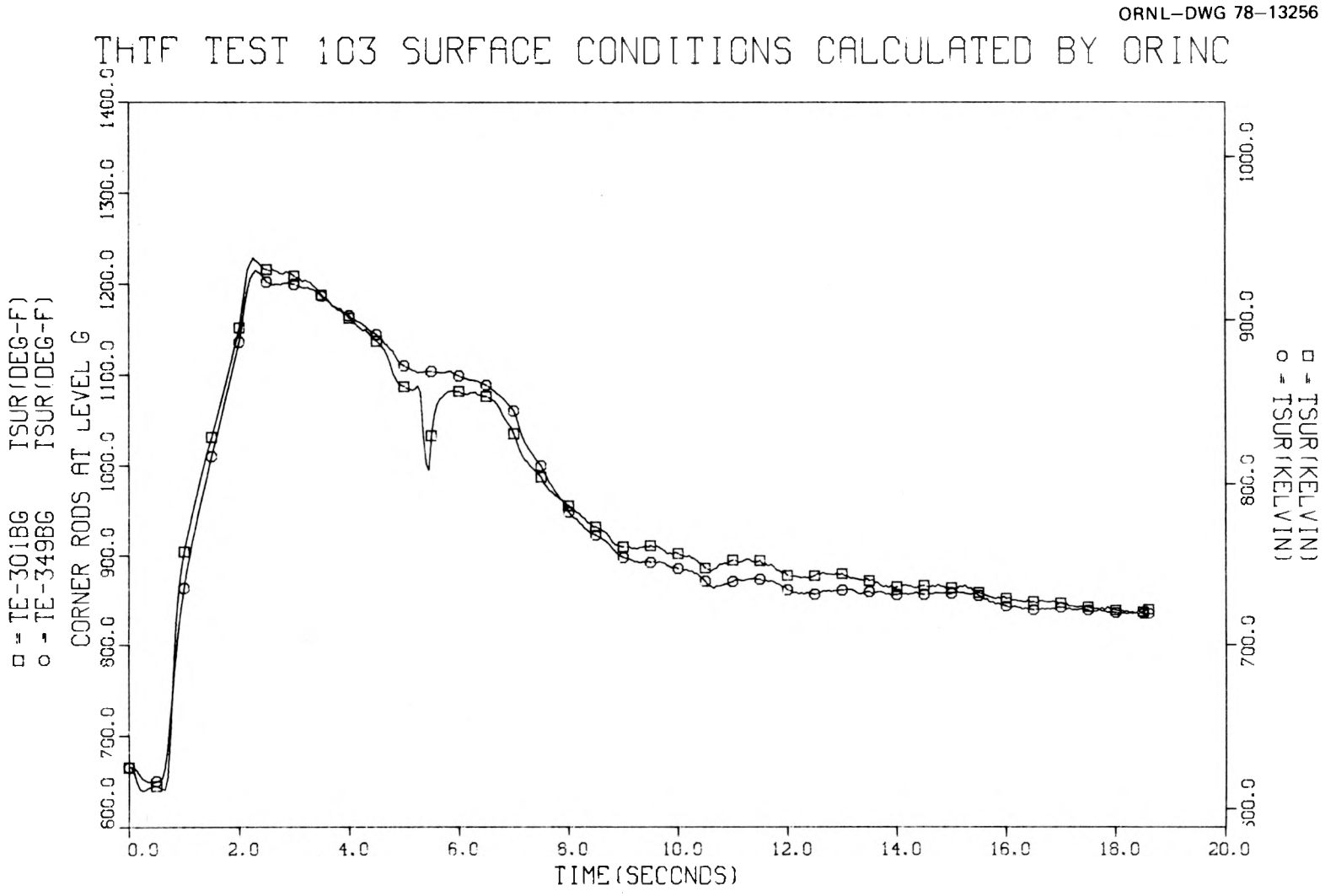

Fig. III.4. Test 103 corner rod ORINC surface temperatures — level G.

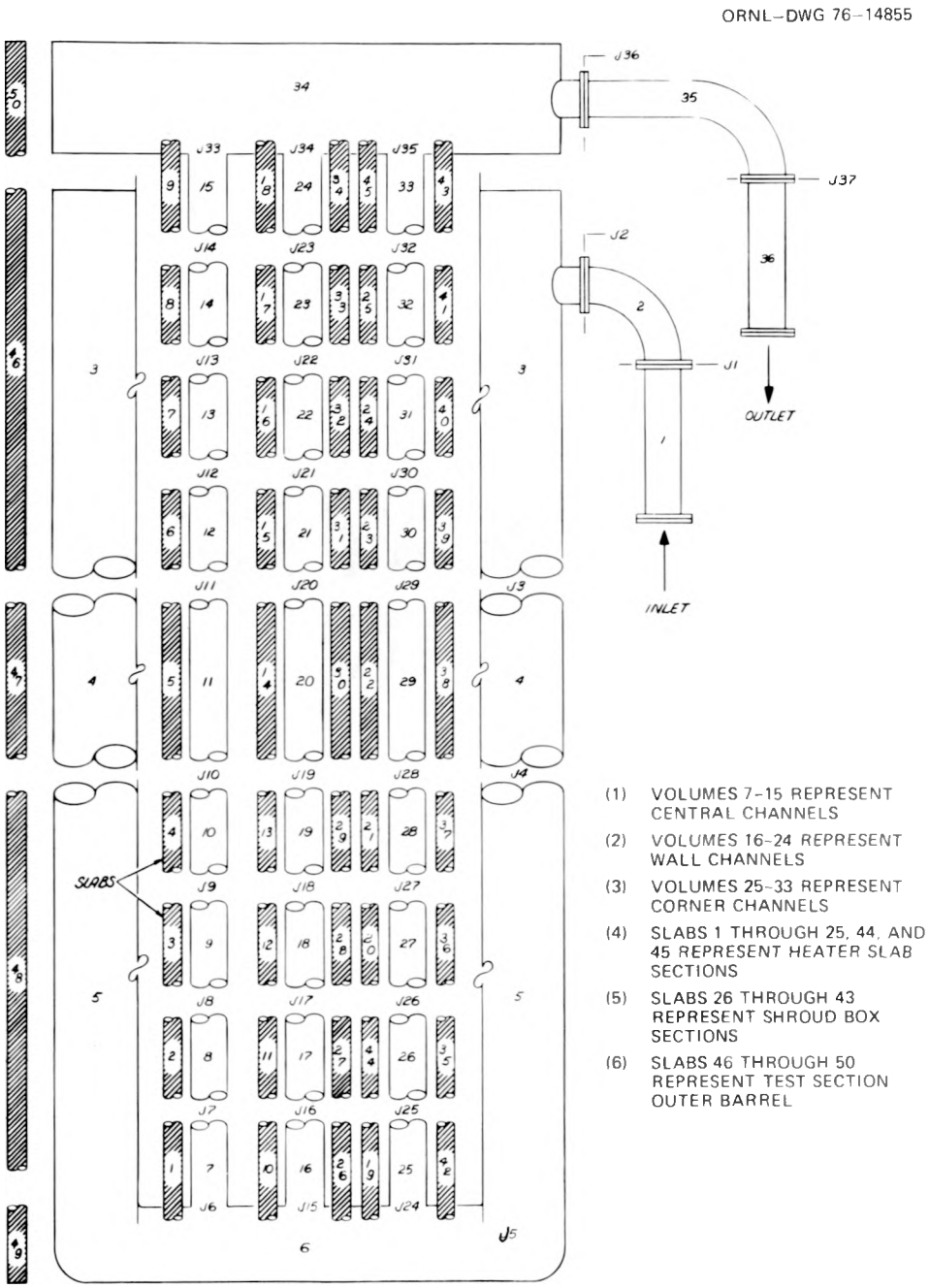

Fig. III.5. THTF (9 axial nodes) three-channel test section model (core model).

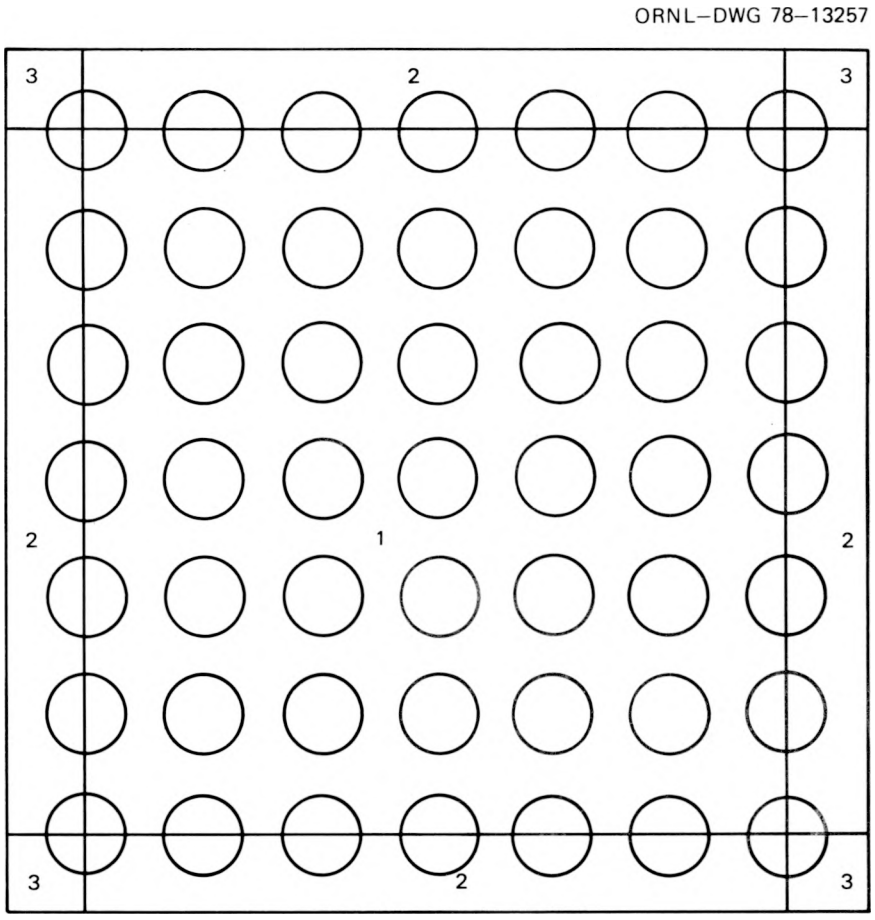

Fig. III.6. Radial boundaries for three-channel test section model (core model) of the THTF. Regions labeled 2 are combined into wall channel. Regions labeled 3 are combined into corner channel. Region 1 is the central channel.

ORNL-DWG 78-13258

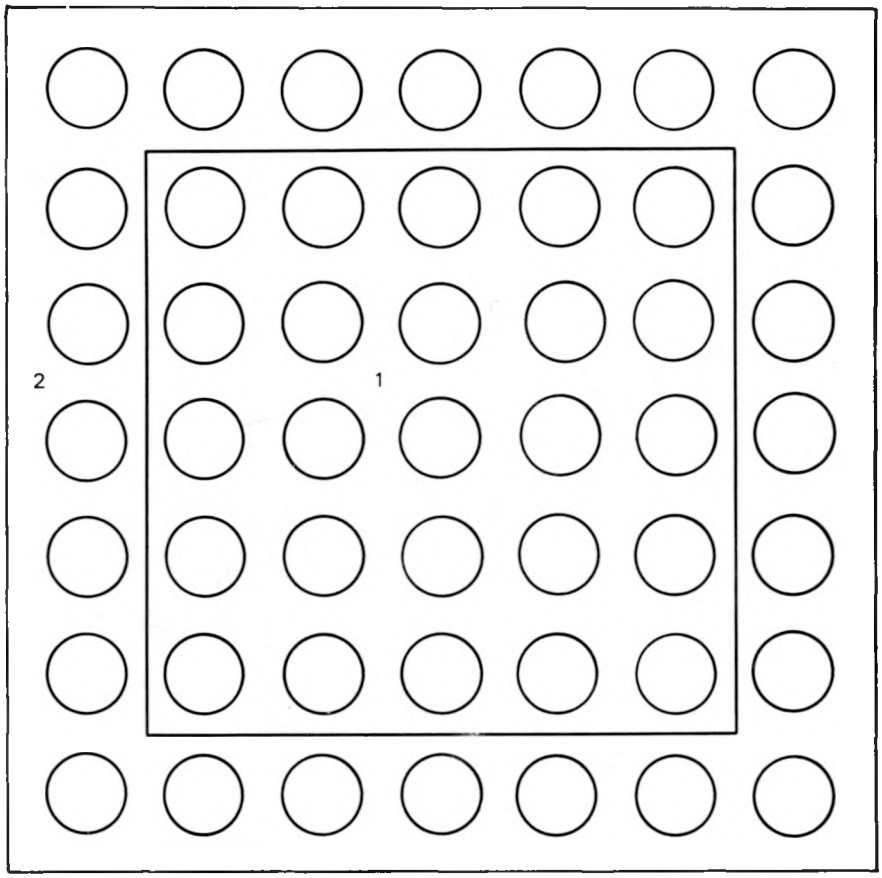

Fig. III.7. Radial boundaries for two-channel test section model (core model) of the THTF. Region 1 is the central channel; region 2 is the wall channel.

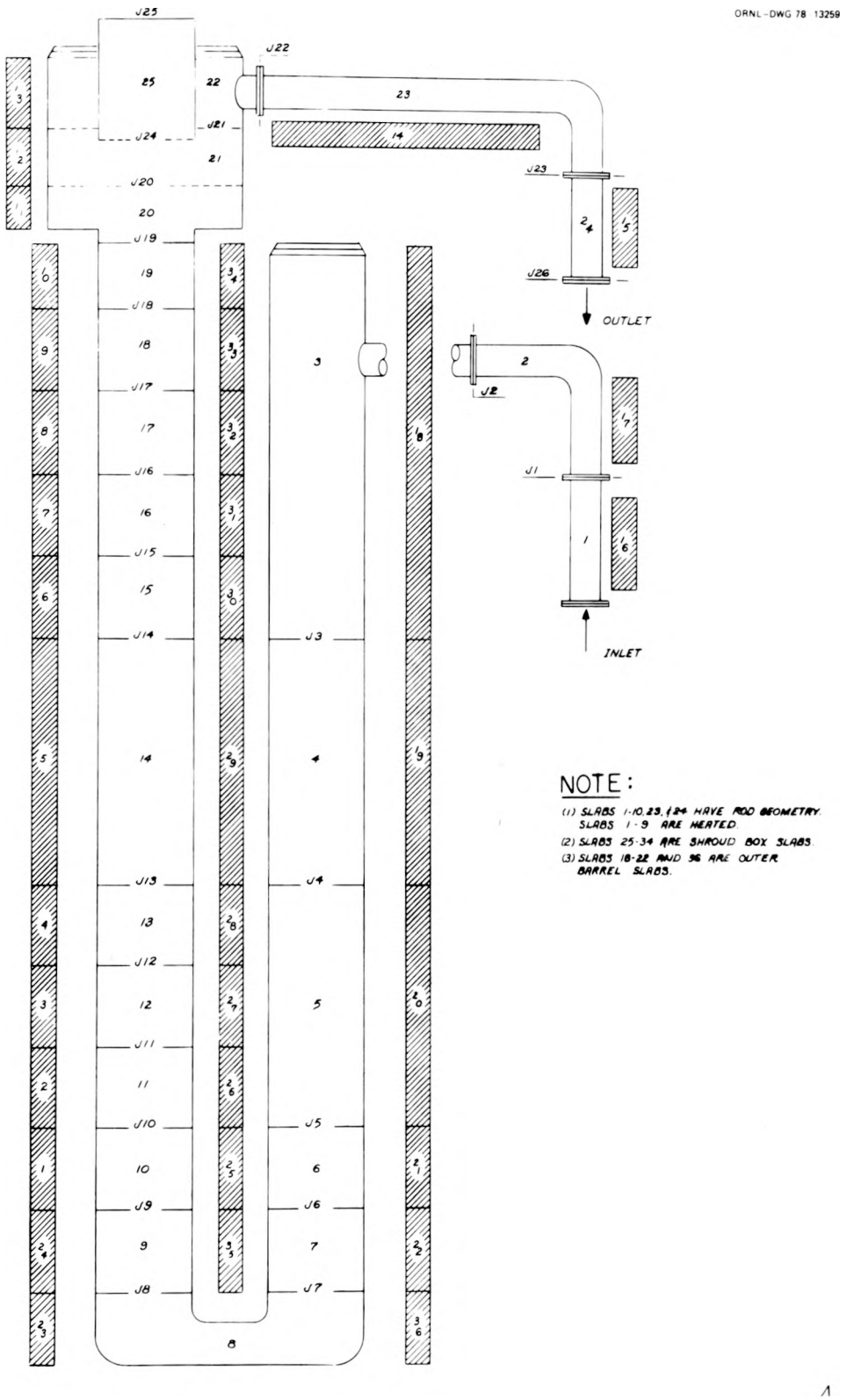

Fig. III.8. THTF (9 axial nodes) single-channel test section model (core model).

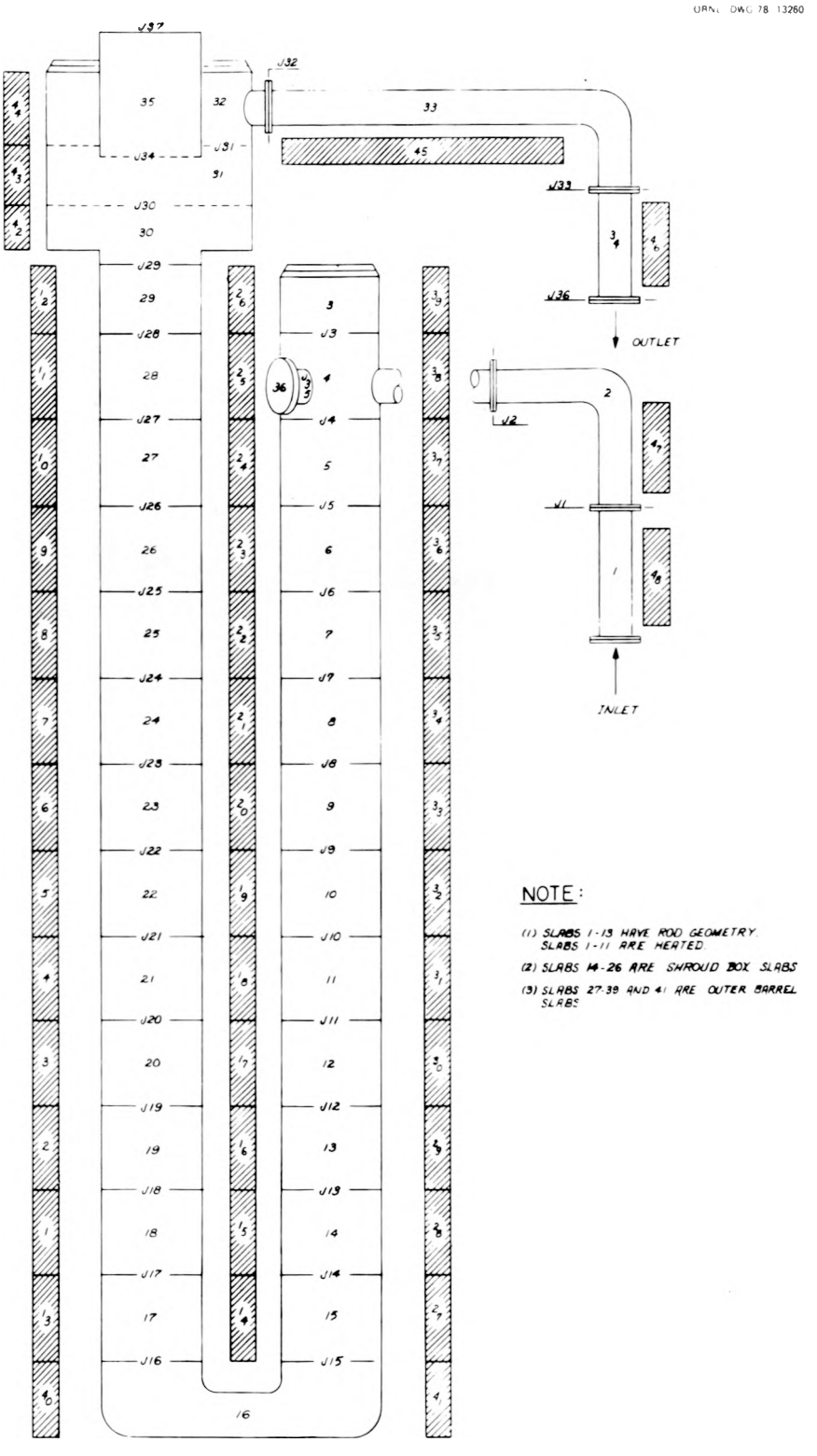

Fig. III.9. THTF (11 axial nodes) single-channel test section model (core model).

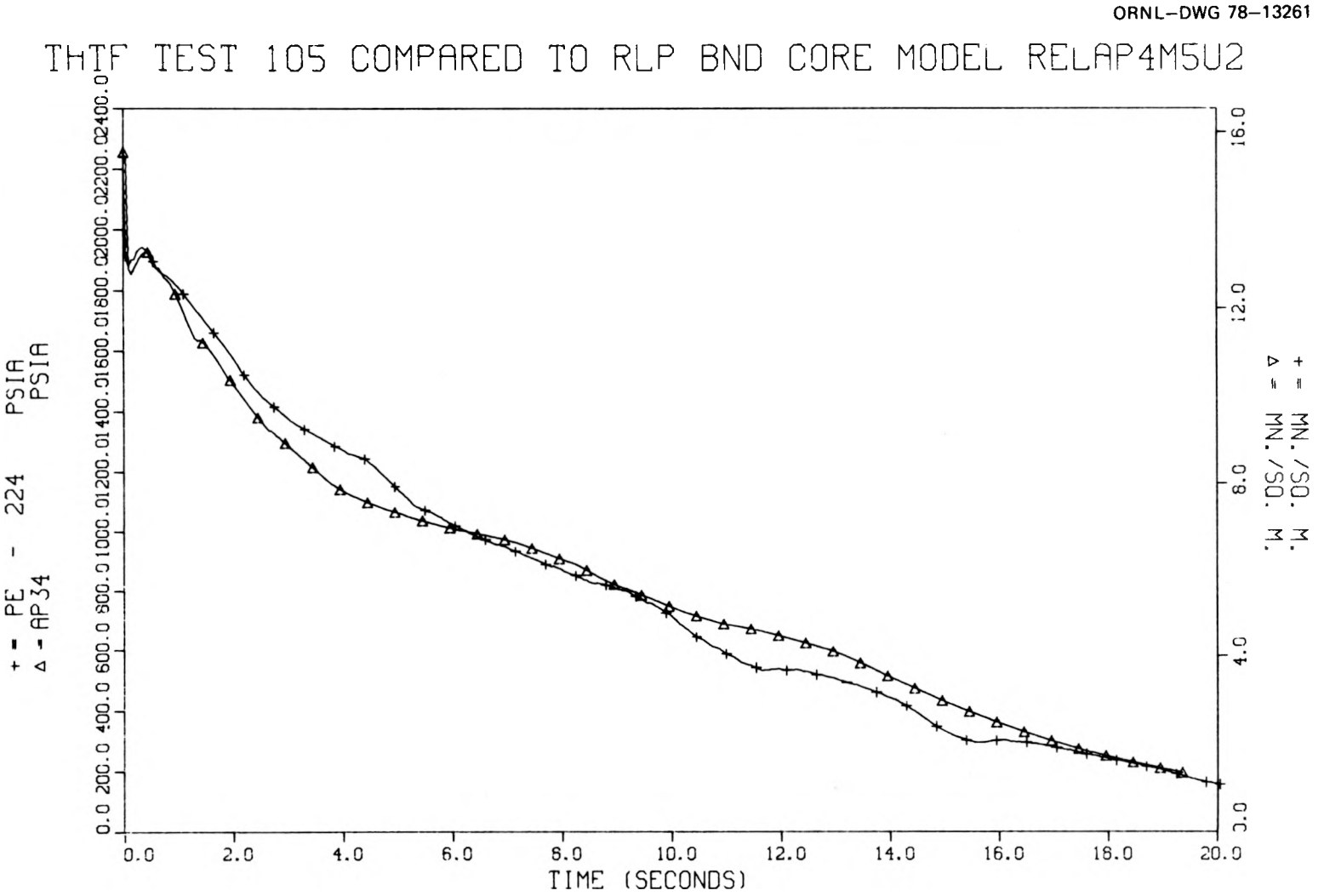

Fig. III.10. RELAP bound core pressure at V0 vs data, test 105.

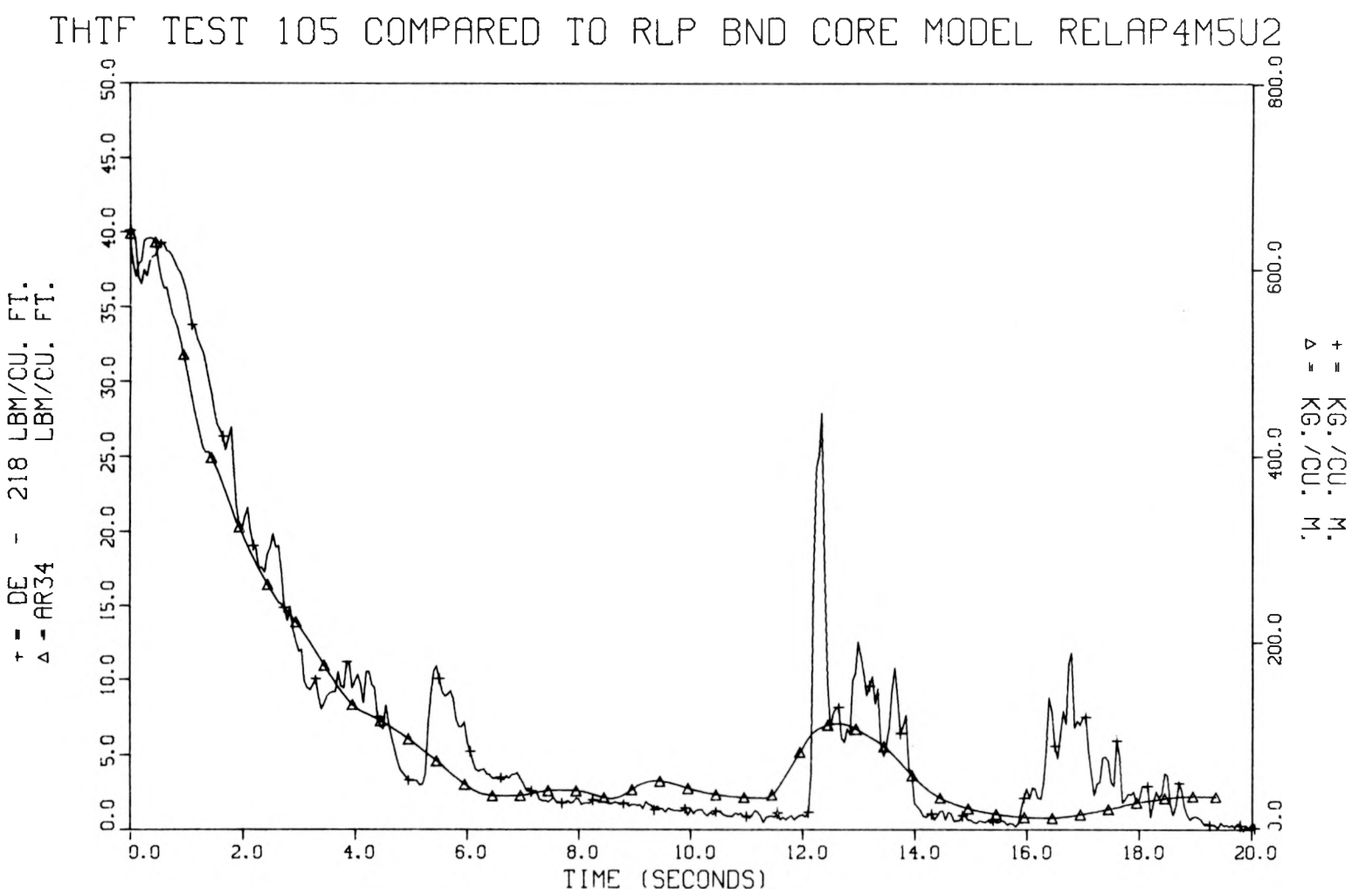

Fig. III.11. RELAP bound core density at V0 vs data, test 105.

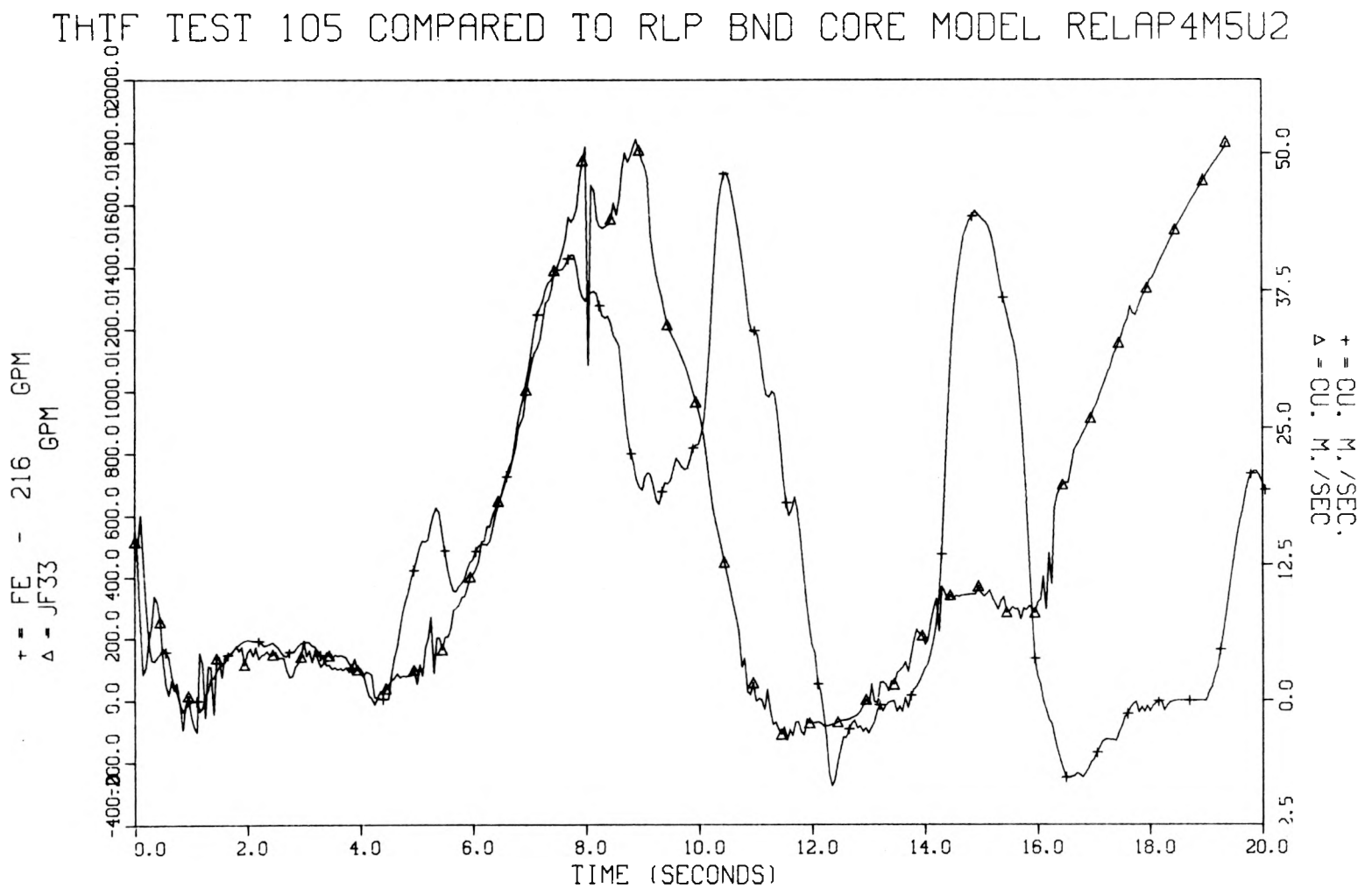

Fig. III.12. RELAP bound core volumetric flow at V0 vs data, test 105.

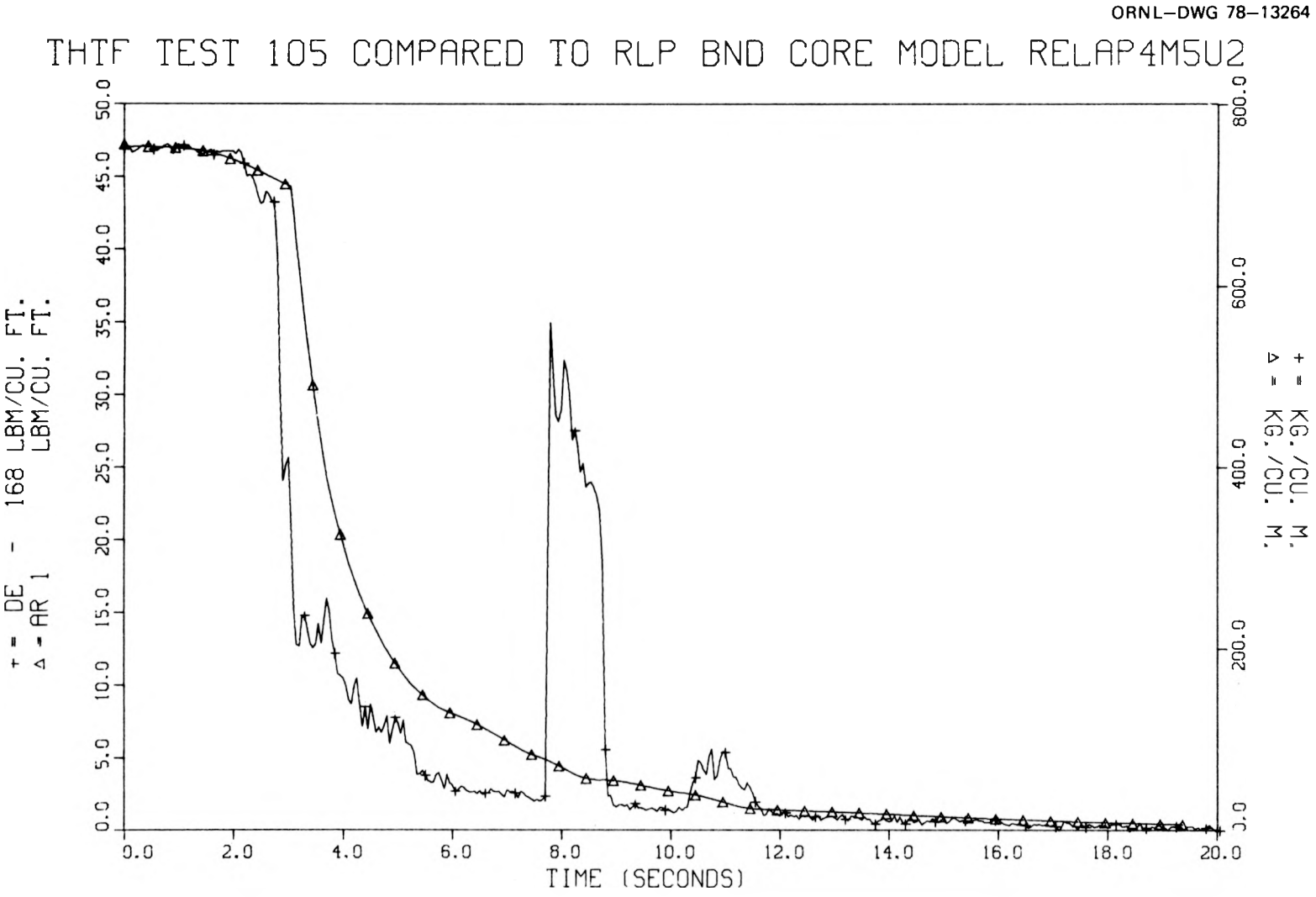

Fig. III.13. RELAP bound core density at VI vs data, test 105.

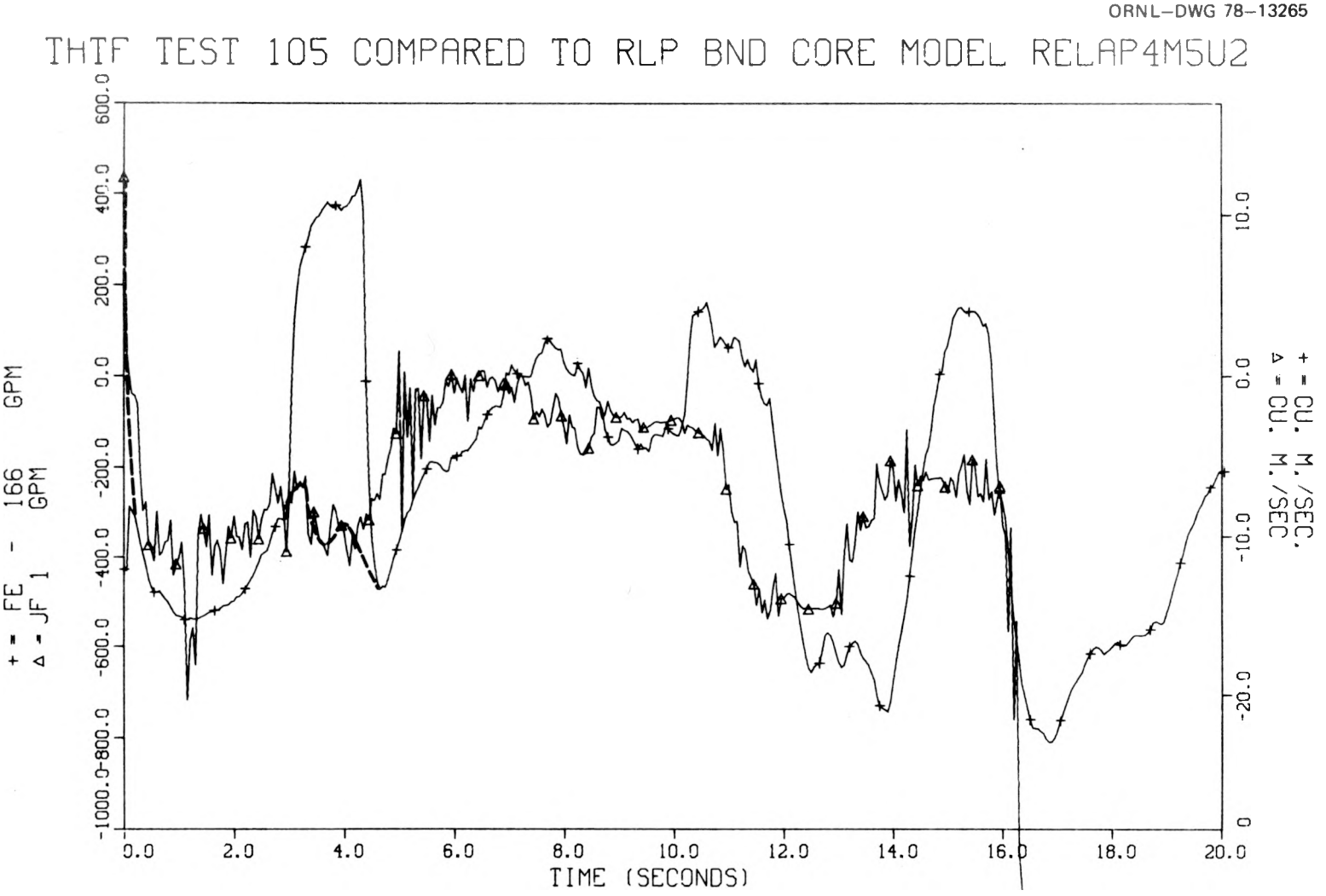

Fig. III.14. RELAP bound core volumetric flow at VI vs data (corrected signal), test 105. (Polarity reversal produced incorrect signs on turbine meter signals at some times. Estimates of the correct signal are indicated by dotted lines.)

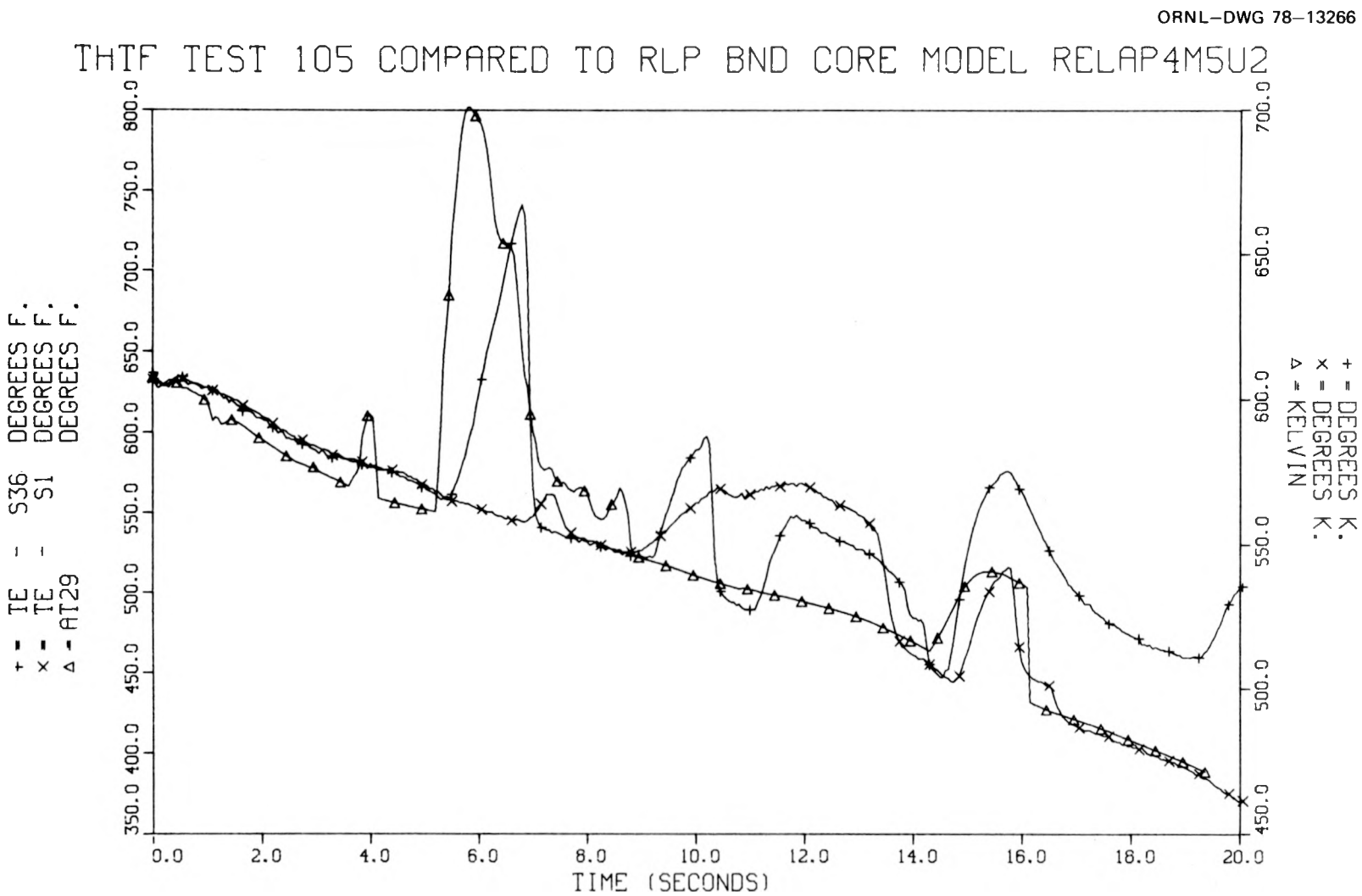

Fig. III.15. RELAP bound core fluid temperatures in subchannel thermocouple region vs data, test 105.

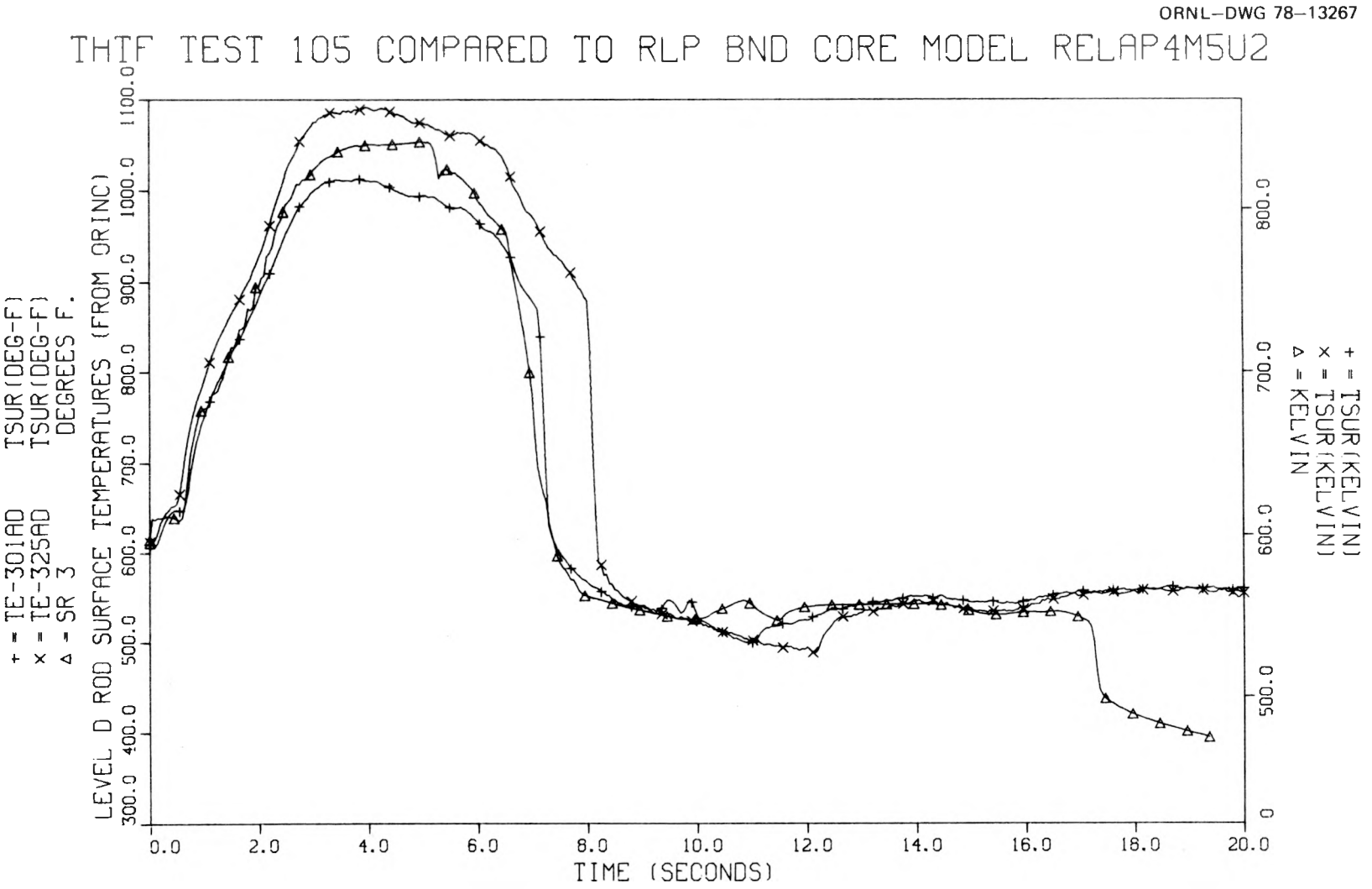

Fig. III.16. RELAP bound core slab surface temperature vs ORINC rod surface temperatures — level D, test 105.

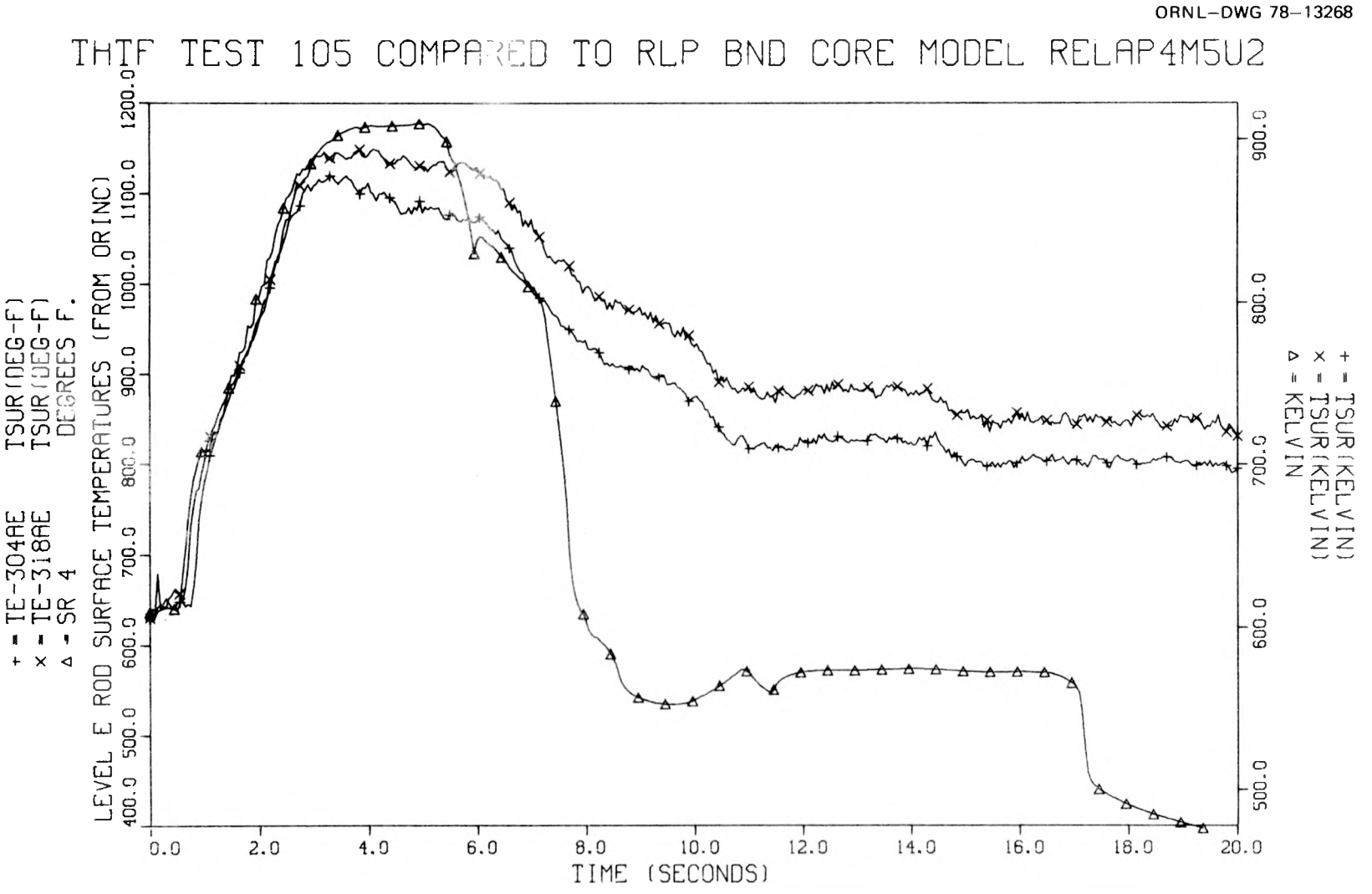

Fig. III.17. RELAP bound core slab surface temperature vs ORINC rod surface temperatures — level E, test 105.

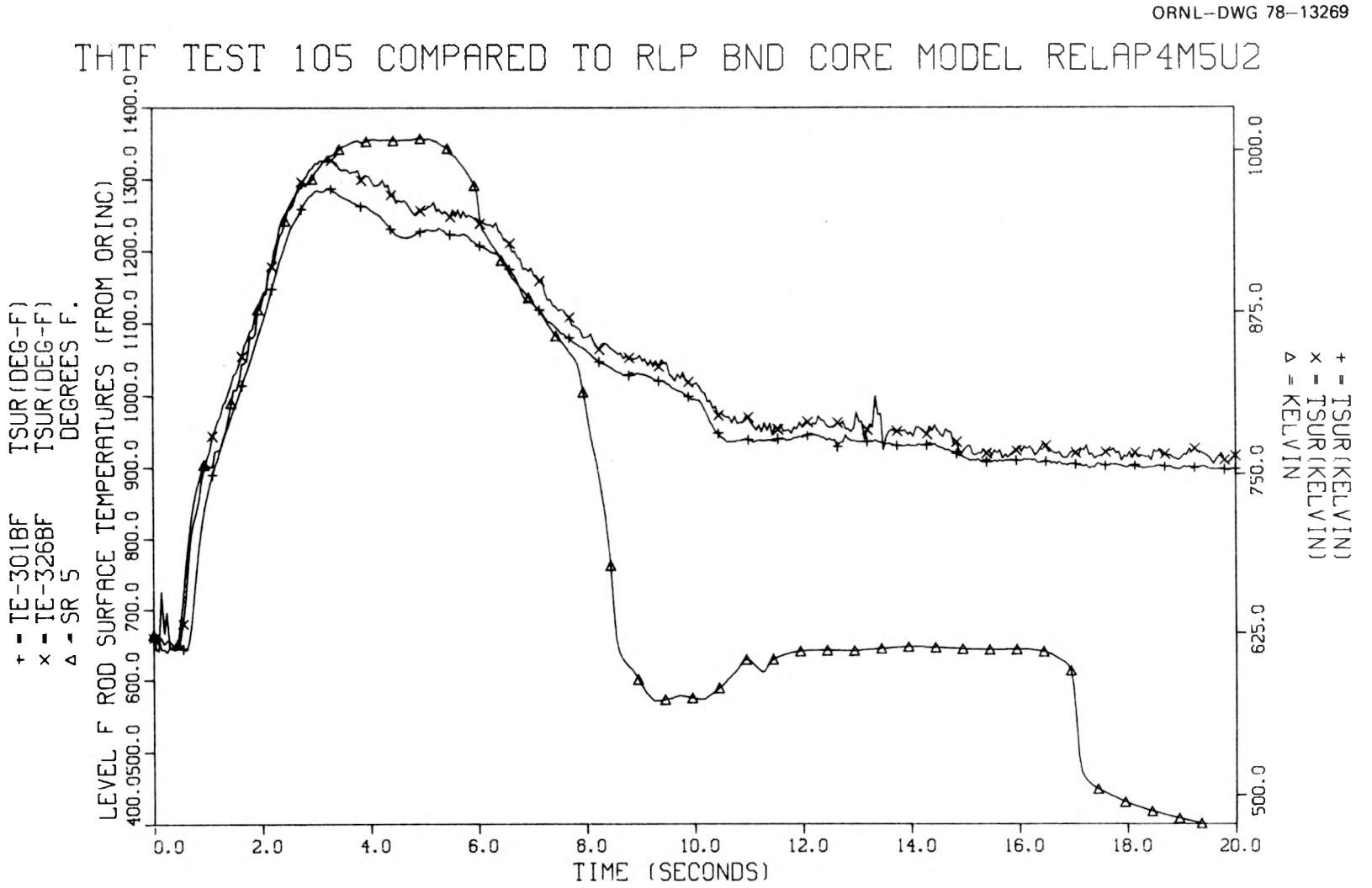

Fig. III.18. RELAP bound core slab surface temperature vs ORINC rod surface temperatures — level F, test 105.

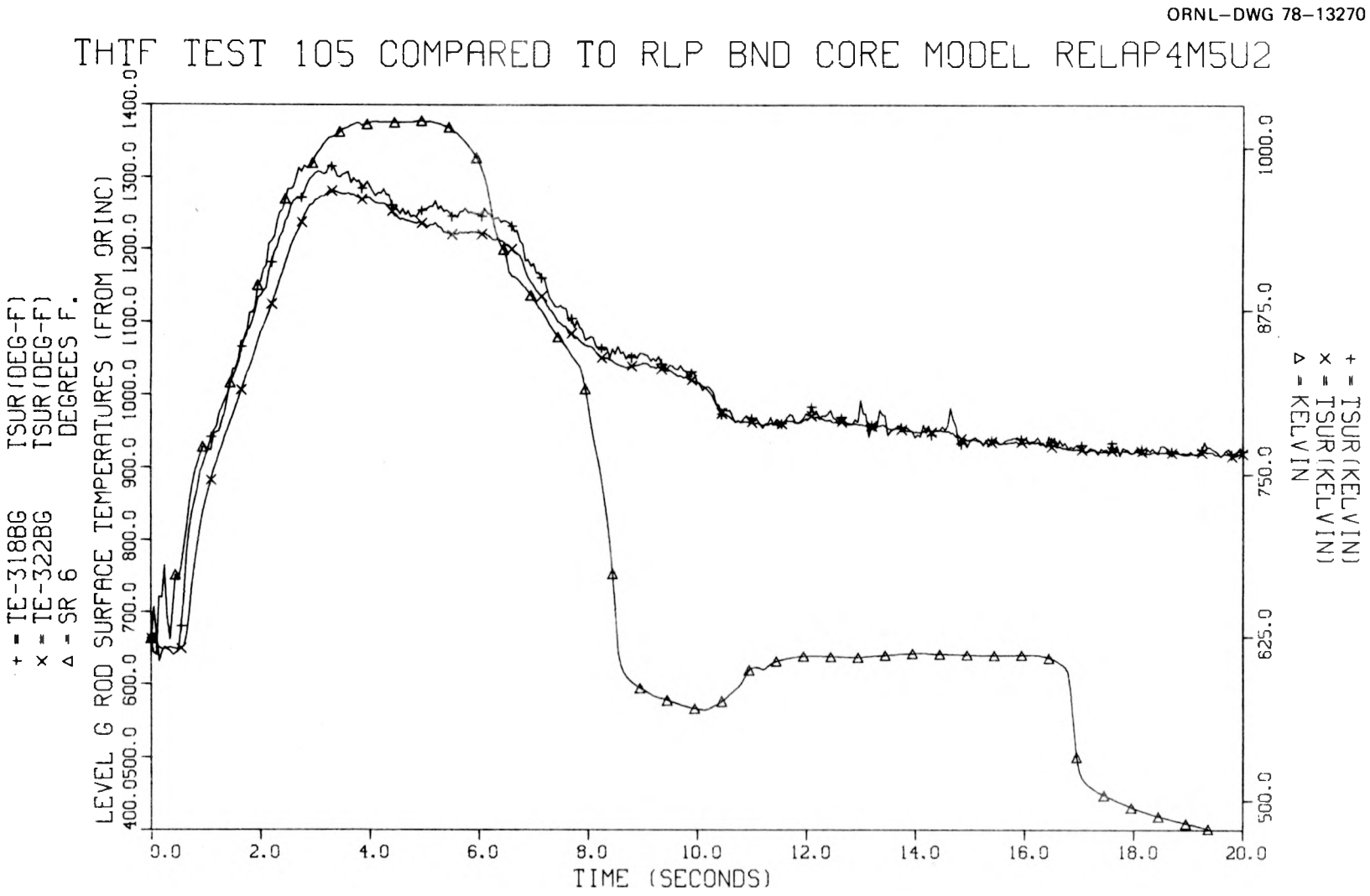

Fig. III.19. RELAP bound core slab surface temperature vs ORINC rod surface temperatures — level G, test 105.

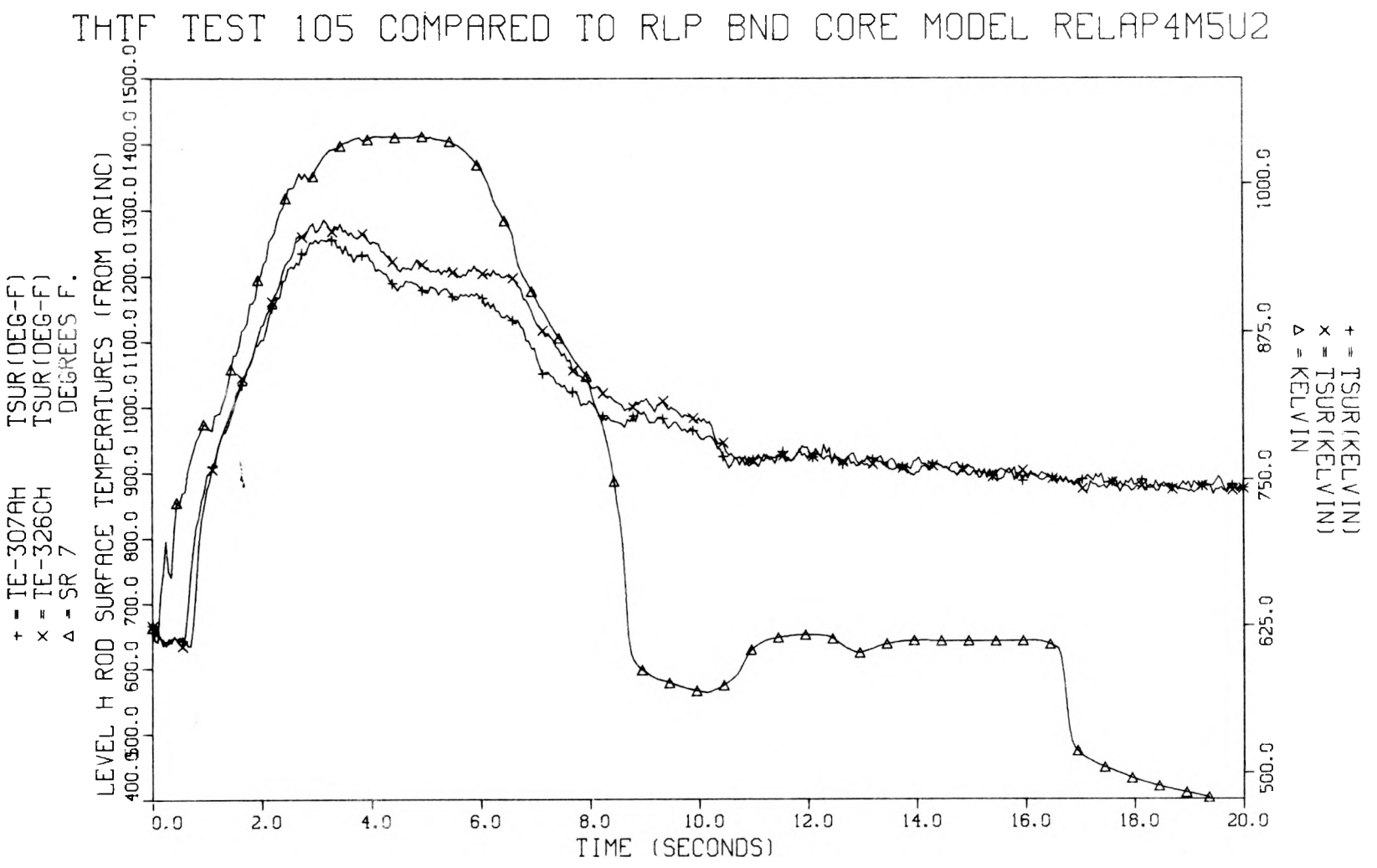

Fig. III.20. RELAP bound core slab surface temperature vs ORINC rod surface temperatures — level H, test 105.

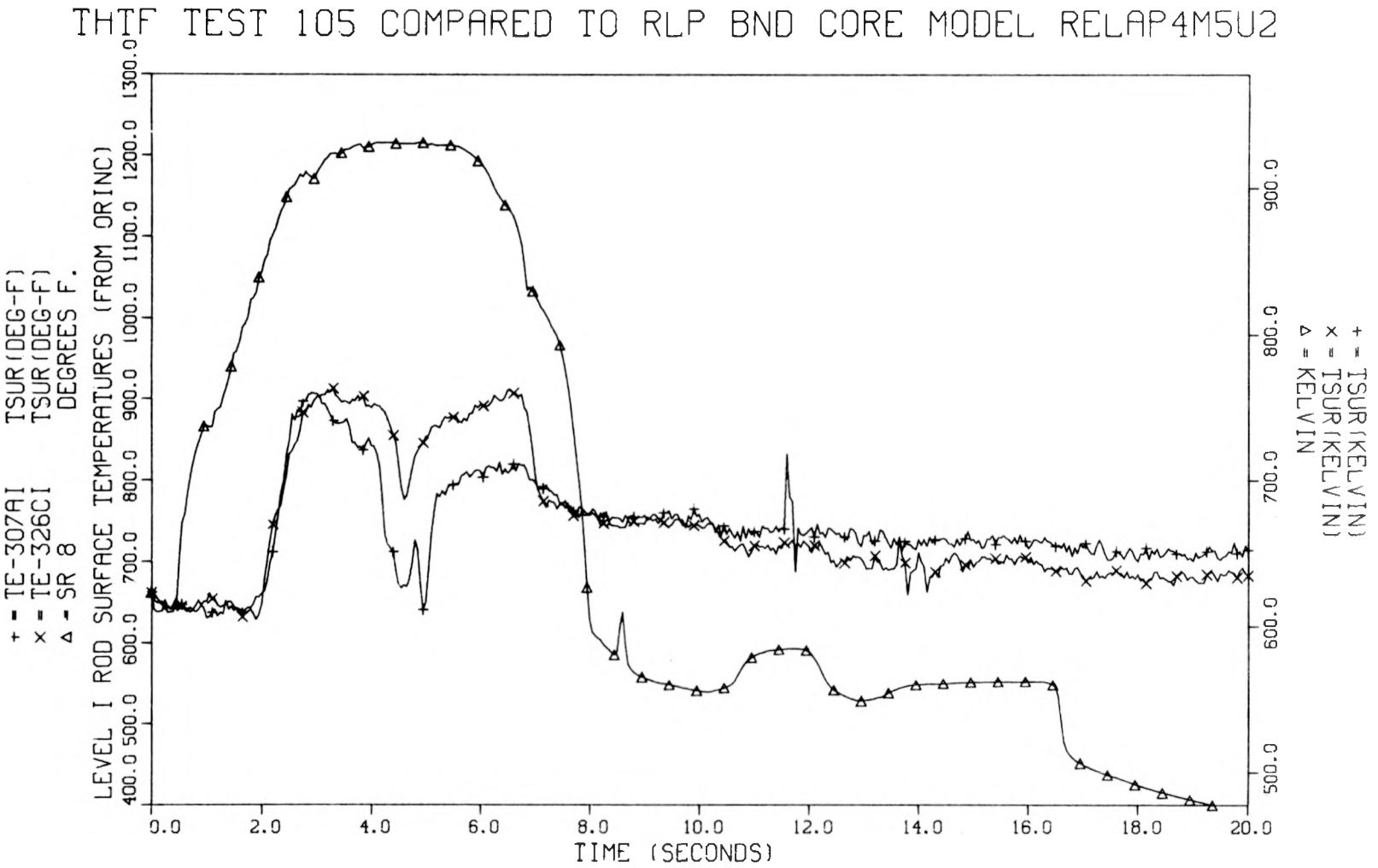

Fig. III.21. RELAP bound core slab surface temperature vs ORINC rod surface temperatures — level I, test 105.

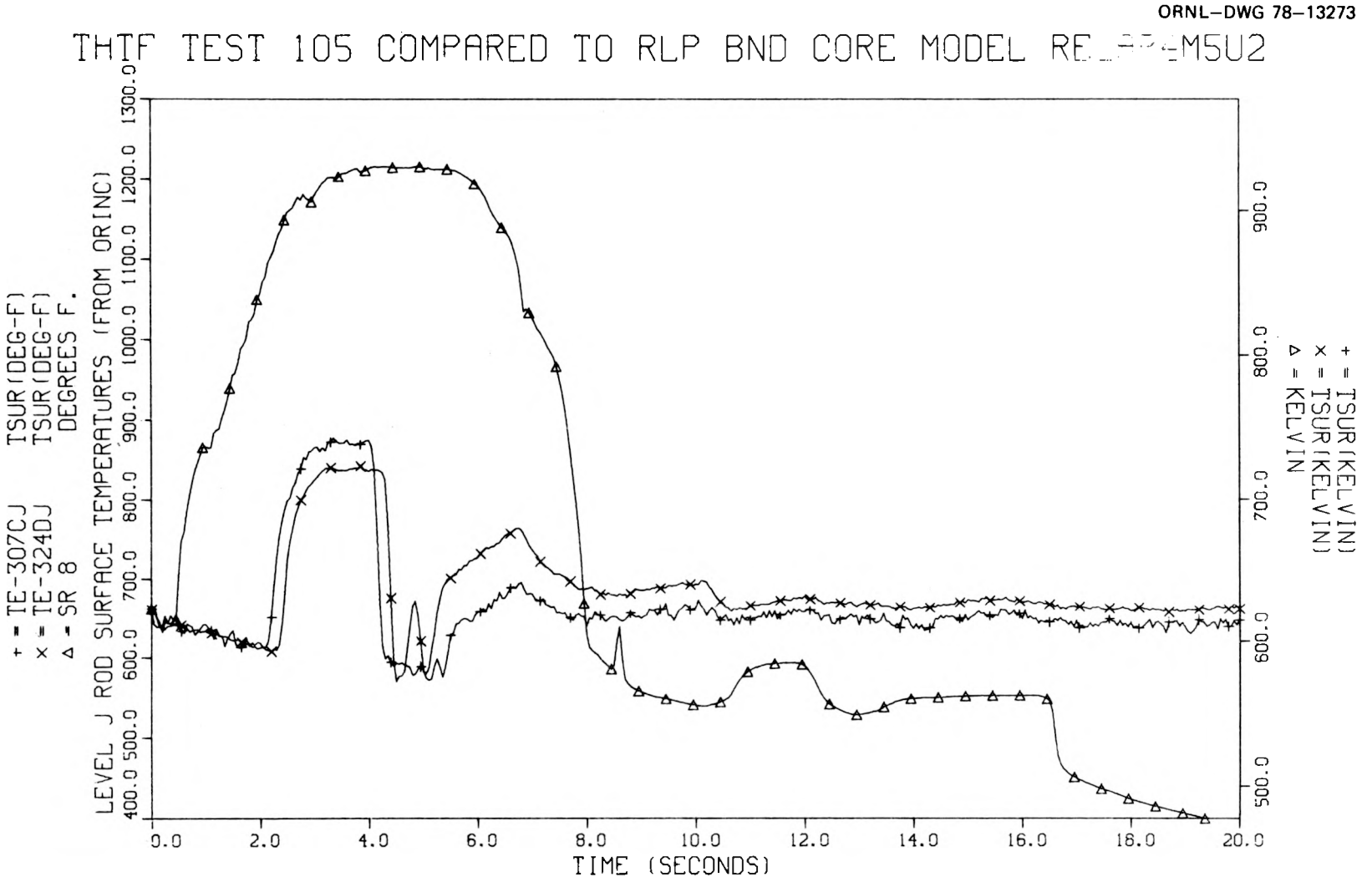

Fig. III.22. RELAP bound core slab surface temperature vs ORINC rod surface temperatures — level J, test 105.

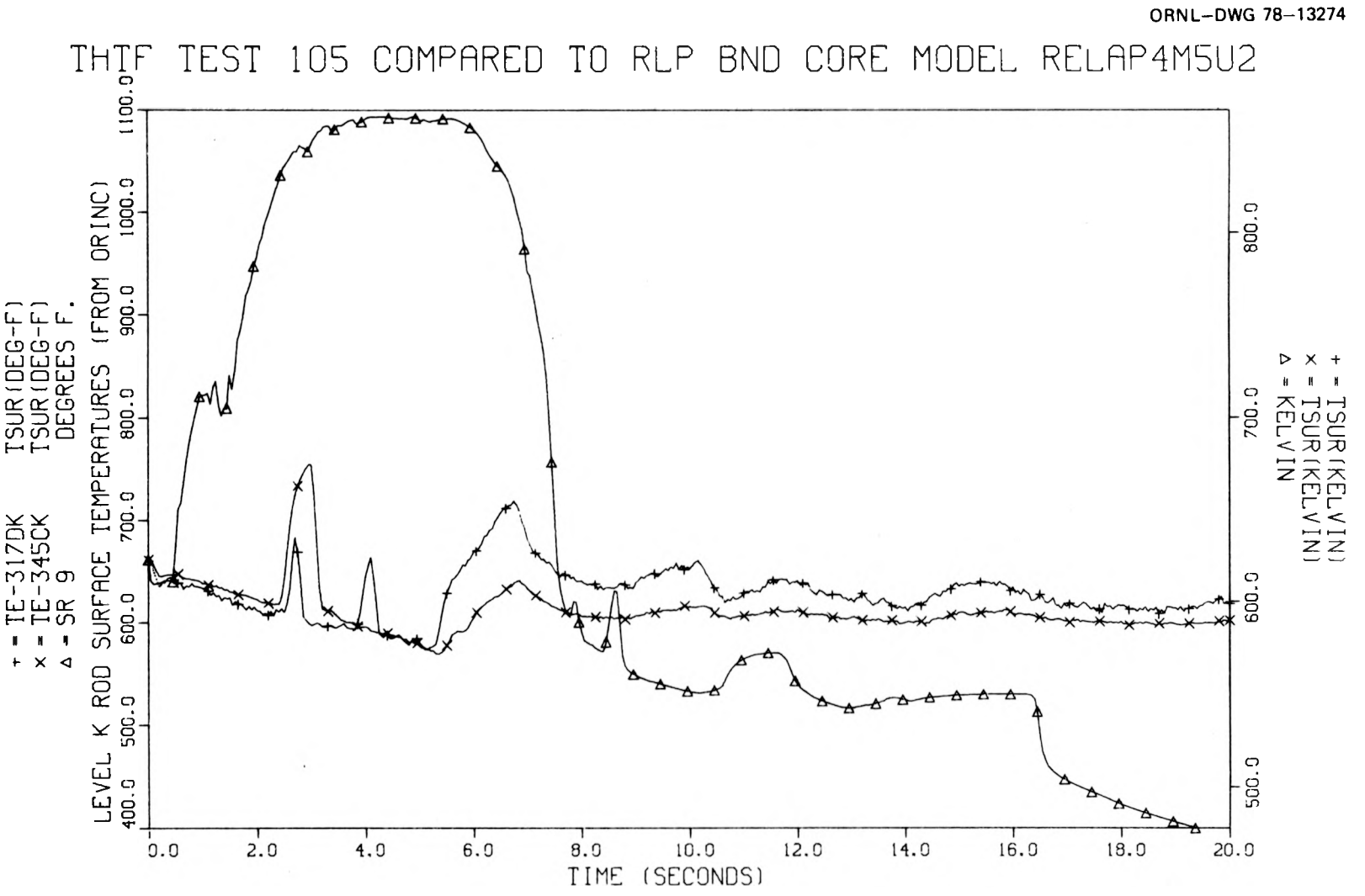

Fig. III.23. RELAP bound core slab surface temperature vs ORINC rod surface temperatures — level K, test 105.

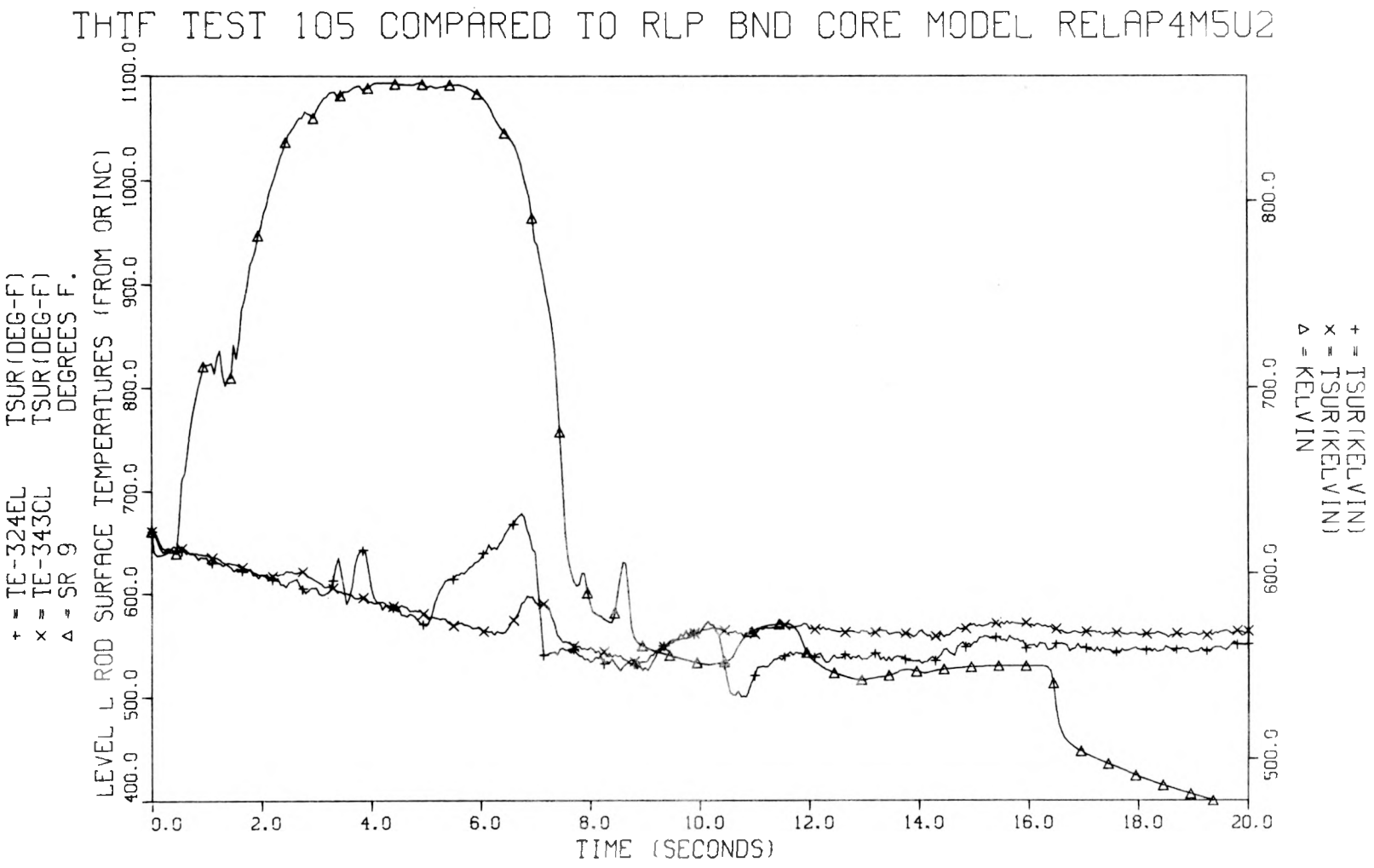

Fig. III.24. RELAP bound core slab surface temperature vs ORINC rod surface temperatures — level L, test 105.

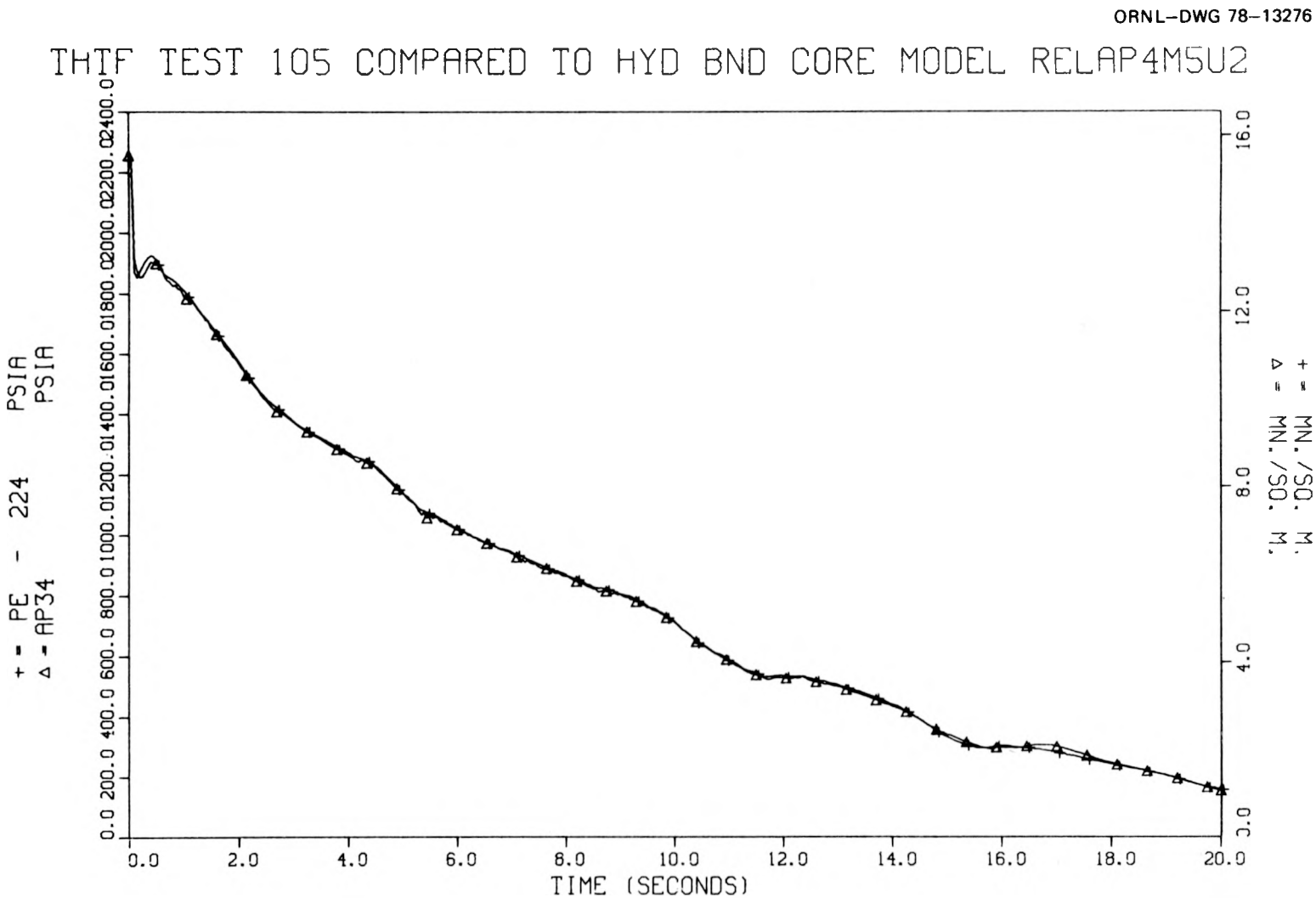

Fig. III.25. Hydraulic bound core pressure at V0 vs data, test 105.

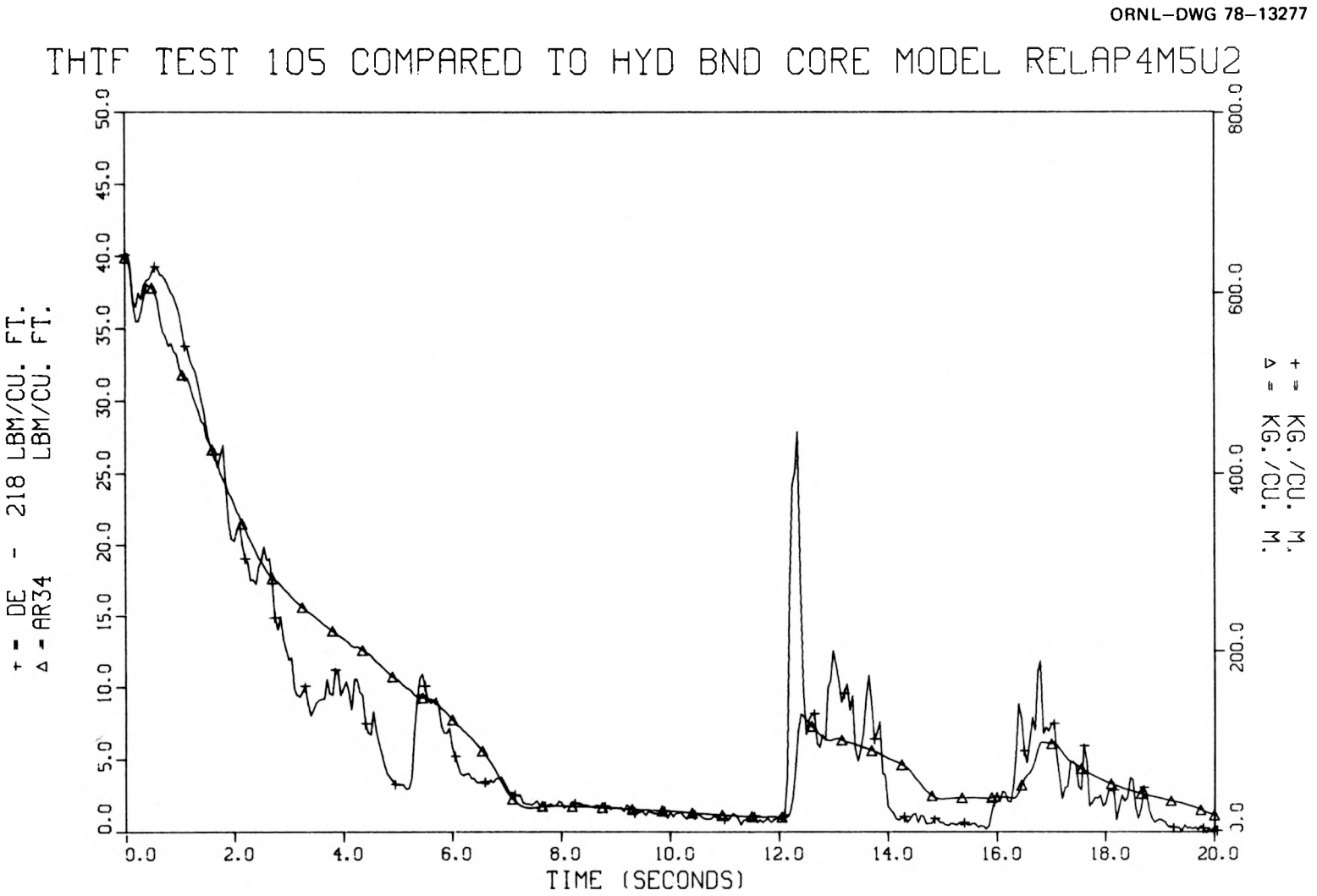

Fig. III.26. Hydraulic bound core density at V0 vs data, test 105.

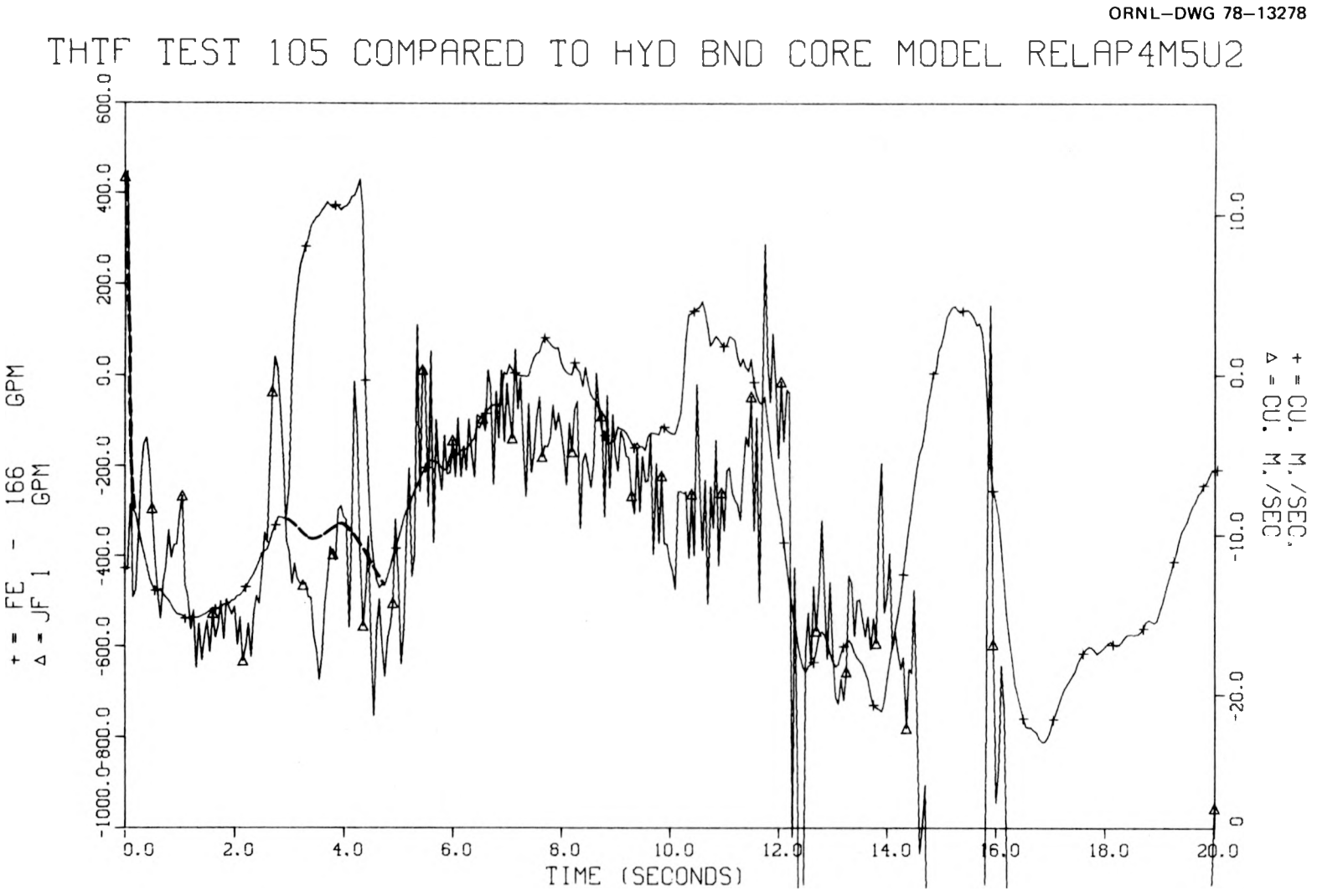

Fig. III.27. Hydraulic bound core volumetric flow at VI vs data (corrected signal), test 105. (Polarity reversal produced incorrect signs on turbine meter signals at some times. Estimates of the correct signal are indicated by dotted lines.)

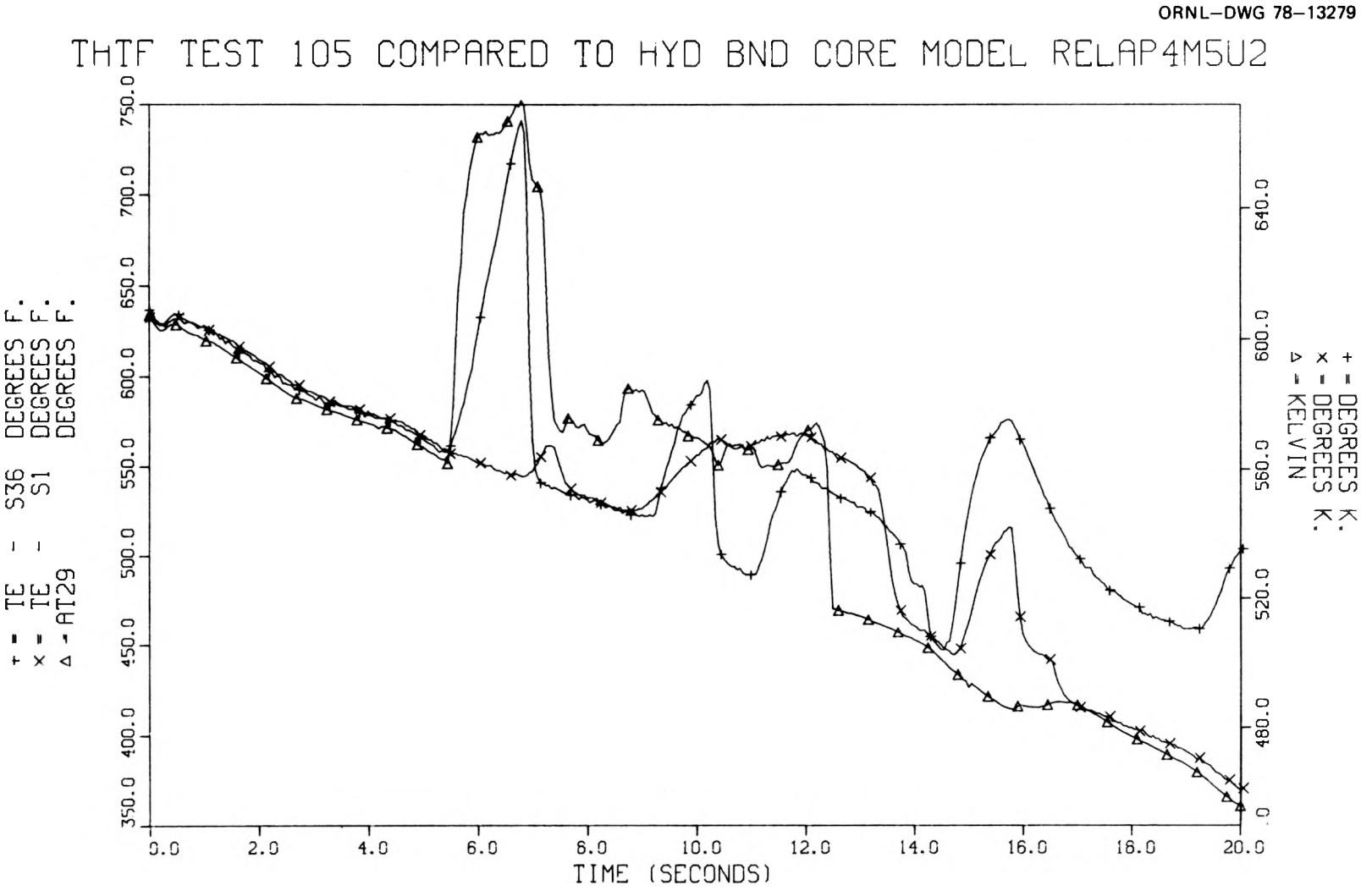

Fig. III.28. Hydraulic bound core fluid temperatures in subchannel thermocouple region vs data, test 105.

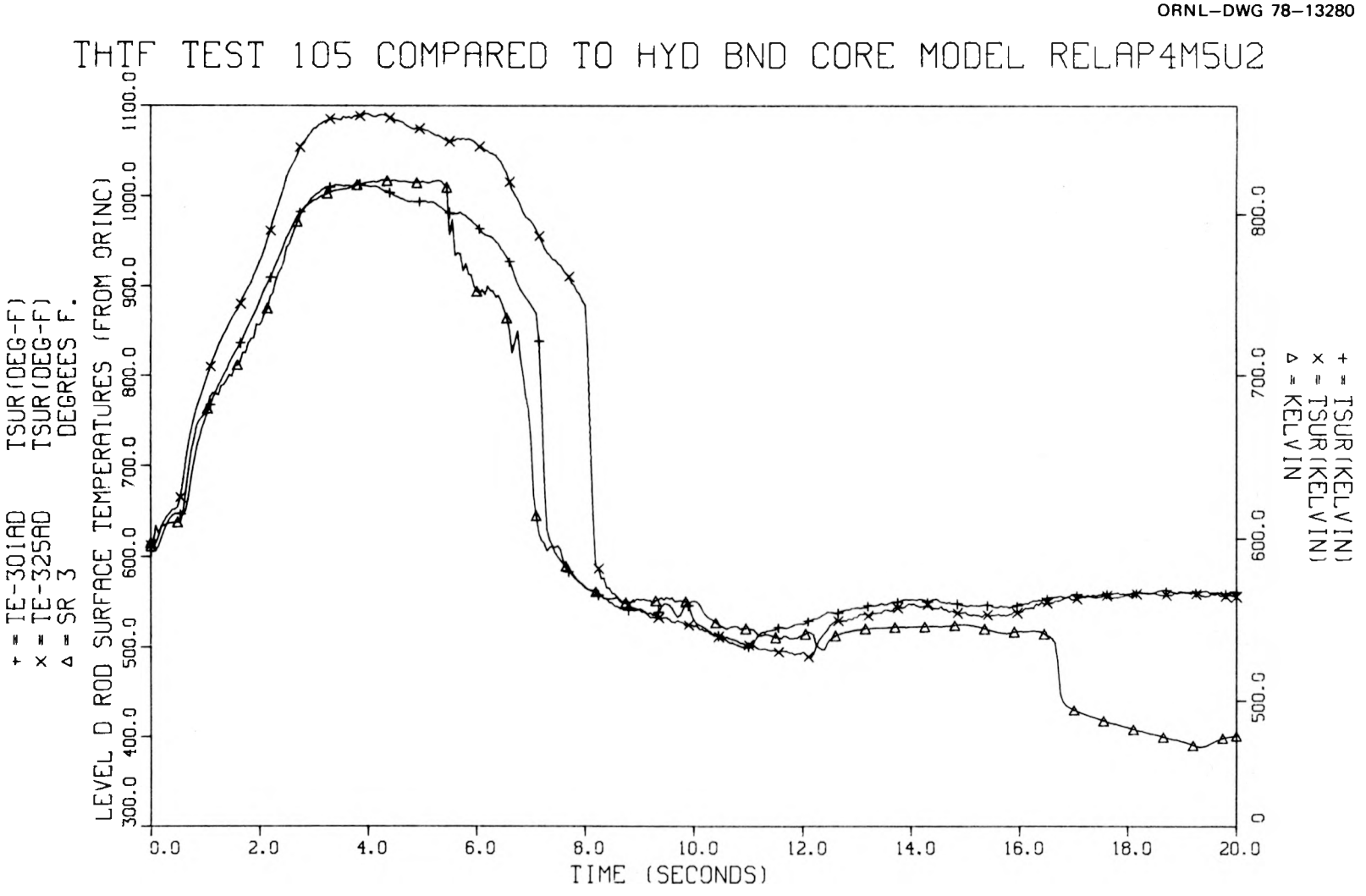

Fig. III.29. Hydraulic bound core slab surface temperature vs ORINC rod surface temperatures — level D, test 105.

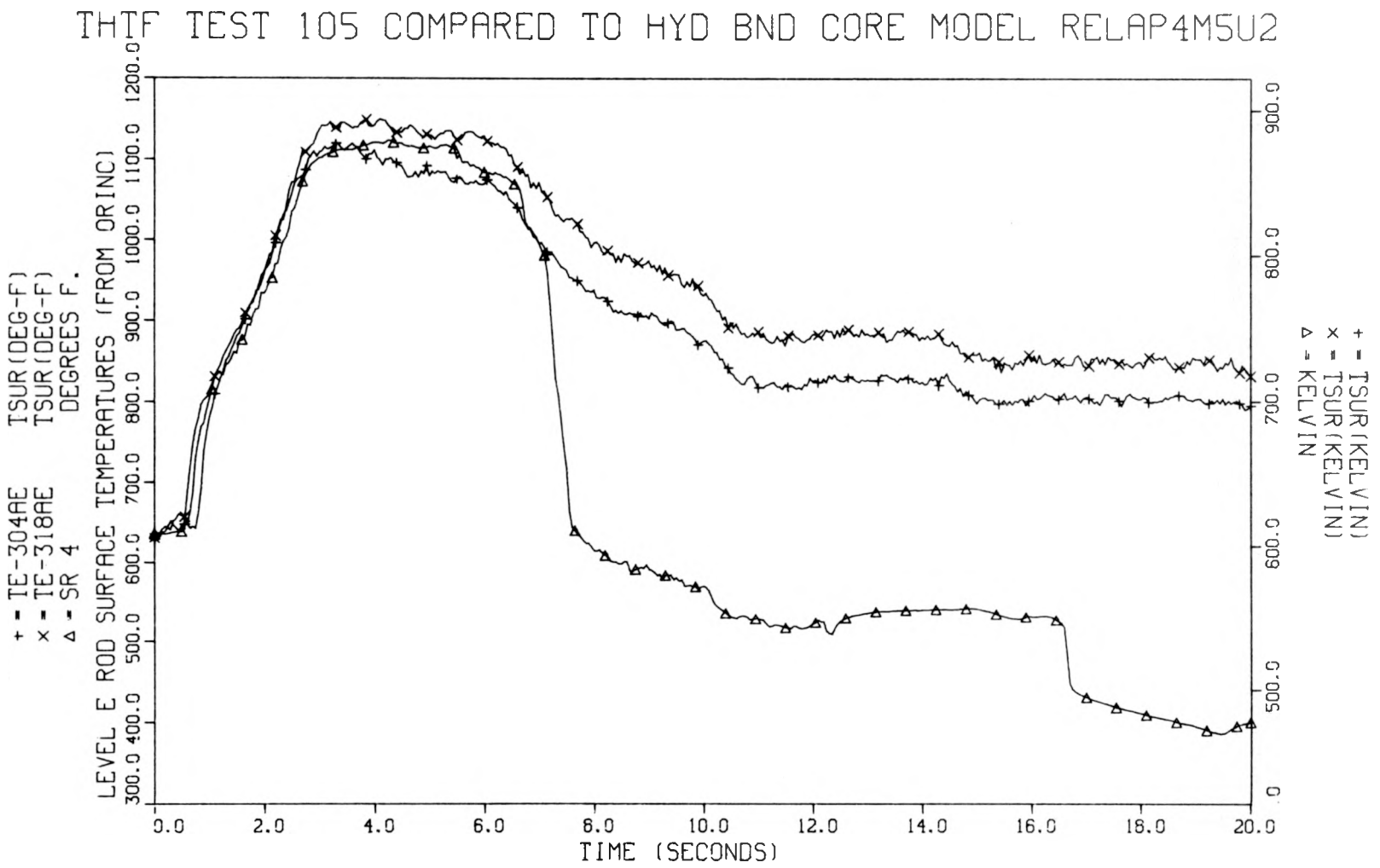

Fig. III.30. Hydraulic bound core slab surface temperature vs ORINC rod surface temperatures — level E, test 105.

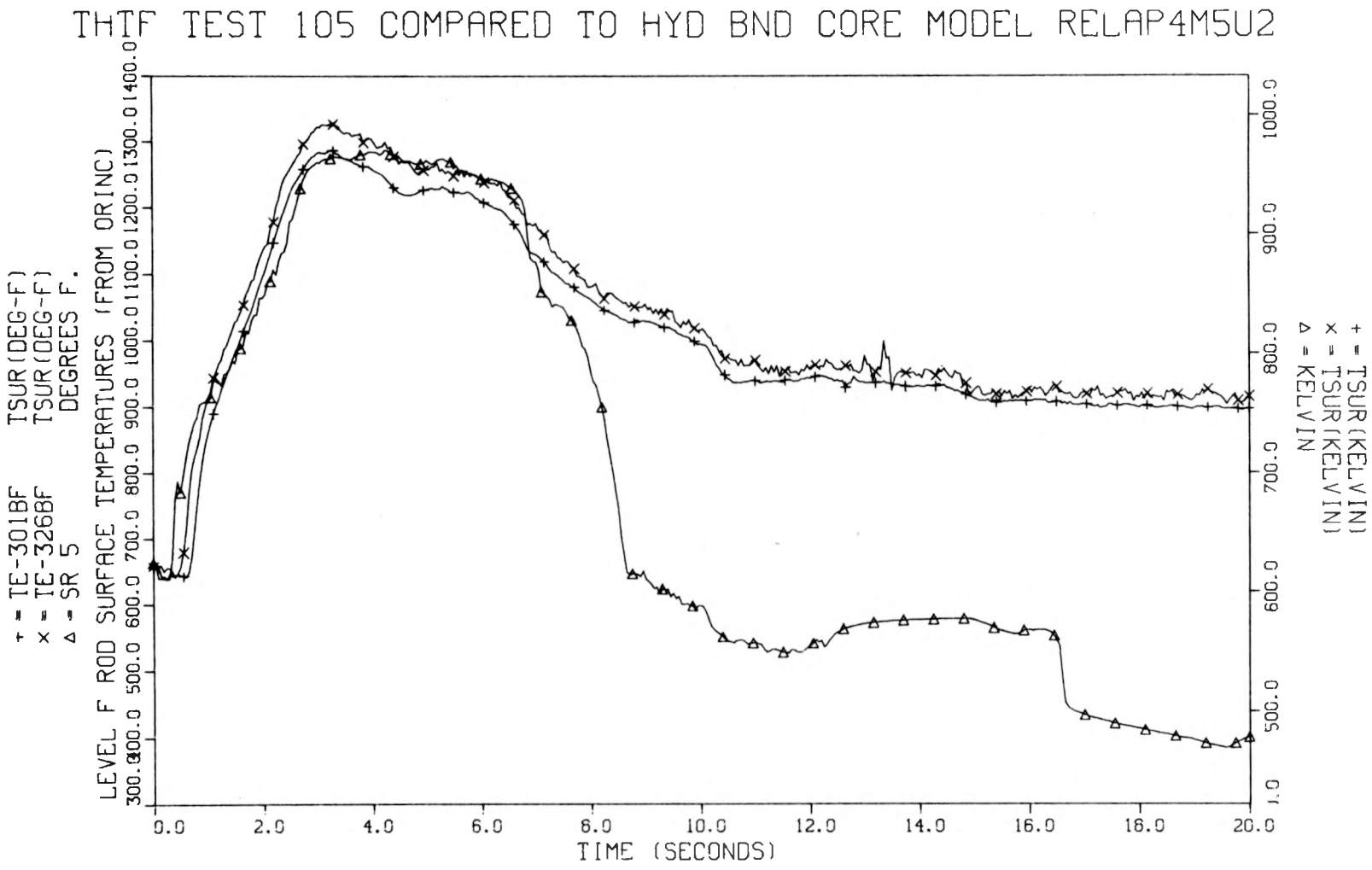

Fig. III.31. Hydraulic bound core slab surface temperature vs ORINC rod surface temperatures — level F, test 105.

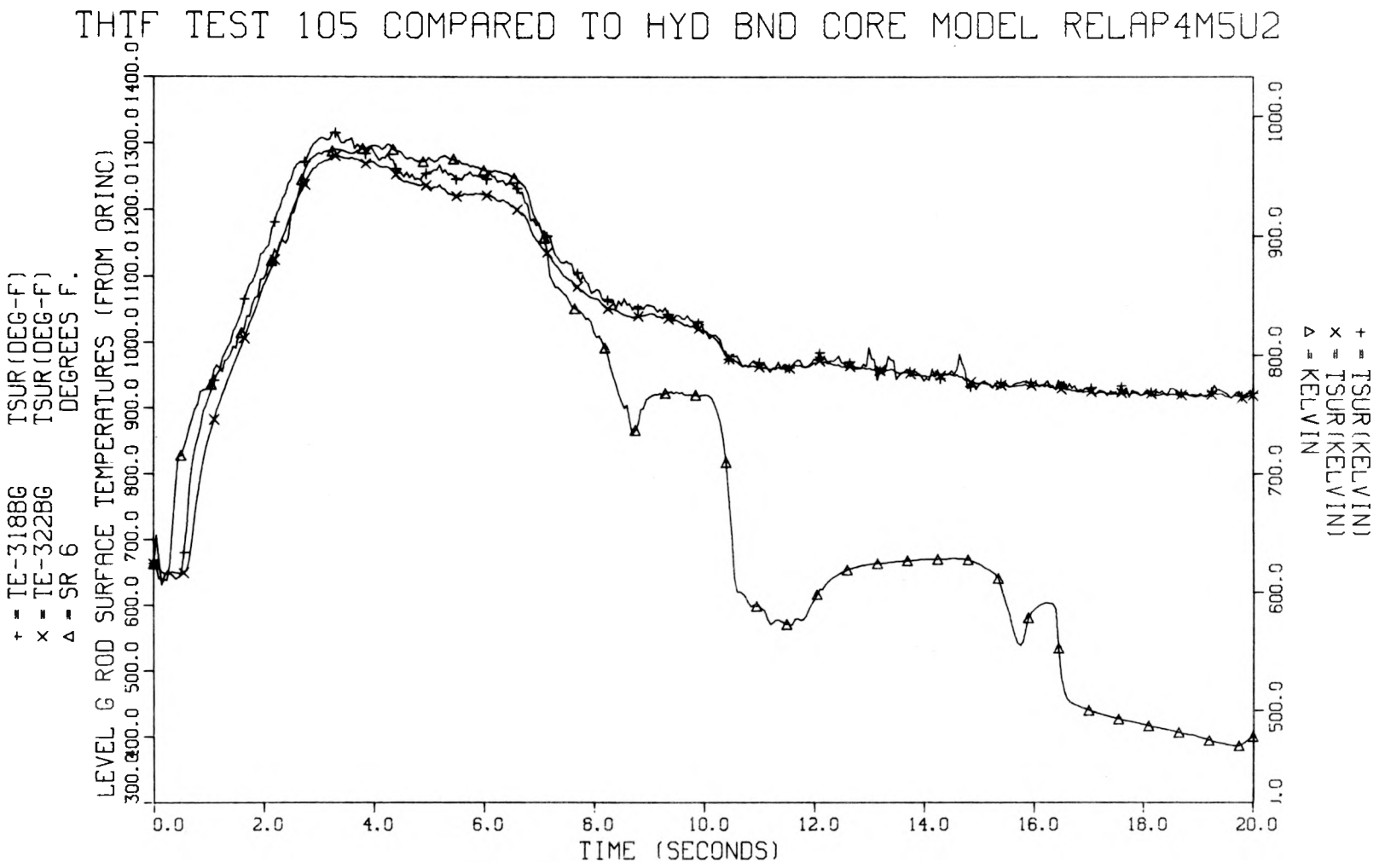

Fig. III.32. Hydraulic bound core slab surface temperature vs ORINC rod surface temperatures — level G, test 105.

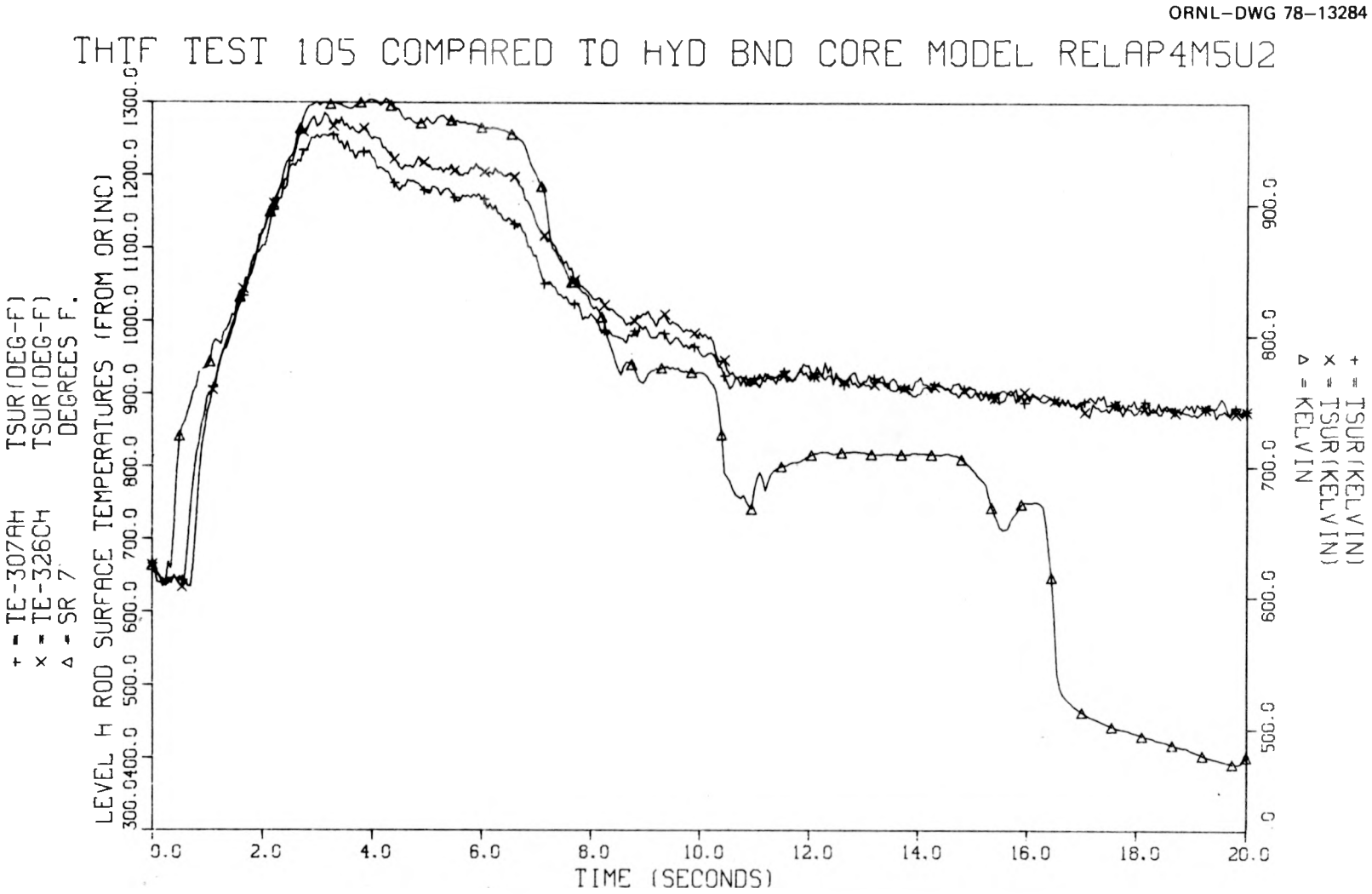

Fig. III.33. Hydraulic bound core slab surface temperature vs ORINC rod surface temperatures — level H, test 105.

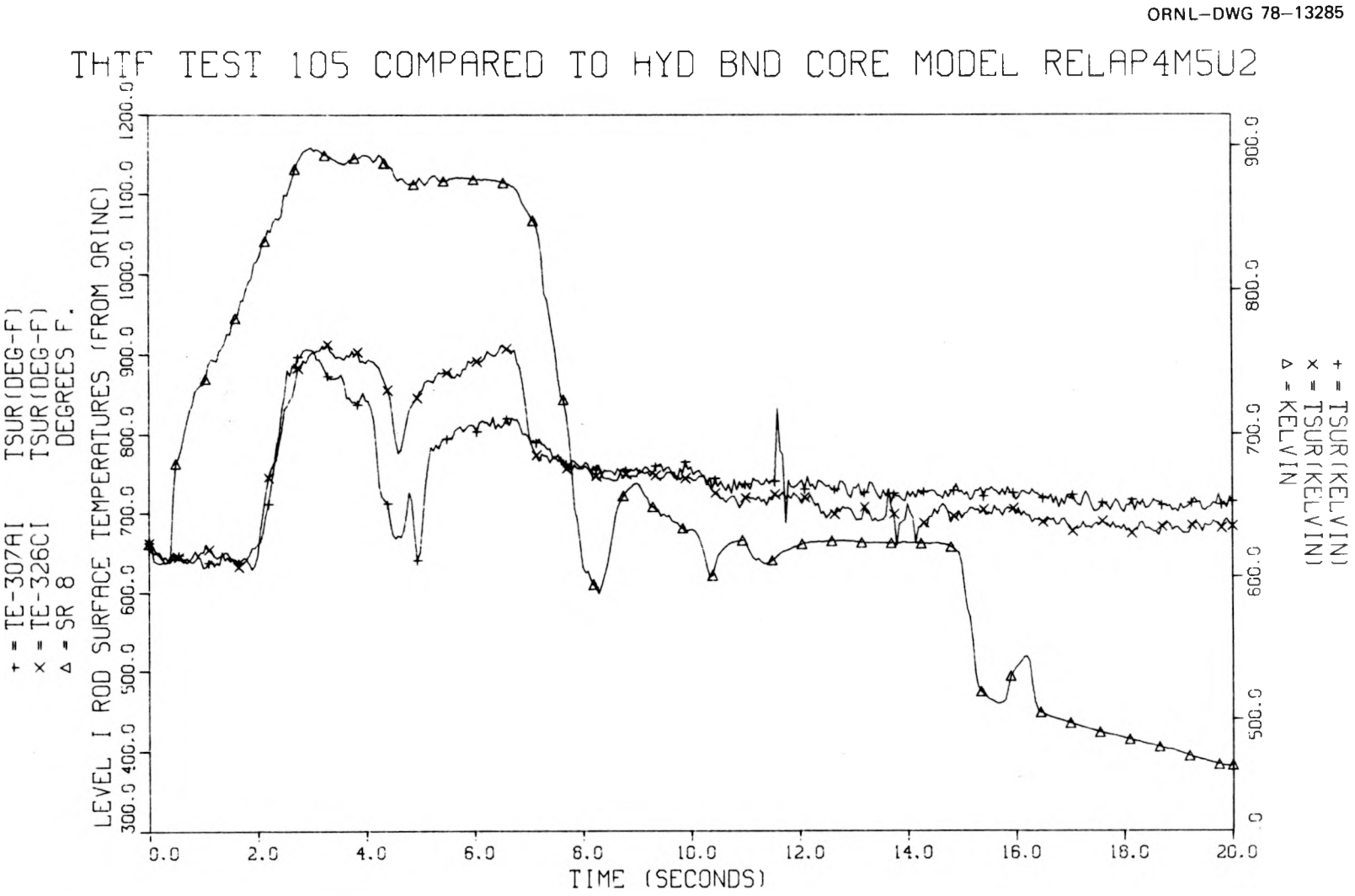

Fig. III.34. Hydraulic bound core slab surface temperature vs ORINC rod surface temperatures — level I, test 105.

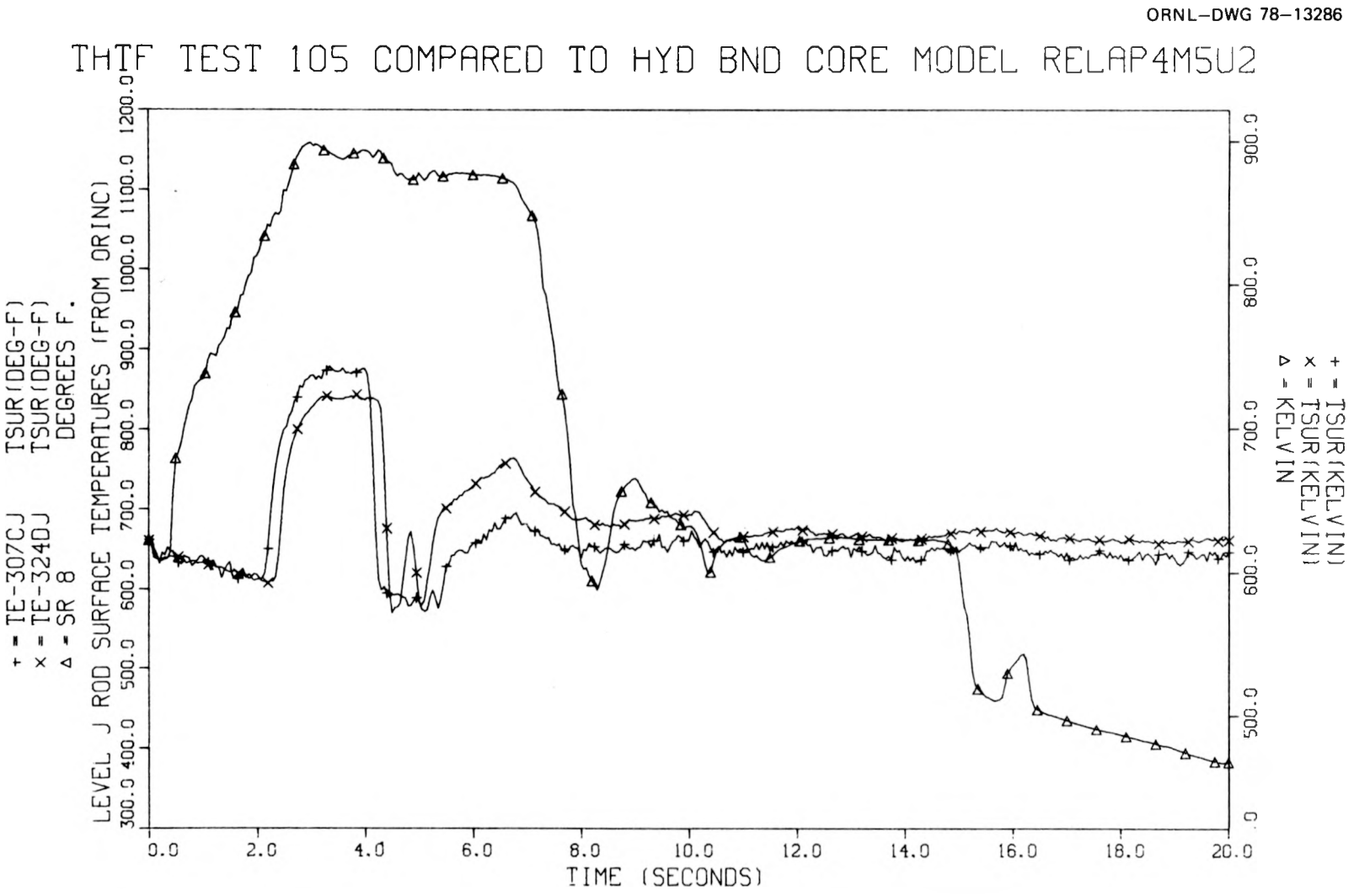

Fig. III.35. Hydraulic bound core slab surface temperature vs ORINC rod surface temperatures — level J, test 105.

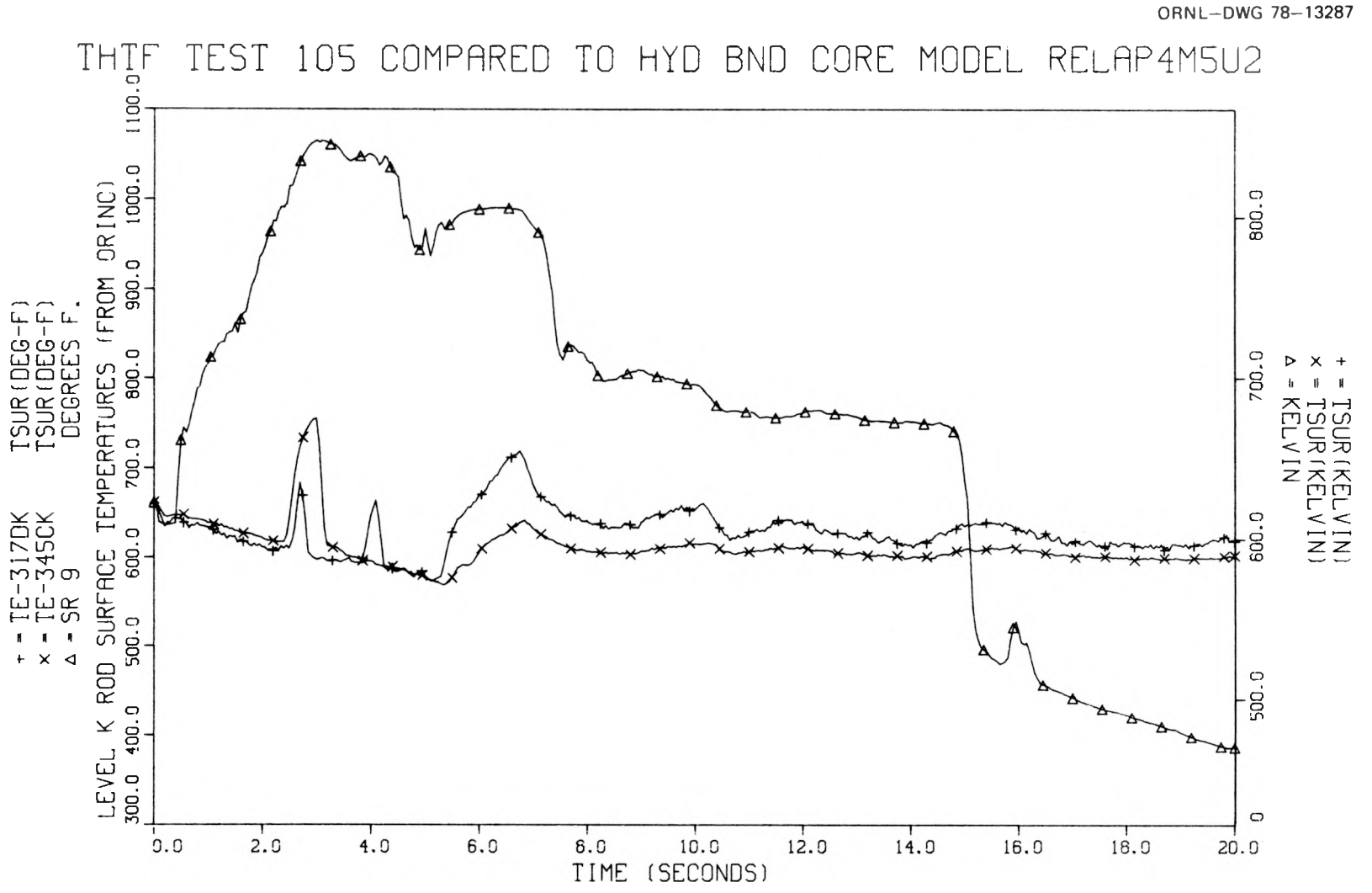

Fig. III.36. Hydraulic bound core slab surface temperature vs ORINC rod surface temperatures — level K, test 105.

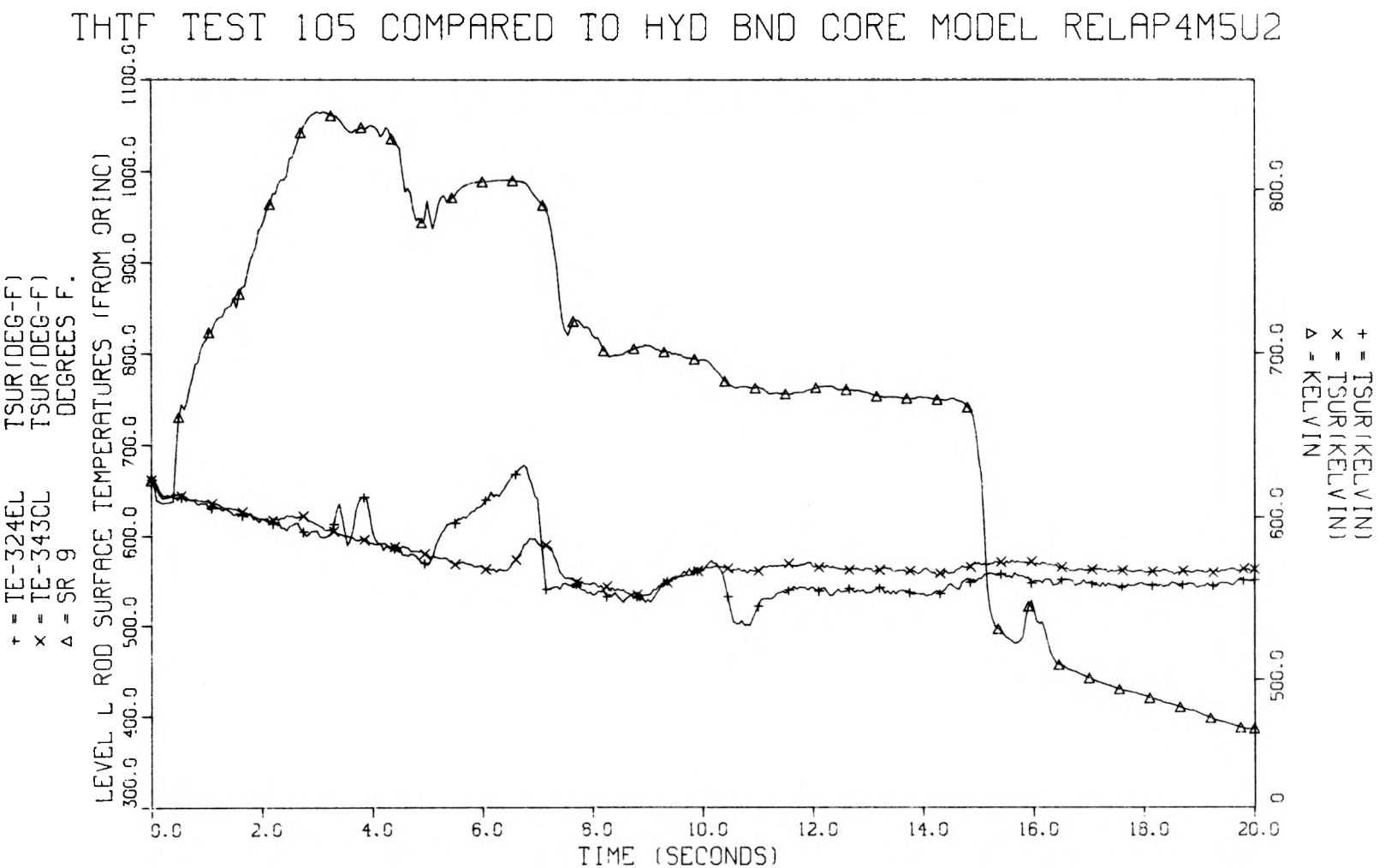

Fig. III.37. Hydraulic bound core slab surface temperature vs ORINC rod surface temperatures — level L, test 105.

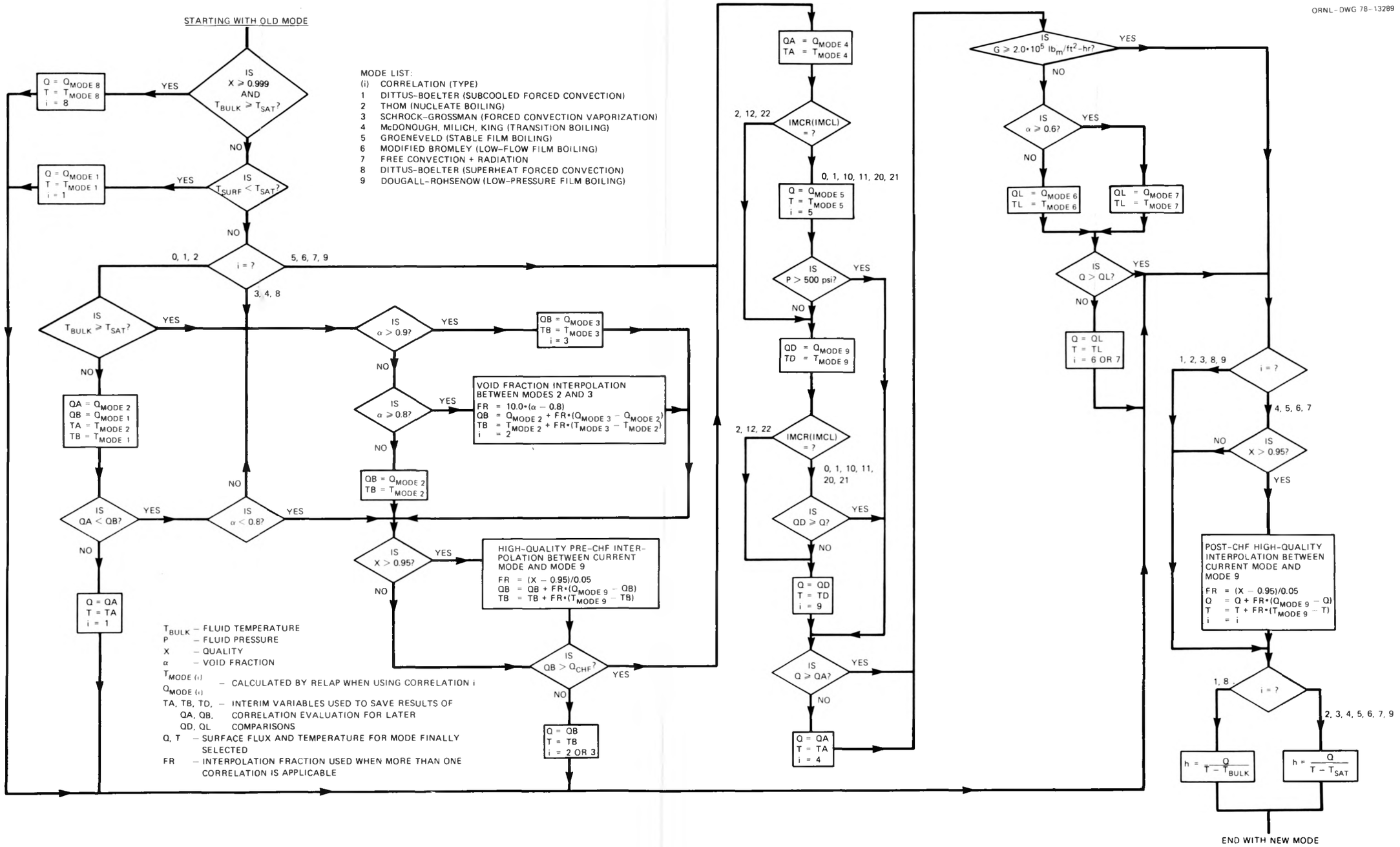

Fig. III.38. RELAP4/M5U2 (minimum controls) heat transfer logic. (See the notes on flow chart for explanation of variables and symbols used. Consult mode list for identification of heat transfer modes and the boiling regime for which the correlation applies.)

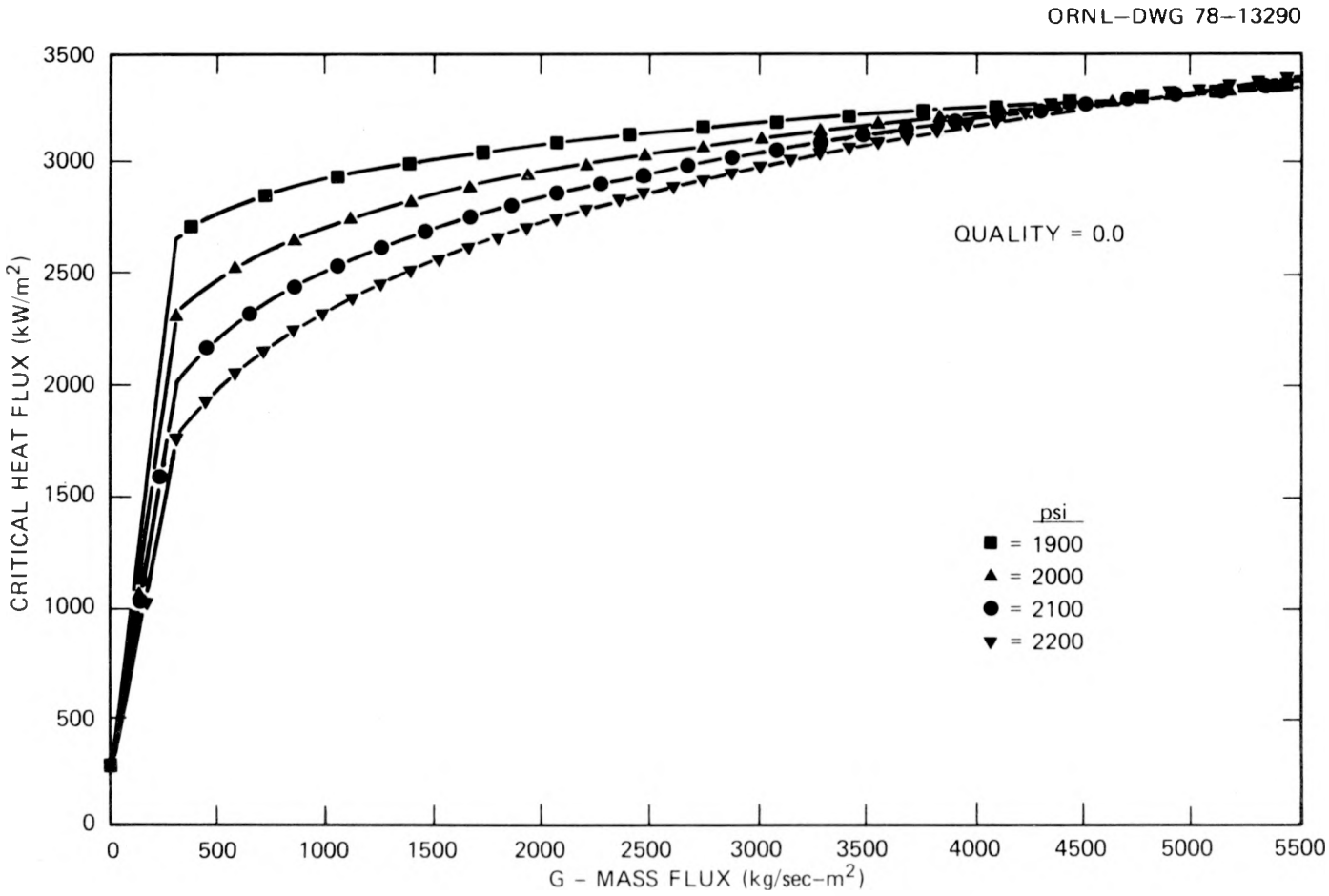

Fig. III.39. Family of pressure curves for RELAP critical heat flux vs mass flux for quality = zero. These curves are a combination of the B&W-2 critical heat flux correlation and linear interpolation between the RELAP minimum critical heat flux and B&W-2 evaluated at 271.10 kg/m^2-s.

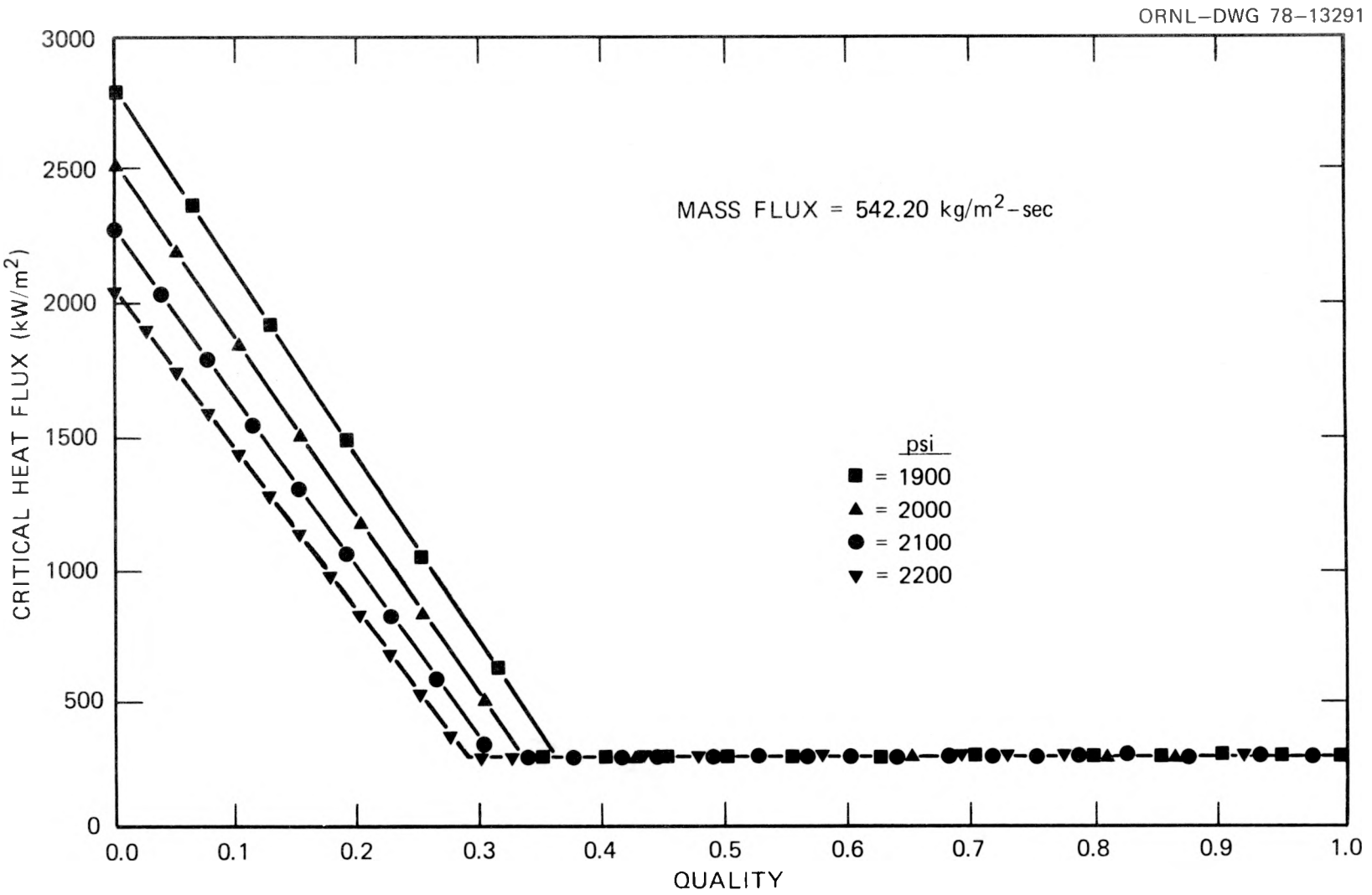

Fig. III.40. Family of pressure curves for RELAP critical heat flux vs quality for mass flux = 542.20 kg/m^2-s. These curves are a combination of the B&W-2 critical heat flux correlation and the RELAP minimum critical heat flux.

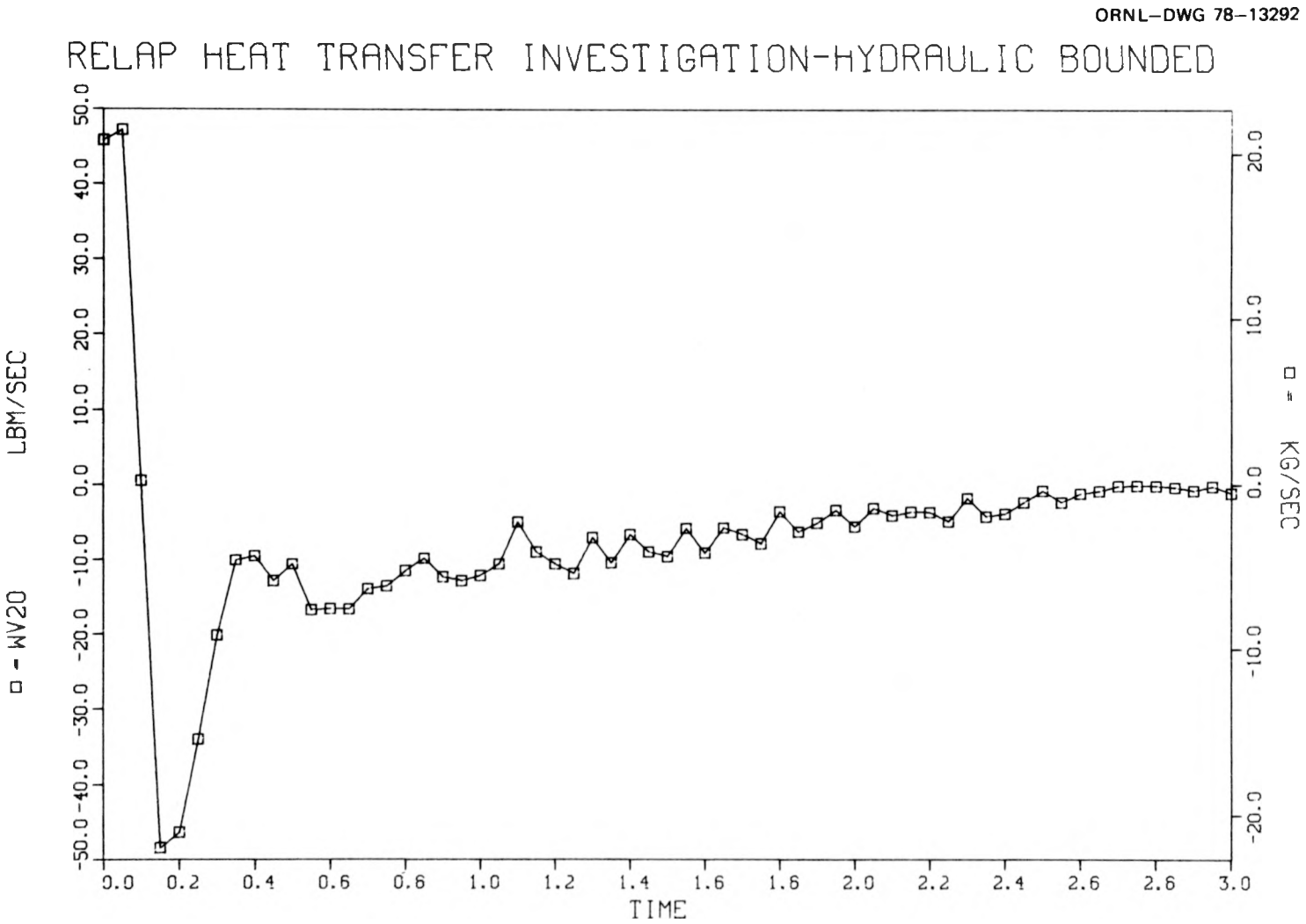

Fig. III.41. Average mass flow volume 20 vs time for hydraulic bound test section model — test 105.

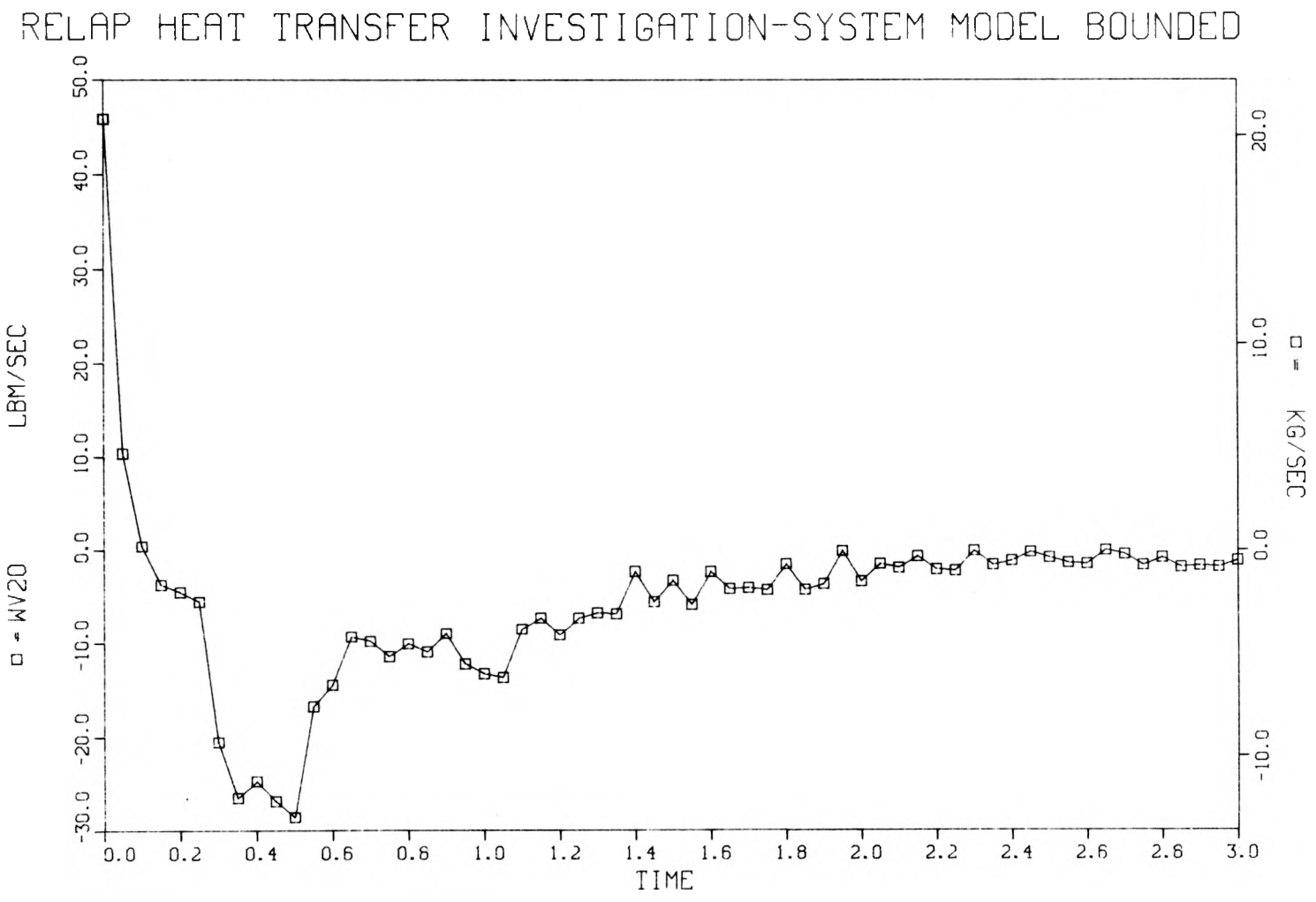

Fig. III.42. Average mass flow volume 20 vs time for system model bound test section model — test 105.

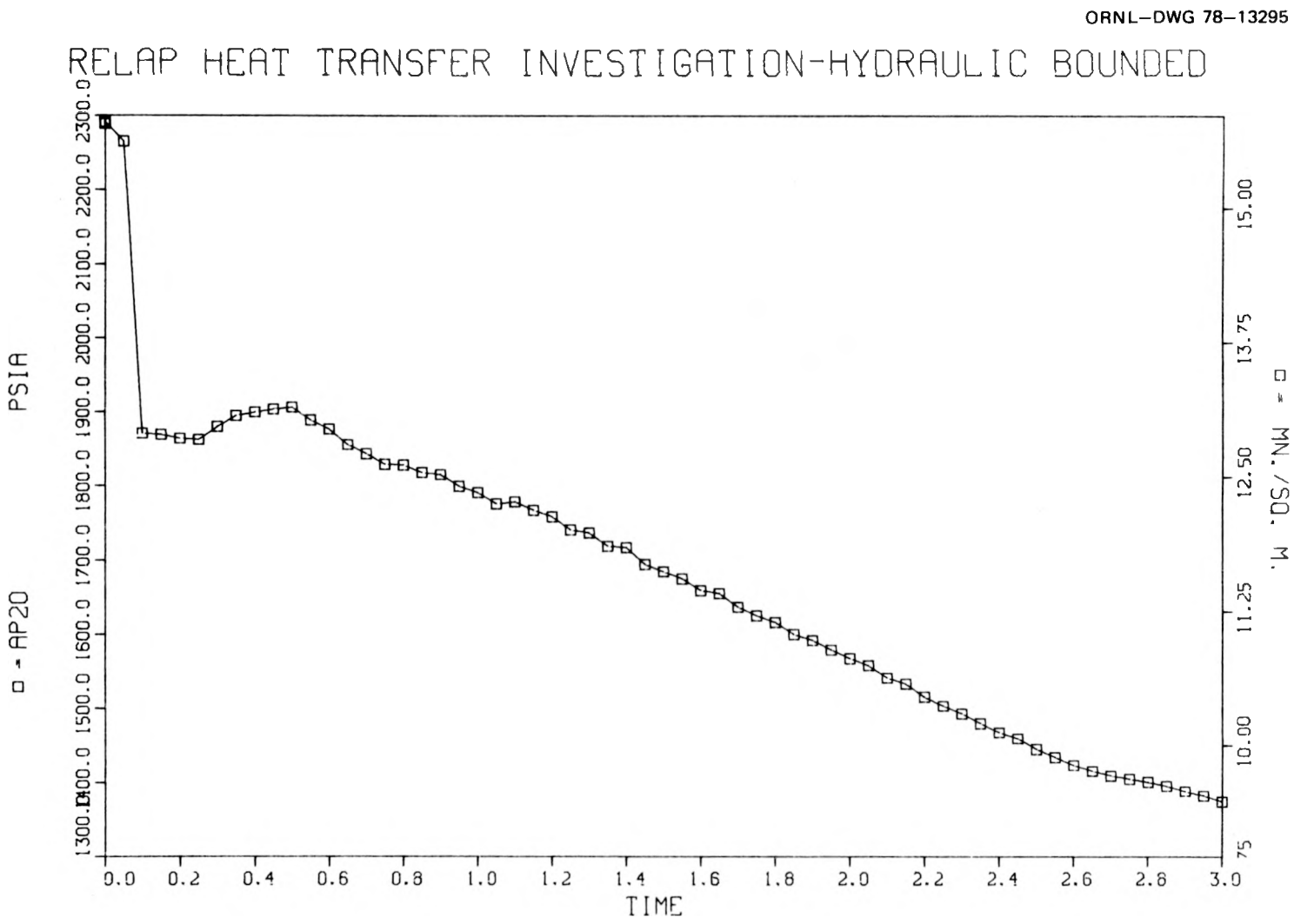

Fig. III.43. Average pressure volume 20 vs time for hydraulic bound test section model — test 105.

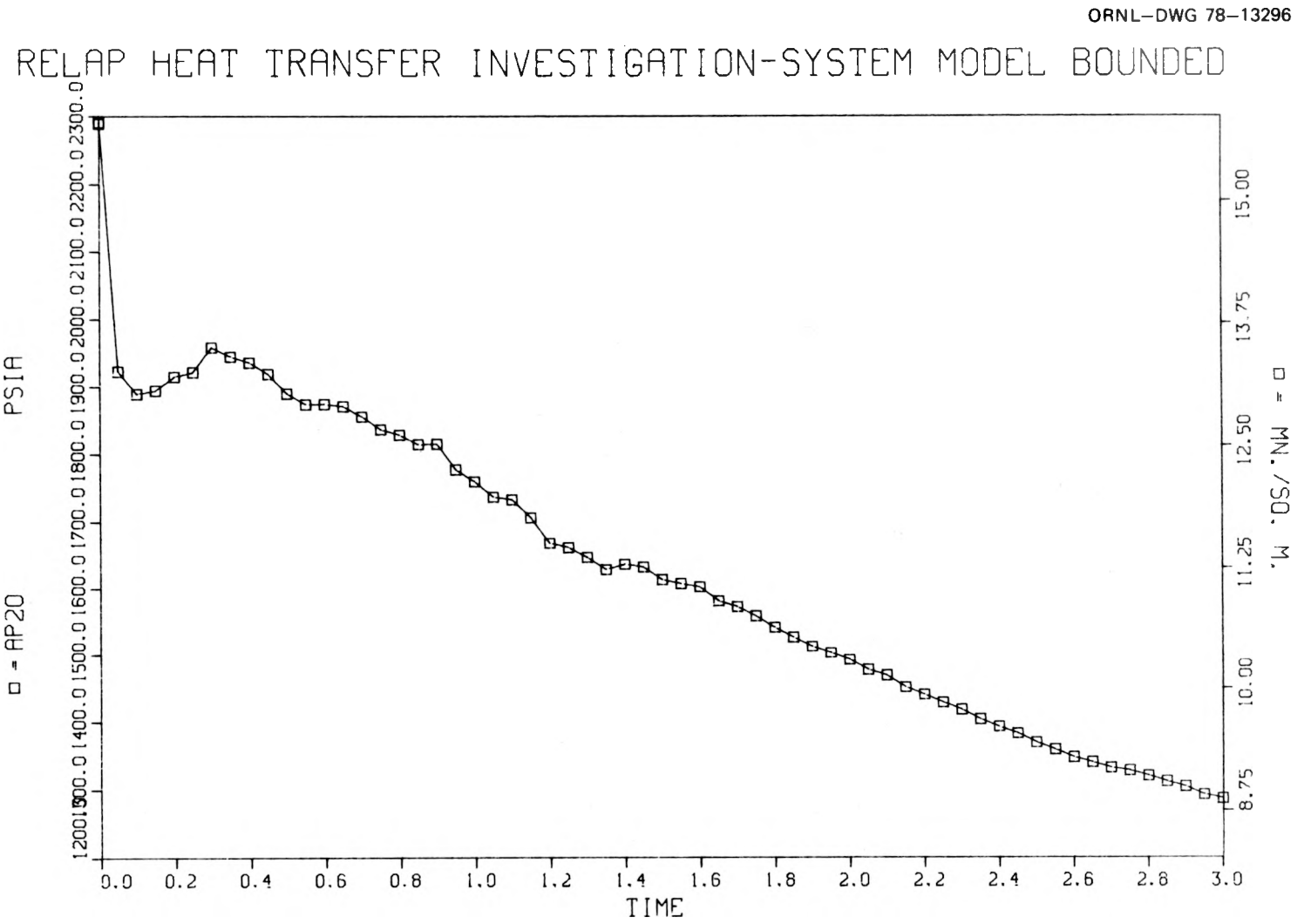

Fig. III.44. Average pressure volume 20 vs time for system model bound test section model — test 105.

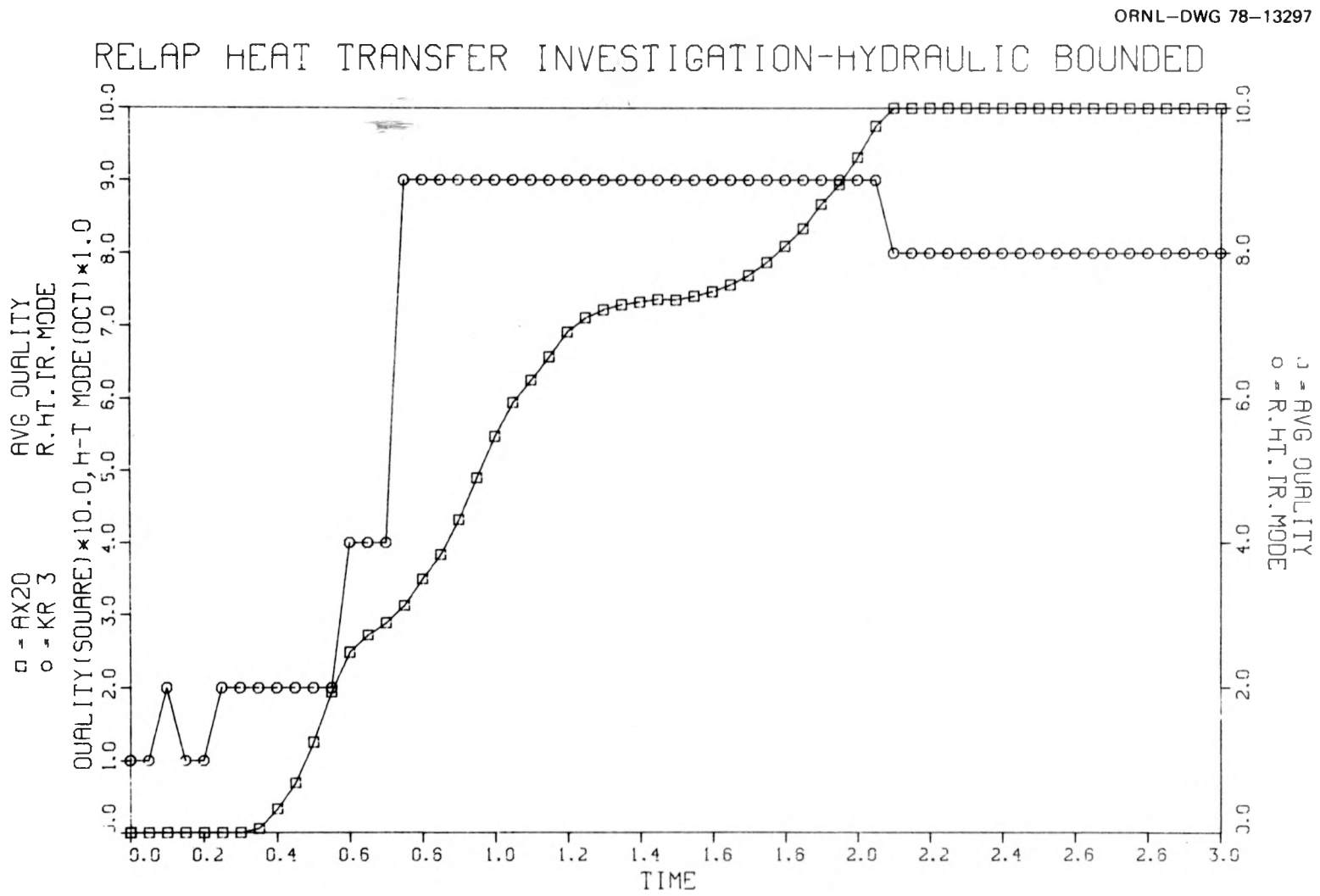

Fig. III.45. Quality and heat transfer mode associated with slab 3 vs time — hydraulic bound test section model — test 105.

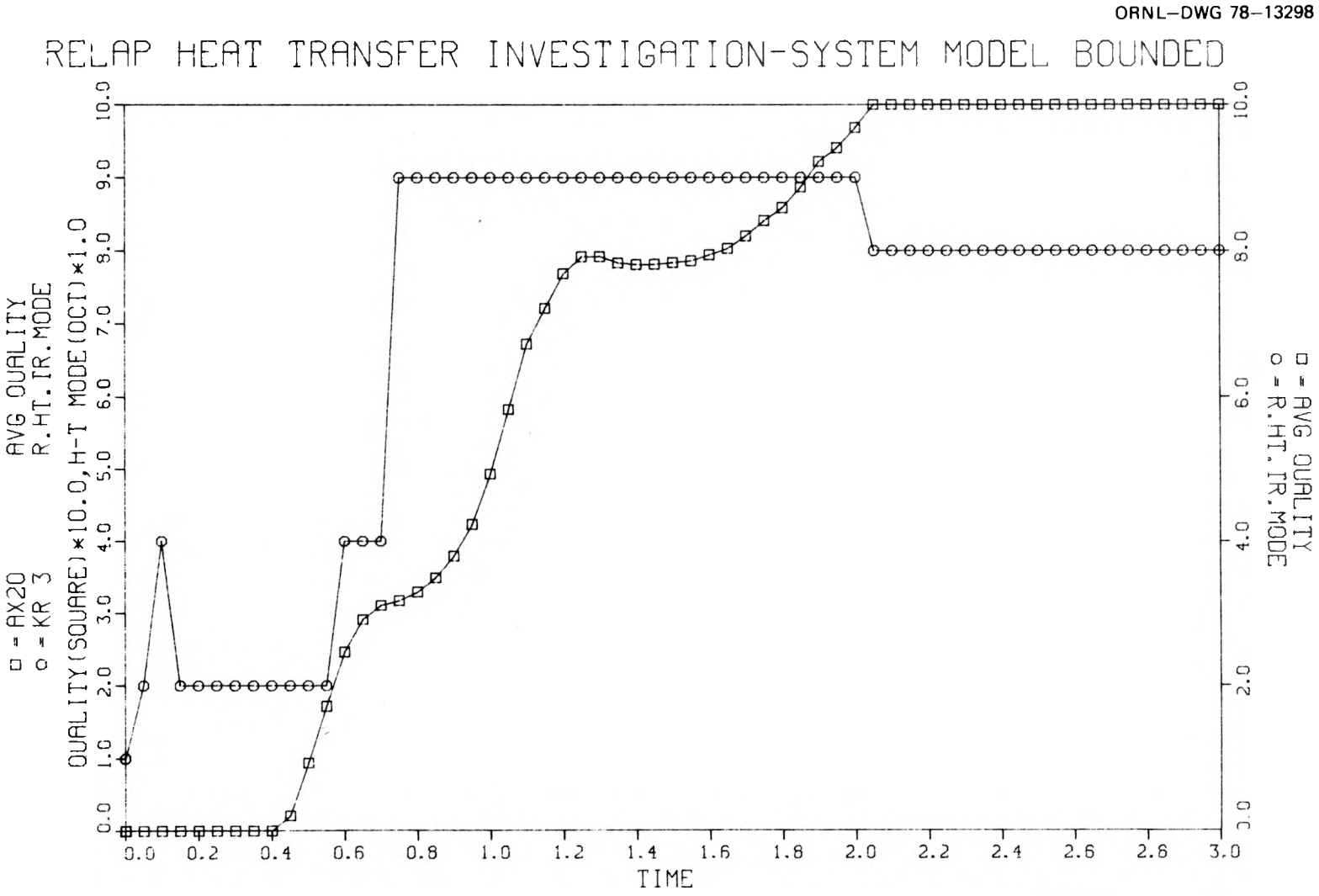

Fig. III.46. Quality and heat transfer mode associated with slab 3 vs time — system model bound test section model — test 105.

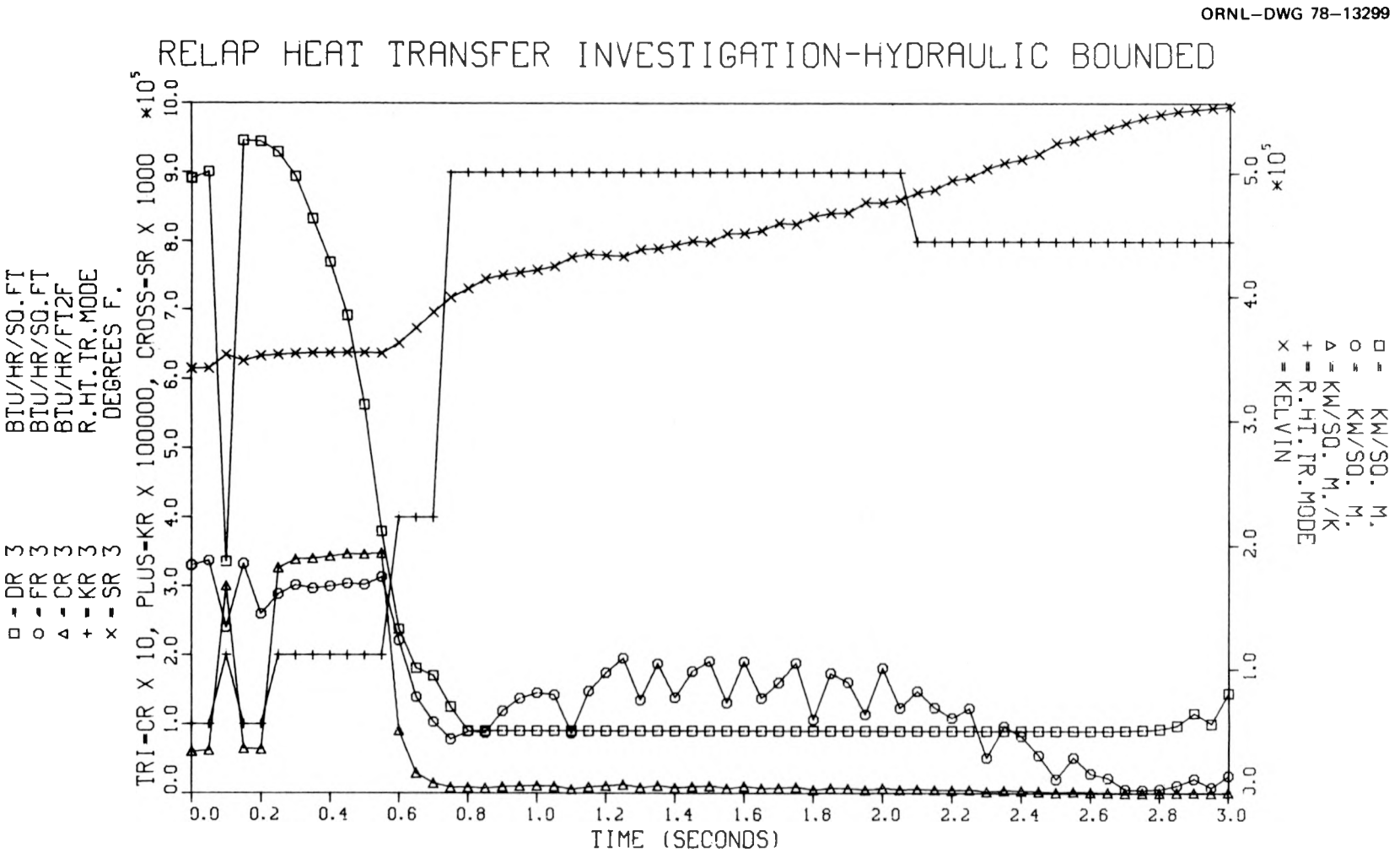

Fig. III.47. Critical heat flux, heat flux, heat transfer coefficient, heat transfer mode, and surface temperature for slab 3 vs time for hydraulic bound test section model — test 105.

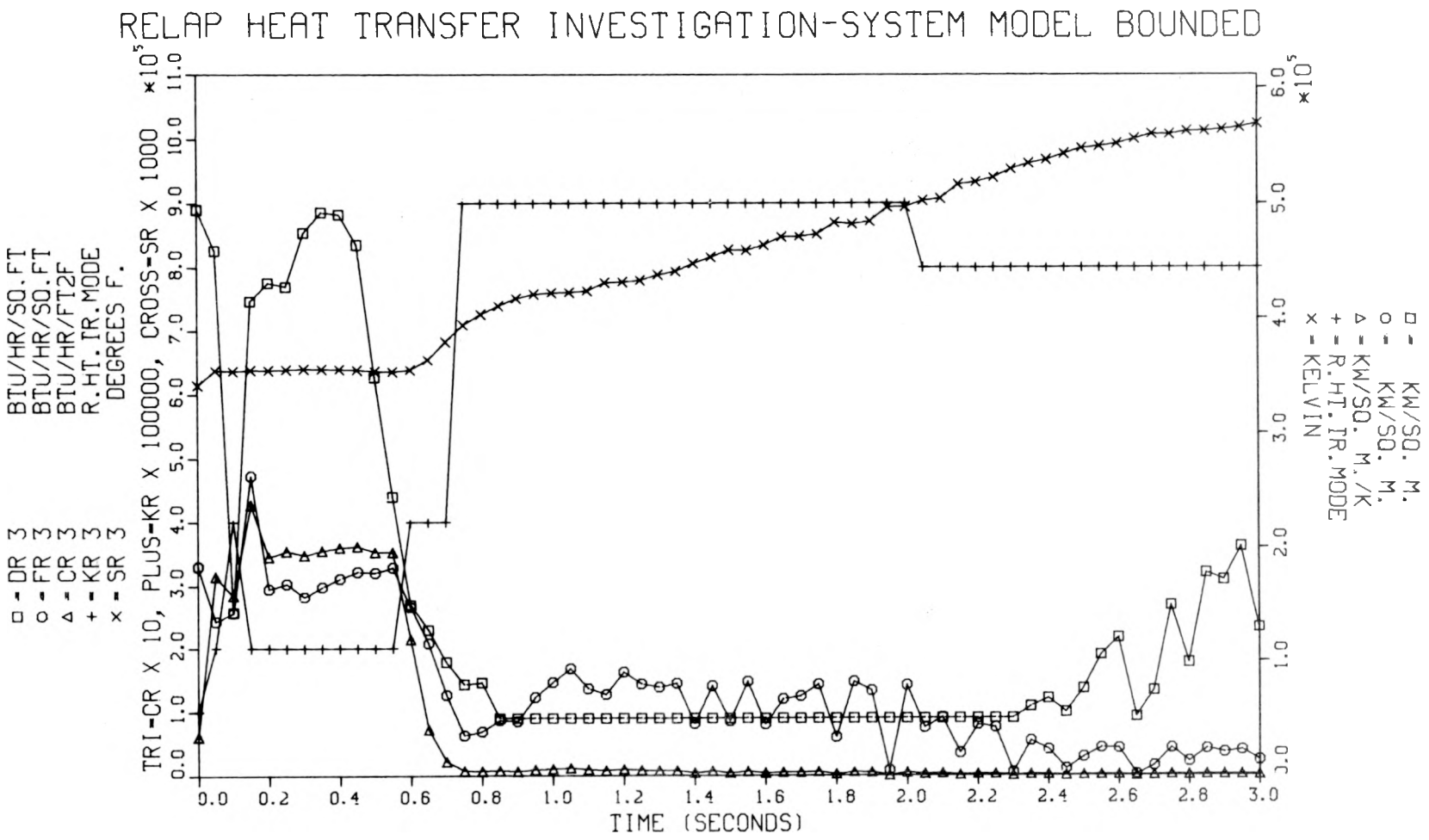

Fig. III.48. Critical heat flux, heat flux, heat transfer coefficient, heat transfer mode, and surface temperature for slab 3 vs time for system model bound test section model — test 105.

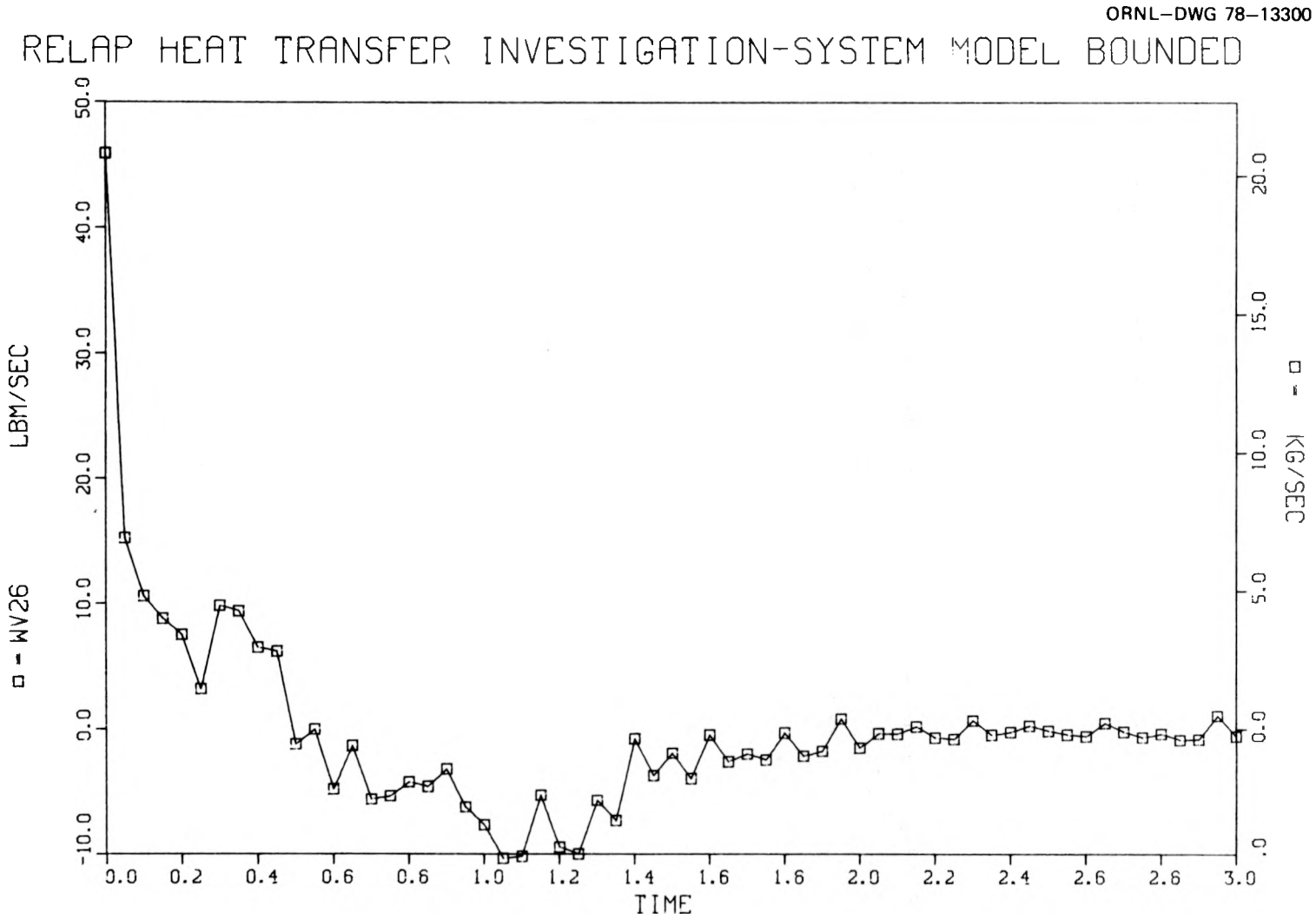

Fig. III.49. Average mass flow volume 26 vs time for system model bound test section model — test 105.

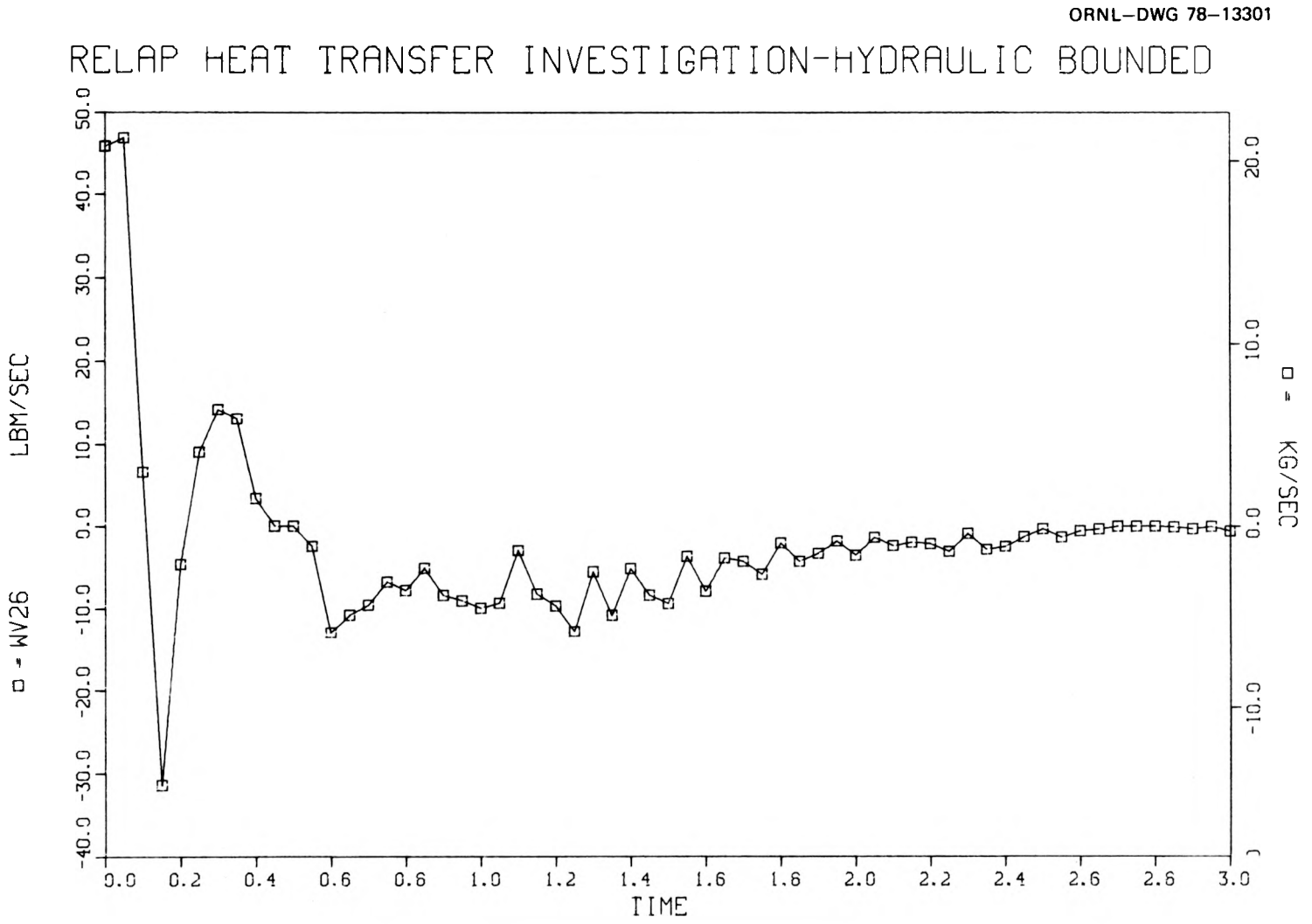

Fig. III.50. Average mass flow volume 26 vs time for hydraulic bound test section model — test 105.

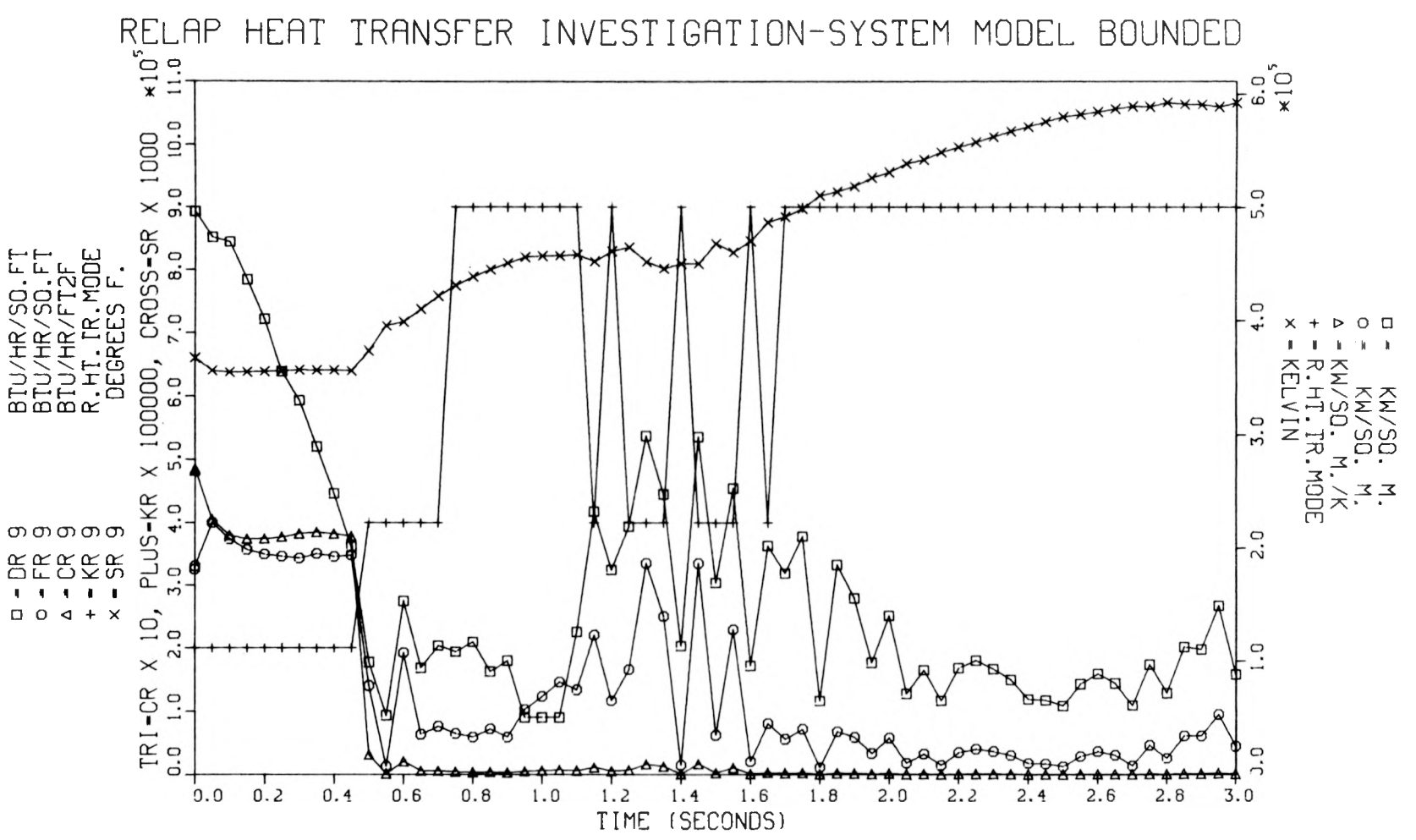

Fig. III.51. Critical heat flux, heat flux, heat transfer coefficient, heat transfer mode, and surface temperature for slab 9 vs time for system model bound test section model — test 105.

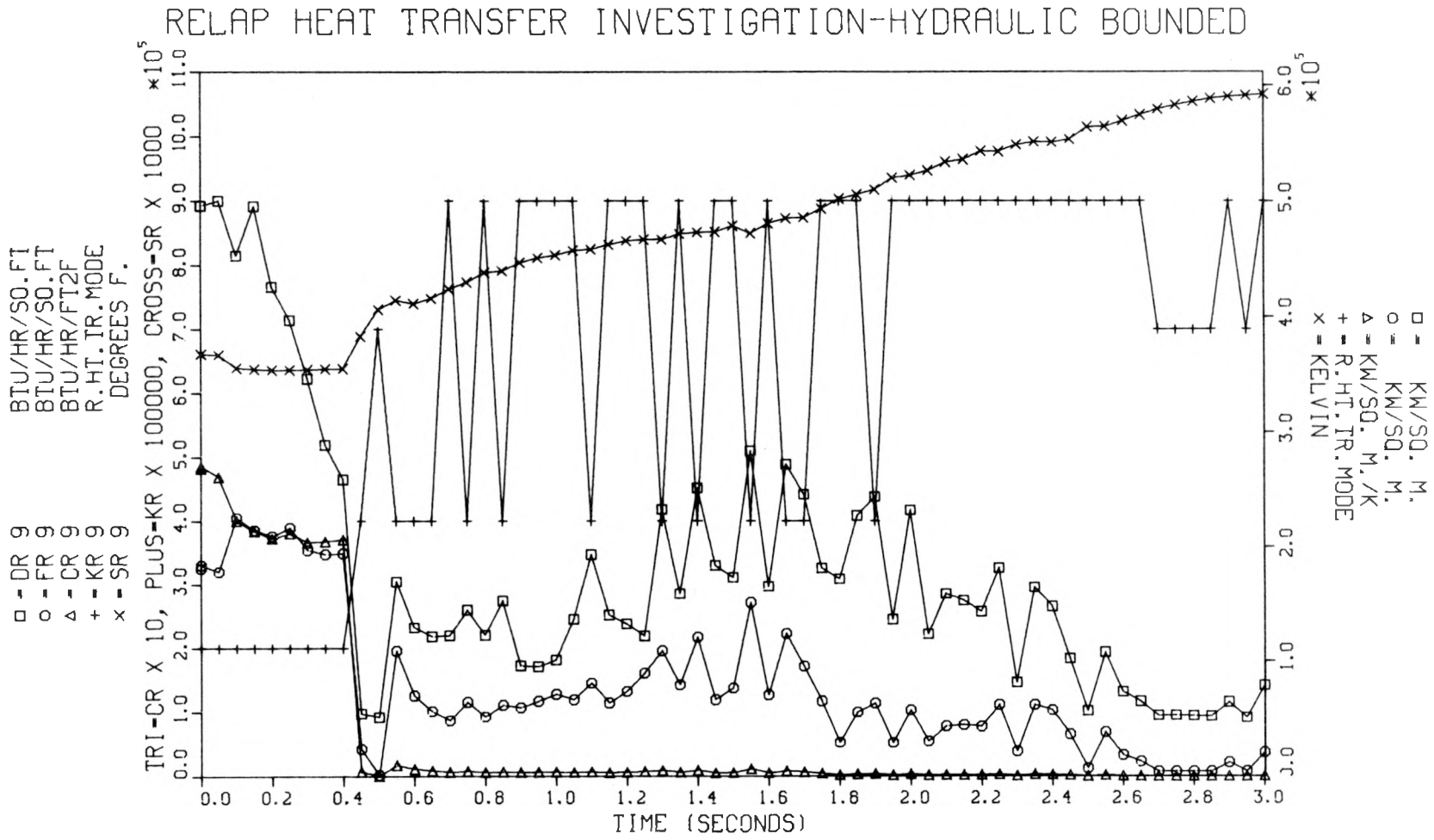

Fig. III.52. Critical heat flux, heat flux, heat transfer coefficient, heat transfer mode, and surface temperature for slab 9 vs time for hydraulic bound test section model — test 105.

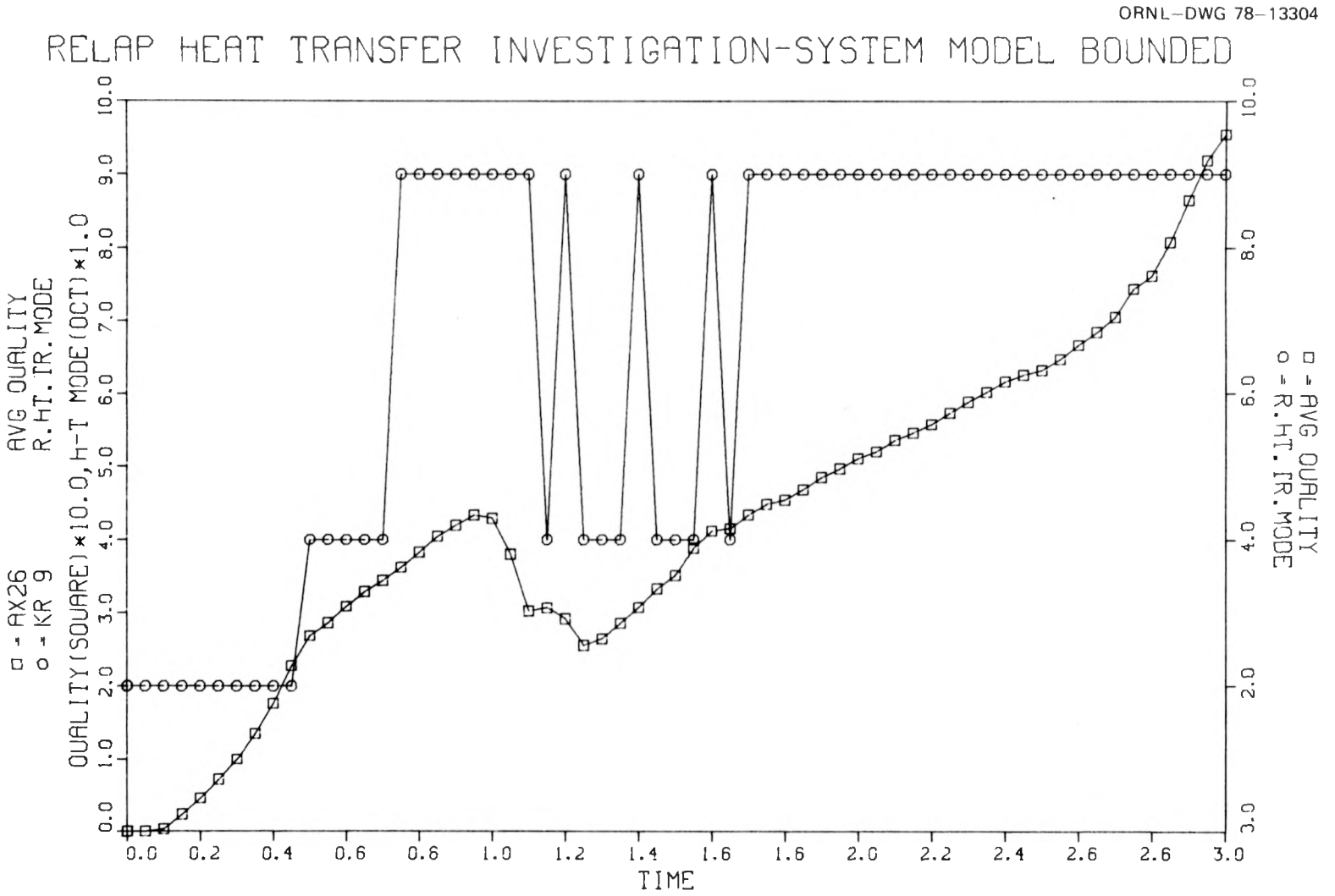

Fig. III.53. Quality and heat transfer mode associated with slab 9 vs time — system model bound test section model — test 105.

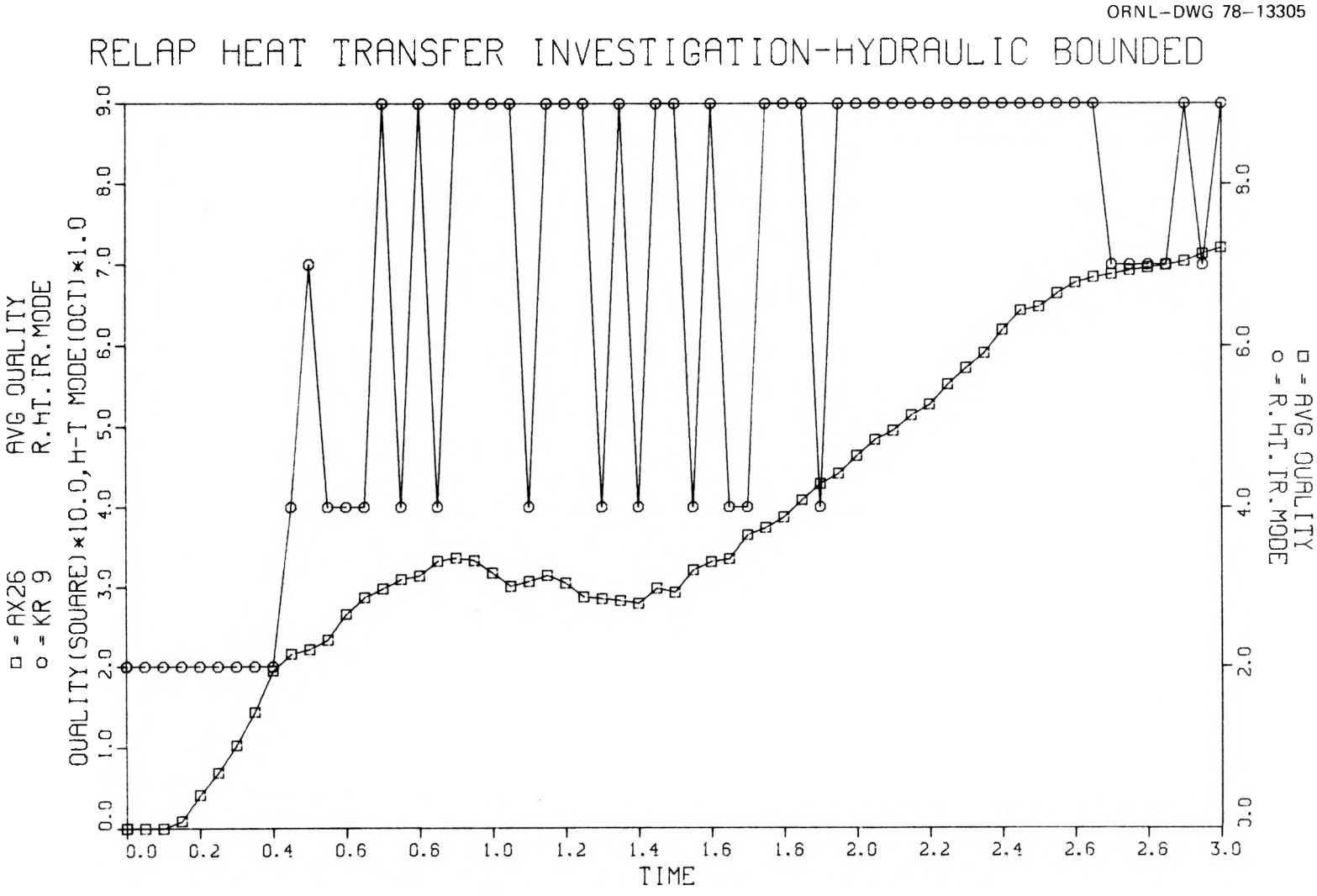

Fig. III.54. Quality and heat transfer mode associated with slab 9 vs time — hydraulic bound test section model — test 105.

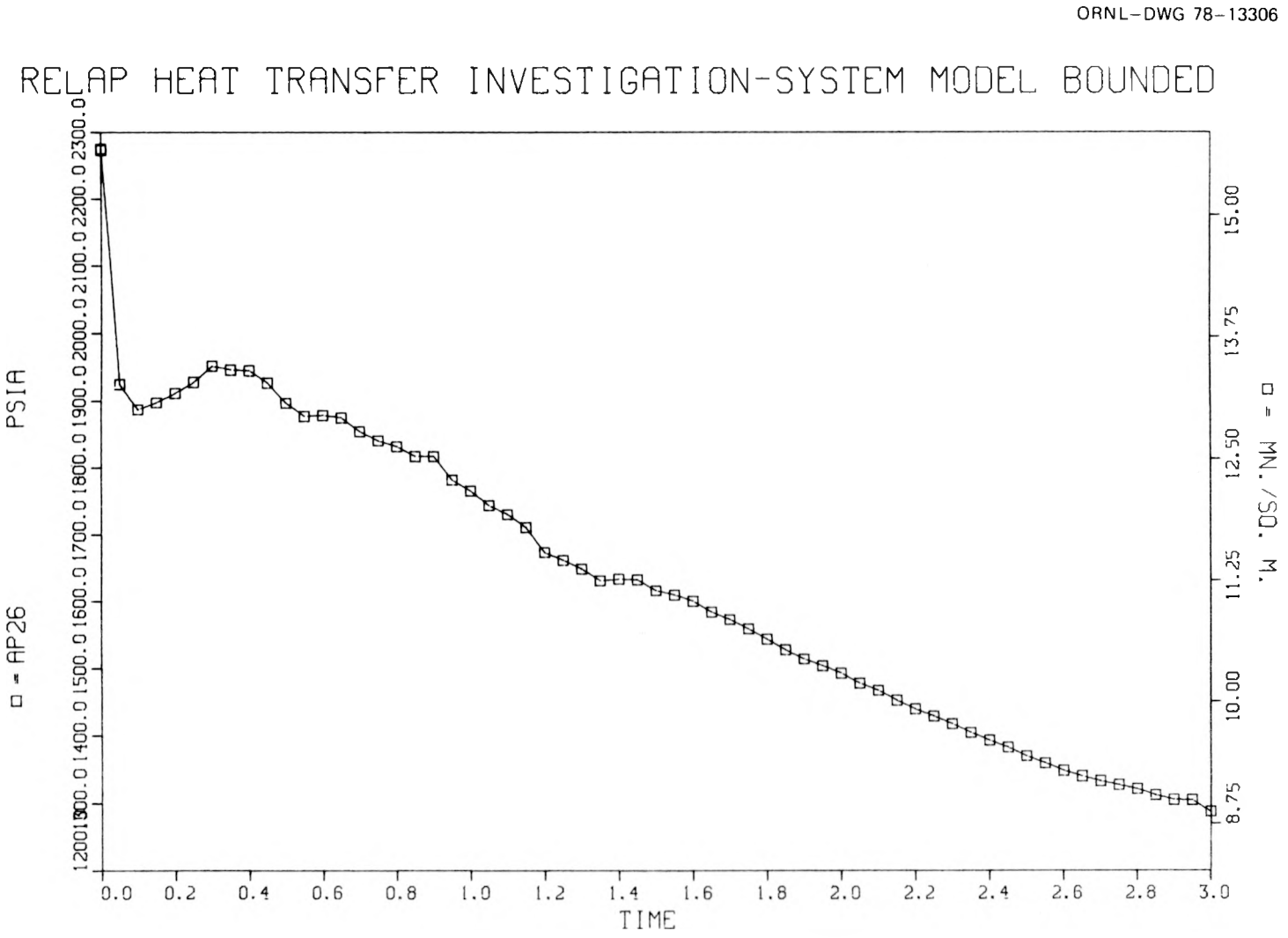

Fig. III.55. Average pressure volume 26 vs time for system model bound test section model — test 105.

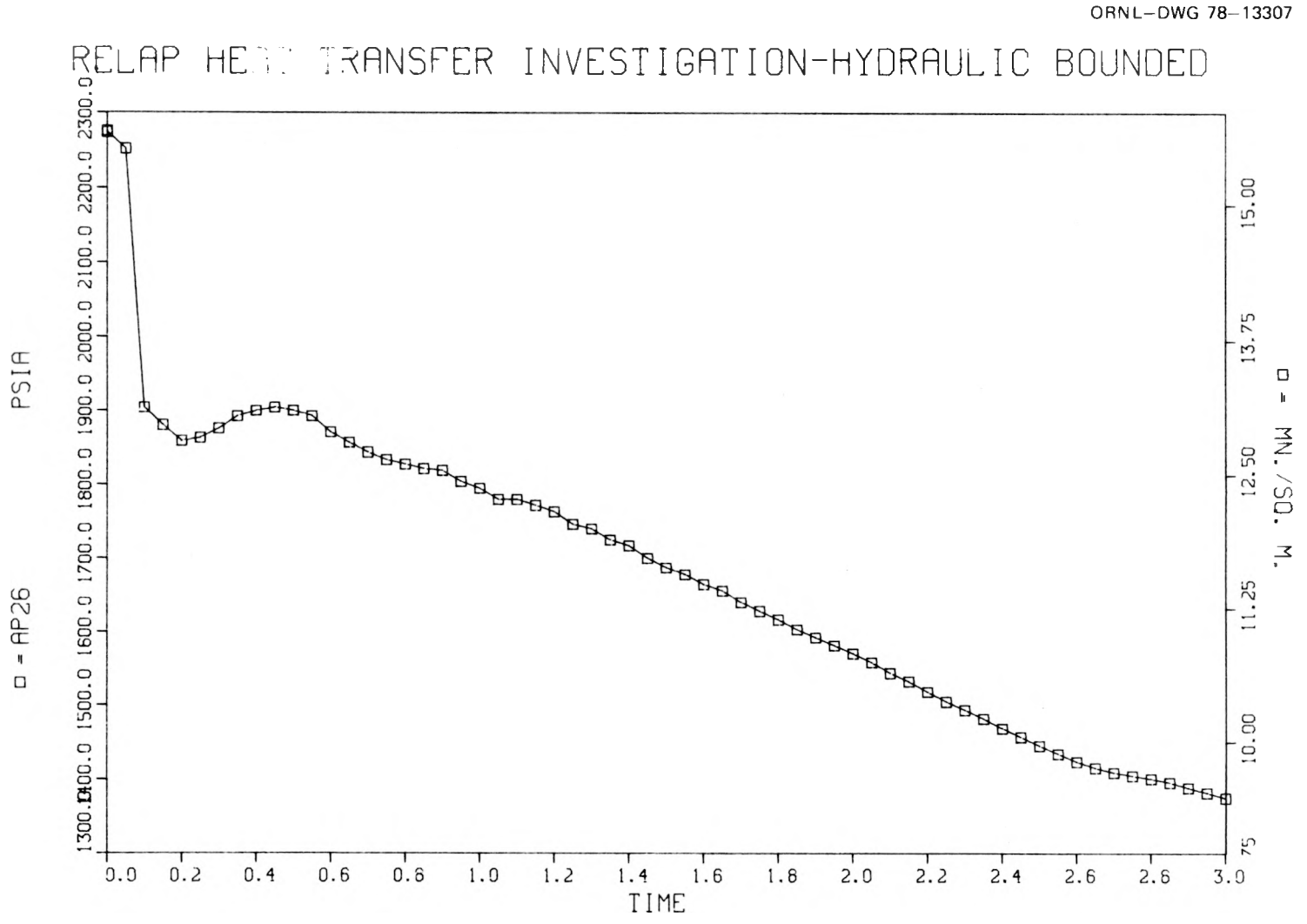

Fig. III.56. Average pressure volume 26 vs time for hydraulic bound test section model — test 105.

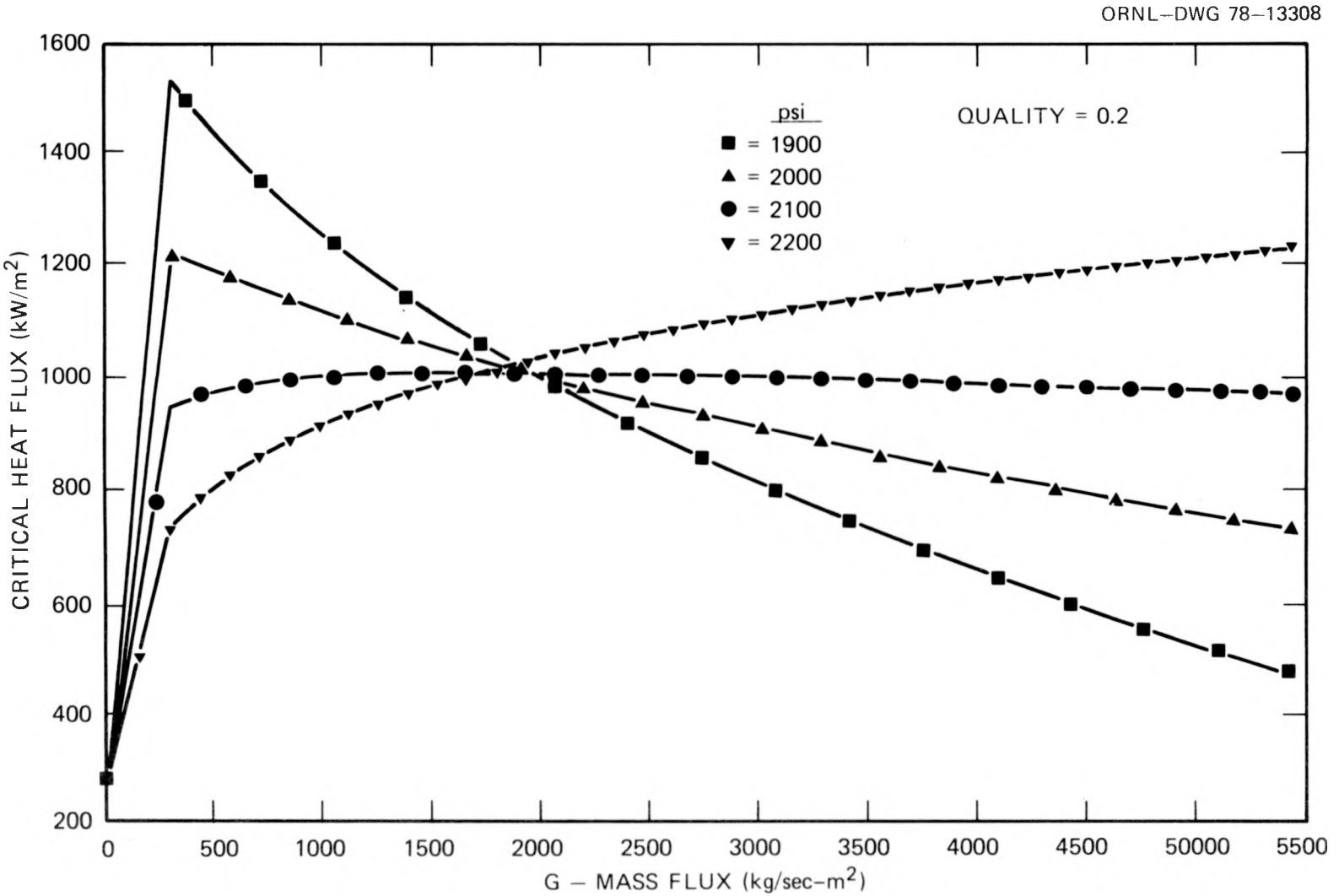

Fig. III.57. Family of pressure curves for RELAP critical heat flux vs mass flux for quality = 0.2. These curves are a combination of the B&W-2 critical heat flux correlation and linear interpolation between the RELAP minimum critical heat flux and B&W-2 evaluated at 271.10 kg/m^2-s.

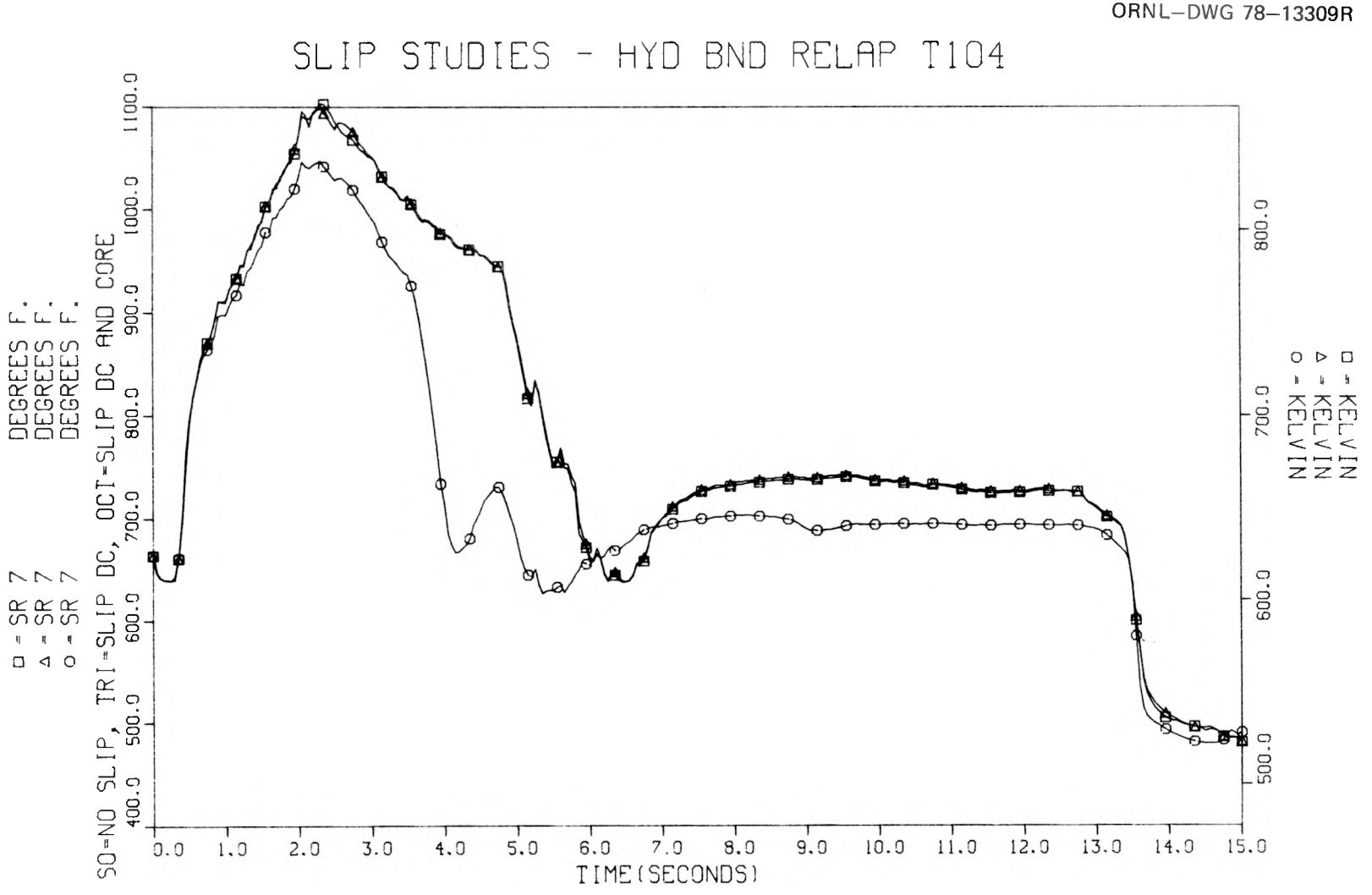

Fig. III.58. Slab 7 surface temperature vs time for various slip combinations for hydraulic bound test section model — test 104.

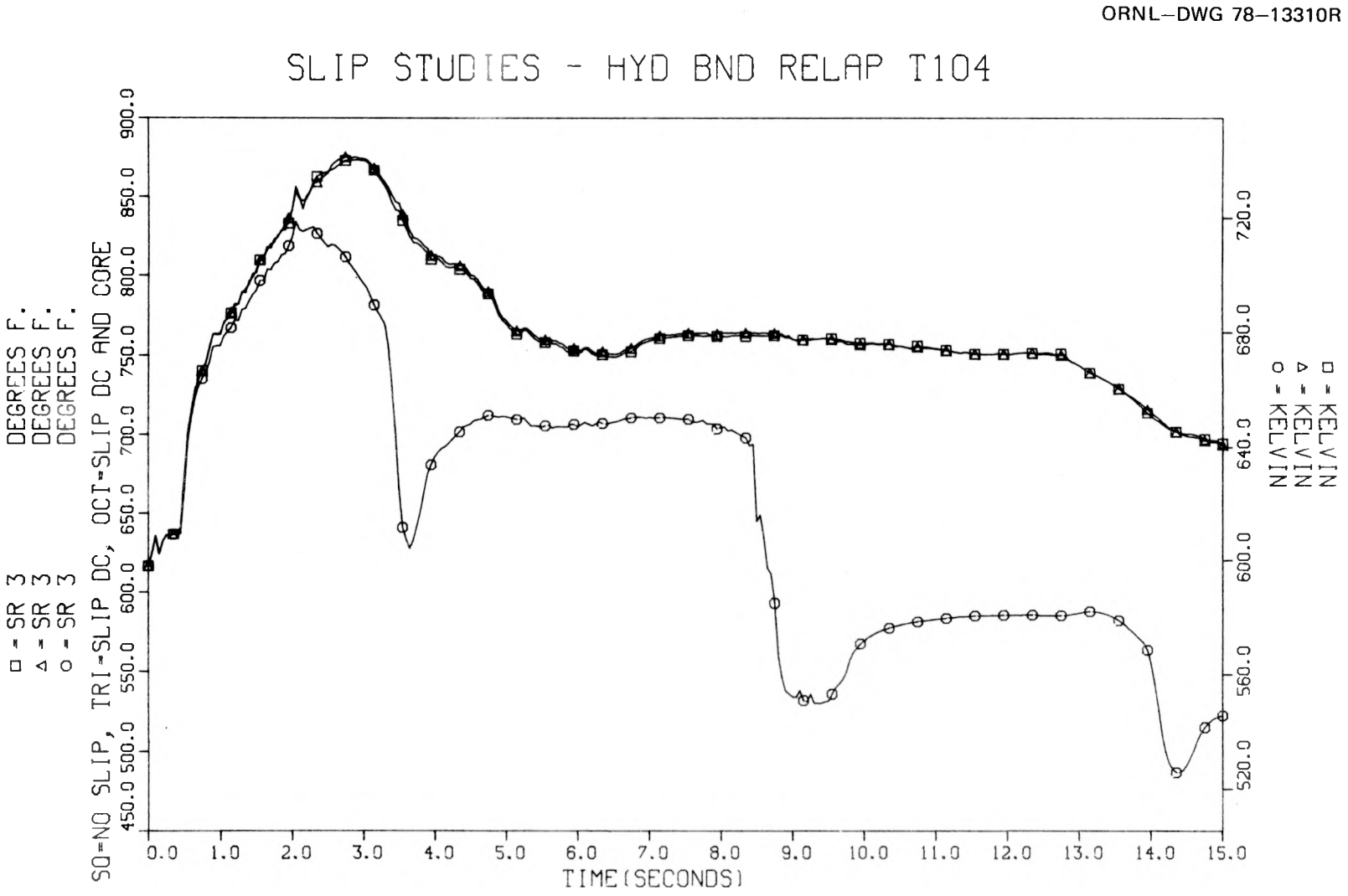

Fig. III.59. Slab 3 surface temperature vs time for various slip combinations for hydraulic bound test section model — test 104.

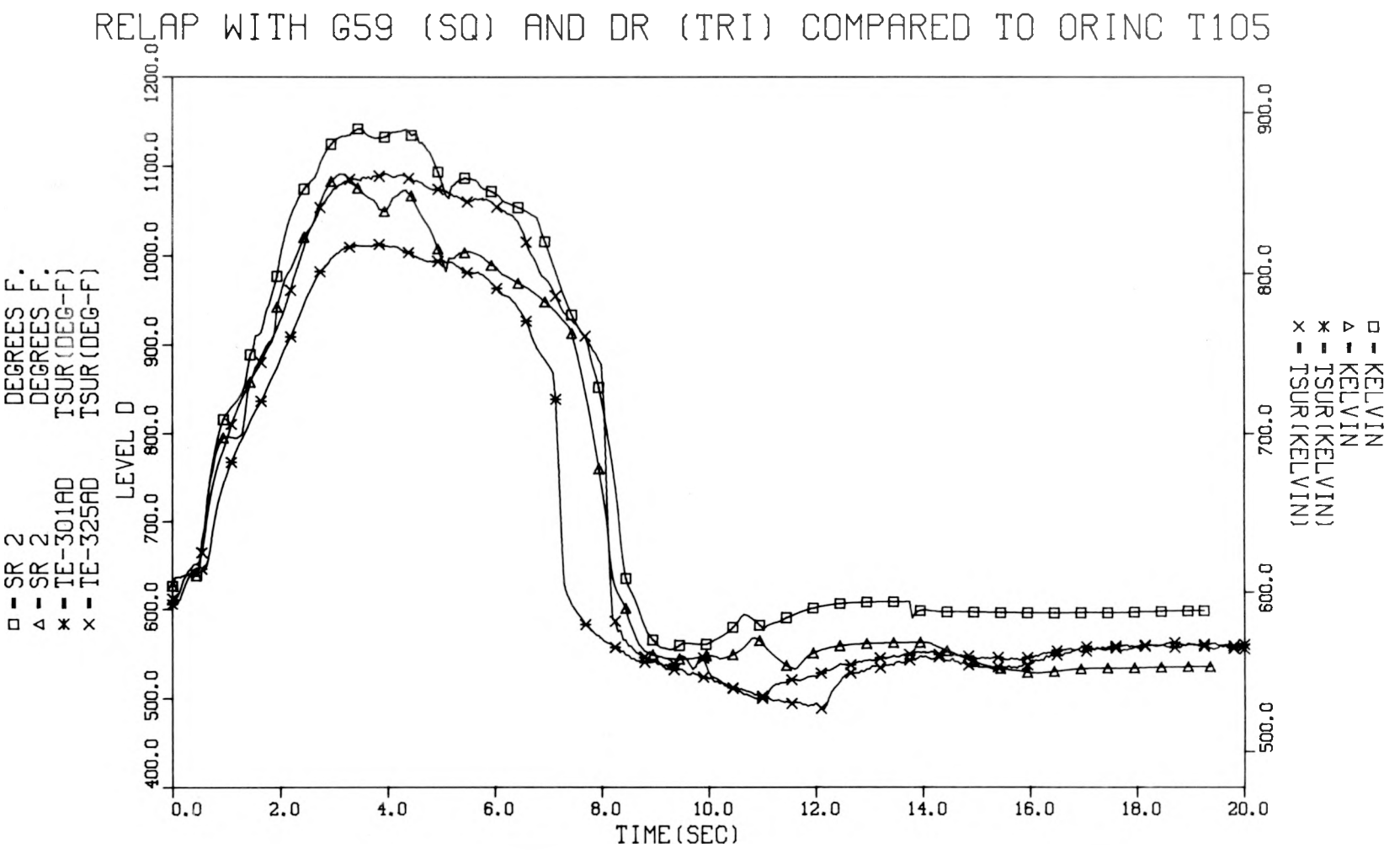

Fig. III.60. Slab 2 surface temperature vs ORINC data (level D) for system model using G59 or DR as film boiling correlation for test 105.

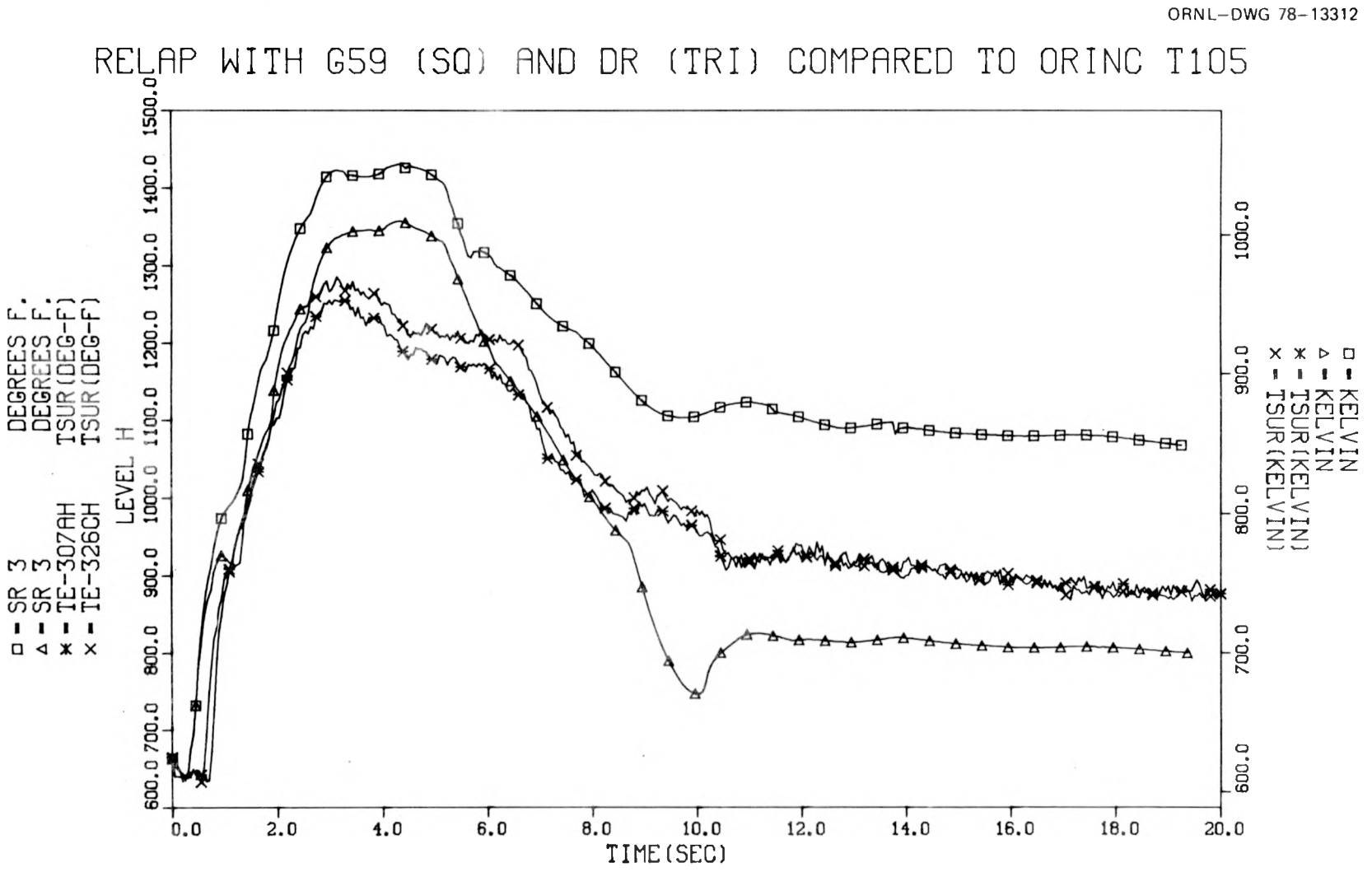

Fig. III.61. Slab 3 surface temperature vs ORINC data (level H) for system model using G59 or DR as film boiling correlation for test 105.

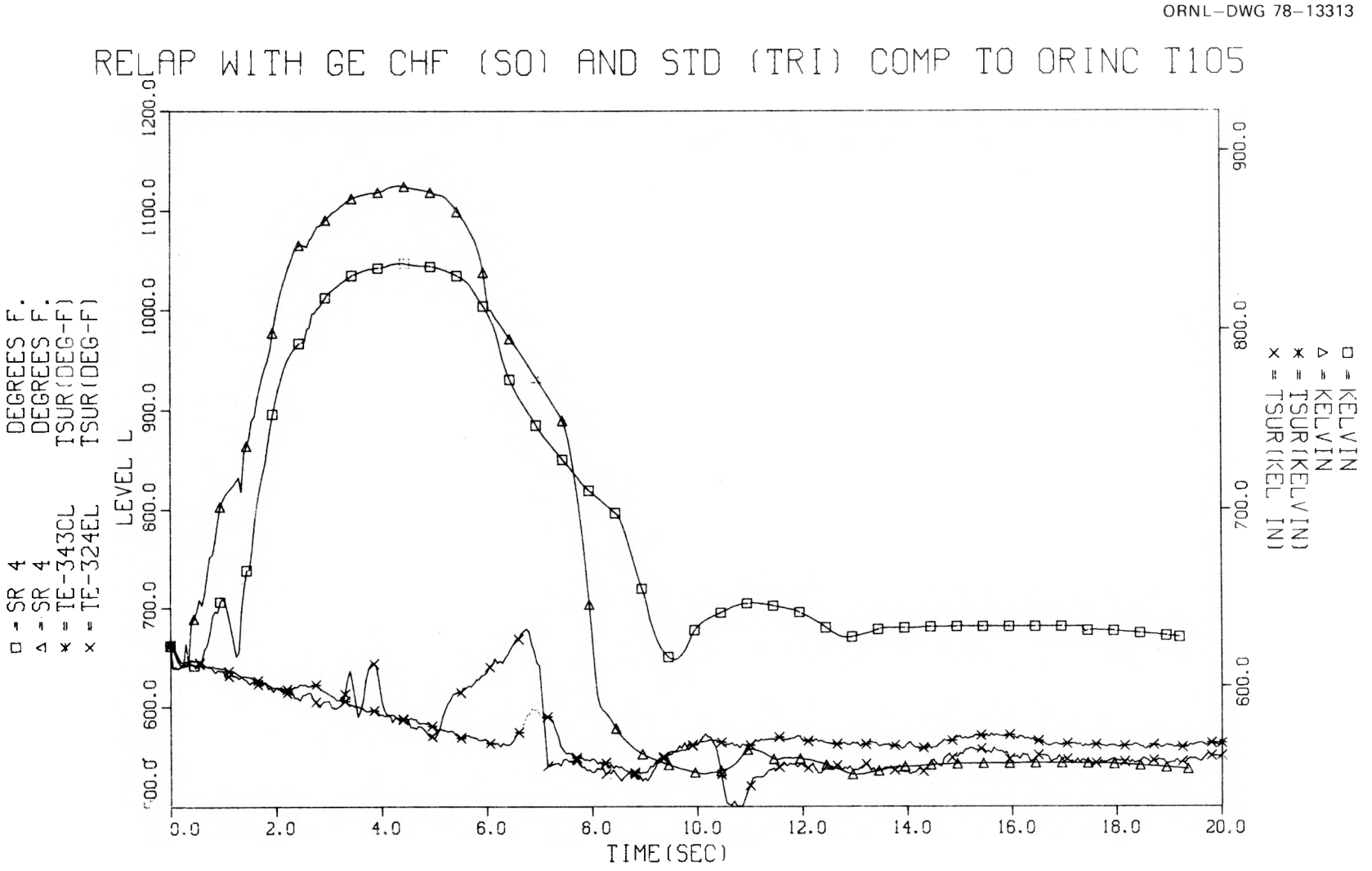

Fig. III.62. Slab 4 surface temperature vs ORINC data (level L) for system model using either the standard or GE critical heat flux correlation for test 105.

IV. HEAT TRANSFER CALCULATIONS

IV.1 Best-Estimate Heat Transfer

In order to perform basic heat transfer calculations, the instantaneous conditions of the receiving medium and the heat source must be known. In experimental determinations, some model that transforms recorded instrument responses into the required receiver and source conditions must be utilized. These models invariably encompass assumptions on the spatial and temporal variation of the parameters. For the THTF the source-receiver pair is the indirect electrically heated rods and the surrounding fluid. Therefore, the conditions that must be determined are the rod surface temperature and surface heat flux and the local fluid conditions.

The current best-estimate heat transfer calculational model is shown in Fig. IV.1. The heater rod surface conditions are supplied by ORINC,[5] which uses the individually recorded rod amperage, voltage, and thermocouple responses. The local fluid conditions are calculated by a special version of RELAP4/MOD5 (Ref. 11) which uses the ORINC heat fluxes in place of the standard RELAP4 heat transfer package and the conditions in the vertical spool pieces obtained from recorded instrument responses as hydraulic boundary conditions. The RELAP4 model used in these calculations is the single-channel 11-node core model (Fig. III.9). The coupling of ORINC, RELAP4, and experimentally determined hydraulic boundary conditions constitutes our current procedure for attempting to solve the transient boundary valued convective transport problem in space and time.

IV.2 Local Fluid Conditions

The calculation of the dynamic and thermodynamic local fluid conditions requires both thermal and hydraulic boundary conditions. The limitations in the generation of these from recorded instrument responses have been discussed in Sect. II.1. Several possible combinations of parameters can be used as hydraulic boundary conditions. The ones chosen (see Sect. III.4) were mass flux at the VO (fill table at junction 36) and absolute pressure at the VI (time-dependent volume at volume 1).

Given these boundary conditions, there are still significant problems involved in their "extrapolation" into the THTF rod bundle. The flow forcing function for junction 36, THTF test 105, is shown in Fig. IV.2, and the calculated upstream flow at junction 33 is shown in Fig. IV.3. The comparison of the two flows (Fig. IV.4) shows the magnitude of the induced flow oscillations. These oscillations do not appear in the reduced response of the vertical outlet turbine meter, FE-216 (Fig. IV.5). Comparison of the reduced response of FE-166, the inlet turbine meter, with the predicted inlet flow, junction 1, also shows oscillations in the predictions relative to the recorded signal (Fig. IV.6). The magnitude and frequency of these oscillations make utilization of the calculated bundle flows in heat transfer correlation calculations highly questionable. Qualitative information may be obtained from such calculations, but quantitative use would be unjustifiable.

The calculated thermodynamic properties (pressure, temperature, and density) are in better agreement with reduced instrument responses. A comparison of the input pressure forcing function for volume 1, THTF test 105, and the reduced response of pressure transducer PE-174, located in the VI, is shown in Fig. IV.7. Comparisons of calculated pressure and reduced pressure transducer responses at other locations are shown in Figs. IV.8 to IV.10. The oscillations noted in the flow are not present in these comparisons, and the agreement is generally within 0.345 MN/m^2 (50 psi). The temperature comparisons (Figs. IV.11 to IV.15) similarly indicate closer agreement. The agreement is quite good during those periods when the fluid was saturated and RELAP4 (Ref. 11) calculated saturation. During other periods, the effects of energy averaging and early prediction of superheat (Fig. IV.13) can be seen.[2] The density comparisons (Figs. IV.16 and IV.17) are not as good as the pressure and temperature comparisons but are better than the flows.

The space- and time-averaged local fluid conditions at TE-309BG resulting from the boundary value calculation for THTF test 105 are given in Table IV.1.

Table IV.1. Space- and time-averaged calculated fluid conditions — THTF test 105, rod 9, thermocouple level G, thermocouple TE-309BG

Time (sec)	Pressure (psia)	Temperature (°F)	Density (lb_m/ft^3)	Enthalpy (Btu/lb_m)	Quality	Mass flux ($lb_m/hr\text{-}ft^2$)	V_f (ft^3/lb_m)	V_g (ft^3/lb_m)	H_f (Btu/lb_m)	H_g (Btu/lb_m)
0.0	2282.20	593.4	4.379E 01	603.98	0.0	2.601E 06	2.716E-02	1.533E-01	705.14	1114.73
5.000E-02	2258.32	593.8					2.701E-02	1.559E-01	702.37	1116.83
1.000E-01	1885.89	595.9					2.508E-02	2.047E-01	658.84	1146.15
1.500E-01	1880.96	610.9					2.505E-02	2.055E-01	658.25	1146.51
2.000E-01	1863.96	625.9					2.498E-02	2.082E-01	656.23	1147.73
2.500E-01	1860.80	625.6					2.497E-02	2.087E-01	655.85	1147.96
3.000E-01	1882.69	627.3					2.506E-02	2.052E-01	658.48	1146.37
3.500E-01	1896.19	628.3					2.512E-02	2.032E-01	660.09	1145.40
4.000E-01	1918.35	629.9					2.523E-02	1.998E-01	662.72	1143.81
4.500E-01	1921.37	630.1	NOTE: The transient in-bundle fluid conditions in this table were calculated by RELAP4 bounded with fluid conditions measured outside the test section. The uncertainty in these fluid conditions cannot be quantified and may be quite large. Therefore the numeric information in these columns has been deleted to prevent misleading the reader.				2.524E-02	1.994E-01	663.07	1143.59
5.000E-01	1922.49	630.2					2.525E-02	1.992E-01	663.20	1143.51
5.500E-01	1928.00	630.6					2.527E-02	1.984E-01	663.85	1143.12
6.000E-01	1890.71	627.9					2.510E-02	2.040E-01	659.44	1145.79
6.500E-01	1863.41	625.8					2.498E-02	2.083E-01	656.17	1147.77
7.000E-01	1843.21	624.3					2.489E-02	2.115E-01	653.73	1149.25
7.500E-01	1825.07	622.9					2.482E-02	2.145E-01	651.52	1150.59
8.000E-01	1814.90	622.2					2.478E-02	2.162E-01	650.27	1151.34
8.500E-01	1817.00	622.3					2.479E-02	2.158E-01	650.53	1151.18
9.000E-01	1817.21	622.3					2.479E-02	2.158E-01	650.56	1151.17
9.500E-01	1816.66	622.3					2.479E-02	2.159E-01	650.49	1151.21
1.000E 00	1802.71	621.2					2.473E-02	2.182E-01	648.81	1152.15
1.050E 00	1785.27	619.9					2.465E-02	2.211E-01	646.75	1153.25
1.100E 00	1783.93	619.8					2.464E-02	2.213E-01	646.59	1153.32
1.150E 00	1766.40	618.4					2.456E-02	2.242E-01	644.53	1154.34
1.200E 00	1762.10	618.1					2.454E-02	2.249E-01	644.03	1154.59
1.250E 00	1752.10	617.3					2.449E-02	2.266E-01	642.85	1155.17
1.300E 00	1735.56	616.0					2.442E-02	2.295E-01	640.89	1156.14
1.350E 00	1731.28	615.6					2.440E-02	2.303E-01	640.37	1156.40
1.400E 00	1713.61	614.2					2.432E-02	2.334E-01	638.26	1157.44
1.450E 00	1700.84	613.2					2.426E-02	2.357E-01	636.72	1158.20
1.500E 00	1693.91	612.6	6.480E 00	955.50	0.6114	−3.351E 05	2.423E-02	2.370E-01	635.88	1158.61

IV.3 Heat Transfer Parameters

The heater rod surface conditions at each sheath thermocouple location are supplied by the computer program ORINC,[5] which solves the inverse heat conduction problem. Given the calculated surface heat flux and surface temperature and the calculated saturation and bulk fluid temperatures, the thermal driving potential and "heat transfer coefficient" can be determined. These calculated space- and time-averaged "heat transfer" parameters at TE-309BG for THTF test 105 are given in Table IV.2. Note that CHF is indicated at ∿0.50 sec.

IV.4 Critical Heat Flux

The phenomenon of CHF and the prediction of its time of occurrence are important aspects of reactor safety analysis. Although the terms CHF and DNB are often used interchangeably, they do not necessarily denote the same event. In this report, the "occurrence of CHF" refers to the beginning of a rapid temperature excursion in the heat source surface which, if uncontrolled, would result in destruction of the surface. CHF is, therefore, a safety problem. DNB merely denotes that a surface which was transferring its heat by nucleate boiling in the receiver is no longer doing so. For example, in the production of steam in steam generators, DNB occurs. DNB carries no safety connotations.

Critical heat flux occurs in the THTF during most blowdowns. In test 105 the majority of the sheath thermocouples indicated CHF. Its occurrence, however, was not instantaneous. The average time to CHF for each thermocouple level (Fig. II.3) in the THTF bundle for test 105 is given in Table IV.3. Columns 2–4 give the number of sheath thermocouples present at each level, the number that indicated the occurrence of CHF, and the number that indicated the occurrence of CHF within 2 sec of break initiation. Since the "early" (<2 sec) occurrences of CHF are of primary interest, the average time to CHF and the standard deviation in that time are computed from the indicated temperature responses of the thermocouples, which compose Col. 4. Note that the inability to determine the time of break initiation to within 0.050 sec places a systematic uncertainty in

Table IV.2. Space- and time-averaged calculated "heat transfer" parameters — THTF test 105, rod 9, thermocouple level G, thermocouple TE-309BG[a]

Time (sec)	Surface flux (Btu/hr-ft^2)	H_{sat} (Btu/hr-ft°F)	H_{bulk} (Btu/hr-ft°F)	Surf. temp. (°F)	$T_s - T_{sat}$ (°F)	$T_s - T_{bulk}$ (°F)
0.0	5.296E 05	6.219E 04	7.581E 03	663.3	8.52	69.86
5.000E-02	5.325E 05	5.510E 04	7.704E 03	662.9	9.66	69.12
1.000E-01	5.576E 05	1.835E 04	8.999E 03	657.9	30.38	61.97
1.500E-01	5.730E 05	2.311E 04	1.396E 04	651.9	24.79	41.03
2.000E-01	5.900E 05	3.148E 04	3.148E 04	644.6	18.74	18.74
2.500E-01	5.731E 05	3.357E 04	3.357E 04	642.7	17.07	17.07
3.000E-01	5.555E 05	3.359E 04	3.359E 04	643.8	16.54	16.54
3.500E-01	5.549E 05	3.576E 04	3.576E 04	643.8	15.52	15.52
4.000E-01	5.516E 05	3.955E 04	3.955E 04	643.9	13.95	13.95
4.500E-01	5.276E 05	2.936E 04	2.936E 04	648.1	17.97	17.97
5.000E-01	4.835E 05	1.693E 04	1.693E 04	658.8	28.55	28.55
5.500E-01	3.194E 05	4.855E 03	4.855E 03	696.4	65.80	65.80
6.000E-01	1.870E 05	1.608E 03	1.608E 03	744.2	116.28	116.28
6.500E-01	6.331E 04	3.663E 02	3.663E 02	798.7	172.85	172.85
7.000E-01	7.500E 04	3.579E 02	3.579E 02	833.9	209.56	209.56
7.500E-01	9.407E 04	3.989E 02	3.989E 02	858.8	235.84	235.84
8.000E-01	1.228E 05	4.842E 02	4.842E 02	875.8	253.63	253.63
8.500E-01	1.279E 05	4.743E 02	4.743E 02	892.0	269.69	269.69
9.000E-01	1.317E 05	4.624E 02	4.624E 02	907.3	284.93	284.93
9.500E-01	1.371E 05	4.586E 02	4.586E 02	921.2	298.92	298.92
1.000E 00	1.374E 05	4.376E 02	4.376E 02	935.2	313.95	313.95
1.050E 00	1.483E 05	4.535E 02	4.535E 02	946.9	327.02	327.02
1.100E 00	1.464E 05	4.310E 02	4.310E 02	959.5	339.77	339.77
1.150E 00	1.836E 05	5.291E 02	5.291E 02	965.5	347.07	347.07
1.200E 00	1.745E 05	4.878E 02	4.878E 02	975.8	357.72	357.72
1.250E 00	1.749E 05	4.741E 02	4.741E 02	986.2	368.89	368.89
1.300E 00	1.566E 05	4.079E 02	4.079E 02	1000.0	383.98	383.98
1.350E 00	1.646E 05	4.164E 02	4.164E 02	1011.0	395.35	395.35
1.400E 00	1.730E 05	4.258E 02	4.258E 02	1020.7	406.45	406.45
1.450E 00	1.756E 05	4.209E 02	4.209E 02	1030.5	417.28	417.28
1.500E 00	1.738E 05	4.059E 02	4.059E 02	1040.9	428.29	428.29

[a]The transient in-bundle fluid conditions used in this table were calculated by RELAP4 bounded with fluid conditions measured outside the test section. The uncertainty in these fluid conditions cannot be quantified and may be quite large.

Table IV.3. Time to CHF determined from recorded sheath thermocouple (T/C) responses — THTF test 105

Level	No. of T/C	No. of T/C to CHF[a]	No. of T/C to CHF (<2 sec)[b,c]	Average time[c] to CHF (sec)	Standard deviation of time (sec)
D	18	17	17	6.6301D-01	6.9285D-02
E	19	18	18	7.3274D-01	1.4336D-01
F	18	18	18	6.2981D-01	1.3969D-01
G	19	19	19	5.6387D-01	7.7565D-02
H	42	41	41	7.2245D-01	1.4203D-01
I	42	37	19	1.0263D-00	5.2733D-01
J	39	39	7	9.1669D-01	4.4515D-01
K	20	14	0	0.0	0.0
L	41	7	0	0.0	0.0
M	4	0	0	0.0	0.0
N	3	0	0	0.0	0.0
O	19	0	0	0.0	0.0

[a]This column lists the number of thermocouples that indicated the occurrence of CHF.

[b]This column lists the number of thermocouples that indicated the occurrence of CHF within 2 sec of break initiation.

[c]There is a systematic uncertainty of ±0.050 sec in the determination of this time.

the calculation of the average time to CHF. The calculation of the standard deviation is also limited by the data acquisition rate of one point every 0.050 sec. Nevertheless, important conclusions can be drawn from the relative magnitude of these numbers. Those levels with small standard deviations incurred CHF uniformly, while those with larger standard deviations, notably I and J, had at least two distinct occurrences of CHF.

The maximum clad temperatures in THTF experiments are also of great interest since clad temperature is the major licensing limit in LOCA analysis. The maximum recorded clad temperature from the indicated thermocouple responses at each level during test 105 is given in Table IV.4. In using this information, one must remember that during this test the electric heater rod behavior did not quantitatively match the performance of nuclear fuel rods.

Table IV.4. Maximum recorded clad temperatures determined from recorded sheath thermocouple responses — THTF test 105

Level	Maximum temperature per level (°F)	Time[a] to maximum temperature (sec)	Instrument name
D	1.1174E 03	3.5996E 00	TE-310AD
E	1.1837E 03	3.3996E 00	TE-320AE
F	1.3840E 03	3.4996E 00	TE-323BF
G	1.4196E 03	3.2496E 00	TE-320BG
H	1.3797E 03	3.2496E 00	TE-312CH
I	1.0258E 03	3.2996E 00	TE-325CI
J	9.4744E 02	4.1995E 00	TE-325DJ
K	8.8553E 02	4.0496E 00	TE-325DK
L	8.4336E 02	0.0	TE-325EL
M	7.1201E 02	5.0000E-02	TE-304EM
N	7.3037E 02	5.0000E-02	TE-325FN
O	7.3787E 02	5.0000E-02	TE-349EO

[a]There is a systematic uncertainty of —0.050 sec in the determination of this time.

The ability to accurately predict the occurrence of CHF is exceedingly important in a coupled thermal-hydraulic analysis since the post-CHF surface temperature excursion is hundreds of degrees per second. A comparison of the predicted DNB flux from several currently used correlations and the calculated surface heat flux from ORINC for TE-309BG during test 105 is presented in Table IV.5. The ORINC-calculated DNB flux occurs at ∿0.50 sec. All the predictions are early, ranging from 0.25 sec [Westinghouse-3 (W-3)][3] to 0.45 sec (GE).[3] In general, the limited analysis to date has indicated that of the correlations examined, the GE correlation produced the best predictions of THTF bundle 1 behavior.

IV.5 Heat Transfer Correlation Comparisons

A comparison of the predicted heat transfer coefficient from several currently used correlations and the appropriate calculated "heat transfer coefficient" from Table IV.2 for TE-309BG during THTF test 105 is presented in Table IV.6. The boiling curve mode is the selected heat transfer mode from a steady-state boiling curve with switching logic similar to that currently employed in transient analysis. The boiling curve is composed of:

Mode	Regime	Correlation[3]
1.0	Subcooled forced convection	Dittus-Boelter
2.0	Nucleate boiling	Thom
3.0	Transition boiling	McDonough-Milich-King
4.0	Film boiling	Dougall-Rohsenow
5.0	Film boiling	Groeneveld 5.9
6.0	Pool boiling	Morgan[12]
7.0	Superheat forced convection	Dittus-Boelter

The mode is selected based on the local fluid conditions (Sect. IV.2) and the surface heat flux from ORINC (Table IV.2). The boiling curve surface temperature is calculated based on the selected mode, the local receiver temperature, and the ORINC surface heat flux.

The surface corresponding to TE-309BG is in subcooled nucleate boiling at steady state, and the comparison with Thom is excellent. During the subcooled decompression (0.050–0.250 sec) and the transition boiling period (0.50–0.750 sec), when the coupling of pin conduction,

Table IV.5. Predictions of departure from nucleate boiling (DNB) correlations — THTF test 105, rod 9, T/C level G, thermocouple TE-309BG[a,b]

Time (sec)	B&W-2	Barnett	Modified Barnett	Press interpolation	W-3	G-E
0.0	2.718E 00	3.775E 00	6.868E 00	2.718E 00	1.133E 00	1.511E 00
5.000E-02	2.704E 00	3.747E 00	6.782E 00	2.704E 00	1.148E 00	1.502E 00
1.000E-01	1.721E 00	1.338E 00	3.008E 00	1.721E 00	9.506E-01	1.506E 00
1.500E-01	1.857E 00	2.552E 00	5.096E 00	1.857E 00	1.147E 00	1.396E 00
2.000E-01	1.508E 00	2.195E 00	4.844E 00	1.508E 00	1.086E 00	1.356E 00
2.500E-01	1.270E 00	1.467E 00	3.469E 00	1.270E 00	8.509E-01	1.316E 00
3.000E-01	1.102E 00	8.105E-01	1.999E 00	1.102E 00	7.954E-01	1.344E 00
3.500E-01	9.365E-01	7.379E-01	1.786E 00	9.365E-01	−1.000E 00	1.238E 00
4.000E-01	7.735E-01	4.964E-01	8.249E-01	7.735E-01	−1.000E 00	1.112E 00
4.500E-01	3.089E-01	1.359E 00	3.383E 00	3.089E-01	−1.000E 00	9.765E-01
5.000E-01	−1.000E 00	1.488E 00	3.704E 00	−1.000E 00	−1.000E 00	8.067E-01
5.500E-01	−1.000E 00	2.333E 00	5.789E 00	−1.000E 00	−1.000E 00	8.176E-01
6.000E-01	−1.000E 00	4.591E 00	1.094E 01	−1.000E 00	−1.000E 00	6.862E-01
6.500E-01	−1.000E 00	1.605E 01	3.649E 01	−1.000E 00	−1.000E 00	1.796E 00
7.000E-01	−1.000E 00	1.231E 01	2.837E 01	−1.000E 00	−1.000E 00	1.840E 00
7.500E-01	−1.000E 00	1.007E 01	2.291E 01	−1.000E 00	−1.000E 00	2.225E 00
8.000E-01	−1.000E 00	6.844E 00	1.590E 01	−1.000E 00	−1.000E 00	2.190E 00
8.500E-01	−1.000E 00	5.637E 00	1.346E 01	−1.000E 00	−1.000E 00	2.545E 00
9.000E-01	−1.000E 00	4.040E 00	9.867E 00	−1.000E 00	−1.000E 00	2.262E 00
9.500E-01	−1.000E 00	6.055E 00	1.411E 01	−1.000E 00	−1.000E 00	1.743E 00
1.000E 00	−1.000E 00	6.134E 00	1.418E 01	−1.000E 00	−1.000E 00	1.572E 00
1.050E 00	−1.000E 00	6.298E 00	1.416E 01	−1.000E 00	−1.000E 00	1.428E 00
1.100E 00	−1.000E 00	4.564E 00	1.088E 01	−1.000E 00	−1.000E 00	1.786E 00
1.150E 00	−1.000E 00	4.486E 00	1.028E 01	−1.000E 00	−1.000E 00	1.130E 00
1.200E 00	−1.000E 00	5.174E 00	1.162E 01	−1.000E 00	−1.000E 00	1.201E 00
1.250E 00	−1.000E 00	4.246E 00	9.862E 00	−1.000E 00	−1.000E 00	1.412E 00
1.300E 00	−1.000E 00	5.549E 00	1.245E 01	−1.000E 00	−1.000E 00	1.317E 00
1.350E 00	−1.000E 00	4.855E 00	1.106E 01	−1.000E 00	−1.000E 00	1.585E 00
1.400E 00	−1.000E 00	4.281E 00	9.816E 00	−1.000E 00	−1.000E 00	1.441E 00
1.450E 00	−1.000E 00	4.904E 00	1.089E 01	−1.000E 00	−1.000E 00	1.132E 00
1.500E 00	−1.000E 00	3.835E 00	8.860E 00	−1.000E 00	−1.000E 00	1.315E 00

[a] Ratio of correlation-predicted DNB flux/calculated "DNB flux" (−1.0 indicates no calculation performed).

[b] The transient in-bundle fluid conditions used in this table were calculated by RELAP4 bounded with fluid conditions measured outside the test section. The uncertainty in these fluid conditions cannot be quantified and may be quite large.

Table IV.6. Predictions of heat transfer correlations — THTF test 105, rod 9, T/C level G, thermocouple TE-309BG[a,b]

Time (sec)	Dittus-Boelter subcooled	Dittus-Boelter superheat	Thom	Groeneveld 5.7	Groeneveld 5.9	Dougall-Rohsenow	Chen	Boiling curve mode	Boiling curve surf. temp.
0.0	7.929E-01	7.798E-01	9.887E-01	4.316E-02	4.798E-02	2.072E-02	−1.000E 00	2.0	663.3
5.000E-02	8.013E-01	7.881E-01	1.219E 00	4.921E-02	5.478E-02	2.371E-02	−1.000E 00	2.0	662.0
1.000E-01	1.287E-01	1.266E-01	6.371E 00	2.883E-02	1.945E-02	1.085E-02	−1.000E 00	2.0	639.3
1.500E-01	3.851E-01	3.788E-01	4.096E 00	8.555E-02	8.678E-02	4.097E-02	−1.000E 00	2.0	639.0
2.000E-01	1.750E-01	1.112E-01	2.214E 00	2.717E-02	2.694E-02	2.041E-02	−1.000E 00	2.0	638.0
2.500E-01	5.412E-02	3.440E-02	1.881E 00	1.190E-02	9.311E-03	7.941E-03	−1.000E 00	2.0	637.8
3.000E-01	1.791E-02	1.139E-02	1.886E 00	5.386E-03	3.295E-03	3.192E-03	−1.000E 00	2.0	639.2
3.500E-01	1.373E-02	8.724E-03	1.698E 00	4.940E-03	2.997E-03	2.947E-03	−1.000E 00	4.0	3769.5
4.000E-01	3.524E-03	2.240E-03	1.429E 00	1.750E-03	7.934E-04	9.091E-04	−1.000E 00	6.0	6101.7
4.500E-01	4.718E-02	2.999E-02	2.493E 00	1.970E-02	1.721E-02	1.469E-02	−1.000E 00	4.0	1542.6
5.000E-01	8.222E-02	5.226E-02	6.879E 00	3.961E-02	3.616E-02	3.094E-02	−1.000E 00	4.0	1351.1
5.500E-01	3.044E-01	1.935E-01	5.578E 01	1.628E-01	1.560E-01	1.341E-01	−1.000E 00	4.0	1034.7
6.000E-01	1.173E 00	7.456E-01	2.804E 02	6.479E-01	6.752E-01	5.680E-01	−1.000E 00	4.0	807.4
6.500E-01	7.106E 00	4.517E 00	1.753E 03	3.790E 00	4.316E 00	3.486E 00	−1.000E 00	4.0	671.4
7.000E-01	6.022E 00	3.827E 00	2.106E 03	3.250E 00	3.506E 00	2.882E 00	−1.000E 00	4.0	688.8
7.500E-01	5.672E 00	3.605E 00	2.066E 03	2.893E 00	3.119E 00	2.515E 00	−1.000E 00	4.0	704.4
8.000E-01	3.753E 00	2.386E 00	1.802E 03	1.882E 00	1.888E 00	1.552E 00	−1.000E 00	4.0	756.9
8.500E-01	2.947E 00	1.873E 00	1.962E 03	1.511E 00	1.408E 00	1.195E 00	−1.000E 00	4.0	800.8
9.000E-01	1.793E 00	1.140E 00	2.127E 03	1.013E 00	8.269E-01	7.517E-01	−1.000E 00	4.0	903.6
9.500E-01	3.877E 00	2.464E 00	2.248E 03	1.999E 00	2.008E 00	1.662E 00	−1.000E 00	4.0	771.8
1.000E 00	4.172E 00	2.652E 00	2.420E 03	2.184E 00	2.221E 00	1.834E 00	−1.000E 00	4.0	765.0
1.050E 00	4.854E 00	3.085E 00	2.366E 03	2.485E 00	2.660E 00	2.142E 00	−1.000E 00	4.0	751.5
1.100E 00	2.855E 00	1.814E 00	2.581E 03	1.573E 00	1.440E 00	1.246E 00	−1.000E 00	4.0	835.7
1.150E 00	3.315E 00	2.107E 00	2.089E 03	1.759E 00	1.775E 00	1.468E 00	−1.000E 00	4.0	815.7
1.200E 00	4.235E 00	2.692E 00	2.319E 03	2.193E 00	2.311E 00	1.871E 00	−1.000E 00	4.0	781.2
1.250E 00	3.098E 00	1.969E 00	2.422E 03	1.687E 00	1.624E 00	1.372E 00	−1.000E 00	4.0	836.0
1.300E 00	4.728E 00	3.005E 00	2.854E 03	2.481E 00	2.570E 00	2.094E 00	−1.000E 00	4.0	770.7
1.350E 00	3.998E 00	2.541E 00	2.860E 03	2.118E 00	2.103E 00	1.741E 00	−1.000E 00	4.0	802.3
1.400E 00	3.437E 00	2.184E 00	2.796E 03	1.872E 00	1.801E 00	1.515E 00	−1.000E 00	4.0	831.4
1.450E 00	4.508E 00	2.865E 00	2.845E 03	2.388E 00	2.469E 00	2.010E 00	−1.000E 00	4.0	787.9
1.500E 00	3.018E 00	1.918E 00	2.995E 03	1.713E 00	1.580E 00	1.360E 00	−1.000E 00	4.0	862.6

[a]Ratio of correlation-predicted heat transfer coefficient/calculated "heat transfer coefficient" (−1.0 indicates no calculation performed).

[b]The transient in-bundle fluid conditions used in this table were calculated by RELAP4 bounded with fluid conditions measured outside the test section. The uncertainty in these fluid conditions cannot be quantified and may be quite large.

surface heat transfer, and receiver energy transport is highly transient, none of the correlations examined produced good comparisons. The boiling curve predicted CHF to occur 0.150 sec early as evidenced by the high predicted surface temperatures. After film boiling was established (>0.75 sec), the correlations for that regime were generally within a factor of 2 of the calculated "heat transfer coefficient." Of the three correlations examined, Dougall-Rohsenow produced the best results, usually by 20%. In both the integral temperature comparisons (conduction equation coupled to the heat transfer — RELAP4; see Sect. III.7) and in these independent time point heat transfer comparisons, Dougall-Rohsenow produced better comparisons in the THTF. It should be noted, however, that similar comparisons made with more accurate fluid conditions could alter this observation.

Some of the numeric information has been deleted from tables in this section because of the lack of confidence in the calculation of the local fluid conditions (Sect. IV.2). This is an attempt to guard against misleading the reader and to prevent misinterpretation by others as to the significance of the information.

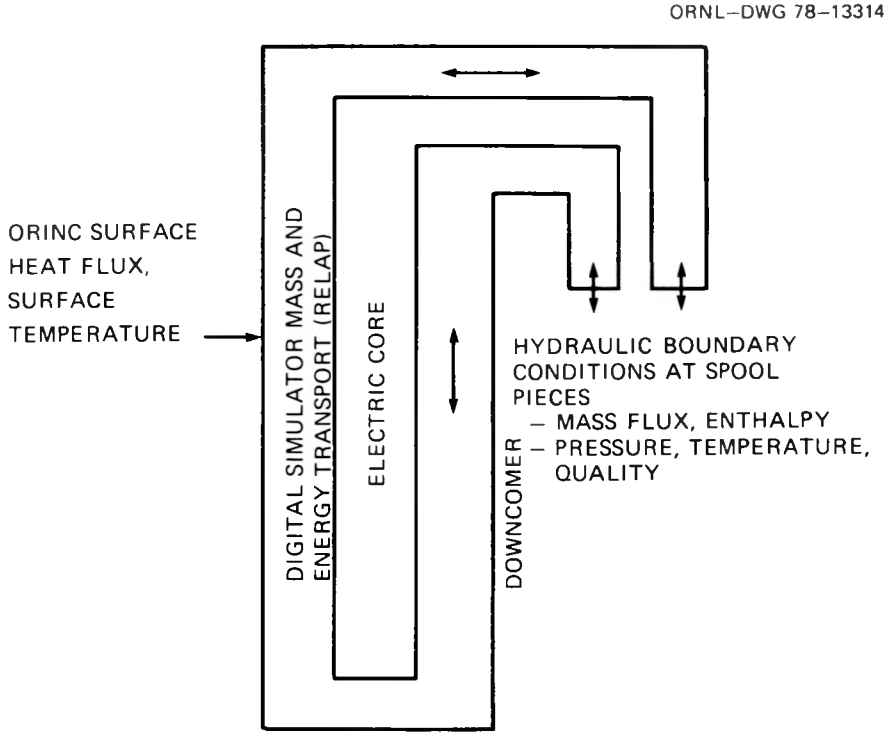

Fig. IV.1. Best-estimate heat transfer calculational model.

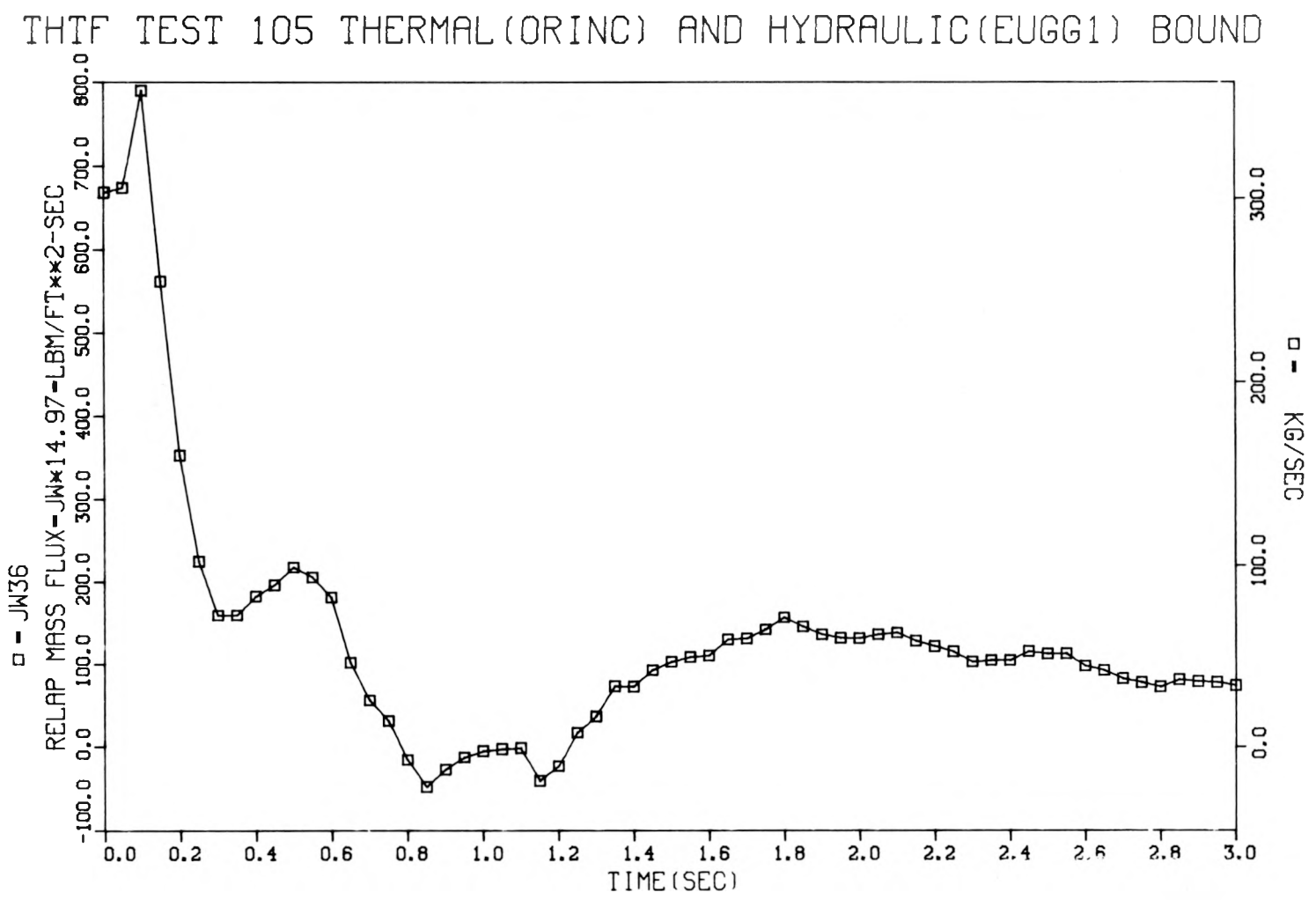

Fig. IV.2. Flow forcing function, junction 36, THTF test 105.

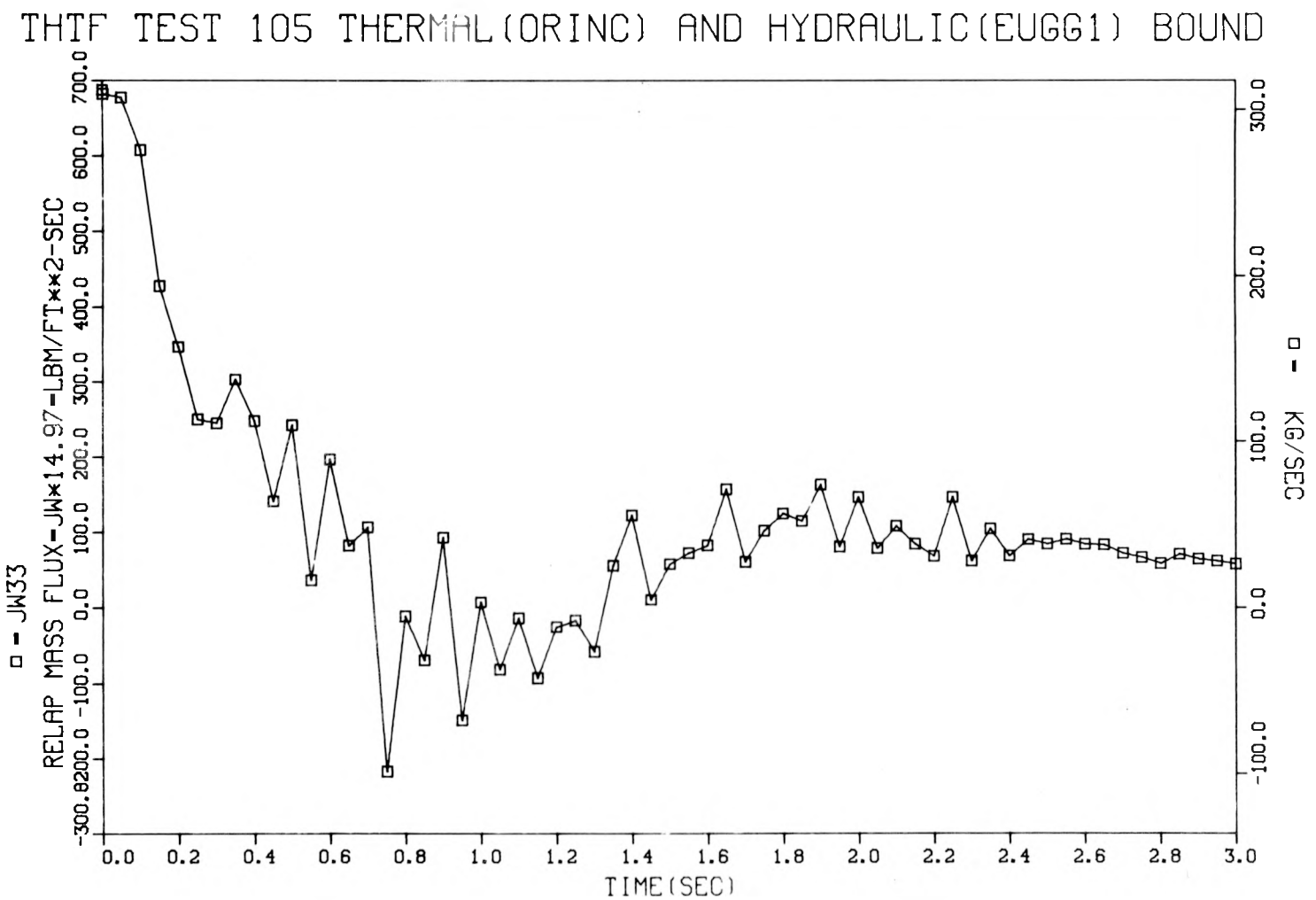

Fig. IV.3. Calculated mass flux, junction 33, THTF test 105, upstream of input forcing function.

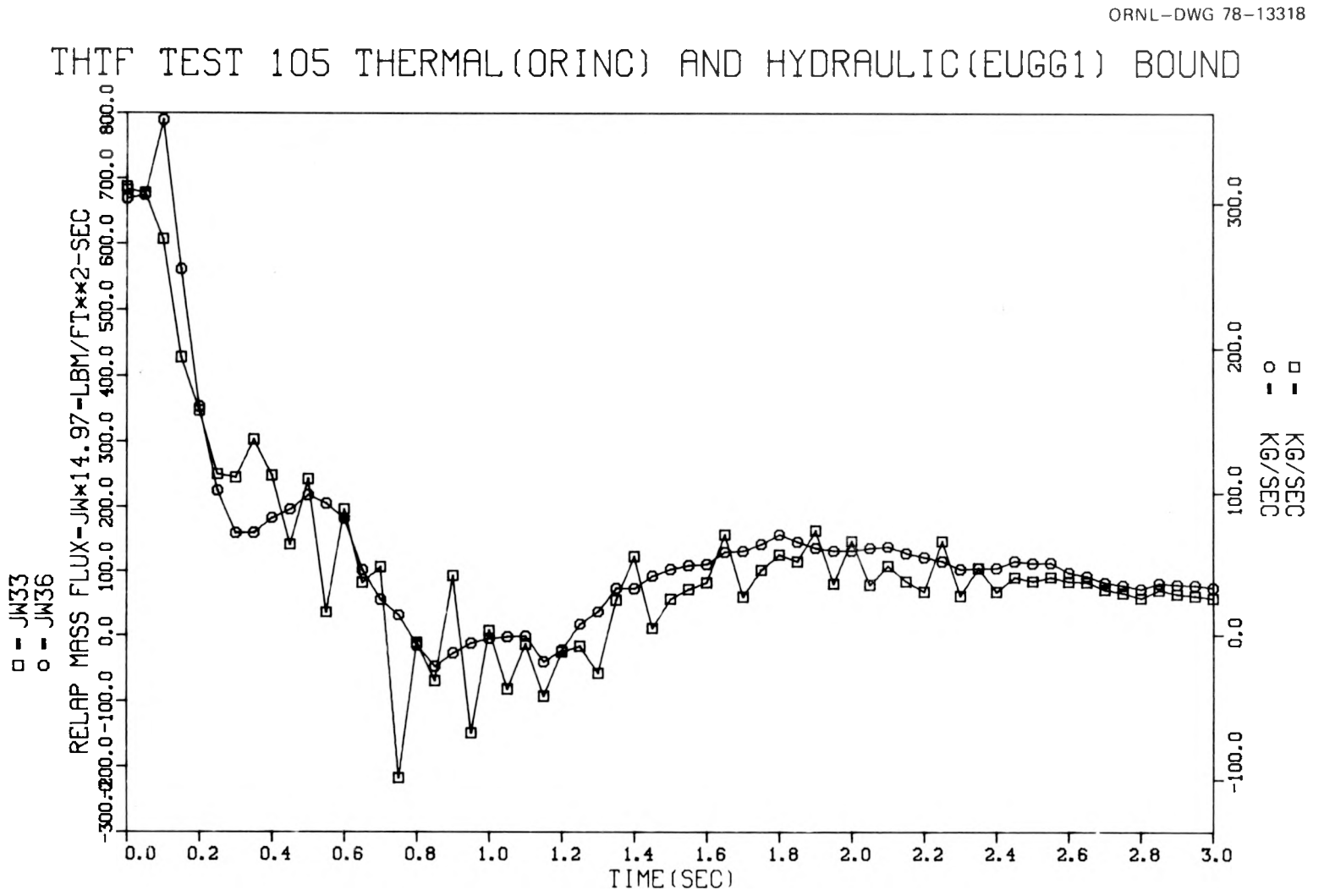

Fig. IV.4. Comparison of junction 36 and 33 mass fluxes, THTF test 105.

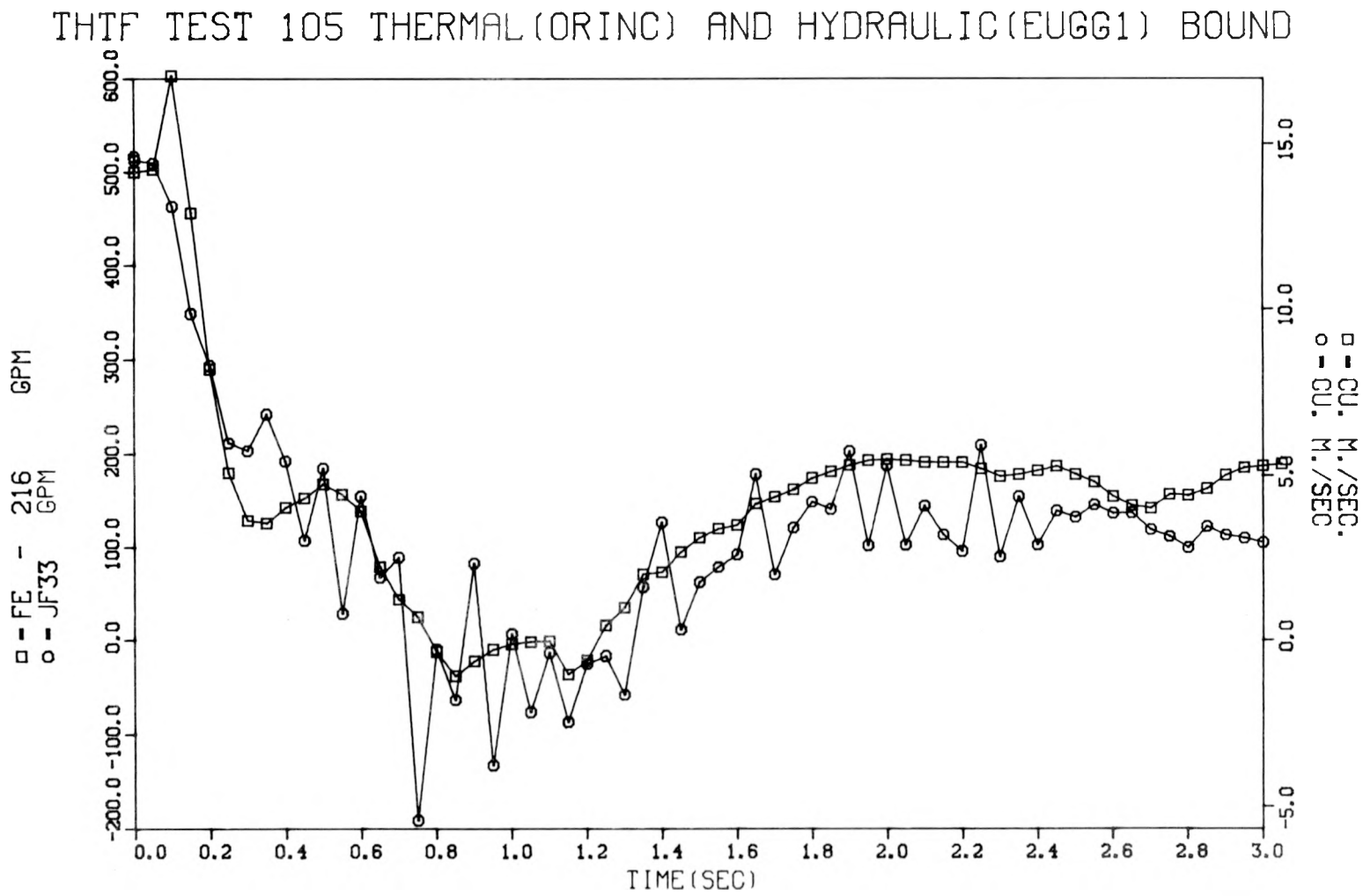

Fig. IV.5. Comparison of vertical outlet turbine meter indicated flow and junction 33 predicted flow, THTF test 105.

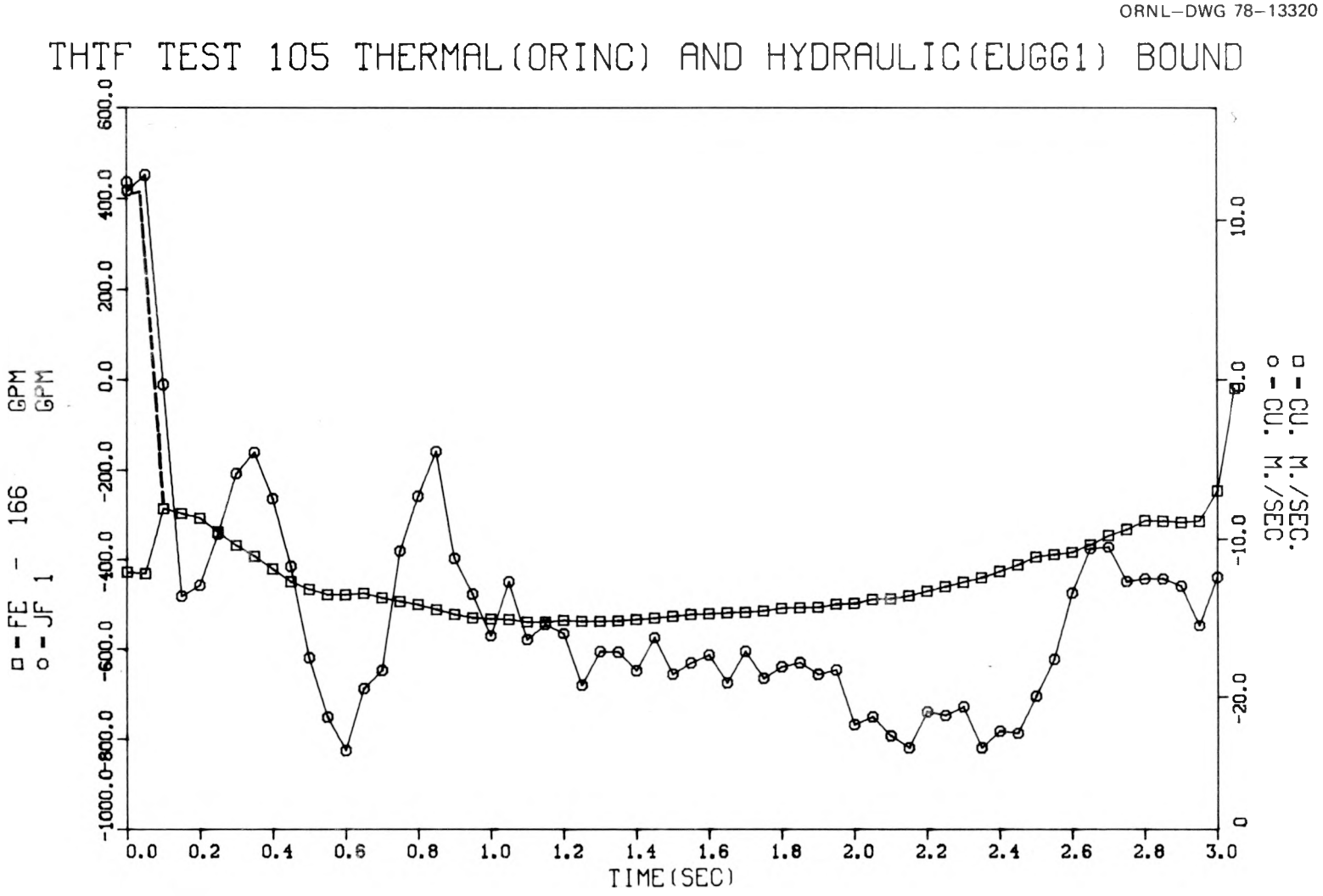

Fig. IV.6. Comparison of vertical inlet turbine meter indicated flow and junction 1 predicted flow, THTF test 105. (Polarity reversal produced incorrect signs on turbine meter signals at some times. Estimates of the correct signal are indicated by dotted lines.)

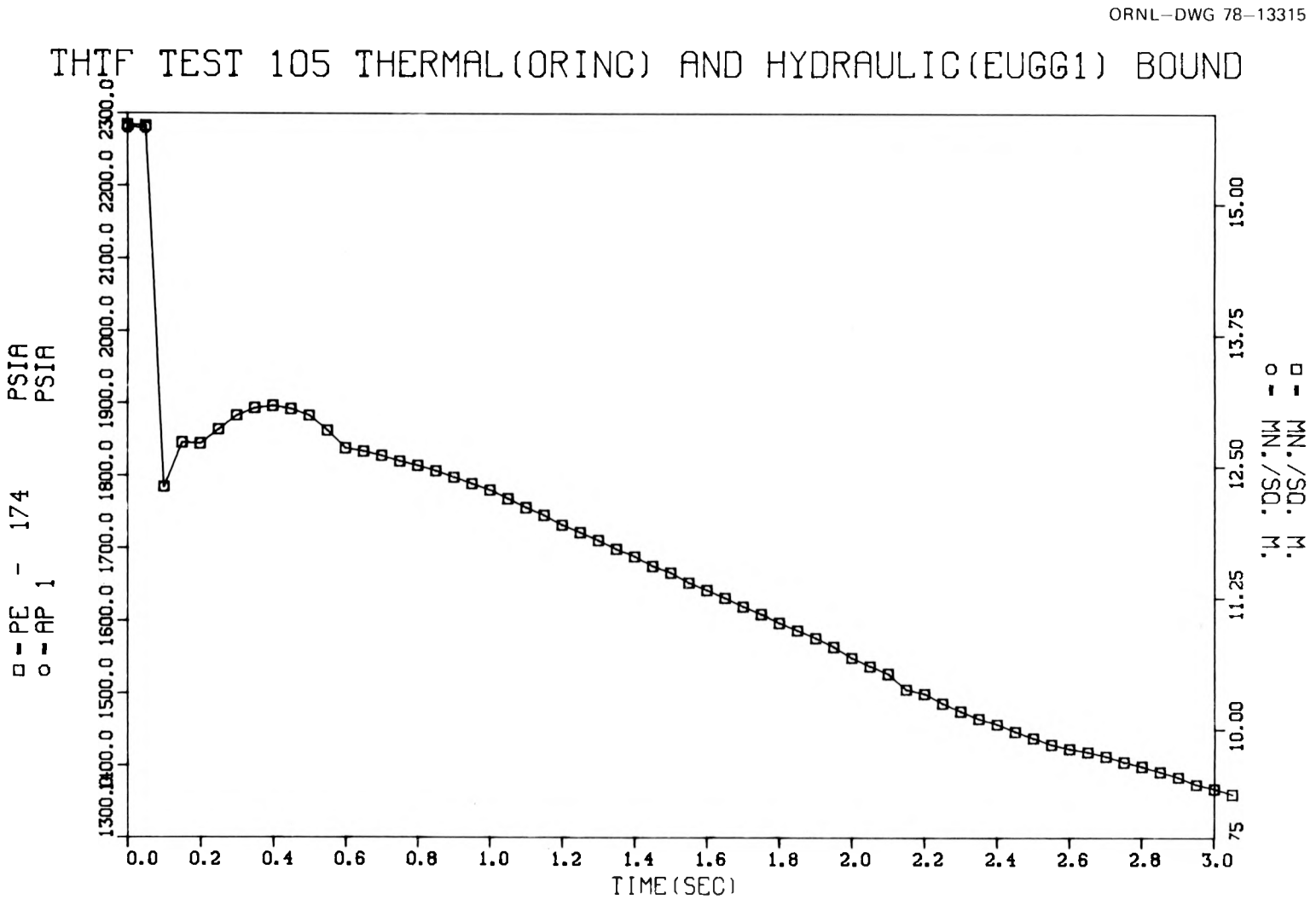

Fig. IV.7. Comparison of vertical inlet pressure transducer reduced response and volume 1 input pressure, THTF test 105.

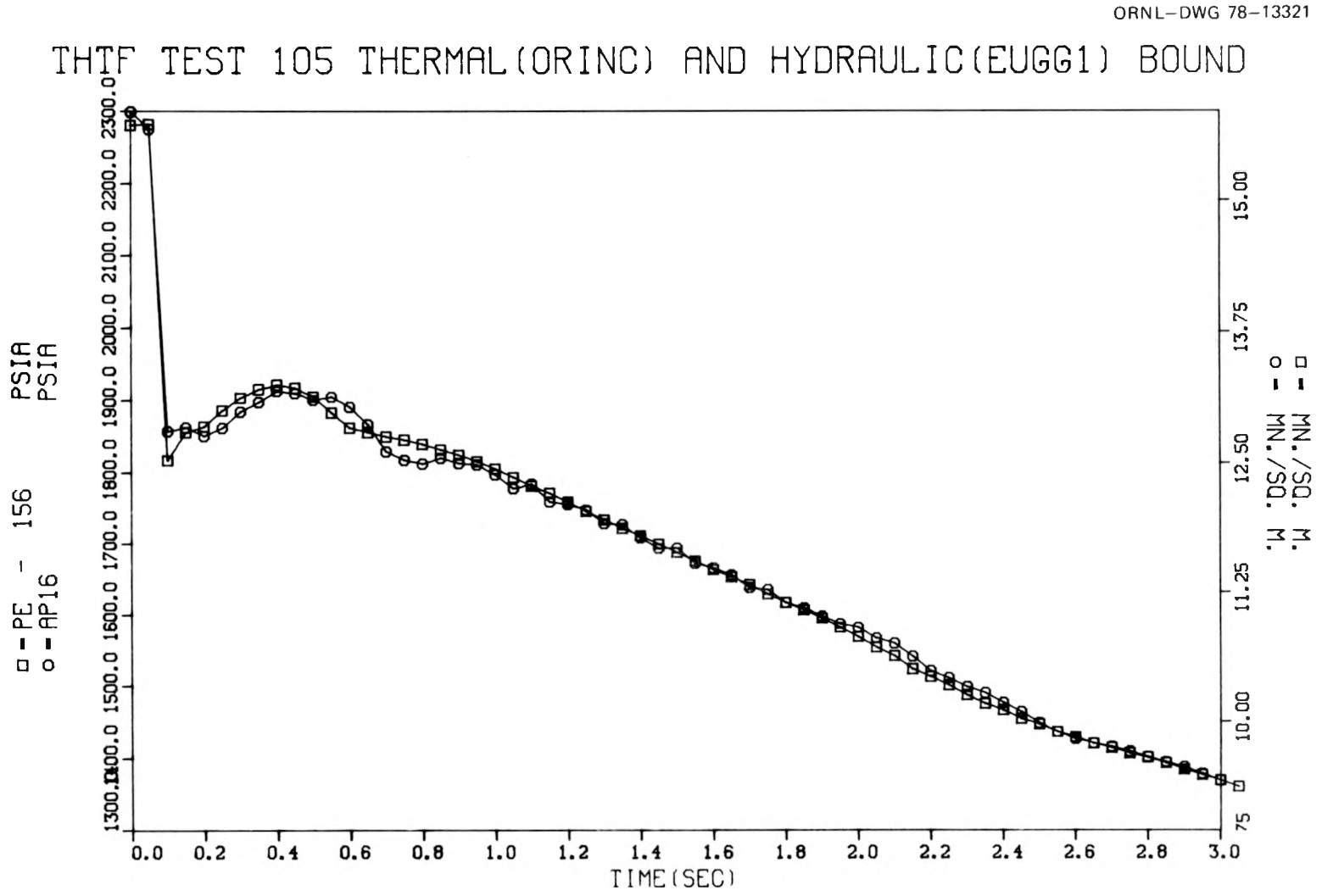

Fig. IV.8. Comparison of lower plenum pressure transducer reduced response and volume 16 pressure, THTF test 105.

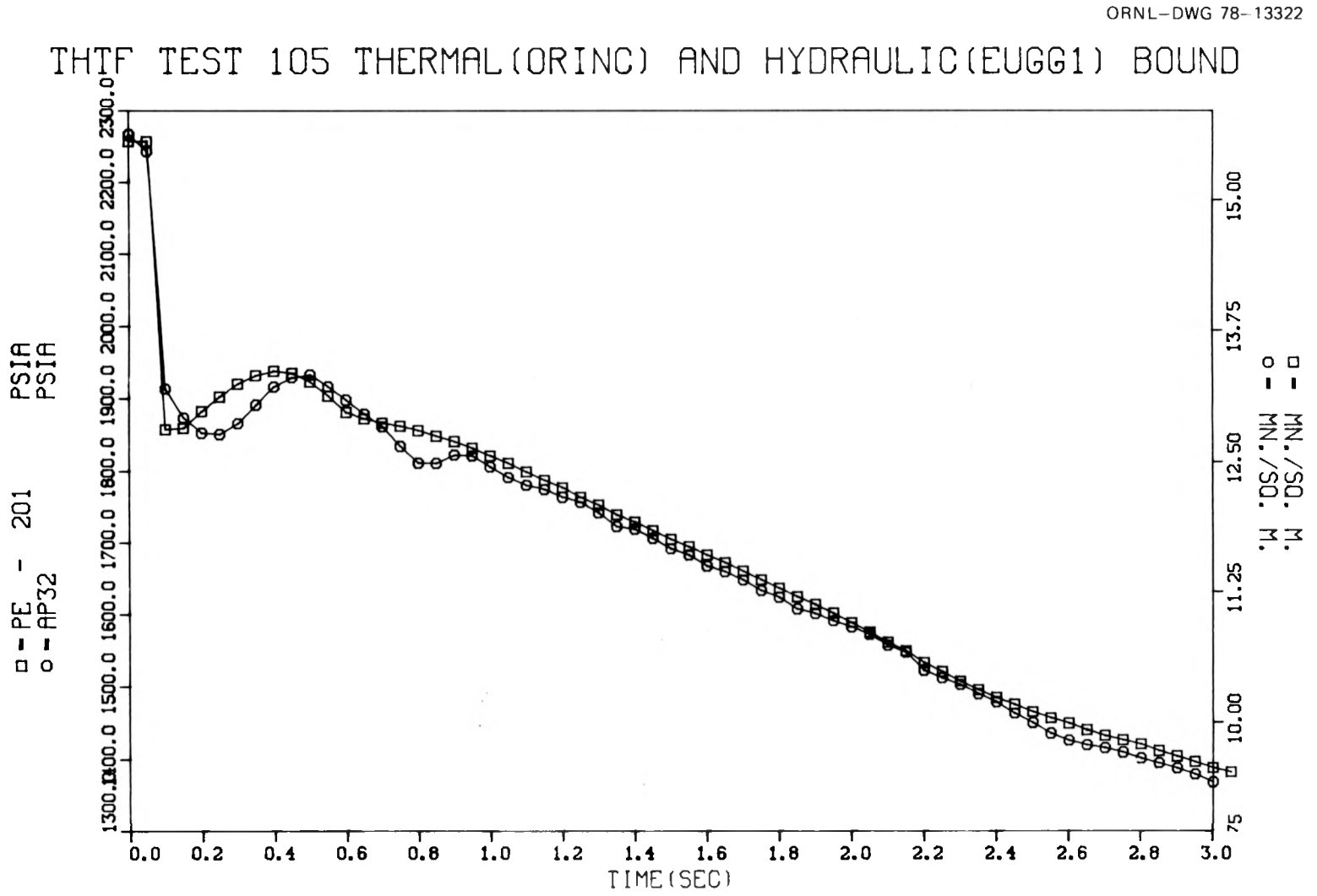

Fig. IV.9. Comparison of upper plenum pressure transducer reduced response and volume 32 pressure, THTF test 105.

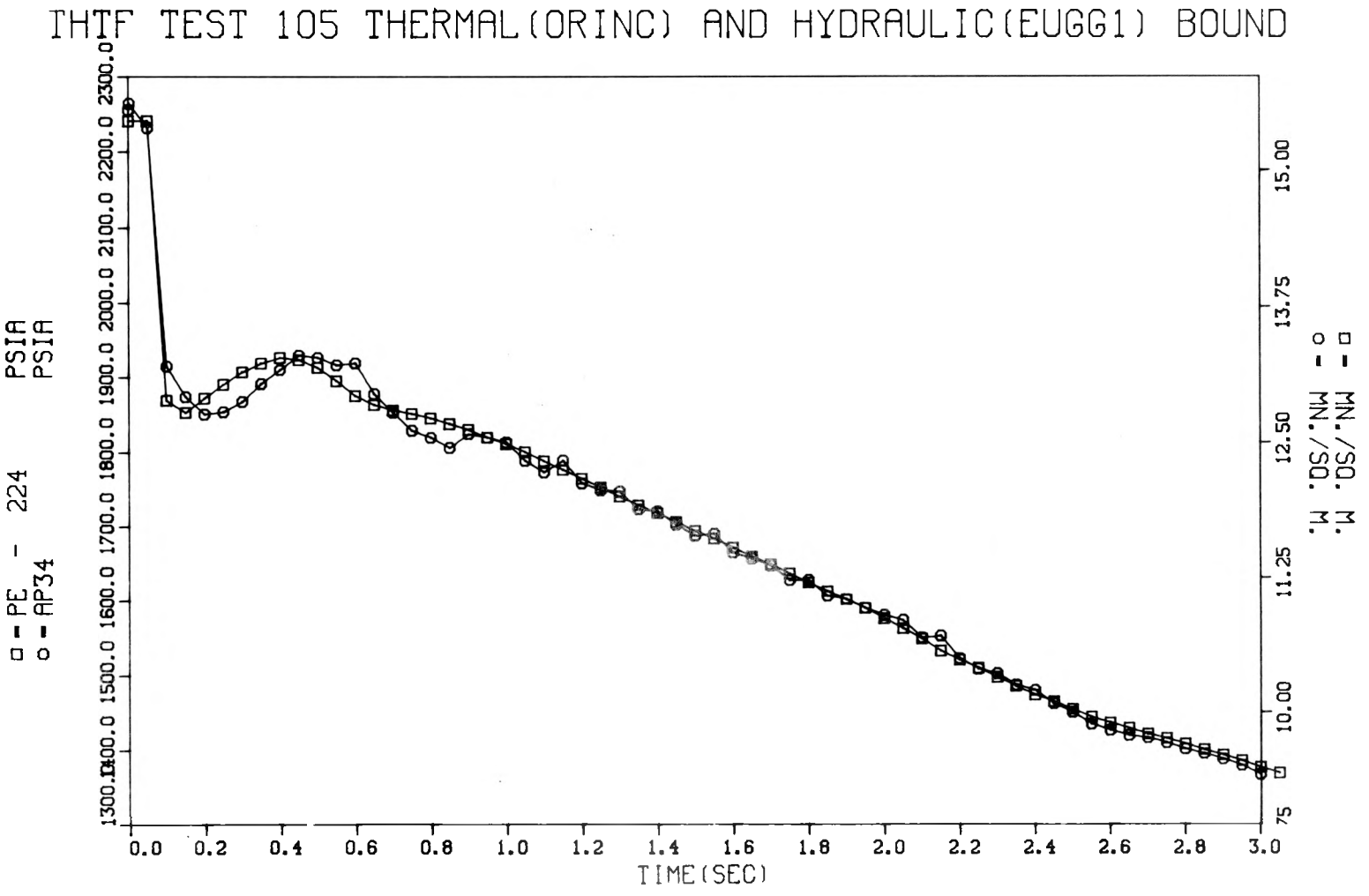

Fig. IV.10. Comparison of vertical outlet pressure transducer reduced response and volume 34 pressure, THTF test 105.

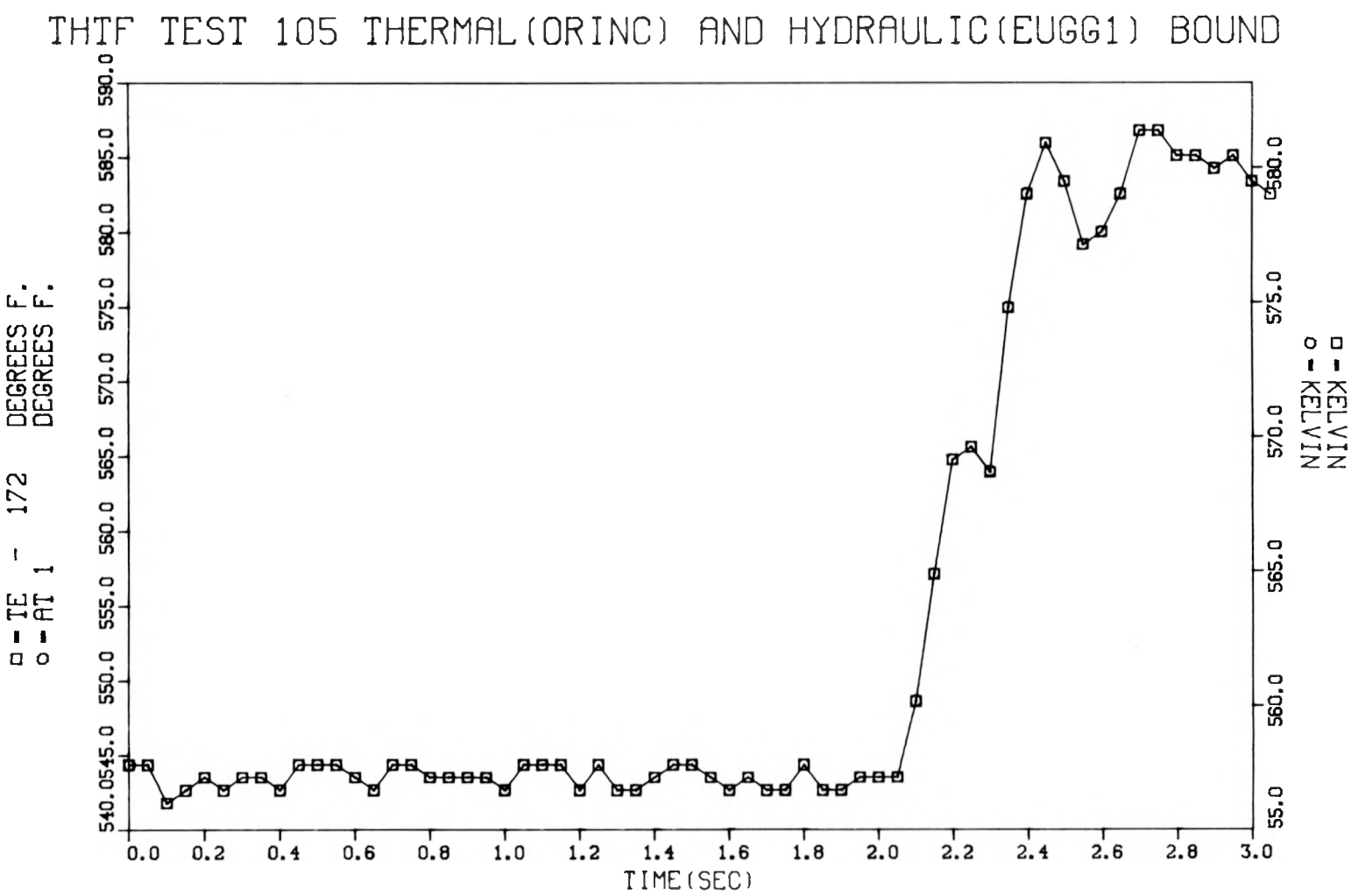

Fig. IV.11. Comparison of vertical inlet thermocouple reduced response and volume 1 input temperature, THTF test 105.

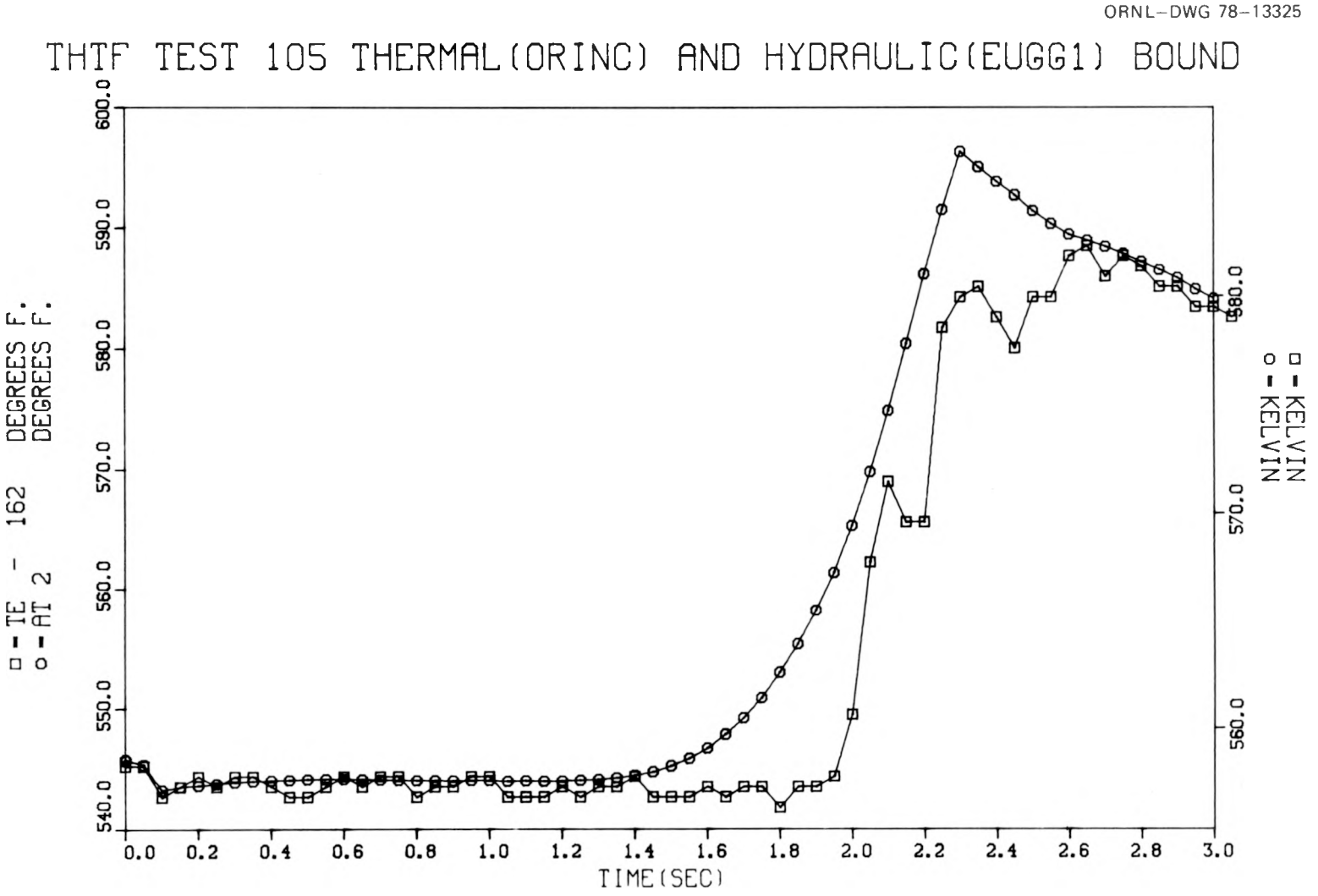

Fig. IV.12. Comparison of inlet line thermocouple reduced response and volume 2 temperature, THTF test 105.

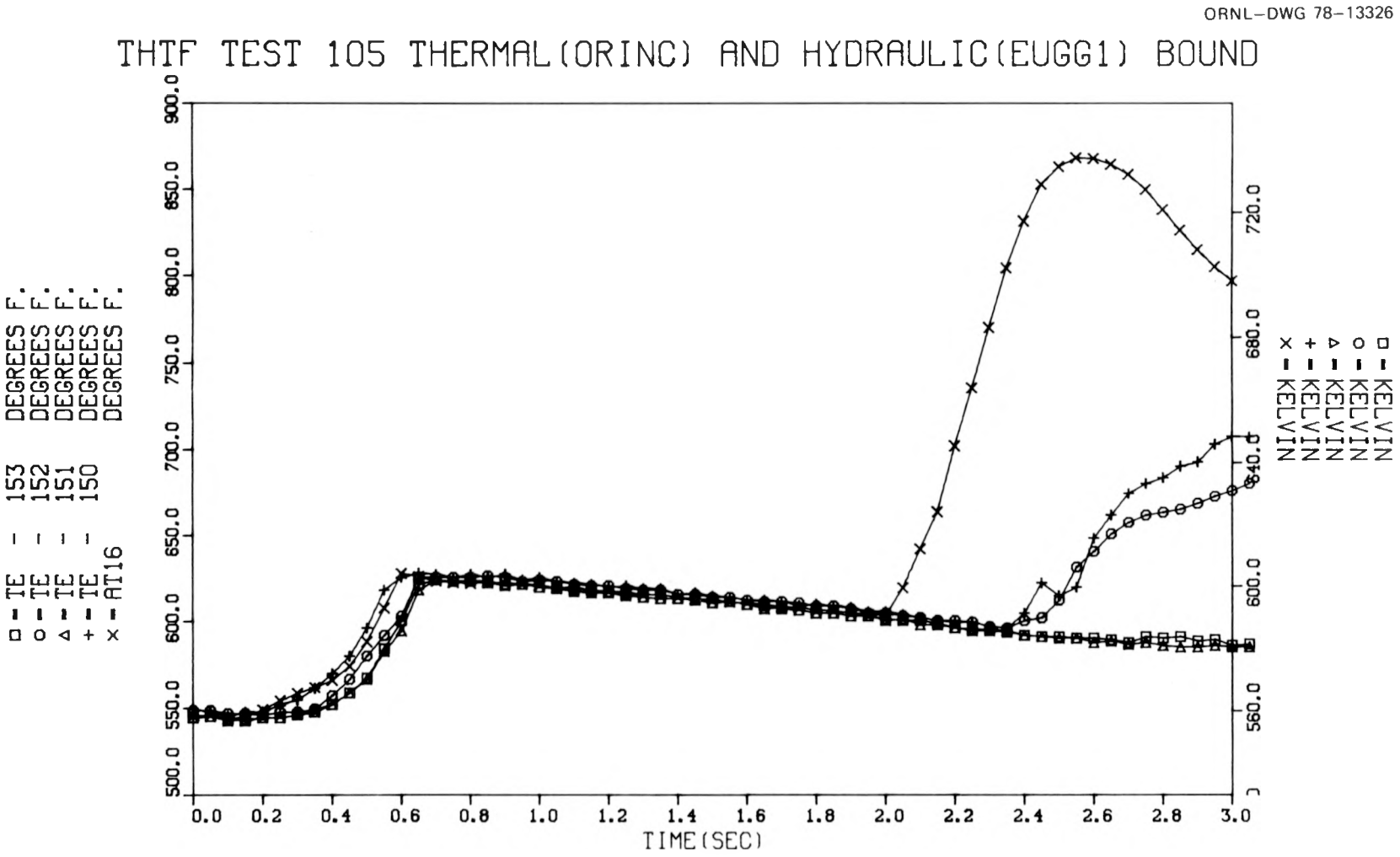

Fig. IV.13. Comparison of lower plenum thermocouple reduced responses and volume 16 temperature, THTF test 105.

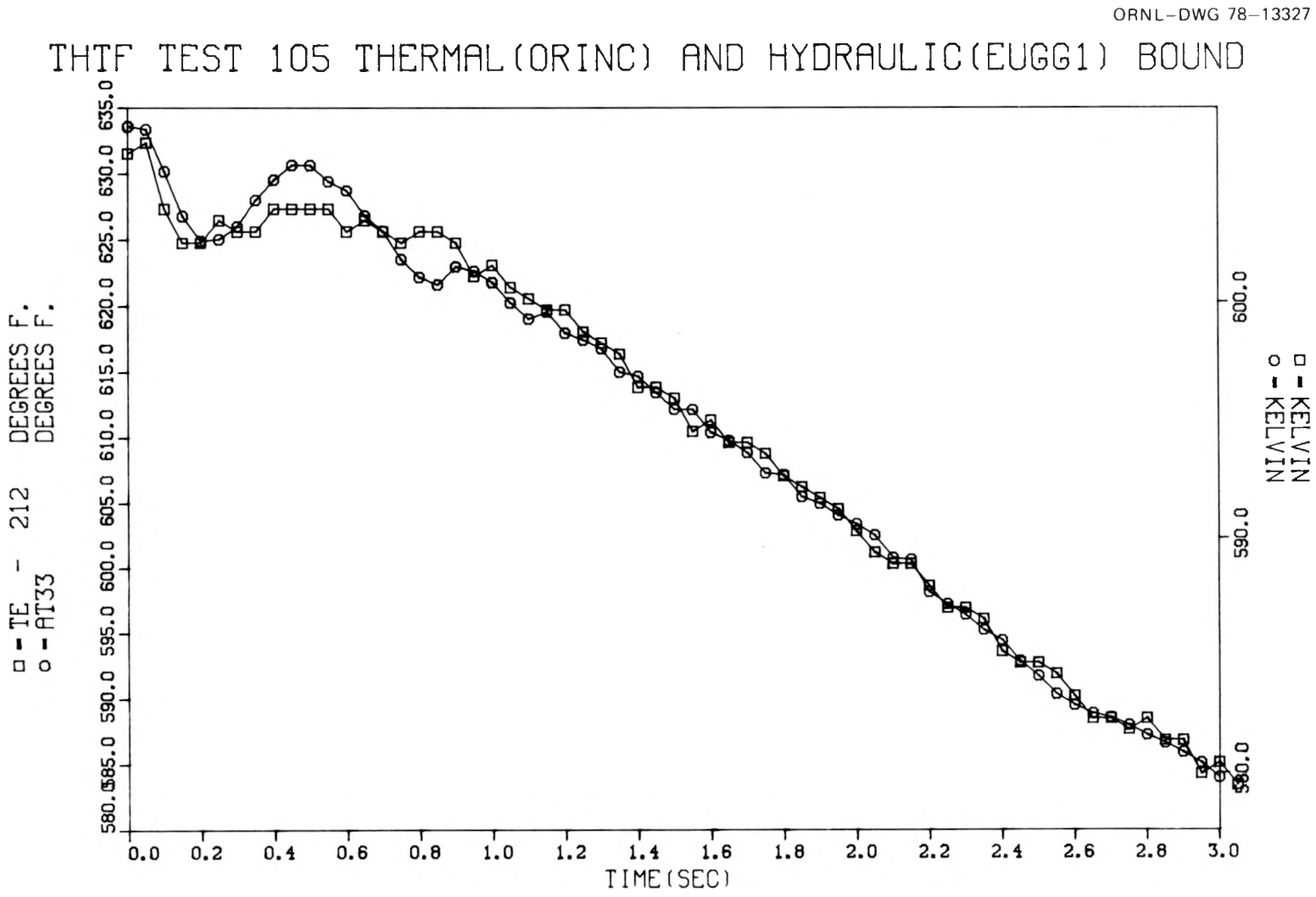

Fig. IV.14. Comparison of outlet line thermocouple reduced response and volume 33 temperature, THTF test 105.

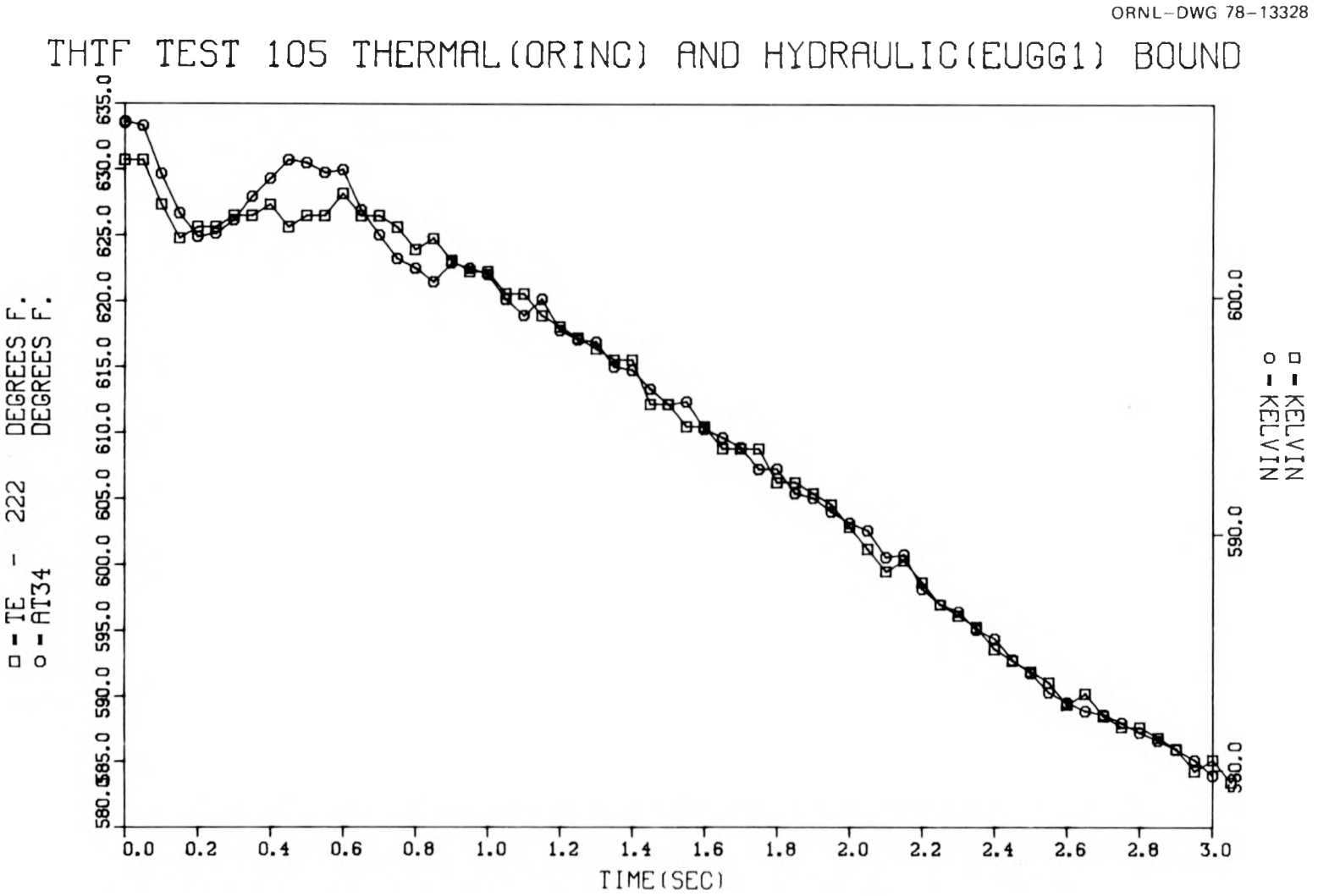

Fig. IV.15. Comparison of vertical outlet thermocouple reduced response and volume 34 temperature, THTF test 105.

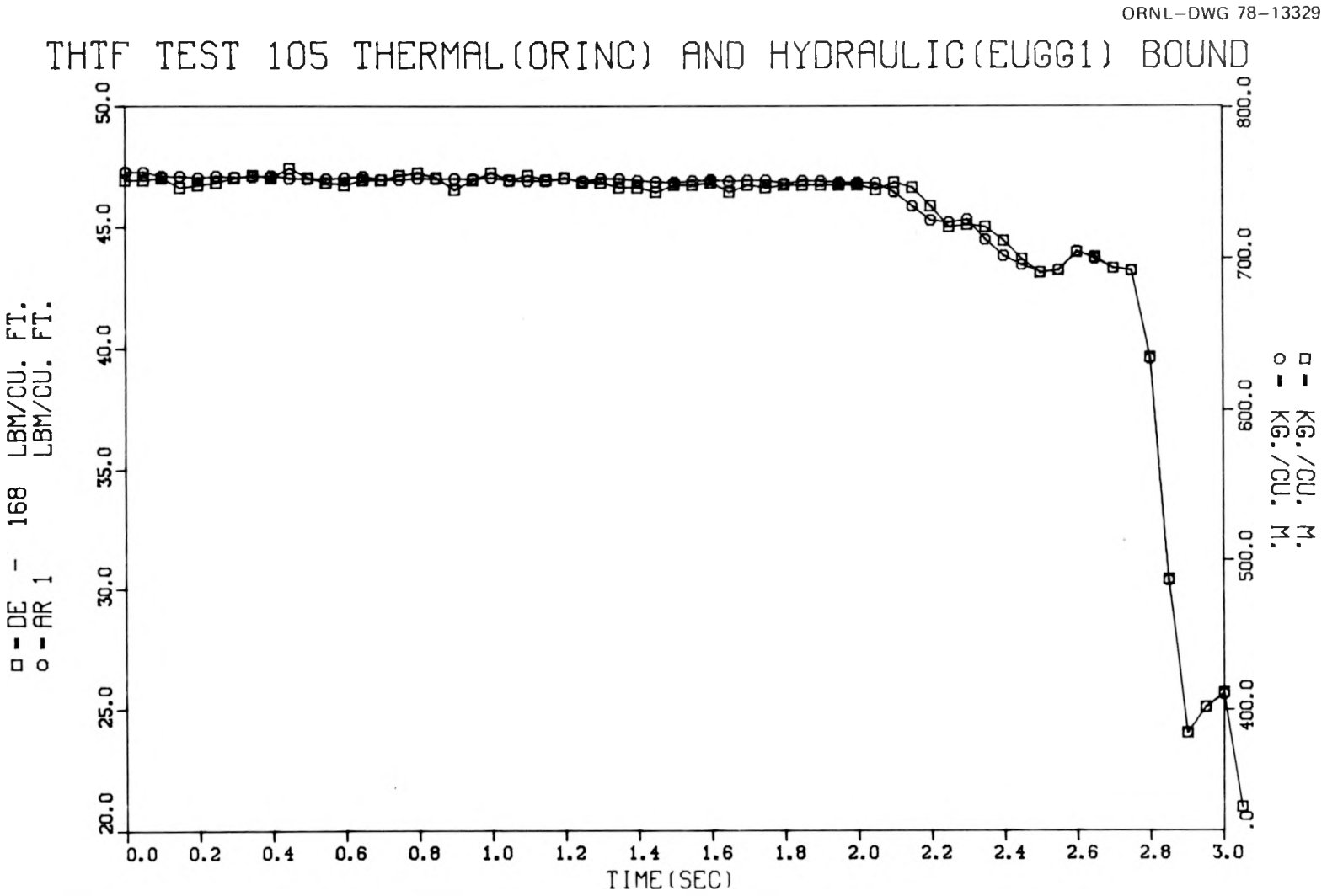

Fig. IV.16. Comparison of vertical inlet densitometer reduced response and volume 1 input density, THTF test 105.

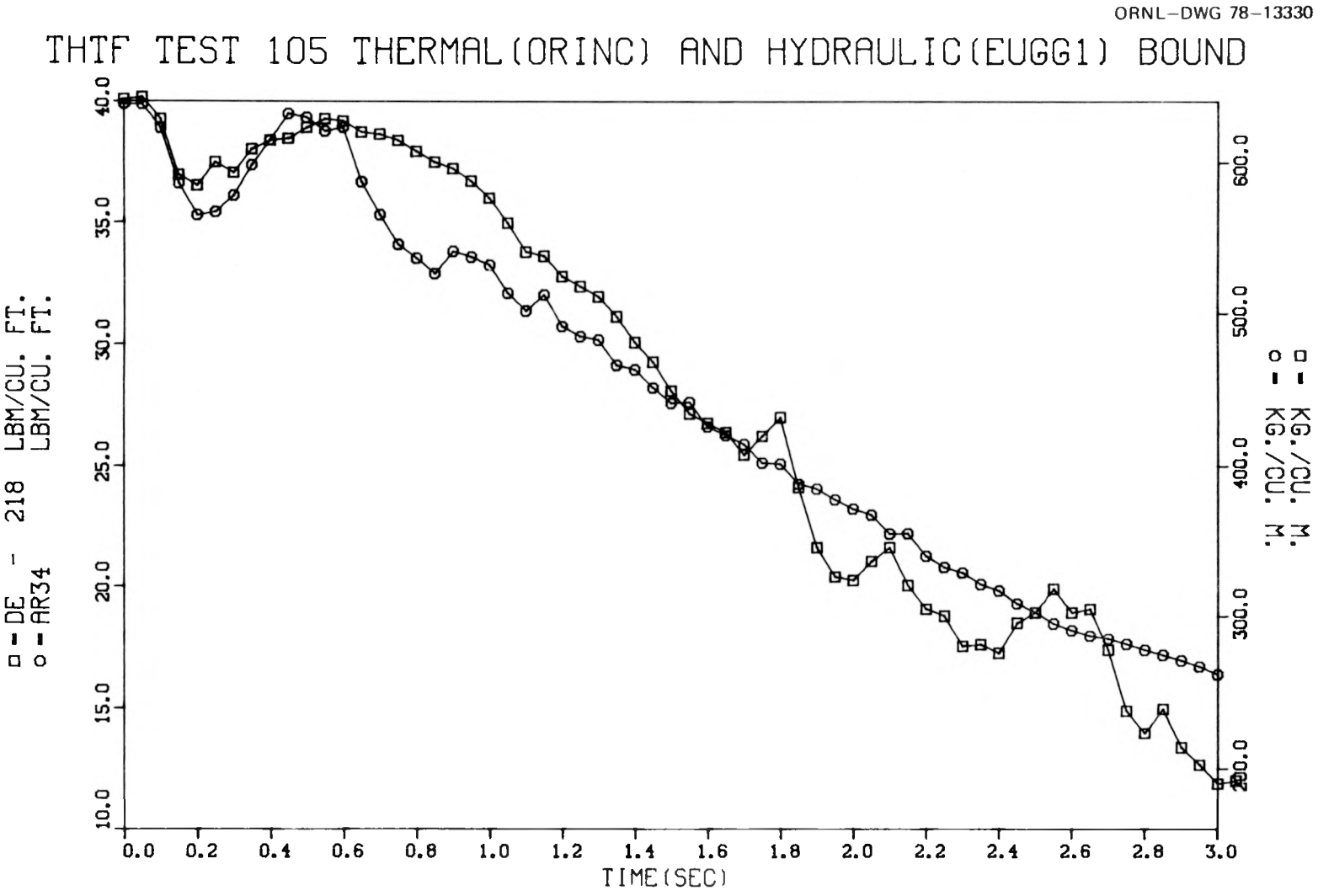

Fig. IV.17. Comparison of vertical outlet densitometer reduced response and volume 34 density, THTF test 105.

V. CONCLUSIONS

The heat transfer phenomena observed in test series 100 of the THTF have been analyzed and described. Three separate occurrences of DNB were observed in these tests. First, CHF occurred from the middle to the bottom of the rod bundle at approximately 0.6 sec (during a period of relatively high flow) because of increased local fluid enthalpy. Second, CHF occurred in the upper part of the rod bundle at approximately 2 sec because of low flow. Third, DNB occurred between 5 and 7 sec because of the passage of superheated steam. A comparison of the tests revealed that the heat transfer and rod surface temperatures are relatively sensitive to changes in the flow pattern, whereas the flow is not as sensitive to changes in rod power or heat transfer. This conclusion has significance for those working to develop codes for margin-of-safety calculations. As heat transfer correlations and logic are improved to better reflect the actual phenomena, they will also reflect this sensitivity to fluid conditions. Therefore, advances in the development of heat transfer correlations for predictive codes without concomitant improvement in the ability to predict fluid conditions is futile.

The ability of RELAP4/M5U2 to predict THTF transient behavior and to calculate local fluid conditions in the test section given experimental boundary conditions was investigated. The surface temperatures calculated by RELAP in both applications share the same characteristics; RELAP's calculated surface temperatures in the lower part of the rod bundle were close to experimental results, while RELAP's surface temperatures were well above experimental results in the upper part of the rod bundle. Departure from nucleate boiling was predicted at approximately 0.6 sec in the lower region when predictions of increasing quality produced large drops in the predicted values for CHF. Critical heat flux predictions decrease similarly in the upper region, but predictions of low flow at approximately 0.4 sec produced a slightly earlier prediction of DNB. Although our current inability to obtain sufficiently accurate local fluid conditions prevents definitive judgment of RELAP's heat transfer correlations and logic, it has been noted that the standard correlation for critical heat flux used early in the transient, B&W-2, is applied

beyond the range of the data for which it was developed when the erroneous DNB in the upper bundle is predicted. This suggests that more experimental data for CHF in regions of high quality (above 0.2), high pressure, and low flow are needed. Similarly, the potential effect of a slip model on calculated fluid conditions emphasizes the desirability of additional experimental work that can provide a basis for a more comprehensive and accurate slip model. Neither the choice of film boiling correlation (Dougall-Rohsenow or Groeneveld 5.9) nor CHF correlation (B&W-2 or General Electric) has an effect on RELAP's calculated surface temperature comparable to the errors in those temperatures in the upper bundle.

The primary hindrance to the analysis effort in the PWR-BDHT Program at present is the poor quality of some experimental measurements necessary for the computation of accurate hydraulic boundary conditions for the test section. Were such accurate boundary conditions available, the ability of RELAP to calculate accurate local fluid conditions given the test section boundary conditions could be determined. (Efforts are in progress to develop additional instrumentation to be used inside the test section which will assist in this determination.) If RELAP's accuracy in this application were judged insufficient, efforts to find or create a satisfactory code would be initiated. Once accurate local fluid conditions are obtained, a valid basis would exist for comparison of current heat transfer correlations and switching logic to heat transfer coefficients calculated directly from experimental data. Limited, preliminary comparisons have been made in Chapter IV.

REFERENCES

1. *Project Description ORNL PWR Blowdown Heat Transfer Separate-Effects Program — Thermal-Hydraulic Test Facility (THTF)*, ORNL/NUREG/TM-2 (February 1976).

2. R. A. Hedrick et al., *PWR Blowdown Heat Transfer Separate-Effects Program Data Evaluation Report — System Response for Thermal-Hydraulic Test Facility Test Series 100*, ORNL/NUREG-19 (November 1977).

3. *RELAP4/MOD5: A Computer Program for Transient Thermal-Hydraulic Analysis of Nuclear Reactors and Related Systems Users' Manual*, Vols. 1–3, Idaho National Engineering Laboratory, Idaho Falls, Idaho, ANCR/NUREG/1335 (September 1976).

4. M. J. Roberts, *Flow Measurement Uncertainty Since Installation of Lightweight Rotors in Turbine Meters*, ORNL intra-laboratory correspondence to B. G. Eads et al., Apr. 6, 1977.

5. L. J. Ott and R. A. Hedrick, *ORINC — A One-Dimensional Implicit Approach to the Inverse Heat Conduction Problem*, ORNL/NUREG-23 (November 1977).

6. L. J. Ott et al., *Error Propagation and Uncertainty Analysis in ORINC Surface Conditions*, ORNL report, to be published.

7. L. J. Ott et al., *Multi-Dimensional Inverse Heat Transfer Code (ORMDIM)*, ORNL report, to be published.

8. Izuo Aya, *A Model to Calculate Mass Flow Rate and Other Quantities of Two-Phase Flow in a Pipe with a Densitometer, a Drag Disk, and a Turbine Meter*, ORNL/TM-4759 (November 1975).

9. M. D. White, *MASFLO: A Computer Code to Calculate Mass Flow Rates in the THTF*, ORNL report, to be published.

10. C. B. Davis, *RELAP4/MOD6 Comparison with PWR-BDHT Test 103 Core Data*, Idaho National Engineering Laboratory, Idaho Falls, Idaho, PG-R-77-27 (July 1977).

11. S. B. Cliff, *RLPSFLUX — RELAP with Surface Flux Modifications*, ORNL/NUREG/CSD/5, to be published.

12. C. D. Morgan, "A Study of Film Boiling from Vertical Surfaces," Ph.D. Dissertation, Lehigh University, 1965.

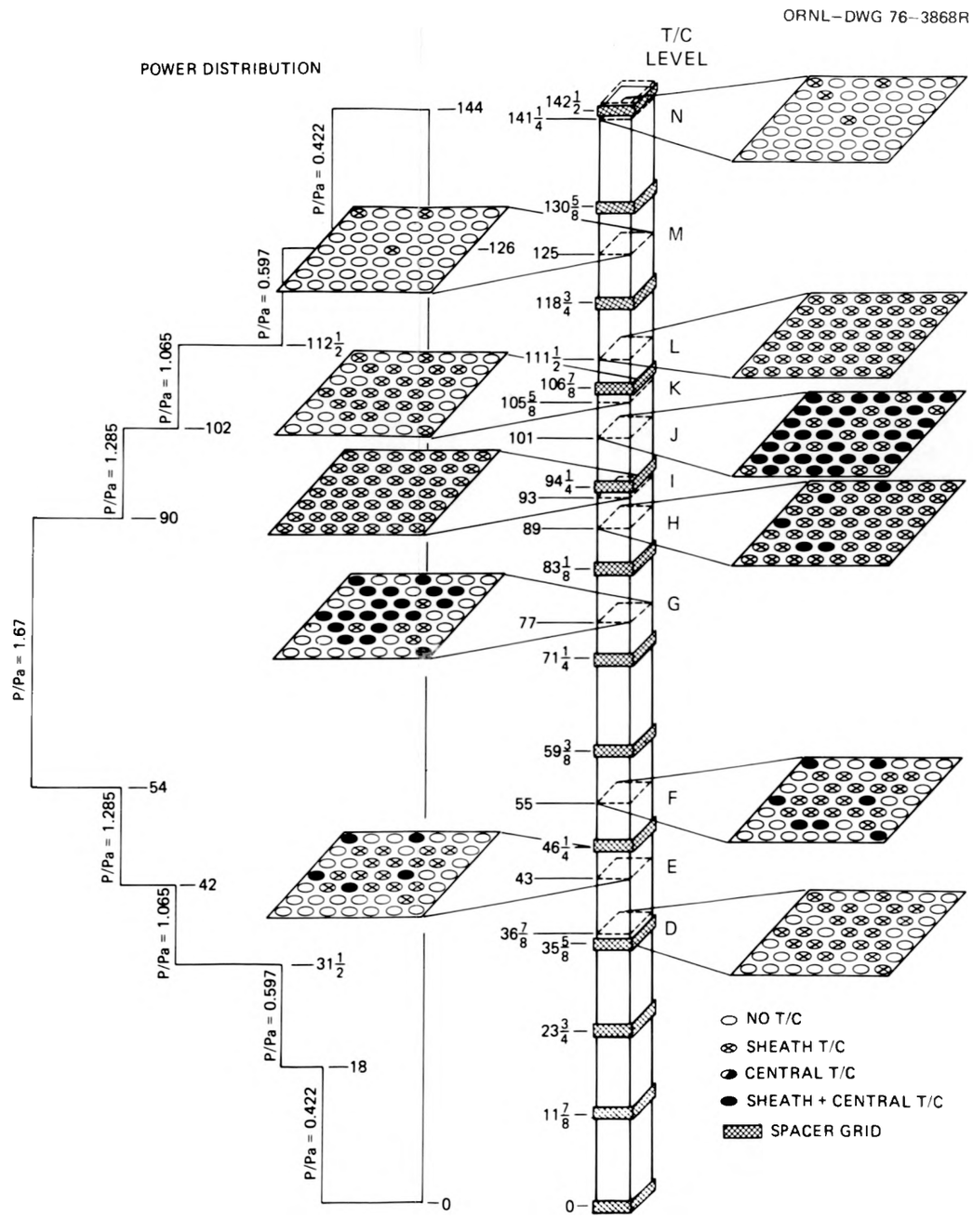

Location of thermocouples in THTF bundle 1.

APPENDICES

Appendix A

SYSTEM HYDRODYNAMICS

The purpose of this appendix is to familiarize the reader with the hydrodynamic response of the THTF to the double-ended breaks of tests 103, 104, and 105. Test 103 will be described in some detail. Since tests 104 and 105 are similar to test 103 in many respects, they will be mentioned only when they differ from test 103 in a way significant to the body of this report. The description of test 103 will proceed chronologically from rupture of the break plenums.

Before the tests themselves are described, a brief discussion of the governing physical interactions may be helpful. In very general terms, phase change controls the rate of depressurization of the THTF. If the system were initially filled with water at a temperature low enough that the saturation pressure were below atmospheric pressure (and no energy were added), the system would depressurize in a small fraction of the time it actually takes. Similarly, if the system were filled solely with steam, the adiabatic depressurization would be more rapid. Depressurization of the THTF is slowed to the observed rate by the presence of water that can change phase from liquid to vapor. Two-phase fluid in the system exerts sufficient force on subcooled fluid to prevent its pressure from rapidly falling to its saturation pressure. Thus, flow in the system will generally tend to be from locations where two-phase fluid is present toward the breaks.

The role of phase change in controlling depressurization rates causes volumetric flow to become an important consideration. Consider an arbitrary container full of a steam and liquid water mixture in equilibrium with phases separated. A leak in the region of steam will produce faster depressurization than a leak in the liquid region if the steam leak produces higher volumetric flow from the container, even though the steam leak may cause a slower loss of mass and energy. This will hold true as long as some liquid remains in the container and as long as the creation of steam from the liquid is at an interface away from the leak; that is, the leak in the liquid region is not losing fluid that was part of an interface where phase change was occurring. This can be understood by

imagining the loss from the container of a small portion of mass and considering the volume it vacates. If already existing steam expanded to fill most of the vacated volume, the pressure of the vapor phase would fall well below that of the liquid phase and thereby cause sufficient phase change to raise the vapor pressure to near its original value. Thus the primary mechanism through which the remaining water fills the vacated volume is phase change. If the mass lost is steam instead of water, more phase change will take place because of the higher volume of the steam. In the absence of any addition of energy, the more phase change that occurs, the farther the pressure will fall.

A quantitative illustration of this effect can be provided by RELAP. A 0.566-m^3 (20-ft^3) container was modeled using RELAP, and two calculations were performed. Each started with the container half full of water and half full of steam, with the phases separated but in thermodynamic equilibrium. In one calculation, there was a leak at the top of the container in the steam region; and in the other calculation, there was a leak of equal size at the bottom in the liquid region. The initial pressure was 15.16 MN/m^2 (2200 psia). RELAP's critical flow model calculated a higher volumetric flow and a lower mass and energy flow for the steam leak than for the liquid leak (Figs. A.1 and A.2). Whether the calculation of the flow at the leaks is correct is irrelevant since the point of interest is the relative conditions in the container if such flows were to exist. RELAP's ability to correctly calculate the conditions in the container should be fairly good, since for a small leak RELAP's assumption of thermodynamic equilibrium at each time step is probably very nearly correct. As expected, RELAP predicted a much slower depressurization rate for the liquid leak than for the steam leak (Fig. A.3), in spite of the loss of more mass and more energy for the liquid leak (Figs. A.1 and A.2). Once the liquid leak had emptied all the liquid from the container, depressurization occurred by steam expansion, which is more rapid, and the pressure fell below that of the container with the steam leak. The preceding discussion leads one to expect a more rapid local rate of depressurization in the THTF when the volumetric flow of the break increases and a slower local rate when it decreases.

Two breaks were used in tests 103, 104, and 105. Each break is connected by horizontal piping to the portion of the system containing the pressurizer, pump, and heat exchangers (referred to as the back side) and by vertical piping to the test section (Fig. II.39). Each connecting pipe contains an instrumented spool piece. The description of the tests will largely be in terms of the readings of the instruments in these spool pieces. The spool pieces will be referred to by location: the horizontal inlet spool piece (HI), the vertical inlet spool piece (VI), the vertical outlet spool piece (VO), and the horizontal outlet spool piece (HO). Before rupture, water from the back side at 559.3 K (547°F) passes from the HI to the VI and into the test section. It leaves the test section at 607 K (633°F) and passes through the VO and HO and into the back side. Flow in the same direction as in steady state is considered positive, and flow in the opposite direction is considered negative. The THTF has no flow instruments beyond the breaks. In the ensuing discussion, statements about volumetric flow out the break will represent inferences drawn from the spool piece flow data. The total break area in all three tests was 12.5 cm^2 (0.0135 ft^2), divided 60% at the outlet and 40% at the inlet for tests 103 and 105 and 50%—50% for test 104. In tests 103 and 104, the power (5.978 MW) was left on for 2 sec after rupture and then dropped immediately to zero. In test 105, there was an exponential decay from full power at 2 sec with a time constant of 0.45 sec until 5.80 sec, when the power was shut off.

The transient is initiated by the simultaneous rupture of both break orifices. Subcooled depressurization causes an initial rapid pressure drop of 2.76 MN/m^2 (400 psi) in less than 0.1 sec (Fig. A.4). The pressure drops below that which would be permitted by the pressurizer fluid (which was saturated initially) during the transit time for the phenomenon to reach the pressurizer and return. The pressurizer resurgence drives the pressure up 0.55 MN/m^2 (80 psi). The hydraulic resistance between the pressurizer and the inlet break rapidly becomes much smaller for a route going past the outlet break and through the test section than for one going past or through the pump and along the HI piping. This decrease is due to the pump being shut off at rupture and the rapid loss of head while the flow control valves near the pump retain their large resistance.

The pump head, initially 5.2 MN/m^2 (750 psi), drops 1.4 MN/m^2 (200 psi) in the first 0.5 sec. Thus, flow in the VO (Fig. A.5), which initially surges more positive, rapidly decreases and goes negative at 0.8 sec. Flow is being driven from outlet to inlet through the test section by the pressurizer fluid. Test 104, with its smaller outlet break, has more negative flow sooner at the VO (Fig. A.6). From this we infer that the early negative flow through the test section is larger for test 104 than for either test 103 or 105. It should be noted that another effect is present which will contribute to the early flow reversal: the initial temperature distribution. If there were no pressurizer in the system, the subcooled depressurization would drop the inlet pressure well below the outlet pressure and thus still produce a flow reversal.

While the initial flow reversal is occurring, density is dropping at the saturated outlet (Figs. A.7 and A.8), producing higher volumetric flow through the outlet break. By approximately 1 sec, this higher volumetric flow has enabled the outlet break to accommodate the expansion of the pressurizer fluid and permit the VO to resume positive flow toward the break. Since the smaller outlet break in test 104 cannot accept as much flow from the VO, flow there is not positive as long, nor is it as strong as in tests 103 and 105 (Fig. A.6). From 1 to 3 sec, flows at both the VO and the VI (Fig. A.9) are toward the breaks, implying the existence of a flow stagnation point within the test section. Since flow at the VI reverses immediately upon rupture, a stagnation point must also have existed within the test section between 0 and 0.8 sec (0 and 0.4 sec for test 104), during which time the VO was positive. At 1.9 sec, hot fluid from the test section begins to arrive at the inlet piping (Fig. A.10) and causes saturation at the VI at 2.5 sec (Fig. A.11). This does not imply, however, that saturated fluid is necessarily exiting through the break. The HI is still subcooled (Fig. A.12) at 559.3 K (547°F), and a comparison of the flows at the VI and HI (Fig. A.13) shows that most of the mass entering the inlet break plenum is from the HI. A calculation of fluid conditions in the break plenum, using calculated mass flows for the spool pieces and assuming complete mixing, indicates that the break fluid would not saturate at this time. The calculated results are such that instrument error bands make it impossible to determine if saturation

occurs, even if the mixing assumption were perfect. Nonetheless, a substantial increase in volumetric flow through the inlet break due to saturation at the VI appears unlikely.

At 3 sec, the HO densitometer (Fig. A.8) shows the arrival of a slug of very low-quality fluid. This fluid was initially between the main heat exchanger outlet and bypass junction and the pressurizer inlet line. The slug sharply decreases the volumetric flow at the HO (Fig. A.14) and thus at the outlet break. The decrease in volumetric flow is large enough that it slows the depressurization rate of the entire system. The effect is strongest at the outlet break itself, causing flow at the VO to drop to near zero at 3.7 sec and to actually become negative from 4.4 to 4.9 sec. At 4.9 sec, departure of the low-quality fluid, which allows resumption of higher volumetric flow and hence more rapid depressurization, leads to a strong, positive surge in VO flow (Fig. A.5). Note that the VO densitometer (Fig. A.7) shows a smaller density increase that coincides in time with the HO density increase (Fig. A.8). While the VO density increase begins at 3.3 sec, the VO turbine at this time still reads 0.013 m^3/s (200 gpm) toward the break and does not show negative flow until after 4.1 sec. This implies that either the turbine meter reading is in error at this time by 0.013 m^3/s (200 gpm) or that countercurrent flow exists. The turbine may be reflecting a relatively high volumetric flow of steam out of the test section while low-quality fluid from the HO passes up the VO piping.

Test 105, which has more energy added to the core than test 103, shows a smaller decrease in VO flow (Fig. A.15) with the arrival of the low-quality fluid at the HO, reflecting its more energetic core fluid. The increase in the VO density for test 105 (Fig. A.16), which again temporally matches the HO density increase, is correspondingly smaller. The VO flow in test 105 never becomes negative, although the instrument reads almost exactly zero for 0.3 sec. Once again, countercurrent flow is suggested by the existence of a density surge at the VO (Fig. A.16) from 3.4 to 4.2 sec while the turbine meter (Fig. A.15) is reading 0.006 m^3/s (100 gpm) toward the break.

Test 104 has no more power than test 103 but has a smaller outlet break area, causing the VO to respond to the arrival of low-quality fluid

at the HO more strongly than in either of the other tests. The turbine meter (Fig. A.6) shows negative flow for most of the period from 3.1 to 5.1 sec. The largest negative surge of the turbine meter, from 4.3 to 4.9 sec, is reflected in a large upward surge in density (Fig. A.17). In all three tests, the VI flow responds to these events at the outlet by increasing its flow toward the break (Fig. A.9) from 3 to 5 sec, reversing the trend of decreasing flow from 1 to 3 sec. In general, the arrival of the low-quality fluid at the HO causes the flow stagnation point to move out of the test section to the outlet break and increases the negative flow through the core.

At approximately 5 sec, the low-quality fluid at the outlet has been expelled and high volumetric flow begins at the outlet break. The resulting more rapid local depressurization rate at the outlet results in decreasing flow at the VI (Fig. A.9) as more core fluid begins to flow toward the outlet. The inlet break is receiving most of its mass as subcooled water from the HI. The high volumetric flow at the outlet finally results in the flow at the VI becoming positive (i.e., into the test section) at 7 sec (Fig. A.9). Thus, between 5 and 7 sec, the flow stagnation point moves from the outlet all the way through the test section to the inlet. This second, complete flow reversal in the core is common to all three tests, although the different break ratio in test 104 delays the reversal approximately 0.3 sec and flow is not as large into the test section at the VI (Fig. A.18). At 6.75 sec, the pressure has fallen far enough to saturate the fluid in the HI (Fig. A.12). As density drops in the HI fluid feeding the break, the increasing volumetric flow at the inlet break and the corresponding increase in the local depressurization rate cause flow in the VI (Fig. A.9) to resume toward the break (negative). While flow in the VI was positive, the VI densitometer (Fig. A.11) shows the passage of lower-quality fluid from the HI toward the test section. A comparison of the VI flow and density suggests that there are three somewhat separate passages of low-quality fluid, at 8, 9.5, and 10.5 sec. Test 104, with its larger inlet break, shows only one occurrence of low-quality fluid passing up the VI, at 8 sec. Test 105 shows two well-separated passages at 8 and 11 sec, the second one being very small.

By 8 sec, the largest concentration of liquid phase left in the system is believed to be in the lowest part, that is, the pump and the piping leading to the HI. Liquid phase may also have collected in the lower plenum of the test section, and some may be left in the main heat exchangers. The flow behavior beyond 8 sec can be explained in terms of these hypotheses. The boiling of fluid in the HI piping will drive flow toward the inlet break. If both breaks have high volumetric flow, the smaller size of the inlet break and the larger size of the outlet break will tend to drive flow in the VI back into the test section (Fig. A.9). We believe that most of the fluid that had collected in the lower plenum has changed phase while rewetting the lower core and thus is not a dominant flow source. At various times the HO densitometer (Fig. A.8) shows the arrival of slugs of lower-quality fluid which probably originate in the main heat exchangers. The arrival of such a slug will decrease the outlet break volumetric flow, slow the local depressurization rate, and therefore oppose the tendency of phase change in the inlet piping to drive flow at the VI into the test section. If a slug at the HO has a large enough effect on the outlet break volumetric flow compared to the flow source in the inlet piping, flow in the VO is driven back into the test section. Thus the interplay of these two effects produces a series of flow reversals in the core, flow being down the core when low-quality fluid reaches the outlet and up the core when such fluid is absent (cf. Figs. A.8, A.9, and A.5). The same alternate increases and decreases in the vertical spool piece flows are seen in test 104 (cf. Figs. A.6 and A.18) except that the larger inlet break area prevents flow at the VI from entering the test section. The arrivals of low-quality slugs at the HO, in addition to affecting the flow pattern, also affect the total volumetric flow leaving the system and produce the undulations in the pressure (Fig. A.4) seen late in the transient.

In summarizing the preceding discussion, several points are worth repeating. The pressurizer dominates the first part of the transient and will always do so as long as the same large pressurizer is used and remains in unhindered communication with the rest of the system. The relatively low hydraulic resistance between the pressurizer and the outlet break, coupled with the relative break sizes, determines the early

flow pattern. It is also clear that the flow pattern after the first few seconds is quite sensitive to density fluctuations in fluid feeding the breaks. Accurate prediction of density gradients would seem essential to accurate prediction of flow patterns in the THTF. The relative sizes of core flows and the movements of flow stagnation points described previously are key factors in producing the rod heat transfer behavior discussed in the body of this report.

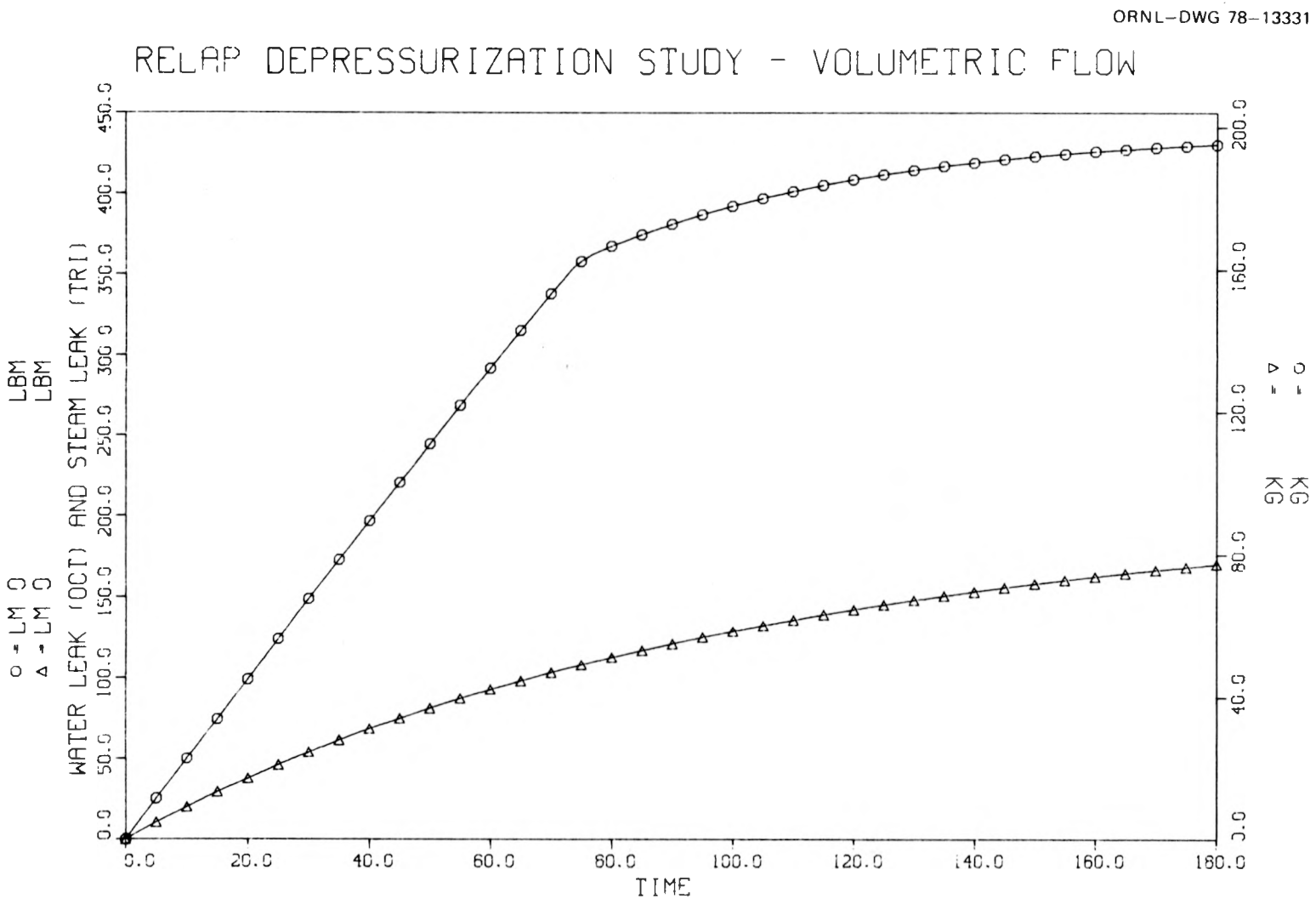

Fig. A.1. RELAP-calculated mass leaked for a system with a water leak vs the same system with a steam leak.

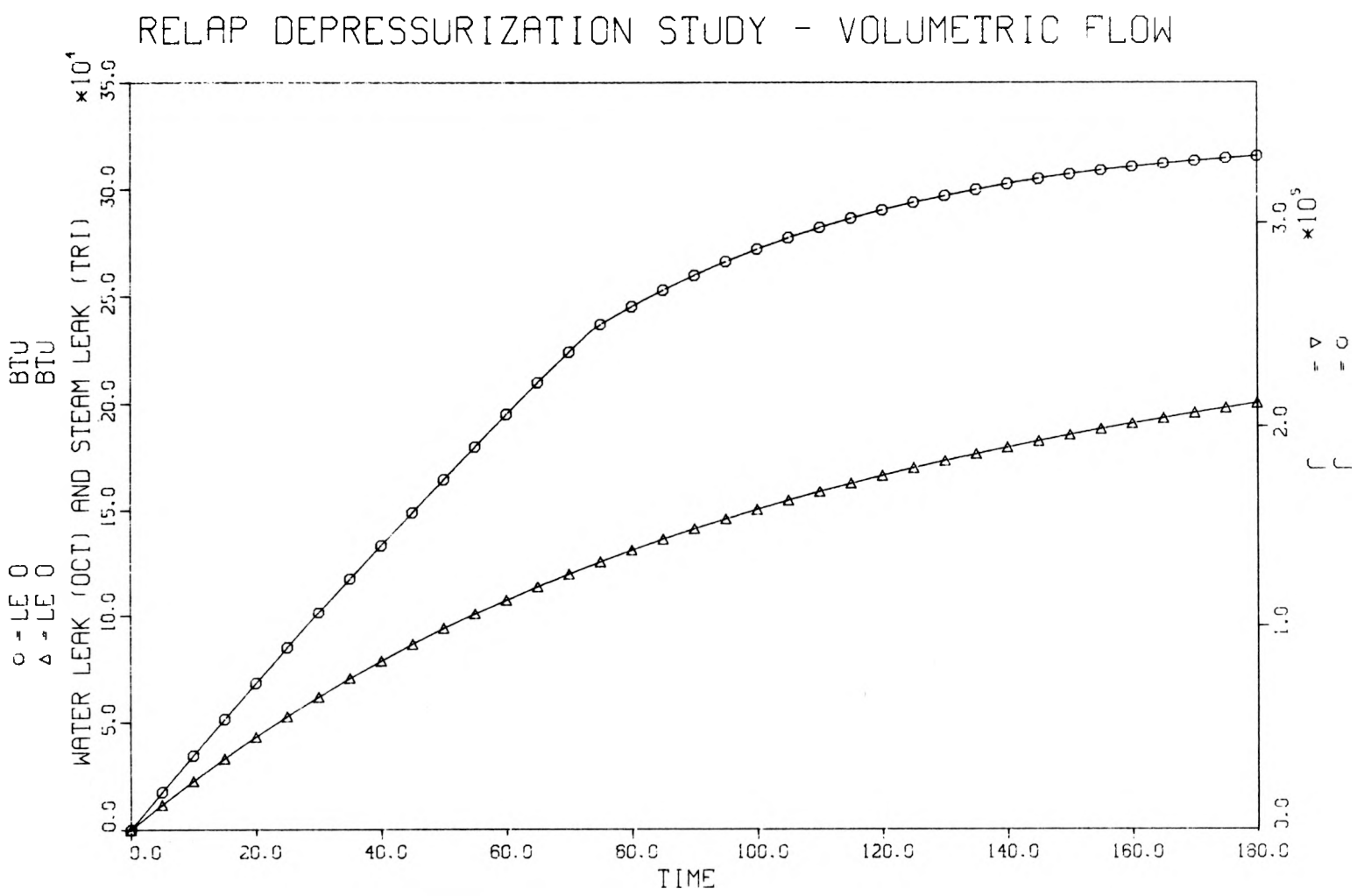

Fig. A.2. RELAP-calculated energy leaked for a system with a water leak vs the same system with a steam leak.

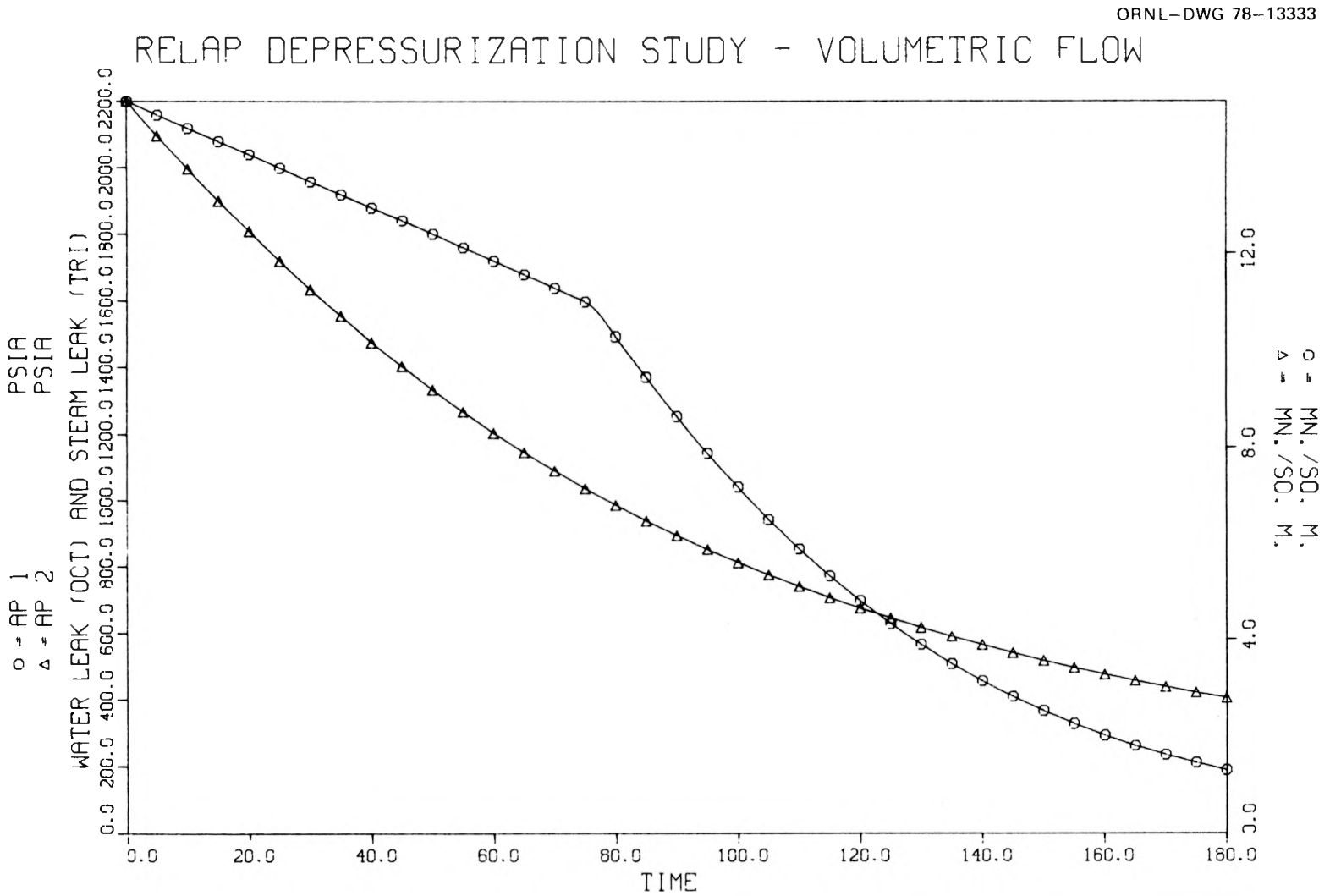

Fig. A.3. RELAP-calculated pressure of system with a water leak vs the same system with a steam leak.

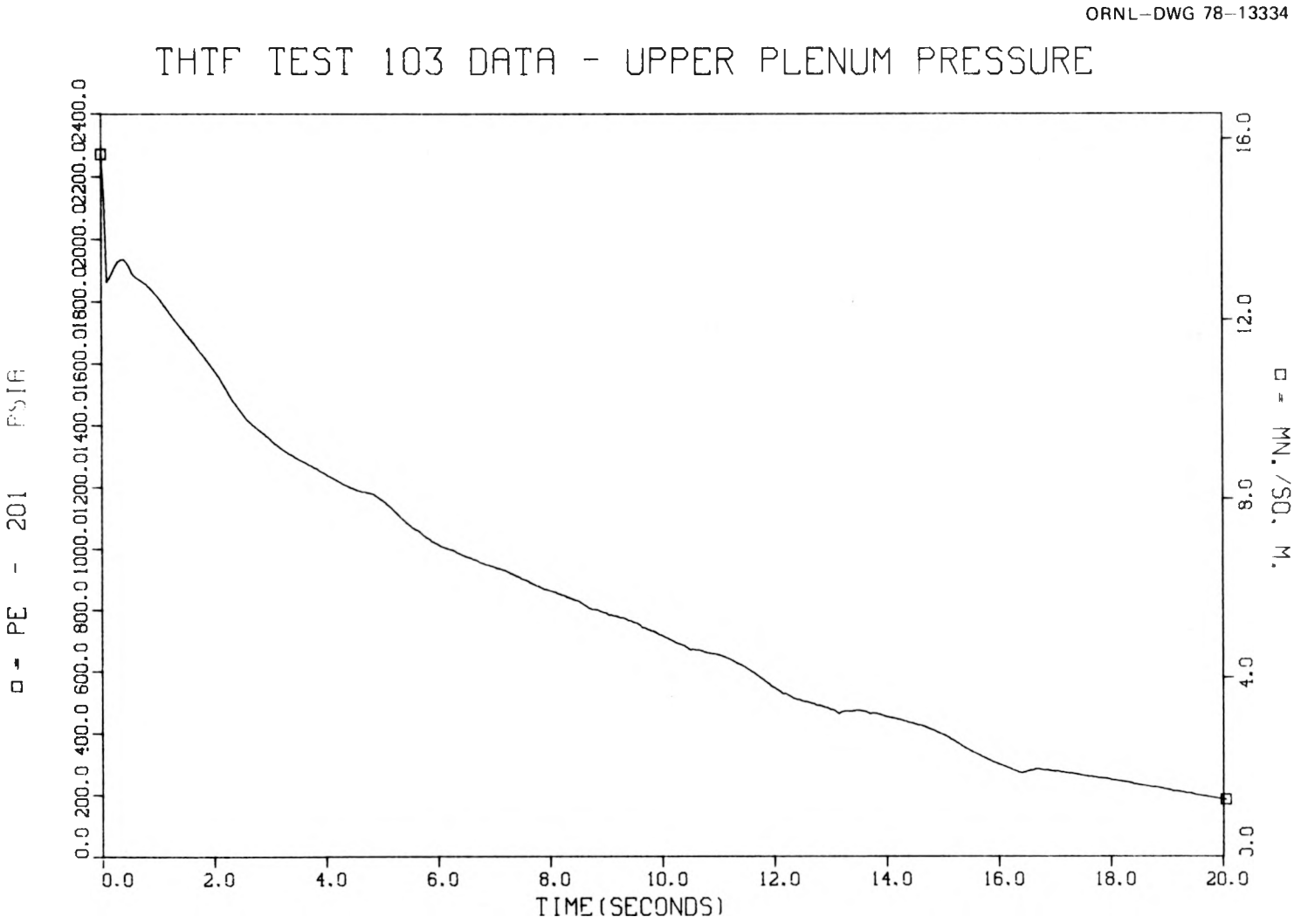

Fig. A.4. Upper plenum pressure for test 103.

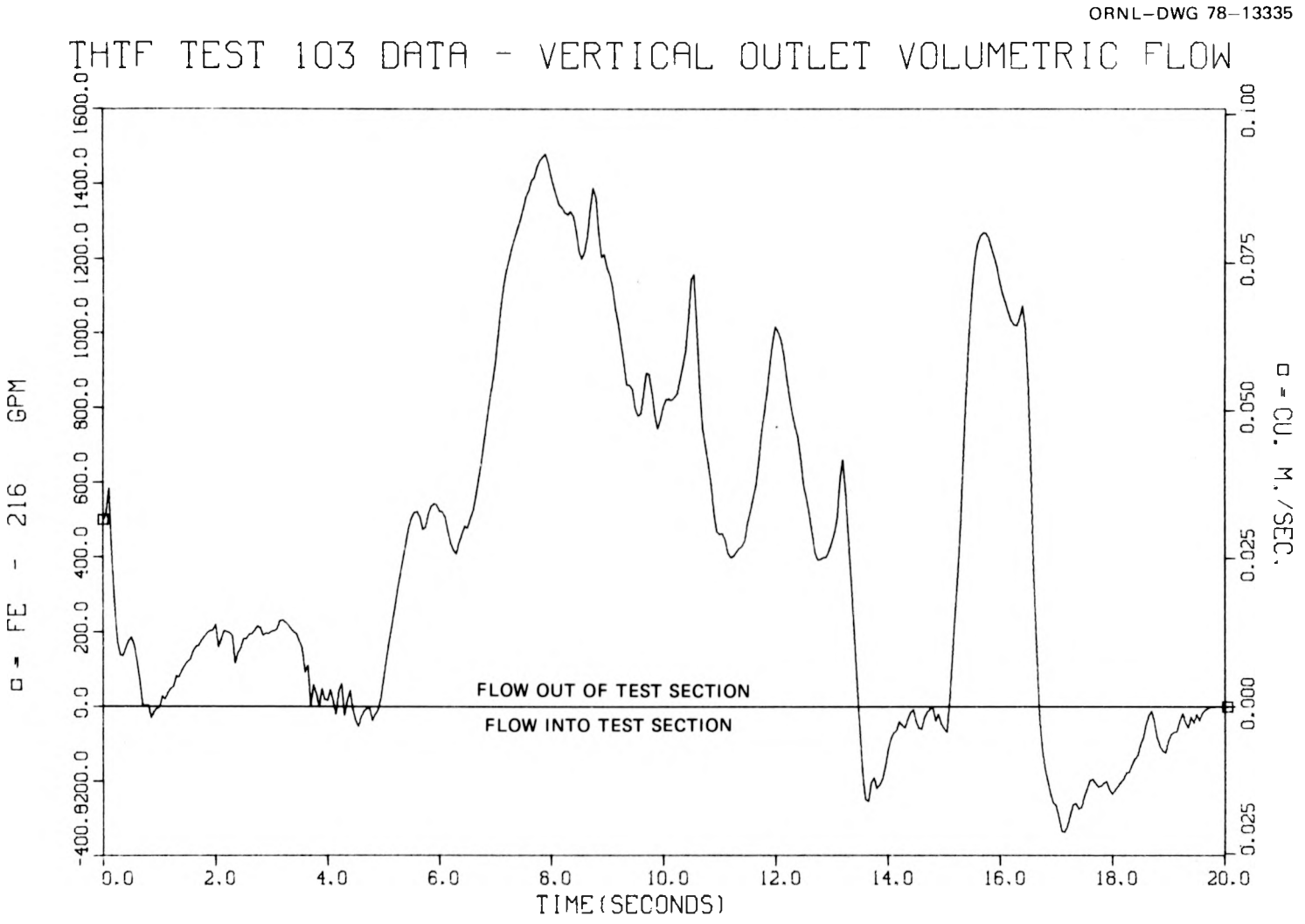

Fig. A.5. Vertical outlet spool piece volumetric flow — test 103.

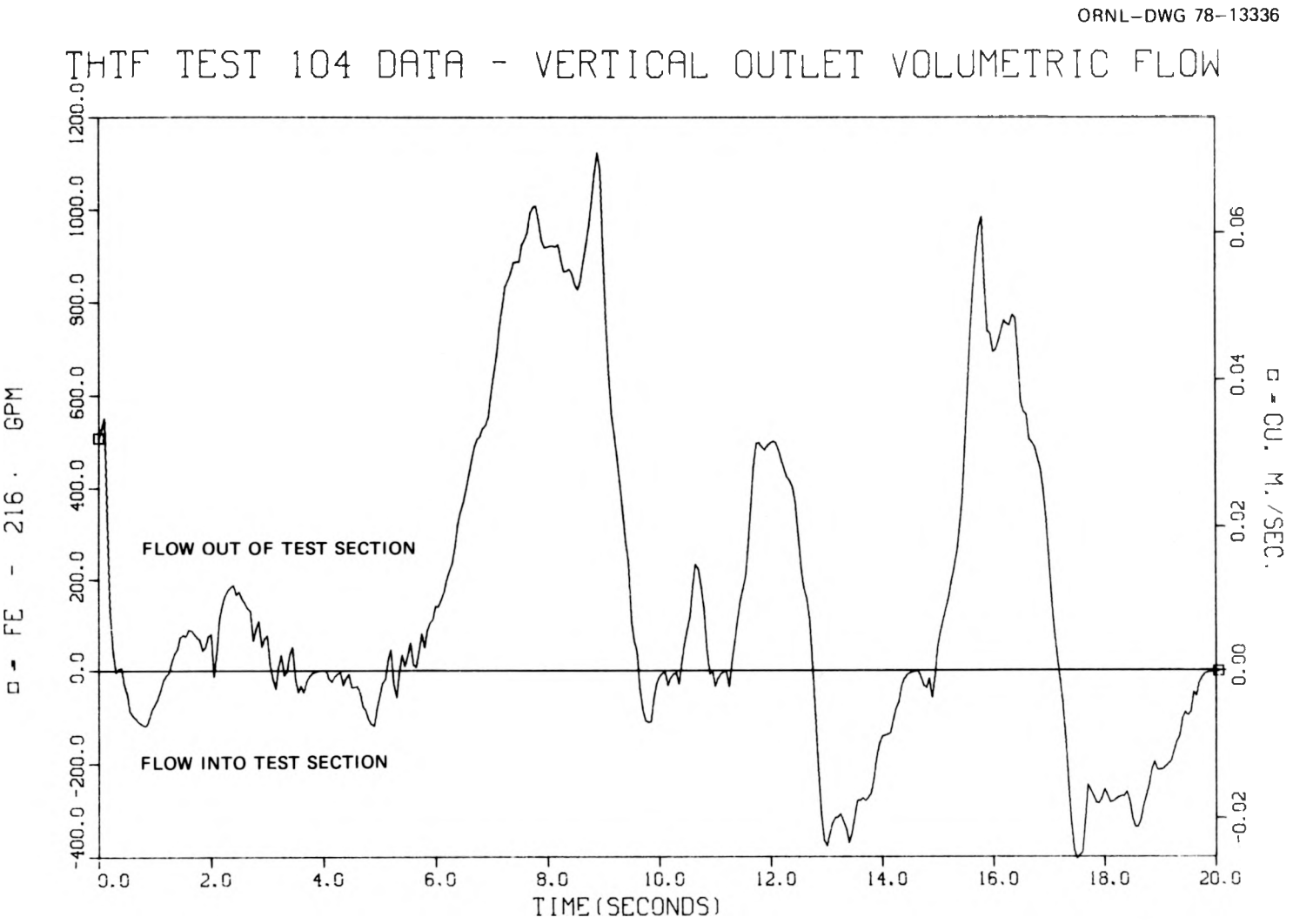

Fig. A.6. Vertical outlet spool piece volumetric flow — test 104.

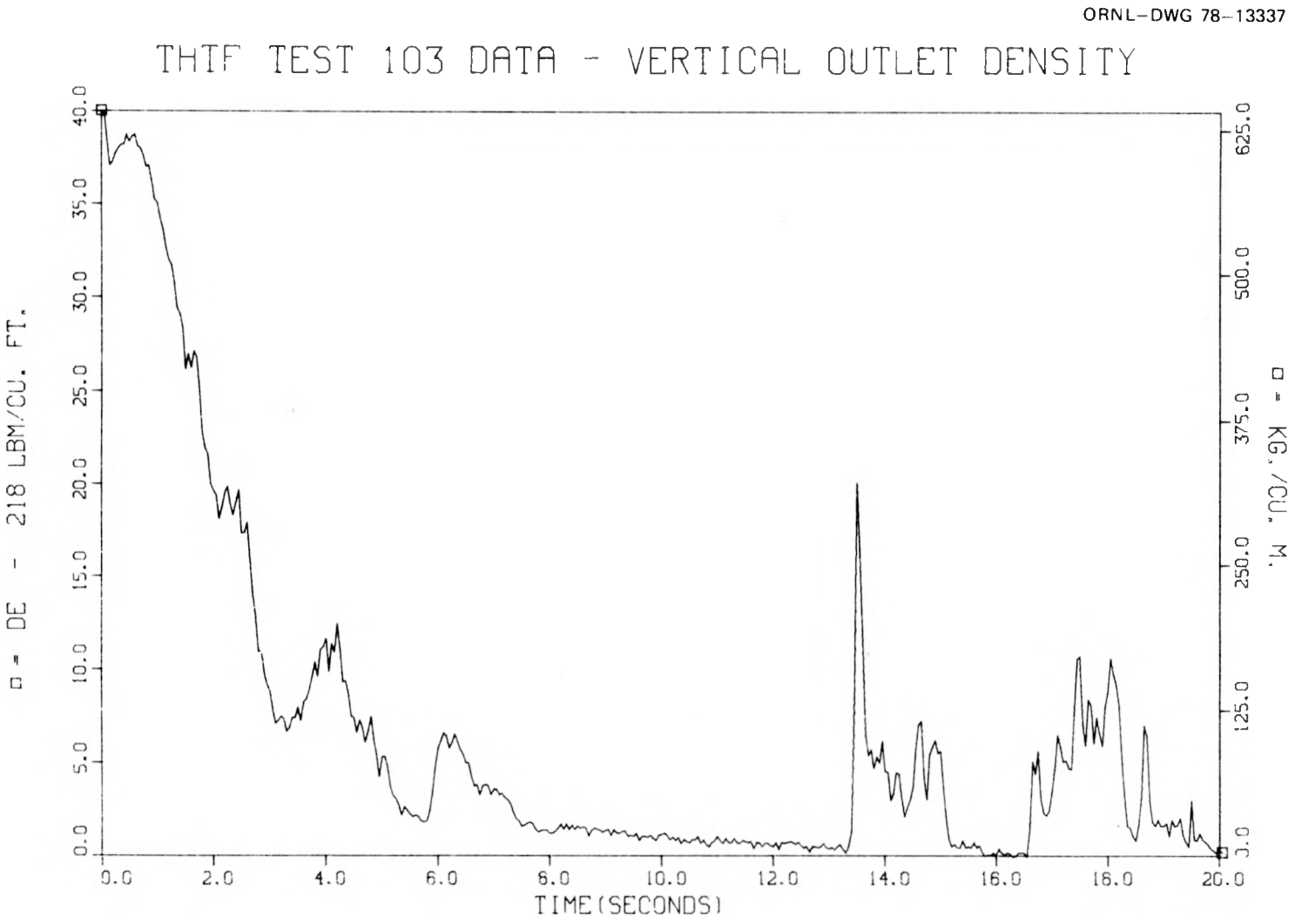

Fig. A.7. Vertical outlet spool piece density — test 103.

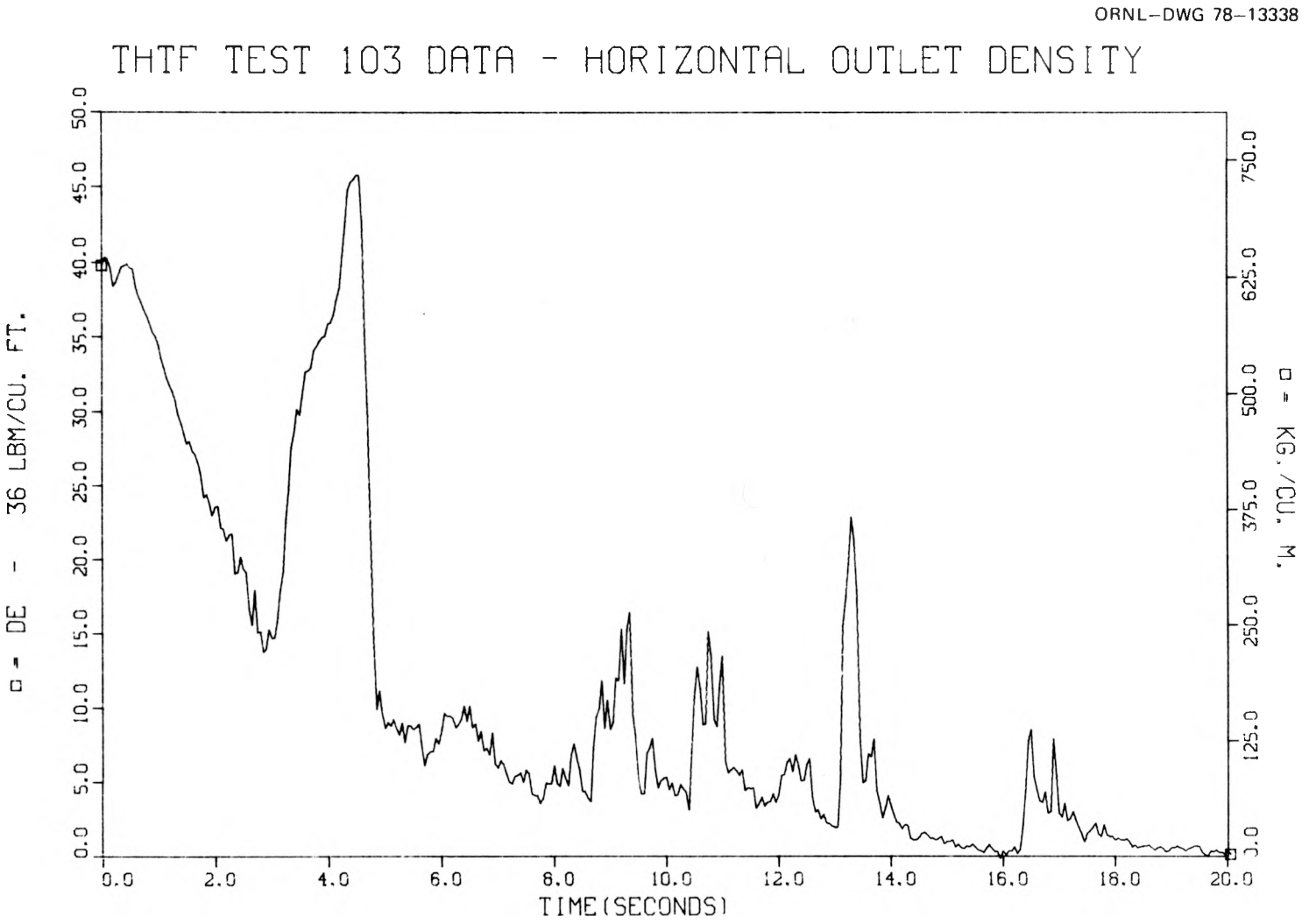

Fig. A.8. Horizontal outlet spool piece density — test 103.

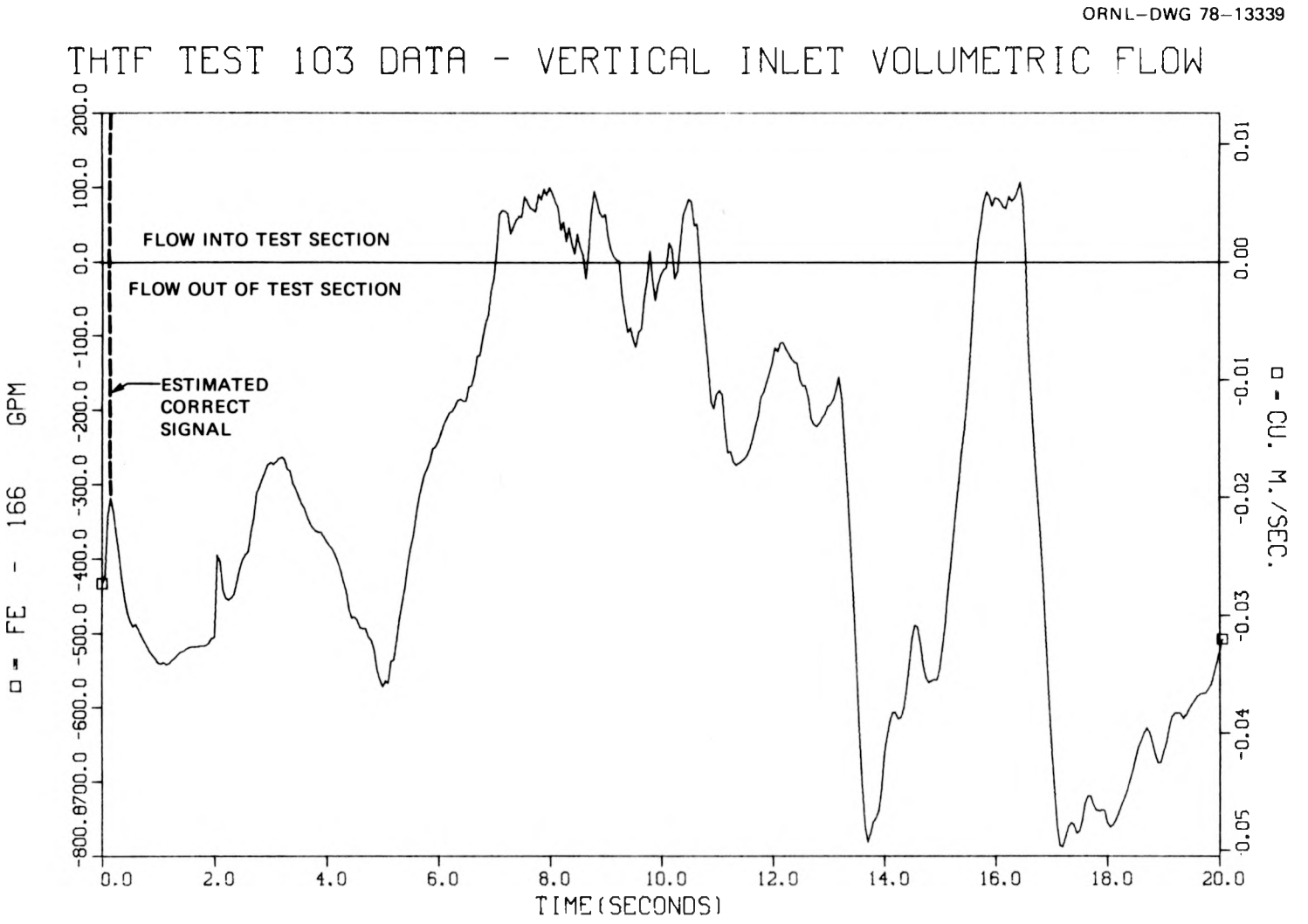

Fig. A.9. Vertical inlet spool piece volumetric flow — test 103 (corrected). (Polarity reversal produced inverted signals in early transient. Dotted line indicates estimated correct signal.)

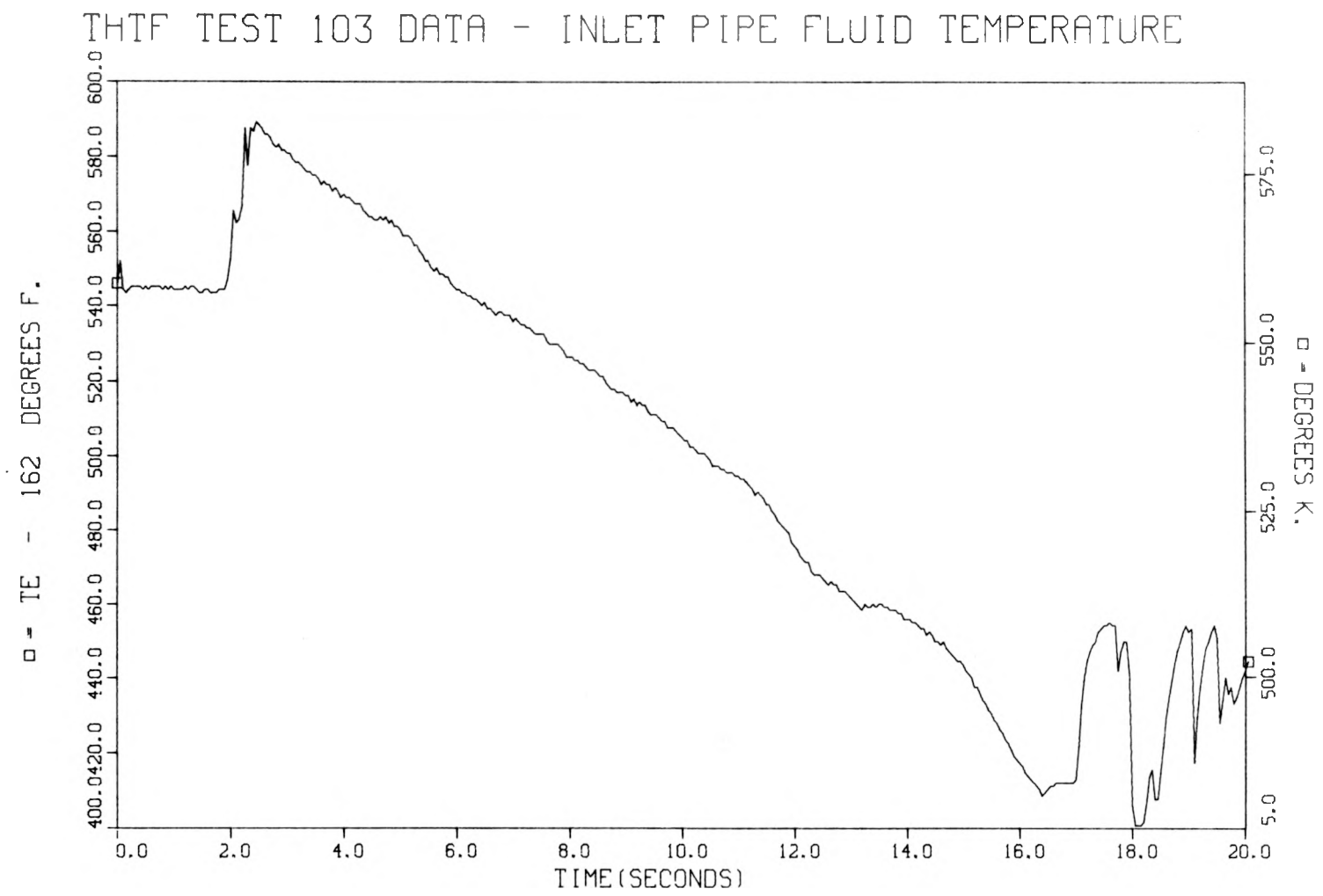

Fig. A.10. Test section inlet pipe fluid temperature — test 103.

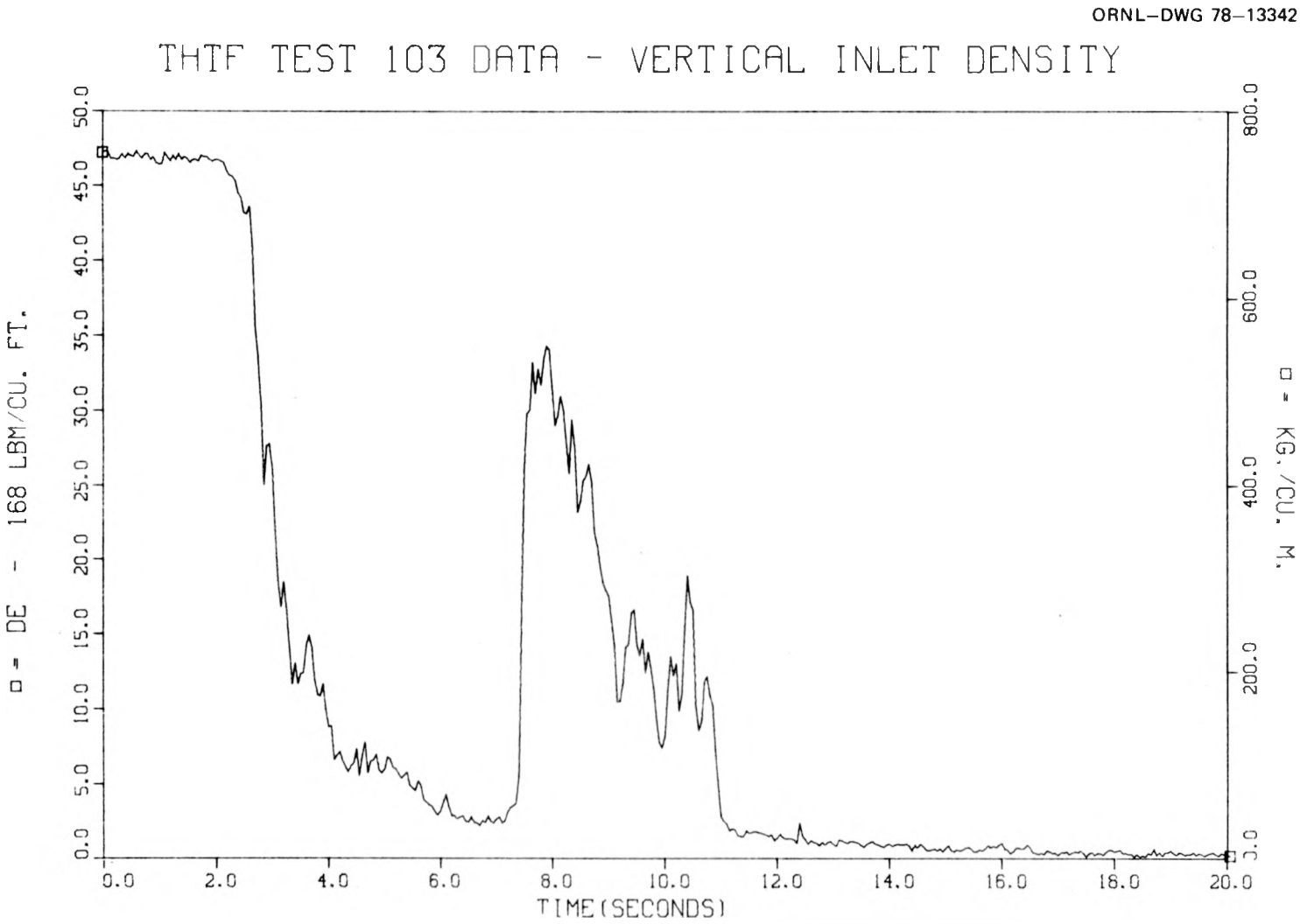

Fig. A.11. Vertical inlet spool piece density — test 103.

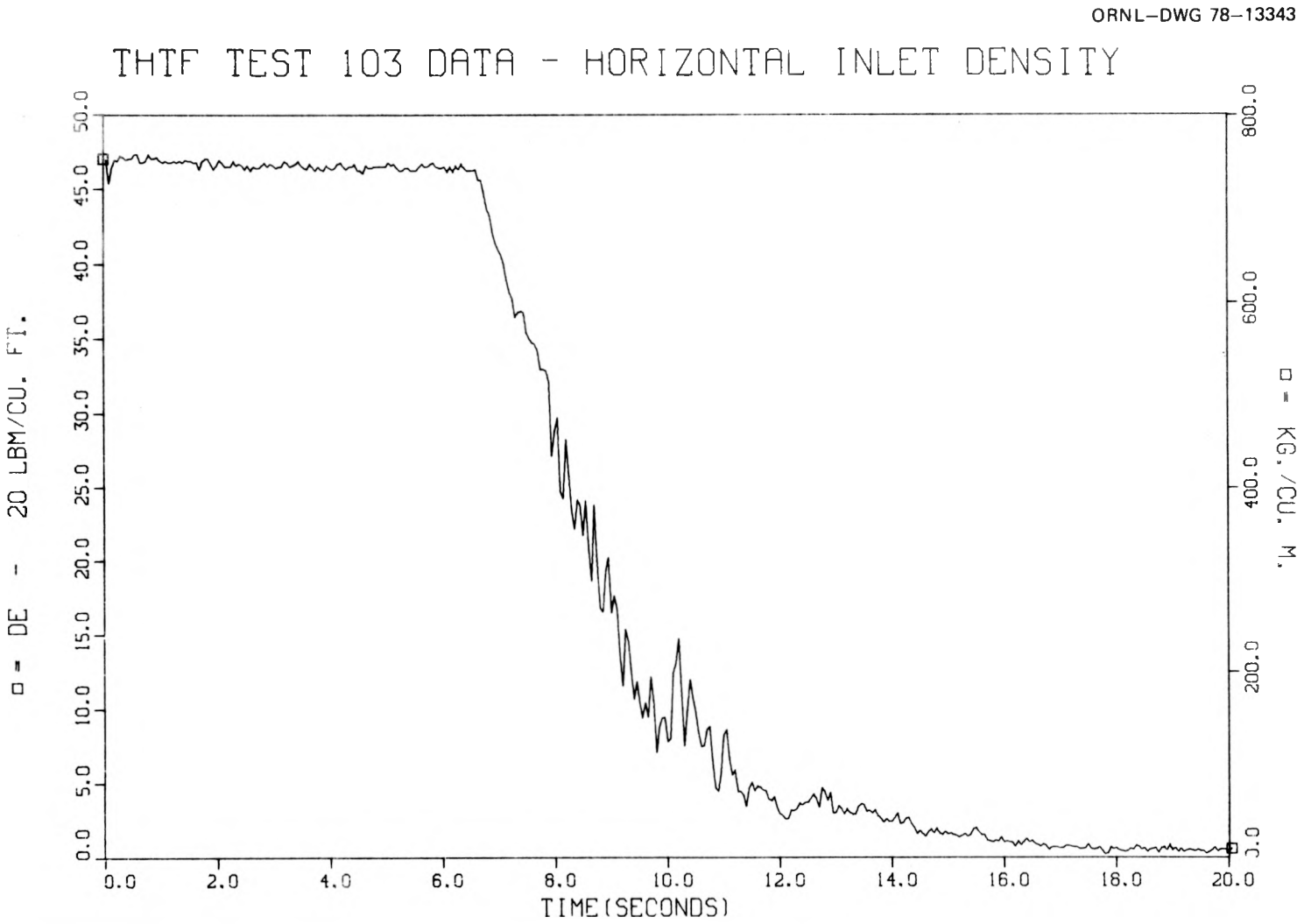

Fig. A.12. Horizontal inlet spool piece density — test 103.

Fig. A.13. Horizontal inlet spool piece volumetric flow — test 103.

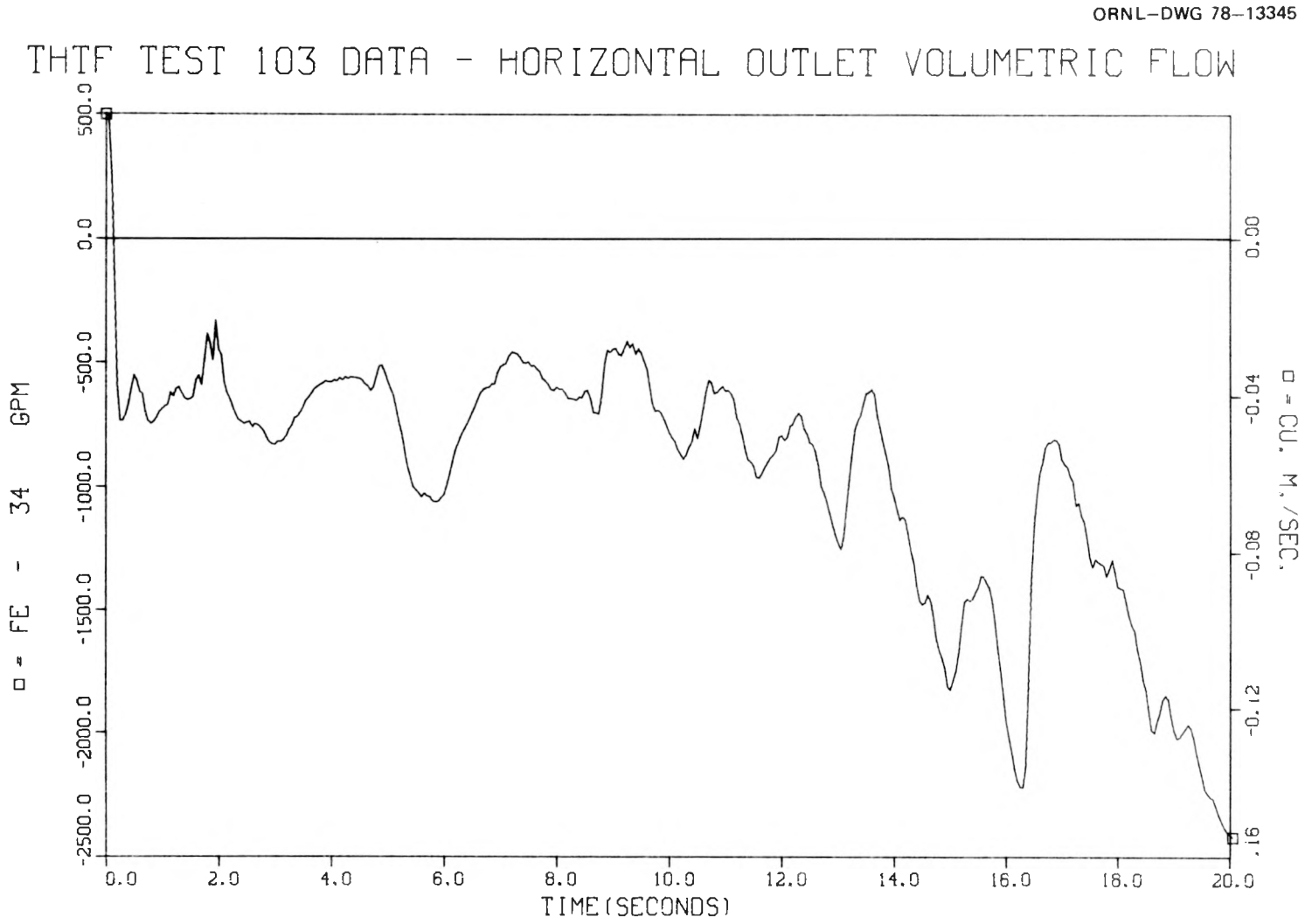

Fig. A.14. Horizontal outlet spool piece volumetric flow — test 103.

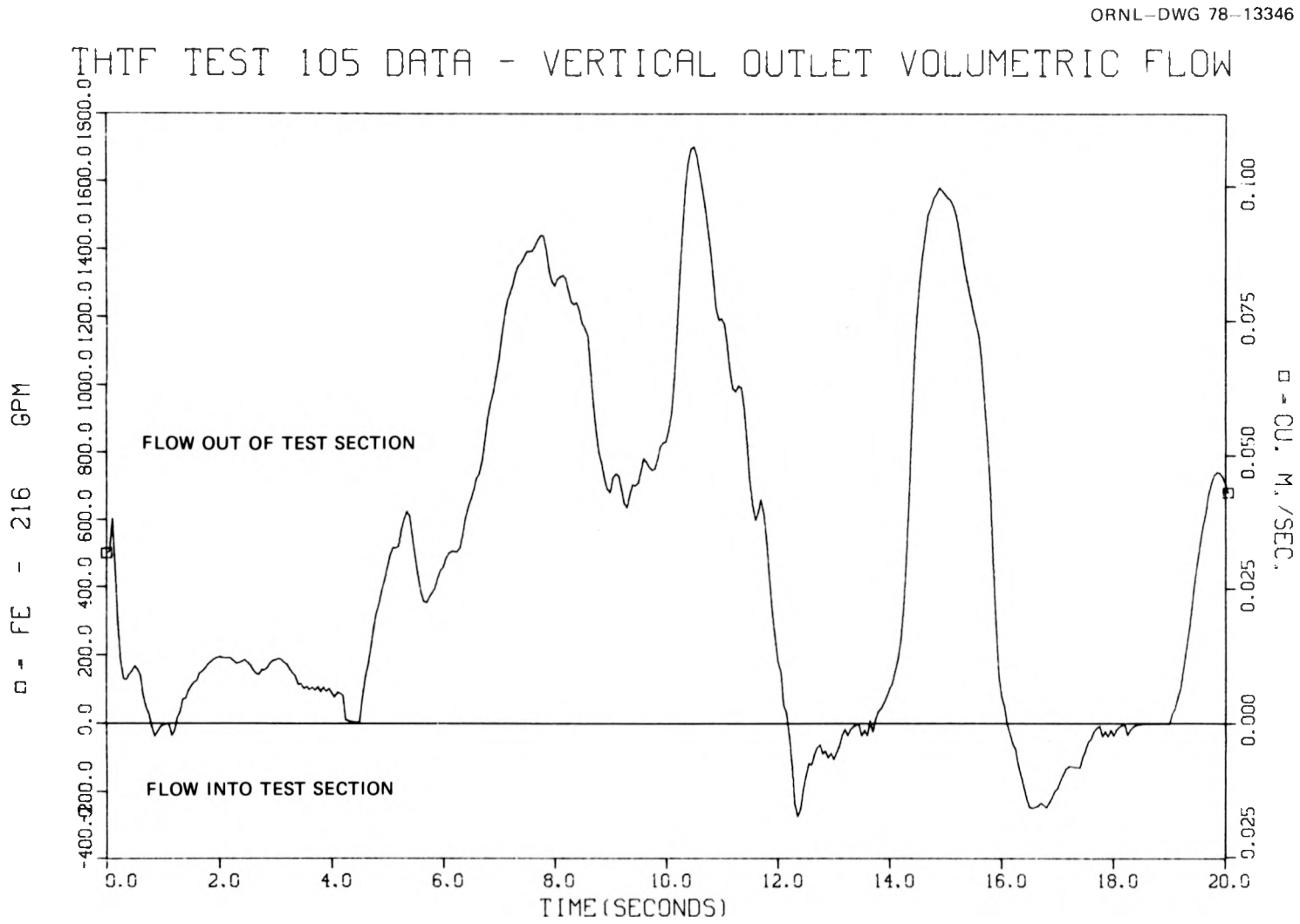

Fig. A.15. Vertical outlet spool piece volumetric flow — test 105.

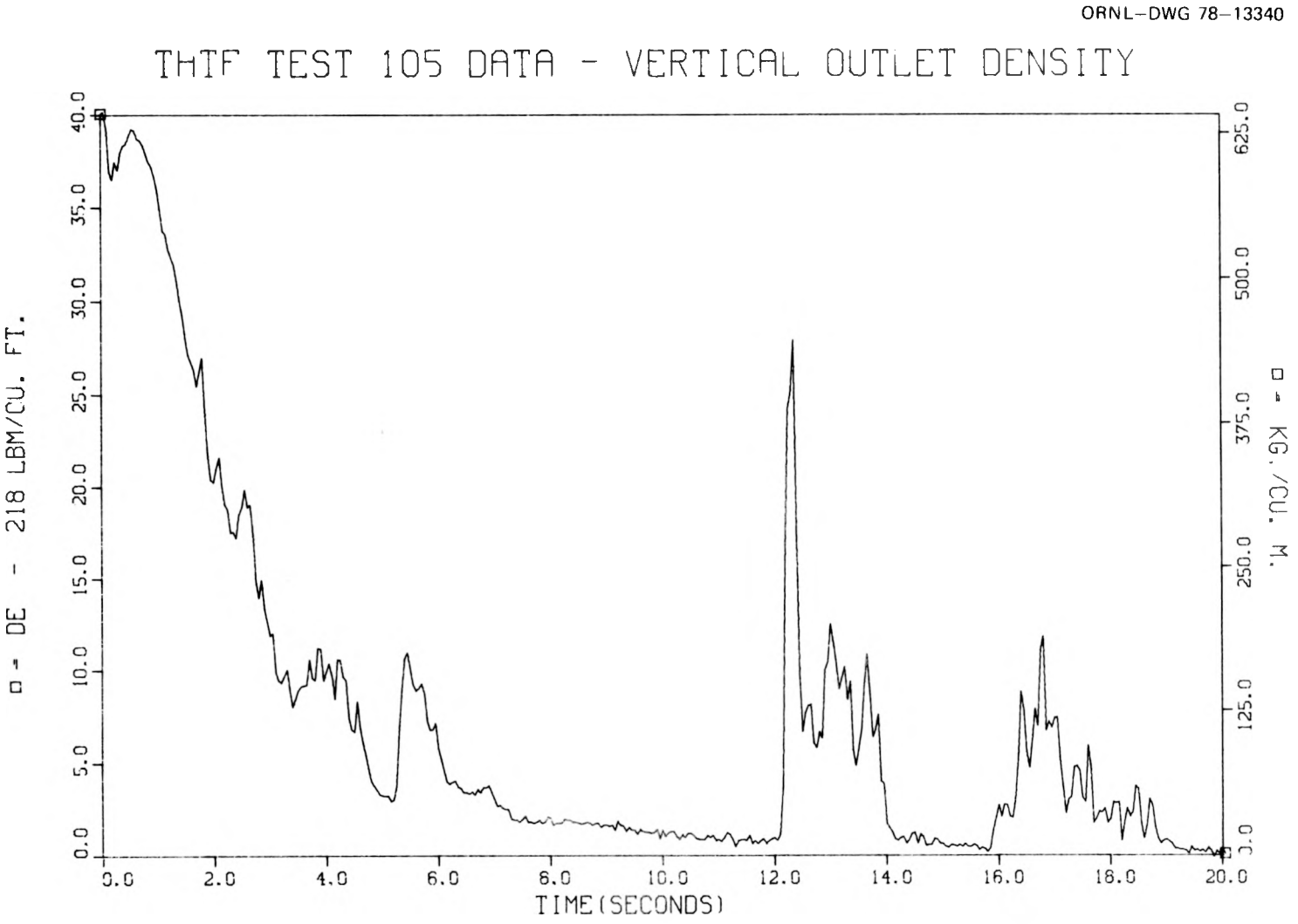

Fig. A.16. Vertical outlet spool piece density — test 105.

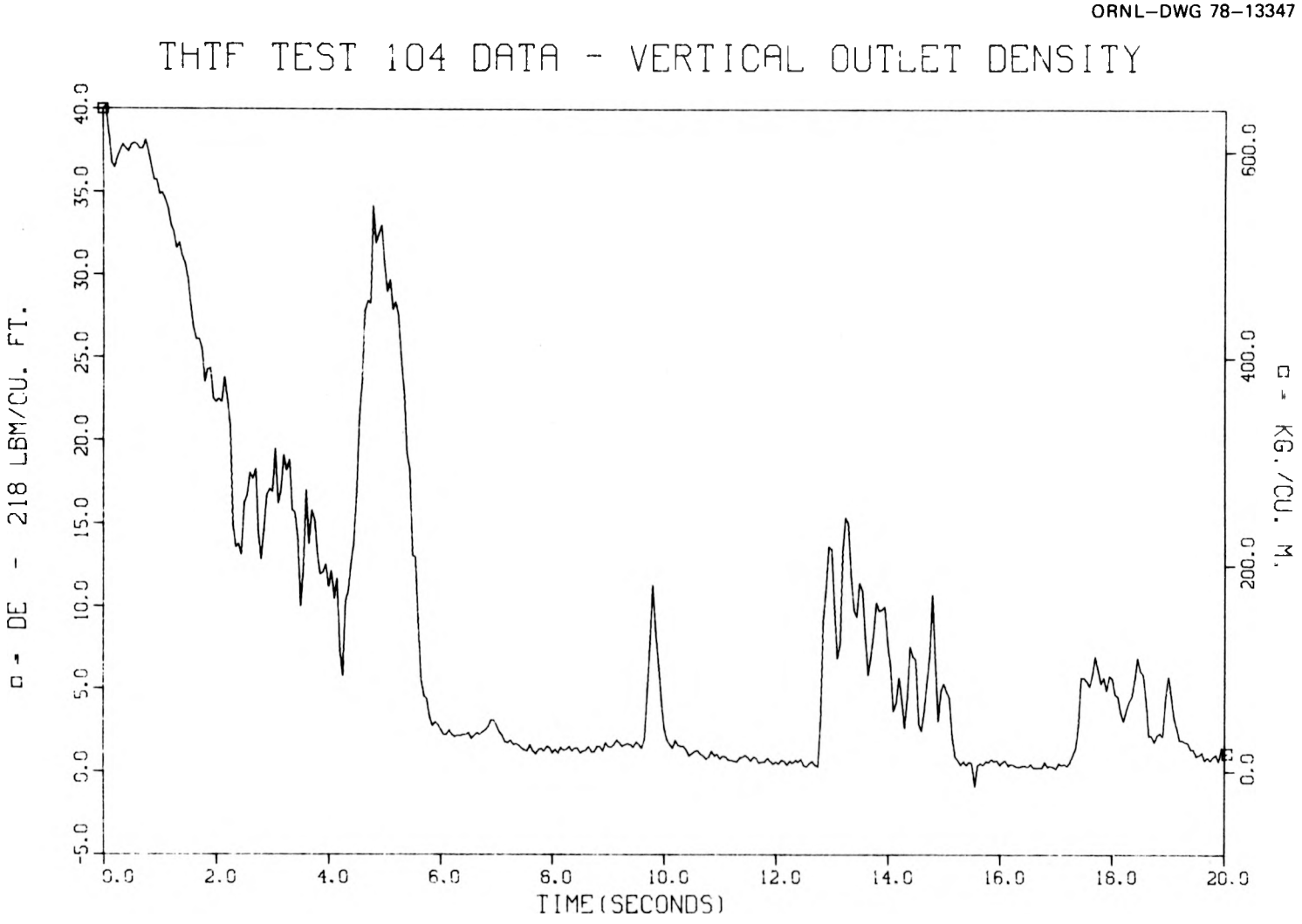

Fig. A.17. Vertical outlet spool piece density — test 104.

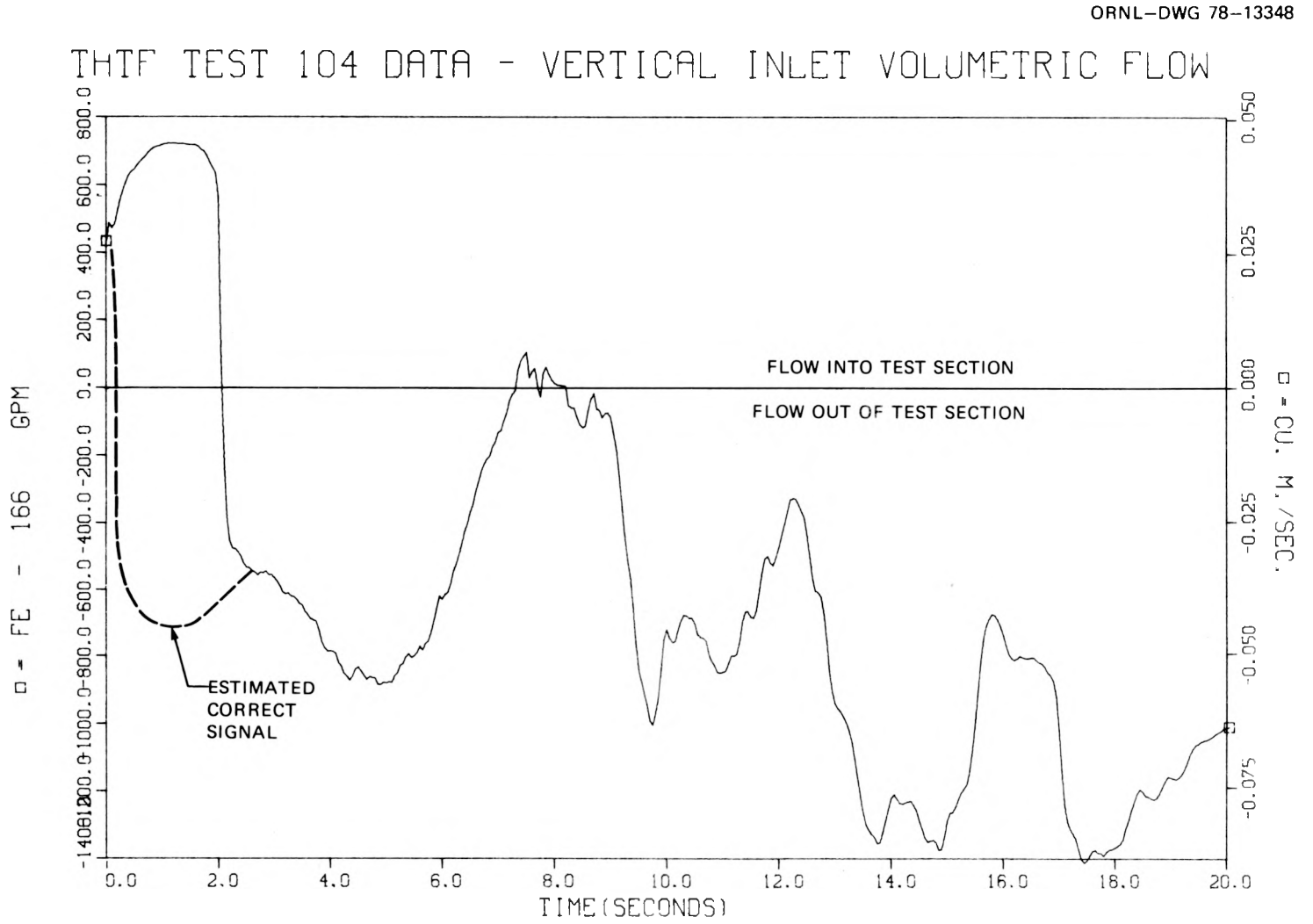

Fig. A.18. Vertical inlet spool piece volumetric flow — test 104 (corrected). (Polarity reversal produced inverted signals in early transient. Dotted line indicates estimated correct signal.)

Appendix B

RELAP CRITICAL HEAT FLUX CORRELATIONS

Appendix B consists of several pages reproduced from Vol. 1 of the RELAP4/MOD5 (update 2) Users' Manual.[3] The information presented describes the various CHF correlations, the ranges over which they are applicable, and the conditions necessary for the selection of desired correlations. A listing of variables and associated units used in the text of the appendix are as follows:

P = pressure, psia

q_{CHF} = critical heat flux valve, Btu/ft^2-hr

G = mass flux, lb_m/ft^2-hr

H = enthalpy, Btu/lb_m

L = channel length, in.

D_{HE}, De = heated equivalent diameter, ft

V = velocity, ft/sec

T_{SUB} = fluid saturation temperature minus fluid temperature, °F

D_r = rod diameter, ft

P_R = pressure at high end of interpolation range, psia

P_L = pressure at low end of interpolation range, psia

H_f = saturated fluid enthalpy, Btu/lb_m

D_{HY} = described in text

H_{in} = described in text

H_{fg} = heat of vaporization, Btu/lb_m

G' = $G/10^6$, lb_m/ft^2-hr

q_{CHF_L} = critical heat flux for low end of interpolation range, Btu/ft^2-hr

q_{CHF_R} = critical heat flux for high end of interpolation range, Btu/ft^2-hr

"(1) Critical Heat Flux Correlations. CHF calculations are made for all heat slab surfaces. The Babcock and Wilcox Company B&W-2[24], Barnett[25], and Modified Barnett[26] correlations are used as follows:

$P > 1,500$	B&W-2
$1,500 > P > 1,300$	Interpolation between B&W-2 and Barnett

$1{,}300 > P > 1{,}000$	Barnett
$1{,}000 > P > 725$	Interpolation between Barnett and Modified Barnett
$725 > P$	Modified Barnett

For a given pressure between 725 and 1,000 lb/in.^{2}, or between 1,300 and 1,500 lb/in.^{2}, the two relevant correlations are evaluated at that pressure and the corresponding enthalpy H_f. The two flux values are then weighted to give

$$q_{CHF} = \frac{(P_R - P)\, q_{CHF_L} + (P - P_L)\, q_{CHF_R}}{P_R - P_L} \tag{54}$$

where P = pressure, and L and R represent the low and high ends of the interpolation range, respectively. A minimum critical heat flux value of 90,000 Btu/ft^2-hr is set if the predicted value falls below this number.

"For a mass flux, G, less than 200,000 lb_m/ft^2-hr, the critical heat flux is interpolated between 90,000 Btu/ft^2-hr and the value given by the chosen correlation, where the former corresponds to G = 0 lb_m/ft^2-hr and the latter to G = 200,000 lb_m/ft^2-hr.

"The inlet enthalpy used in the Barnett and Modified Barnett Correlations is dependent on the flow direction and is determined in the following manner:

Flow at Major Inlet	Flow at Major Outlet	H_{in}
>0	≧0	H at normal inlet
≦0	<0	H at normal outlet
All other cases		H of core volume

If the term $H_f - H_{in}$ is negative, it is set to 0 in the correlations.

"The heated equivalent diameter term, D_{HE}, is input in feet and converted to inches in the correlations. The other "diameter" used in the Barnett and Modified Barnett correlations is calculated as $D_{HY} = \sqrt{D_r\,(D_r + D_{HE})} - D_r$, where D_r is rod diameter. For a cylindrical heat slab with a left conduction surface, the D_r used for that surface is the actual inside diameter of the slab (pipe, tank, etc.). If the right

side of the slab is a conducting surface, the D_r used for that surface is the outside diameter of the slab (pin, pipe, etc.). In some cases, D_{HY} will fall outside of the range of the correlations.

"If the heat slab geometry is rectangular rather than cylindrical, then D_{HY} for each side of the slab is set to the hydraulic diameter of the volume on that side.

"The B&W-2 Correlation can be evaluated down to a pressure of 1,300. The actual value of the term (P − 2,000) is used even if it is negative.

"(a) Babcock & Wilcox Company, B&W-2[24]. The B&W-2 correlation[24] is:

$$q_{CHF} = \frac{1.15509 - 0.40703(12De)}{12.71 \times (3.0545G')^{A}}$$

$$\left[(0.3702 \times 10^{8})\ (0.59137G')^{B} - 0.15208XH_{fg}G\right] \tag{55}$$

where

$$A = 0.71186 + (2.0729 \times 10^{-4})\ (P - 2,000) \tag{56}$$

$$B = 0.834 + (6.8479 \times 10^{-4})\ (P - 2,000) \tag{57}$$

and where

$$G = \frac{G}{10^{6}}$$

H_{fg} = heat of vaporization

"The correlation was developed from rod bundles in water data over the parametric ranges given by:

Equivalent diameter	0.2 to 0.5 in.
Length	72 in.
Pressure	2,000 to 2,400 psia
Mass flux	0.75×10^{6} to 4.0×10^{6} lb_m/ft^2-hr
Burnout quality	−0.03 to 0.20.

"(b) Barnett. The Barnett Correlation[25] is:

$$q_{CHF} = 10^{6}\left[\frac{A + B(H_f - H_{in})}{C + L}\right] \tag{58}$$

where

$$A = 67.45\ D_{HE}^{0.68} G'^{0.192} \left[1.0 - 0.744e^{(-6.512\ D_{HY} G')}\right] \quad (59)$$

$$B = 0.2587\ D_{HE}^{1.261} G'^{0.817} \quad (60)$$

$$C = 185.0\ D_{HY}^{1.415} G'^{0.212} \quad (61)$$

"For a rectangular conductor geometry, D_{HY} is set equal to the input value for the right side hydraulic diameter for the conductor. The correlation can be applied to rod bundles using equivalent diameters. The parametric range of the data is as follows:

Equivalent diameters	0.258 in. < D_{HE} < 3.792 in.
	0.127 in. < D_{HY} < 0.875 in.
Length	24 to 108 in.
Pressure	1,000 psi
Mass flux	0.14 × 10^6 to 6.20 × 10^6 lb_m/ft^2-hr
Inlet subcooling	0 to 412 Btu/lb_m

"(c) Modified Barnett[26]. The modified Barnett Correlation is:

$$q_{CHF} = 10^6 \left[\frac{A + B(H_f - H_{in})}{C + L}\right] \quad (62)$$

where

$$A = 73.71\ D_{HE}^{0.052} G'^{0.663} \left[1.0 - 0.315e^{(-11.34 D_{HY} G')}\right] \quad (63)$$

$$B = 0.104\ D_{HE}^{1.445} G'^{0.691} \quad (64)$$

$$C = 45.44\ D_{HY}^{0.0817} G'^{0.5866} \quad (65)$$

"Data were from rod bundles containing water and were over parametric ranges given by:

Rod diameter	0.395 to 0.543 in.
Length	32.9 to 174.8 in.
Pressure	150 to 725 psia
Mass flux	0.03 × 10^6 to 1.7 × 10^6 lb_m/ft^2-hr
Inlet subcooling	6 to 373 Btu/lb_m

"(2) Additional Critical Heat Flux Correlations. There are two alternatives to using the B&W-2, Barnett, and Modified Barnett Correlations. These are a pair of General Electric CHF Correlations[27] and a Savannah River Correlation[28] for aluminum heaters. These may be selected by use of IMCL (or IMCR) on the Heat Slab Data Cards.

"(a) General Electric Company. The General Electric Company Correlations are:

$$q_{CHF} = 10^6 \ (0.8 - X) \tag{66}$$

for

$$G \geq 0.5 \times 10^6 \ lb_m/ft^2\text{-hr}$$

and

$$q_{CHF} = 10^6 \ (0.84 - X) \tag{67}$$

for

$$G < 0.5 \times 10^6 \ lb_m/ft^2\text{-hr} \ .$$

"(b) Savannah River. The Savannah River Correlation is:

$$Q_{CHF} = 188{,}000 \ (1.0 + 0.0515V) \ (1.0 + 0.069 \ T_{SUB}) \tag{68}$$

where

V = fluid velocity, ft/sec

T_{SUB} = fluid saturation temperature minus fluid temperature."

Appendix C

RELAP THTF SYSTEM MODEL LISTING

```
=BE105          TEST 105 FOR CDER
*
*
*    MODEL PHILOSOPHY-----THIS IS A RELAP4M5U2 LOOP MODEL OF THE THTF.
*    THIS MODEL IS DIFFERENT FROM THE LOOP DER MODEL IN THE FOLLOWING
*    WAYS:(1) THE BAFFLE OUTLET ZONE ORIFICE (BOZO) CONNECTION IS
*    MODELED (2) THE PUMP RATED TORQUE REFLECTS THE EFFICIENCY AND
*    HORSEPOWER OF THE PUMP AS TAKEN FROM THE PUMP HEAD CURVE, AND THE
*    PUMP INERTIA HAS BEEN ADJUSTED TO MATCH THE EXPERIMENTALLY
*    OBSERVED SLOWDOWN RATE (3) THE UNHEATED LENGTH VOLUME IN THE TEST
*    SECTION IS NOW INCLUDED IN THE NODE NEAREST THAT UNHEATED LENGTH
*    (4) THE VOLUME OF THE DEAD LEG IN THE DOWNCOMER IS INCLUDED IN THE
*    VOLUME SIMULATING THE UPPER PART OF THE DOWNCOMER(VOLUME 25) (5)
*    NEW HYDRAULIC DIAMETERS AND K'S HAVE BEEN CALCULATED AND UTILIZED
*    IN THIS MODEL (6) THE POWER USED IS THE ACTUAL POWER IN THE RODS,
*    DURING THE BEGINNING OF BLOWDOWN, AVERAGED THROUGH TIME (7) INITIAL
*    CONDITIONS (FRACTION OF POWER REMOVED BY HX'S ABC,D,MASSFLOW
*    THROUGH THE TEST SECTION,ETC.) WERE OBTAINED FROM FLOTT DATA
*    (8) HX'S ABC, AND D ARE NOW MODELED WITH A CONDUCTION HX
*    MODEL;HX-D IS MODELED WITH A CONSTANT SINK HX MODEL.
*
*
*    MODEL SPECIFICS-----
*
*    (1) THE MIXTURE LEVEL IN THE PRESSURIZER HAS BEEN ADJUSTED.
*
*    (2) THE SLAB GEOMETRY GAPS FOR THE CORE SLABS HAVE BEEN
*        ADJUSTED.
*
*    (3) THE POWER TRACE HAS BEEN ADJUSTED.
*
*    (4) THE BREAK RATIOS HAVE BEEN ADJUSTED.
*
*    (5) THIS RUN WAS RECORDED ON TAPE
*
*        VOL=SER=029445
*
*        DSN=LT105
*
*    (6) THE RINPUT INPUT USED TO GENERATE THIS MODEL IS SHOWN BELOW
*         45.9 73.72 0.0 5.9681
*         25.48 24.9 .9462 541.71 325.95 0.05
*         34 633.6 2266.9
*         19 0 0 1 7 8 12 13 14 38 52 54 50 51
*         0 1 1 1 1
*         18 400.0
*         700.0 1945.87
*         55 0.01
*         8 9 10
*         52 51 50 49 48
*         56 55 54 53
*         55 34 57 -1
*         56 55 58 -1
*         57 17 60 1
*         37 14 39 1
*        -36 37 38 1
*         0
*
*
*
* PROBLEM DIMENSIONS
*
010001 -2  9  6  5 57  1  2 62  1  0  2  0 50 11 6  5  0  0
010002   5.9681  1.0
*
```

```
* MINOR EDIT VARIABLES
020000 AP 28 AP 34 JH 31 JW 31 JH 36 JW 36 TD 28 TD 36 TD 31
*
*
*   ENTHALPY TRANSPORT SHUT DOWN
030003  0  0.  0.  .000001
*
*
* TIME STEP CARDS
*
030010  500  10  1  0  .0001  .00001     .001
030020   50  10  1  0  .001   .00001     .05
030030    5  10  1  0  .01    .00001     .5
030040    5  10  1  0  .01    .00001    5.0
030050   50  10  1  0   .001  .00001    6.0
030060    5  10  1  0  .01    .00001  210.
*
* TRIP CARDS
*
040010  1  1  0  0  20.0   0.0 * TRIP END
040020  2  1  0  0   0.0   0.0 * TRIP LEAK TO FIRST POWER CURVE
040030  3  1  0  0   0.0   0.09* TRIP PUMP
040040  4  1  0  0   0.0   1.965 *TRIP SEC FLOW ON HEAT-X
040050  1  -4 36  0  200.  0.  * TRIP END BELOW 200 PSI
*
* VOLUME DATA CARDS
*
050011 0   0 2255.5330 633.5142 -1.000 0.200400  3.0000  3.0000 *S.P.1 OUTLET
050021 0   0 2247.2729 633.4626 -1.000 0.202600  2.0140  2.0140 *BLOWDOWN TEE
050031 0   0 2236.6587 633.3960 -1.000 0.200400  0.2920  0.2920 *S.P.2 OUTLET
050041 0   0 2226.8127 633.3342 -1.000 0.304700  0.2920  0.2920
050051 0   0 2225.3618 633.3250 -1.000 0.436000  6.9000  6.9000
050061 0   0 2221.9995 633.3040 -1.000 0.304500  0.2920  0.2920
050071 0   0 2222.0132 633.3040 -1.000 0.233200  0.2920  0.2920 *INLET HEADR
050081 0   0 2222.4026 572.9595 -1.000 0.591400  4.1000  4.1000 *HEX FIRST PT
050091 0   0 2222.8760 437.4390 -1.000 0.591400  0.9000  0.9000 *HX SECOND PT
050101 0   0 2223.1270 317.1306 -1.000 0.591400  2.1500  2.1500 *HX THIRD PT
050111 0   0 2200.0081 262.2756 -1.000 0.560700  0.2920  0.2920 *OUT HEADER
050121 0   0 2199.9226 633.1646 -1.000 0.495900  7.0400  7.0400 *HX BYPASS
050131 0   0 2200.6431 550.9937 -1.000 0.295600  4.8000  4.8000
050141 0   0 2202.5088 550.9961 -1.000 0.403000  0.2920  0.2920 *HORZ TO PRES
050151 0   0 2198.6184 543.5400 -1.000 0.481300  0.2920  0.2920
050161 0   0 2832.5332 546.1812 -1.000 0.490500  4.2000  4.2000
050171 0   0 2430.7561 545.8762 -1.000 0.196300  0.2920  0.2920 *BYPASS TEE
050181 0   0 2428.2292 545.8740 -1.000 0.114100  0.3000  0.3000 *BY-PASS
050191 0   0 2339.8884 545.7583 -1.000 0.462300  0.2920  0.2920
050201 0   0 2328.9106 545.7888 -1.000 0.373500  2.3330  2.3330 *VERT TO SP I
050211 0   0 2320.2012 545.7813 -1.000 0.200400  0.2920  0.2920 *S.P. 1 INLET
050221 0   0 2312.7041 545.7747 -1.000 0.267800  1.9140  1.9140 *B.D.TEE INLET
050231 0   0 2302.9951 545.7661 -1.000 0.200400  3.0000  3.0000 *S.P.2 INLET
050241 0   0 2294.0217 545.7581 -1.000 0.170200  1.2600  1.2600 *T.S. INLET
050251 0   0 2294.5593 545.7585 -1.000 0.990491  5.0210  5.0210 *TOP DOWNCOMER
050261 0   0 2295.7727 545.7595 -1.000 0.525400  2.9500  2.9500 *MID DOWNCOMER
050271 0   0 2296.9065 545.7605 -1.000 0.834000  4.5130  4.5130 *BOT DOWNCMER
050281 0   0 2297.7441 545.7615 -1.000 0.159619  0.8740  0.8740 *LOWER PLENUM
050291 0   0 2292.6707 551.2791 -1.000 0.212380  3.3438  3.3438 *1ST HEATED
050301 0   0 2287.1023 565.6982 -1.000 0.119090  1.8750  1.8750 *2ND HEATED
050311 0   0 2281.7246 593.4170 -1.000 0.190550  3.0000  3.0000 *3RD HEATED
050321 0   0 2276.1272 618.4387 -1.000 0.119090  1.8750  1.8750 *4TH HEATED
050331 0   0 2270.1201 629.6189 -1.000 0.206650  3.3125  3.3125 *5TH HEATED
050341 0   0 2266.8999 633.5852 -1.000 0.571900  1.8240  1.8240 *UPPER PLENUM
050351 0   0 2264.8506 633.5723 -1.000 0.334300  0.8500  0.8500 *OUTLET LINE
050361 1   0 2198.7415   0.0     0.0   7.450000 12.4000  5.8900 *PRESSURIZERTMDP
050371 0   0 2201.3760 550.9946 -1.000 0.658100  6.1000  6.1000 *PRNSS LN
050381 0   0 2516.0640 544.8728 -1.000 1.490000  2.0000  2.0000 * PUMP
```

```
050391 0    0 2226.5627 633.3325 -1.000 0.370400  0.2920   0.2920
050401 0    0 2223.1926 633.3115 -1.000 0.436000  6.7000   6.7000
050411 0    0 2222.0088 633.3040 -1.000 0.353300  1.6500   1.6500
050421 0    0 2201.9612 550.9954 -1.000 0.295600  4.8000   4.8000
050431 0    0 2198.0591 543.5396 -1.000 0.704000  1.0300   1.0300
050441 0    0 2198.0454 543.5396 -1.000 0.543000  3.8100   3.8100
050451 0    0 2831.2415 546.1802 -1.000 0.479900  0.2920   0.2920
050461 0    0 2339.6001 545.7981 -1.000 0.462300  0.2920   0.2920
050471 0    0 2339.3118 545.7979 -1.000 0.462300  0.2920   0.2920
050481 0    1  250.0000  70.0002 -1.000 0.491200  1.2500   1.2500 *4X-MAIN
050491 0    0  238.9509  93.5496 -1.000 0.491200  0.9500   0.9500 *4X-MAIN
050501 0    0  237.6119 146.6505 -1.000 0.491200  0.9500   0.9500 *4X-MAIN
050511 0    0  236.2688 213.2093 -1.000 0.491200  0.9500   0.9500 *4X-MAIN
050521 0    2  234.7875 250.0255 -1.000 0.491200  3.1537   3.1537 *4X-MAIN
050531 0    0 2202.2937 530.9480 -1.000 0.114100  0.9000   0.9000 *BY-PASS
050541 0    0 2206.7180 442.8044 -1.000 0.121042  0.6000   0.6000 *4X-D
050551 0    0 2267.0347 448.1494 -1.000 0.21870   2.306    2.306 *BOZO VOL 3
050561 0    0 2269.9258 220.2700 -1.000 0.023200  8.9400   8.9400 *BOZO VOL 2
050571 0    0 2434.0159 545.8789 -1.000 0.015000  3.0000   3.0000 *BOZO VOL 1
050012 0  0.0668100   0.2916999  930.7100  0                      *S.P.1 OUTLET
050022 0  0.1104000   0.3750000  928.7078  0                      *BLOWDOWN TEE
050032 0  0.0668100   0.2916999  929.7078  0                      *S.P.2 OUTLET
050042 0  0.0668100   0.2916999  929.7078  0
050052 0  0.0668100   0.2916999  929.7078  0
050062 0  0.0668100   0.2916999  943.0999  0
050072 0  0.0668100   0.2916999  941.3528  0                      *INLET HEADR
050082 0  0.0573000   0.0562158  937.2537  0                      *4X FIRST PT
050092 0  0.0573000   0.0562158  936.3606  0                      *4X SECOND PT
050102 0  0.0573000   0.0562158  934.2610  0                      *4X THIRD PT
050112 0  0.0668200   0.2916999  934.2620  0                      *JET HEADER
050122 0  0.0668100   0.2916999  934.4170  0                      *4X BYPASS
050132 0  0.0668100   0.2916999  929.6250  0
050142 0  0.0668100   0.2916999  924.7920  0                      *4ORZ TO PRES
050152 0  0.0668100   0.2916999  924.7920  0
050162 0  0.0668100   0.2916999  919.9900  0
050172 0  0.0668100   0.2916999  923.9368  0                      *BYPASS TEE
050182 0  0.0341375   0.0807868  923.9368  0                      *BY-PASS
050192 0  0.0668100   0.2916999  923.9368  0
050202 0  0.0668100   0.2916999  924.0828  0                      *VERT TO SP 1
050212 0  0.0668100   0.2916999  926.2710  0                      *S.P. 1 INLET
050222 0  0.1104000   0.3750000  925.2710  0                      *B.D.TEE INLET
050232 0  0.0668100   0.2916999  927.1089  0                      *S.P.2 INLET
050242 0  0.0668100   0.2916999  930.1050  0                      *T.S. INLET
050252 0  0.1848000   0.1791300  927.7317  0                      *TOP DOWNCOMER
050262 0  0.1848000   0.1791300  924.7830  0                      *4TH DOWNCOMER
050272 0  0.1848000   0.1791300  920.2737  0                      *BOT DOWNCMER
050282 0  0.3019000   0.1791300  919.4500  0                      *LOWER PLENUM
050292 0  0.0634800   0.0205230  919.5518  0                      *1ST HEATED
050302 0  0.0634800   0.0205230  922.8926  0                      *2ND HEATED
050312 0  0.0634800   0.0205230  924.7654  0                      *3RD HEATED
050322 0  0.0634800   0.0205230  927.7625  0                      *4TH HEATED
050332 0  0.0634800   0.0205230  929.6355  0                      *5TH HEATED
050342 0  0.2987900   0.2291923  932.9451  0                      *UPPER PLENUM
050352 0  0.0668100   0.2916999  933.7000  0                      *OUTLET LINE
050362 0  0.6010000   0.8750000  930.9397  0                      *PRESSURIZERTMDP
050372 1  0.0668100   0.2916999  924.8997  0                      *PRNSS LN
050382 0  0.0668100   0.2916999  918.0000  0                      * PUMP
050392 0  0.0668100   0.2916999  929.7078  0
050402 0  0.0668100   0.2916999  936.5496  0
050412 0  0.0668100   0.2916999  941.5000  0
050422 0  0.0668100   0.2916999  924.9380  0
050432 0  0.0668100   0.2916999  923.7898  0
050442 0  0.0668100   0.2916999  919.9900  0
050452 0  0.0668100   0.2916999  923.9368  0
050462 0  0.0668100   0.2916999  923.9368  0
```

```
050472 0   0.0668100   0.2916999   923.9368   0
050482 0   0.0695100   0.2974943   934.2610   0                    *4X-MAIN
050492 0   0.0695100   0.0472000   935.4600   0                    *4X-MAIN
050502 0   0.0695100   0.0472000   936.3606   0                    *4X-MAIN
050512 0   0.0695100   0.0472000   937.2537   0                    *4X-MAIN
050522 0   0.0695100   0.2974943   938.2000   0                    *4X-MAIN
050532 0   0.0341375   0.0807868   923.9368   0                    *3Y-PASS
050542 0   0.0072975   0.0406700   923.4888   0                    *4X-D
050552 0   0.0778400   0.0454000   932.8108   0                    *3020 VOL 3
050562 0   0.0004974   0.0251700   926.9397   0                    *3020 VOL 2
050572 0   0.0004974   0.0251700   923.9500   0                    *3020 VOL 1
*
* BUBBLE RISE CARD
060011              0.8          3.0
*
*
*      TIME DEPENDENT VOLUME DATA
*
070100  1
070200  6  2.  232.  250.  0.  3.1537
070201     5.  246.2  250.  0.  3.1537
070202     7.  247.5  250.  0.  3.1537
070203    12.  247.8  250.  0.  3.1537
070204    20.  248.0  250.  0.  3.1537
*
* JUNCTION DATA CARDS
*
*THE AREA OF JUNCTIONS WITH ORIFICES OR VALVES IS = ADJACENT VOL CS AREA
*
080011 35  1   0  0 45.899994 0.0668100  933.70459  0.0   7.500   7.500
080021  1  2   0  0 45.899994 0.0668100  930.71094  0.0   7.500   7.500
080031  2  3   0  0 45.899994 0.0668100  929.85376  0.0   7.500   7.500
080041  3  4   0  0 45.899994 0.0668100  929.85376  0.0   7.500   7.500
080051 39  5   0  0 45.899994 0.0668100  929.85376  0.0   0.0     0.0
080061 40  6   0  0 45.899994 0.0668100  943.19971  0.0   0.0     0.0
080071 41  7   0  0 45.899994 0.0668100  941.54932  0.0   0.0     0.0
080081  7 12   0  0 33.438293 0.0668100  941.39966  0.0   0.0     0.0
080091  7  8   0  0 12.461686 0.0573000  941.35303  0.0   0.0     0.0
080101  8  9   0  0 12.461686 0.0573000  937.25977  0.0   0.0     0.0
080111  9 10   0  0 12.461686 0.0573000  936.36084  0.0   0.0     0.0
080121 10 11   0  0 12.461686 0.0573000  934.29932  0.0   0.0     0.0
080131 11 13   0  0 12.461686 0.0668100  934.41797  0.0   0.0     0.0
080141 12 13   0  0 33.438293 0.0668100  934.41968  0.0   0.0     0.0
080151 42 14   0  0 45.899994 0.0668100  924.93970  0.0   0.0     0.0
080161 14 15   0  0 45.899994 0.0668100  924.93970  0.0   0.0     0.0
080171 38 16   1  0 73.719986 0.0668100  919.99463  0.0   0.0     0.0
080181 45 17   0  0 73.719986 0.0668100  924.09961  0.0   0.0     0.0
080191 17 18   0  0 27.819992 0.0250000  923.93970  0.0   0.0     0.0
080201 43 15   0  0 27.819992 0.0250000  924.79932  0.0   0.0     0.0
080211 17 19   0  0 45.899994 0.0668100  924.09961  0.0   0.0     0.0
080221 47 20   0  0 45.899994 0.0668100  924.08472  0.0   9.000   9.000
080231 20 21   0  0 45.899994 0.0668100  926.29932  0.0   7.500   7.500
080241 21 22   0  0 45.899994 0.0668100  926.29932  0.0   7.500   7.500
080251 22 23   0  0 45.899994 0.0668100  927.13965  0.0   7.500   7.500
080261 23 24   0  0 45.899994 0.0668100  930.10669  0.0   7.500   7.500
080271 24 25   0  0 45.899994 0.0668100  931.29932  0.0   0.0     0.0
080281 25 26   0  0 45.899994 0.1848000  927.73218  0.0   0.0     0.0
080291 26 27   0  0 45.899994 0.1848000  924.78467  0.0   0.0     0.0
080301 27 28   0  0 45.899994 0.1848000  920.27588  0.0   0.300   0.300
080311 28 29   0  0 45.899994 0.0635180  919.55225  0.0   1.575   1.575
080321 29 30   0  0 45.899994 0.0635180  922.89307  0.0   1.816   1.816
080331 30 31   0  0 45.899994 0.0635180  924.76636  0.0   1.697   1.697
080341 31 32   0  0 45.899994 0.0635180  927.76294  0.0   1.697   1.697
080351 32 33   0  0 45.899994 0.0635180  929.63599  0.0   1.805   1.805
080361 33 34   0  0 45.899994 0.0580634  932.94727  0.0   1.201   1.201
```

```
C80371 34 35    C   0 45.899994 C.0668100  934.50000    0.0          0.500      0.500
C80381 36 37    C   0  0.0      C.0668100  930.94971    0.0          1.000      1.000
C80391 37 14    0   0  0.0      C.0668100  924.91968   90.00000      1.000      1.000
C80401 44 38   -1   0 73.719986 C.0668100  919.99463    0.0          0.0        0.0
C80411  4 39    C   0 45.899994 C.0668100  929.85376    0.0          0.0        0.0
C80421  5 40    C   0 45.899994 C.0668100  936.59961    0.0          0.0        0.0
C80431  6 41    0   0 45.899994 C.0668100  943.14258    0.0          0.0        0.0
C80441 13 42    0   0 45.899994 C.0668100  929.69971    0.0          0.0        0.0
C80451 15 43    0   0 73.719986 C.0668100  924.79932    0.0          0.0        0.0
C80461 43 44    0   0 73.719986 0.0668100  923.79468    0.0          0.0        0.0
C80471 16 45    0   0 73.719986 C.0668100  924.08252    0.0          0.0        0.0
C80481 19 46    0   0 45.899994 0.0668100  924.09961    0.0          0.0        0.0
C80491 46 47    0   0 45.899994 0.0668100  924.09961    0.0          0.0        0.0
C80501 18 54    0   0  2.090632 C.0049950  924.00000  100.00000      0.0        0.0
C80511 54 53    0   0  2.090632 C.0049950  924.00000  100.00000      0.0        0.0
C80521 18 53    0   0 25.729355 C.0205000  923.93970    0.0          0.0        0.0
C80531 48 49    0   0 29.689972 C.0347500  935.46045   10.00000      8.000      8.000
C80541 49 50    C   0 29.689972 C.0695100  936.36060   10.00000      0.500      0.500
C80551 50 51    0   0 29.689972 C.0695100  937.29932   10.00000      0.500      0.500
C80561 51 52    0   0 29.689972 C.0695100  938.20142   10.00000      0.500      0.500
C80571 55 34    0   0  0.120000 C.0389000  933.00000    0.0          0.0        0.0
C80581 56 55    0   0  0.120000 C.0004974  935.10093    0.0          0.0        0.0
C80591 57 56    C   0  0.120000 C.0004974  926.94434    0.0          0.0        0.0
C80601 17 57    0   0  0.120000 C.0004974  923.95459    0.0          0.0        0.0
C80611 22  C    2   0  0.0      C.0135000  925.29932    0.0          0.0        0.0
C80621  2  C    1   0  0.0      C.0135000  928.70972    0.0          0.0        0.0
C80012 0  0  2  C 0.0     C.ECC    C 0 0.0     0
C80022 0  0  2  C 0.0     0.ECC    C 0 0.0     0
C80032 0  0  2  C 0.0     0.ECC    C 0 0.0     0
C80042 0  0  2  0 0.0     0.ECC    C 0 0.0     0
C80052 0  0  3  C 0.0     0.ECC    C 0 0.0     0
C80062 0  0  3  0 0.0     C.ECC    C 0 0.0     0
C80072 0  0  3  C 0.0     C.ECC    C 0 0.0     0
C80082 0  0  3  C 0.0     0.ECC    C 0 0.0     0
C80092 0  0  3  3 0.0     C.ECC    C 2 C.0     0
C80102 0  0  3  C 0.0     C.ECC    C 3 0.0     0
C80112 0  0  3  C 0.0     0.ECC    C 3 C.0     0
C80122 0  0  3  C 0.0     C.ECC    C 1 0.0     0
C80132 0  0  3  3 0.0     C.ECC    C 0 C.0     0
C80142 0  0  3  C 0.0     C.ECC    C 0 0.0     0
C80152 0  0  3  C 0.0     C.ECC    C 0 0.0     0
C80162 0  0  3  0 0.0     0.ECC    C 0 0.0     0
C80172 0  0  3  C 0.0     C.ECC    C 0 0.0     0
C80182 0  0  3  C 0.0     C.ECC    C 0 0.0     0
C80192 0  0  3  3 0.0     0.ECC    C 0 C.0     0
C80202 0  0  3  3 0.0     C.ECC    C 0 C.0     0
C80212 0  0  3  C 0.0     C.ECC    C 0 0.0     0
C80222 0  0  2  C 0.0     0.ECC    C 0 0.0     0
C80232 0  0  2  0 0.0     0.ECC    C 0 0.0     0
C80242 0  0  2  C 0.0     C.ECC    C 0 C.0     0
C80252 0  0  2  0 0.0     0.ECC    C 0 0.0     0
C80262 0  0  2  C 0.0     0.ECC    C 0 0.0     0
C80272 0  0  3  C 0.0     0.C      C 0 C.0     0
C80282 0  0  3  0 0.0     0.C      C 0 1.000   0
C80292 0  0  3  C 0.0     0.C      C 0 1.000   0
C80302 0  0  2  0 0.0     0.C      C 0 1.000   0
C80312 0  0  2  0 0.0     0.C      C 2 0.0     0
C80322 0  0  2  0 0.0     0.0      C 3 0.0     0
C80332 0  0  2  C 0.0     0.0      C 3 C.0     0
C80342 0  0  2  C 0.0     0.C      C 3 C.0     0
C80352 0  0  2  C 0.0     0.C      C 3 C.0     0
C80362 0  0  2  0 0.0     0.0      C 1 C.0     0
C80372 0  0  2  C 0.0     0.C      C 0 C.0     0
C80382 0  0  2  C 0.0     0.ECC    C 0 0.0     0
C80392 0  0  0  3 0.0     C.ECC    C 0 0.0     0
```

```
C80402 0  0  3  C 0.0      0.ECC    C 0 0.0      0
C80412 0  C  3  0 0.0      0.ECC    C 0 C.0      C
C80422 0  0  3  C 0.0      C.ECC    C 0 0.0      C
C80432 C  0  3  C 0.0      0.ECC    C 0 0.0      0
C80442 0  0  3  C 0.0      C.ECC    C 0 0.0      C
C80452 0  0  3  0 0.C      0.ECC    C 0 0.0      0
C80462 0  0  3  C 0.0      C.ECC    C 0 C.0      C
C80472 0  0  3  C 0.0      0.ECC    C 0 0.0      0
C80482 0  0  3  C 0.0      0.ECC    C 0 C.0      0
C80492 0  0  3  C 0.0      0.ECC    C 0 0.0      0
C805C2 0  0  C  C 0.0      1.CCC    C 2 0.0      0
C80512 C  0  0  0 0.0      1.CCC    C 1 0.0      C
C80522 0  0  3  3 0.C      C.ECC    C 0 C.0      0
C80532 0  0  C  3 0.0      1.CCC    C 2 C.0      0
C80542 0  0  C  3 0.0      1.CCC    C 3 C.0      C
C80552 C  0  0  3 0.C      1.CCC    C 3 C.0      0
C80562 C  0  C  3 0.0      1.CCC    C 1 0.0      C
C80572 0  5  3  C 0.0      1.CCC   11 0 C.0      0
C80582 0  5  3  C 0.C      1.CCC   11 0 0.0      0
C80592 C  5  3  C 0.0      1.CCC   11 C 0.0      0
C80602 0  5  3  C 0.0      1.CCC   11 0 0.0      0
C80612 0  5  3  0 0.0      1.CCC   11 0 C.0      0
C80622 0  5  3  C 0.C      1.CCC   11 0 0.0      0
*
* HENRY-FAUSKE-HEM CRITICAL FLCW MCDEL DIALS
*
C82003   .9  C.8  0.8  0.01
*
* PUMP CATA CARCS
*
C90011  3 3 C C C 3560. 1. 734. 1560.C 395.31  62.75  47.10
C90012  0.0CC    0.0  00.000  C.00C   0.00
*
* PUMP CURVE INPLT INDICATOR
*
100CC0  C  C  E  C
*
* PUMP CURVES
*
103011  1  1  5   0.C      1.1357  C.2847  1.1253  0.5694  1.0944   *     V/A.LT.1
103012             0.8541  1.0427  1.0     1.0                      *     HEAD V/A
103021  1  2  7  C.       C.0     C.524   C.1135   0.562   0.1753  *     A/V.LT.1
103022             0.689   0.3768   0.7024   0.4127   0.8781 0.7324 *     HEAD A/V
103023             1.      1.
103031  2  1  5   0.0      0.55    C.2857  0.708   0.5714  0.826    *     V/A.LT.1
103032             0.8571  0.944   1.0     1.0                      *     TORQ V/A
103041  2  2  8   0.      -0.2     C.389   0.25    0.437   0.2933   *     A/V.LT.1
103042             0.5      0.3538  C.583   0.4415  0.67    0.529    *     TORQ A/V
103043             0.875    0.8128  1.      1.                       *     TORQ A/V
103051 1 3 3 -1.0 2.0 -0.3 1.15 0.C 1.1357
103061 2 3 4 -1.C 1.0 -C.7 C.6C -.3 0.5 0.C 0.59
*
* LEAK JUNCTION CARDS:
*
120100  2  2  14.7  C.0 0.6  210. C.6
120200  2  2  14.7  0.0 0.4  21C. C.4
*
* KINETIC CONSTANTS CARD
*
140CC0  0  C  C.  0.
*
* SCRAM POWER CARC
*
141C01 20 2 C. 1.C  2.04 1.0  2.1C 0.8247  2.15 C.7491  2.20 0.6804
141002  2.25 C.618  2.3  0.5614  2.40 0.4634  2.5 0.3827  2.65 0.2874
```

```
141003  2.8 C.2161  3.0 0.1482  3.25 C.C931  3.6 0.0495  4.C 0.0252
141004  4.35 0.C172  4.8 C.01C31  5.8 C.00458  5.85 0.  50.  0.
*
* SLAB CARDS -- DOUGALL-ROHSENOW
*
150011  C 29  3 C 0  2  2  0.C        14.4285980 0.12769961 0.0        0.03760000
150021  0 30  2 1 0  2  2  0.C        10.0949984 0.08959997 0.0        0.03760000
150031  0 31  1 1 0  2  2  0.C        16.0525938 0.14199996 0.0        0.03760000
150041  0 32  2 1 0  2  2  0.C        10.0799990 0.08909971 0.0        0.03760000
150051  0 33  3 1 0  2  2  0.C        14.2539988 0.12599999 0.0        0.03760000
150061 23  0  7 C 0  2  2  2.7500000  0.0        0.13089997 0.0        0.0
150071 24  C  7 0 0  2  2  2.3339987  0.0        0.11109996 0.0        0.0
150081 35  0  7 0 0  2  2  3.2089987  0.0        0.15289962 0.0        0.0
150091 28  0  4 0 0  2  2  2.0019999  0.0        0.18579996 0.0        0.0
150101 25  0  4 0 0  2  2 11.5029984  0.0        1.06799984 0.0        0.0
150111 26  0  4 0 0  2  2  6.7579985  0.0        0.62699986 0.0        0.0
150121 27  0  4 0 0  2  2 10.3399992  0.0        0.95999998 0.0        0.0
150131 34  C  4 0 0  2  2  4.1699982  0.0        0.38709962 0.0        0.0
150141 29 27  5 0 0  2  2  3.5379982  5.0869961 0.31309950 0.02760000 0.0
150151 30 27  5 0 0  2  2  2.4799986  3.5629969 0.21939993 0.02760000 0.0
150161 31 26  5 C 0  2  2  3.9359980  5.6539965 0.34819978 0.02760000 0.0
150171 32 25  5 C 0  2  2  2.4679976  3.5459967 0.21839952 0.02760000 0.0
150181 33 25  5 C 0  2  2  3.4979992  5.0229979 0.30959994 0.02760000 0.0
150191 39  C  7 0 0  2  2  5.2012892  0.0        0.24777436 0.0        0.0
150201 40  C  7 0 0  2  2  6.0949984  0.0        0.29014987 0.0        0.0
150211 41  C  7 0 0  2  2  5.2044325  0.0        0.24759996 0.0        0.0
150221 42  0  7 0 0  2  2  4.3299990  0.0        0.20614988 0.0        0.0
150231 43  0  7 C 0  2  2  8.3426204  0.0        0.39796788 0.0        0.0
150241  1  0  7 0 0  2  2  2.7500000  0.0        0.13089997 0.0        0.0
150251  3  C  7 0 0  2  2  2.7500000  0.0        0.13089997 0.0        0.0
150261  4  C  7 0 0  2  2  4.2787066  0.0        0.20382524 0.0        0.0
150271  5  0  7 0 0  2  2  6.0949984  0.0        0.29014987 0.0        0.0
150281  6  C  7 0 0  2  2  4.4855652  0.0        0.21339995 0.0        0.0
150291  7  C  7 0 0  2  2  3.2099991  0.0        0.15269995 0.0        0.0
150301 11  C  7 C 0  2  2  7.2199984  0.0        0.34379995 0.0        0.0
150311 12  C  7 0 0  2  2  7.1929989  0.0        0.34249961 0.0        0.0
150321 13  0  7 0 0  2  2  4.3299990  0.0        0.20614988 0.0        0.0
150331 14  0  7 0 0  2  2  5.5299988  0.0        0.26309997 0.0        0.0
150341 15  0  7 0 0  2  2  5.7172289  0.0        0.27207661 0.0        0.0
150351 16  0  7 0 0  2  2  7.0259161  0.0        0.33456481 0.0        0.0
150361 17  0  7 0 0  2  2  2.7500000  0.0        0.13089997 0.0        0.0
150371 19  C  7 0 0  2  2  6.4866629  0.0        0.30893320 0.0        0.0
150381 20  C  7 0 0  2  2  5.3399992  0.0        0.25439996 0.0        0.0
150391 21  C  7 0 0  2  2  2.7500000  0.0        0.13089997 0.0        0.0
150401 38  0  7 0 0  2  2 20.4299927  0.0        0.97289968 0.0        0.0
150411 36  0  8 0 0  2  2 34.0312958  0.0        3.53230000 0.0        0.0
150421 37  0  7 0 0  2  2  7.1931992  0.0        0.34249961 0.0        0.0
150431  8 51 11 0 0  2  2 30.0159760 35.5979767 0.13396078 0.04392000 0.0
150441  9 50 11 0 0  2  2 30.0159760 35.5979767 0.13396078 0.04392000 0.0
150451 10 49 11 0 0  2  2 30.0159760 35.5979767 0.13396078 0.04392000 0.0
150461 44  0  7 0 0  2  2  6.4501467  0.0        0.30695534 0.0        0.0
150471 45  0  7 0 0  2  2  6.8740EC7  0.0        0.32733464 0.0        0.0
150481 46  0  7 0 0  2  2  6.4866629  0.0        0.30893320 0.0        0.0
150491 47  0  7 0 0  2  2  6.4866629  0.0        0.30893320 0.0        0.0
150501 54 -1  6 0 0  2  2  7.7299986  9.6299992 0.03540700 0.03360000 0.0
150012 0.0        0.0471000  0.0        0.0        0.718800  0.0       .0        0.0
150022 0.0        0.0471000  0.0        0.0        0.0       0.0       .0        0.0
150032 0.0        0.0471000  0.0        0.0        0.0       0.0       .0        0.0
150042 0.0        0.0471000  0.0        0.0        0.0       0.0       .0        0.0
150052 0.0        0.0471000  0.0        0.0        0.0       0.0       .0        0.0
150062 0.0        0.0        3.000000   0.0        0.0       0.0       .0        0.0
150072 0.0        0.0        2.549994   0.0        0.0       0.0       .0        0.0
150082 0.0        0.0        4.000000   0.0        0.0       0.0       .0        0.0
150092 0.0        0.0        0.0        0.0        0.0       0.0       .0        0.0
150102 0.0        0.0        0.0        0.0        0.0       0.0       .0        0.0
150112 0.0        0.0        0.0        0.0        0.0       0.0       .0        0.0
```

```
150122 0.0        0.0        0.0        0.0        0.0        0.0        .0         0.0
150132 0.0        0.0        0.0        0.0        0.0        0.0        .0         0.0
150142 0.0        0.0        0.0        2.653996   0.0        2.653996   .0         0.0
150152 0.0        0.0        0.0        1.858994   2.655000   4.509996   .0         0.0
150162 0.0        0.0        0.0        2.950000   0.0        0.0        .0         0.0
150172 0.0        0.0        0.0        1.849998   0.001000   1.839998   .0         0.0
150182 0.0        0.0        0.0        2.622993   1.851000   4.591000   .0         0.0
150192 0.0        0.0        5.678620   0.0        0.0        0.0        .0         0.0
150202 0.0        0.0        6.649998   0.0        0.0        0.0        .0         0.0
150212 0.0        0.0        5.677073   0.0        0.0        0.0        .0         0.0
150222 0.0        0.0        4.724998   0.0        0.0        0.0        .0         0.0
150232 0.0        0.0        9.124336   0.0        0.0        0.0        .0         0.0
150242 0.0        0.0        3.000000   0.0        0.0        0.0        .0         0.0
150252 0.0        0.0        3.000000   0.0        0.0        0.0        .0         0.0
150262 0.0        0.0        4.671371   0.0        0.0        0.0        .0         0.0
150272 0.0        0.0        6.649998   0.0        0.0        0.0        .0         0.0
150282 0.0        0.0        4.892920   0.0        0.0        0.0        .0         0.0
150292 0.0        0.0        3.500000   0.0        0.0        0.0        .0         0.0
150302 0.0        0.0        7.879993   0.0        0.0        0.0        .0         0.0
150312 0.0        0.0        7.849998   0.0        0.0        0.0        .0         0.0
150322 0.0        0.0        4.724998   0.0        0.0        0.0        .0         0.0
150332 0.0        0.0        6.030000   0.0        0.0        0.0        .0         0.0
150342 0.0        0.0        6.237988   0.0        0.0        0.0        .0         0.0
150352 0.0        0.0        7.667850   0.0        0.0        0.0        .0         0.0
150362 0.0        0.0        3.000000   0.0        0.0        0.0        .0         0.0
150372 0.0        0.0        7.079988   0.0        0.0        0.0        .0         0.0
150382 0.0        0.0        5.830000   0.0        0.0        0.0        .0         0.0
150392 0.0        0.0        3.000000   0.0        0.0        0.0        .0         0.0
150402 0.0        0.0       22.299588   0.0        0.0        0.0        .0         0.0
150412 0.0        0.0       12.379993   0.0        0.0        0.0        .0         0.0
150422 0.0        0.0        7.849998   0.0        0.0        0.0        .0         0.0
150432 0.0439200  0.0        6.042996   7.066998   0.0        0.930000   .0         0.0
150442 0.0439200  0.0        6.042996   7.066998   0.0        0.890000   .0         0.0
150452 0.0439200  0.0        6.042996   7.066998   0.0        0.930000   .0         0.0
150462 0.0        0.0        7.037663   0.0        0.0        0.0        .0         0.0
150472 0.0        0.0        7.502144   0.0        0.0        0.0        .0         0.0
150482 0.0        0.0        7.079988   0.0        0.0        0.0        .0         0.0
150492 0.0        0.0        7.079988   0.0        0.0        0.0        .0         0.0
150502 0.0        0.0        8.160000   0.0        0.0        0.0       .08747 2624.9
*
* CORE CARDS
*
160010  1  5  8  9 0.0      0.1110400 0.0        0.0
160020  2  5 12 13 0.0      0.1858799 0.0        0.0
160030  3  5 12 13 0.0      0.4131899 0.0        0.0
160040  4  5 12 13 0.0      0.1798900 0.0        0.0
160050  5  5  8  9 0.0      0.1100000 0.0        0.0
*
* SLAB GEOMETRY CARDS
*
170101 2 6 3 2 0. .009067 0.
170102  0     1  2  1.100E-03   1.0
170103  0     4  3  4.167E-03    0.
170104 0   2 4 .0025 0.
170105   0   6   1   5.489E-6 0.
170106 0   2 2 .000833 0.
170201 2 6 3 2 0. .008579 0.
170202  0     1  2            1.588E-03    1.0
170203  0     4  3            4.167E-03    0.
170204 0   2 4 .0025 0.
170205  0  6  1  3.702E-6   0.
170206 0   2 2 .000833 0.
170301 2 6 3 2 0. .007666 0.
170302  0     1  1            1.783E-03    0.5
170303  0     5  1            7.18E-04    0.5
170304  0     4  3            4.167E-03    0.
```

```
170305  0   6  1  1.667E-6     0.
170306 0    2 5 3.333E-3 0.
170901 2 6 3 2 0. .008579 0.
170902  0      1  2              1.588E-03     1.0
170903  0      4  3              4.167E-03     0.
170904 0    2 4 .0025 0.
170905  0   6  1  5.204E-6    0.
170906 0    2 2 .000833 0.
171001 2 6 3 2 0. .007666 0.
171002  0      1  1              1.783E-03     0.5
171003  0      5  1              7.18E-04     0.5
171004  0      4  3              4.167E-03     0.
171005  0   6  1  4.105E-6    0.
171006 0    2 5 3.333E-3 0.
170401  2   2  2  3  0.365  0.0333      0.
170402  0      2  1           0.05        0.
170501  1   1  2  4  0.      0.08333     0.
170601  2 1   2  4    .01675   .004083  0.0
170701  2   2  2  3  0.1459 0.01666     0.
170702  0      2  1           0.025       0.
170801 2 2 2 3 0.4375 0.0375  0.
170802  0   2  2  .05625  0.
171101  2   1  2  4  0.02196  0.004083  0.
*
*    VOLUMETRIC HEAT CAPACITY  BTU/F-FT**3  MATERIAL 1 - INCONNEL
*
190101 20        0.     51.41        200.     57.434       300.     59.327   * INCONNEL
190102          400.    61.167       500.     62.476       600.     63.372   * INCONNEL
190103          700.    64.578       800.     65.612       900.     66.795   * INCONNEL
190104         1000.    68.247      1100.     70.088      1200.     72.439   * INCONNEL
190105         1300.    75.420      1400.     79.150      1500.     83.750   * INCONNEL
190106         1600.    89.341      1700.     96.042      1800.    103.973   * INCONNEL
190107         1900.   113.255      2000.    124.008                         * INCONNEL
*
*    THERMAL CONDUCTIVITY BTU/FT-HR-F    MATERIAL 1 - INCONNEL
*
180101 20        0.      8.4294      200.      9.098       300.      9.495  *9INCONNEL
180102          400.     9.930       500.     10.398       600.     10.896   * INCONNEL
180103          700.    11.420       800.     11.967       900.     12.532   * INCONNEL
180104         1000.    13.113      1100.     13.704      1200.     14.303   * INCONNEL
180105         1300.    14.906      1400.     15.509      1500.     16.109   * INCONNEL
180106         1600.    16.701      1700.     17.282      1800.     17.849   * INCONNEL
180107         1900.    18.397      2000.     18.922                         * INCONNEL
*
*    VOLUMETRIC HEAT CAPACITY  BTU/F-FT**3  MATERIAL 2 - 316 SS
*
190201 20        0.     51.68        200.     56.923       300.     59.020   * 316-STST
190202          400.    60.846       500.     62.447       600.     63.855   * 316-STST
190203          700.    65.141       800.     66.308       900.     67.400   * 316-STST
190204         1000.    68.444      1100.     69.463      1200.     70.450   * 316-STST
190205         1300.    71.508      1400.     72.563      1500.     73.552   * 316-STST
190206         1600.    74.782      1700.     75.952      1800.     77.152   * 316-STST
190207         1900.    78.406      2000.     79.672                         * 316-STST
*
*    THERMAL CONDUCTIVITY BTU/FT-HR-F    MATERIAL 2 - 316 SS
*
180201 20        0.      7.2458      200.      8.225       300.      8.691   * 316-STST
180202          400.     9.144       500.      9.586       600.     10.020   * 316-STST
180203          700.    10.448       800.     10.872       900.     11.294   * 316-STST
180204         1000.    11.718      1100.     12.145      1200.     12.577   * 316-STST
180205         1300.    13.017      1400.     13.467      1500.     13.929   * 316-STST
180206         1600.    14.406      1700.     14.900      1800.     15.414   * 316-STST
180207         1900.    15.948      2000.     16.507                         * 316-STST
*
*    VOLUMETRIC HEAT CAPACITY  BTU/F-FT**3  MATERIAL 3 - MGO
*
190301 20 0. 47.5516 200. 52.2156 300. 54.2084 400. 55.9468 500. 57.4944
```

```
190302 600. 58.8512 700. 60.0384 800. 61.0348 900. 61.9040 1000. 62.6460
190303 1100. 63.2608 1150. 63.5364 1200. 63.7908 1250. 64.0240 1300. 64.2360
190304 1400. 64.5964 1500. 64.9144 1600. 65.1900 1700. 65.4444 1800. 65.9776
*
*    THERMAL CONDUCTIVITY BTU/FT-HR-F    MATERIAL 3 - MGO
*
180301 20 0. 8.4435  200.  6.4805  300.  5.7049  400.  5.0470  500.  4.4937
180302  600.  4.0326  700.  3.6523  800.  3.3423  900.  3.0930
180303  1000.  2.8959  1100.  2.7431  1200.  2.6281  1300.  2.5450
180304  1400.  2.4888  1500.  2.4558  1600.  2.4428  1700.  2.4428
180305 1800.  2.4428  1900.  2.4428  2000.  2.4428
*
*    VOLUMETRIC HEAT CAPACITY  BTU/F-FT**3  MATERIAL 4 - BN
*
190401 20       0.     20.98       200.     29.896      300.     33.012  *        BN
190402         400.    36.265      500.     39.178      600.     41.775  *        BN
190403         700.    44.078      800.     46.112      900.     47.900  *        BN
190404        1000.    49.466     1100.     50.834     1200.     52.026  *        BN
190405        1300.    53.067     1400.     53.980     1500.     54.789  *        BN
190406        1600.    55.517     1700.     56.188     1800.     56.826  *        BN
190407        1900.    57.453     2000.     58.094                       *        BN
*
*    THERMAL CONDUCTIVITY BTU/FT-HR-F    MATERIAL 4 - BN
*
180401  20    0.      21.0962  300.   18.6490  500.   17.0927  600.   15.3442
180402        700.    15.6187  750.   15.2554  800.   14.9186  850.   14.5788
180403        900.    14.2463  950.   13.9212  1000.  13.6040  1050.  13.2950
180404        1100.   12.9944  1150.  12.7025  1200.  12.4196  1300.  11.8821
180405        1400.   11.3844  1500.  10.9287  1700.  10.1531  2000.  9.3650
*
*    VOLUMETRIC HEAT CAPACITY  BTU/F-FT**3  MATERIAL 5 - 70CU30NI
*
190501 20       0.     52.55       200.     55.512      300.     58.317  * 70CU30NI
190502         400.    58.032      500.     59.179      600.     60.280  * 70CU30NI
190503         700.    61.358      800.     62.435      900.     63.532  * 70CU30NI
190504        1000.    64.672     1100.     65.876     1200.     67.157  * 70CU30NI
190505        1300.    68.567     1400.     70.098     1500.     71.752  * 70CU30NI
190506        1600.    73.641     1700.     75.697     1800.     77.973  * 70CU30NI
190507        1900.    80.489     2000.     83.269                       * 70CU30NI
*
*    THERMAL CONDUCTIVITY BTU/FT-HR-F    MATERIAL 5 - 70CU30NI
*
180501 20       0.     16.802      200.     17.972      300.     19.314  * 70CU30NI
180502         400.    20.960      500.     22.833      600.     24.919  * 70CU30NI
180503         700.    27.261      800.     29.964      900.     33.193  * 70CU30NI
180504        1000.    37.174     1100.     42.190     1200.     48.339  * 70CU30NI
180505        1300.    56.774     1400.     67.212     1500.     80.429  * 70CU30NI
180506        1600.    97.010     1700.    117.602     1800.    142.911  * 70CU30NI
180507        1900.   173.704     2000.    210.807                       * 70CU30NI
*
*
*    VOLUMETRIC HEAT CAPACITY  BTU/F-FT**3  MATERIAL 6 - AIR IN GAP
*
190601 20  25. .01973    68. .01812    100. .01708   200. .01449
190602    300. .01258   400. .01111    500. .00995   600. .00901
190603    700. .00824   800. .00758    900. .00702  1000. .00654
180602    300. .01948   400. .02164    500. .02380   600. .02596
180603    700. .02812   800. .03028    900. .03244  1000. .03460
180604   1100. .03676  1200. .03892   1300. .04108  1400. .04324
180601 20  25. .01354    68. .0144688  100. .01516   200. .01732
190604   1100. .00612  1200. .00575   1300. .00543  1400. .00513
190605   1500. .00487  1600. .00463   1700. .00442  2000. .00388
180605   1500. .04540  1600. .04756   1700. .04972  2000. .05620
*
```

Appendix D

RELAP THTF TEST SECTION MODEL LISTING

```
=BE105            T105 EXP HYDRAULIC  BOUNDED
*
*
* THIS RUN HAS EU GG1 NONINVERTED FILL TABLE AT THE OUTLET
*  AND OXREPT V3 AT THE INLET. (2/6/78)
*
* THIS RUN HAS SLIP ONLY IN THE DOWNCOMER AND TS INLET JUNCTIONS.
*  1-15. (2/7/78)
*
* THE LOOP MODEL TIME STEP REGIME DOES NOT WORK BETWEEN 12
*  AND 13 SEC BECAUSE OF A FLOW SPIKE IN THE MASS FLOW INTO THE
*  TS.  ADDED TWO NEW TIME STEP CARDS.  (2/8/78)
*
* REPEAT OF CRH2C256 FOR PRODUCTION OF LOCAL FLUID CONDITIONS TO
*  BE FED TO ORINC FOR CALCULATION OF HEAT TRANSFER COEFFICIENTS
*  FOR THE THTF TEST 105.(2/17/78)
*
* THIS RUN HAS CORRECTED POWER AT 4.8 SEC. (2/23/78)
*
* INSERTED 2 NEW TIME STEP CARDS FOR BOMB AT 15.5 SEC.(2/23/78)
*
* PROBLEM DIMENSIONS
010001  -2 9 9 2 36 0 0  37 0 0 0 2 48 13 6 11 0 0
*
C10002   5.9681  1.0
*
* MINOR EDIT VARIABLES
*
020000 JW 34  JW 29  JW 27  SR 11  SR 10  SR 09  SR 08  SR 07  SR J5
*
*   ENTHALPY TRANSPORT SHUT DOWN
*
C30003  0  0.  C.  .000001
*
*
* TIME STEP CARDS
*
030010  500  10  1  0  .0001  .00001     .001
030020   50  10  1  0  .001   .00001     .05
030030   5   10  1  0  .01    .00001     5.0
030040   50  10  1  0  .001  .00001  6.0
030050    5  10  1  0  .01    .00001  12.0
030060   50  10  1  0  .001  .00001  13.0
030070    5  10  1  0  .01    .00001  15.0
030080    5  10  1  0  .01     .000001   16.0
C30090    5  10  1  0  .01     .00001   210.0
*
* TRIP CARDS
*
040010  1  1  0  0   20.00   0.0 * TRIP END
040020  2  1  0  0   0.0   0.0 * TRIP LEAK TO FIRST POWER CURVE
*
* VOLUME DATA CARDS:
*    IBUB IREAD PRESS     TEMP     QUAL   VOLUME      HT     MIXT LVL
050011 0  -3 2304.1624 545.7659 -1.000 0.200400  3.0000  3.0000 *VERT INLET
050021 0   0 2295.1892 545.7578 -1.000 0.170200  1.2600  1.2600 *TS INLET
050031 0   0 2295.3254 545.7581 -1.000 0.097507  0.5175  0.5175 *TOP DWNCOM
050041 0   0 2295.3269 545.7581 -1.000 0.282630  1.5000  1.5000 *  DWNCOM#1
050051 0   0 2295.6941 545.7583 -1.000 0.211970  1.1250  1.1250 *  DWNCOM#2
050061 0   0 2295.9619 545.7585 -1.000 0.164870  0.8750  0.8750 *  DWNCOM#3
050071 0   0 2296.2097 545.7588 -1.000 0.188420  1.0000  1.0000 *  DWNCOM 4
050081 0   0 2296.4810 545.7590 -1.000 0.188420  1.0200  1.0200 *  DWNCOM#5
```

```
C50091 0    0 2296.7490 545.7593 -1.000 0.188420  1.0000   1.0000 *  DWNCOM#6
C50101 0    0 2297.0139 545.7595 -1.000 0.188420  1.0000   1.0000 *  DWNCOM#7
C50111 0    0 2297.2820 545.7598 -1.000 0.188420  1.0000   1.0000 *  DWNCOM#8
050121 0    0 2297.5298 545.7600 -1.000 0.164870  0.8750   0.8750 *  DWNCOM#9
050131 0    0 2297.7976 545.7603 -1.000 0.211970  1.1250   1.1250 *  DWNCOM#10
050141 0    0 2298.1648 545.7605 -1.000 0.282630  1.5000   1.5000 *  DWNCOM#11
050151 0    0 2298.3337 545.7607 -1.000 0.102110  0.7188   0.7188 #BOT DWNCOM
050161 0    0 2298.5322 545.7607 -1.000 0.057509  0.1560   0.1560 #LOWER PLEN
050171 0    0 2296.0771 545.7585 -1.000 0.045656  0.7188   0.7188 #UNHT L CORE
050181 0    0 2293.7156 548.4595 -1.000 0.095276  1.5000   1.5000 #1ST HTD CORE
050191 0    0 2290.9116 553.9443 -1.000 0.071457  1.1250   1.1250 #2ND HTD CORE
C50201 0    0 2288.7449 560.4861 -1.000 0.055578  0.8750   0.8750 #3RD HTD CORE
050211 0    0 2286.6841 569.3481 -1.000 0.063518  1.0000   1.0000 #4TH HTD CORE
050221 0    0 2284.4583 580.9963 -1.000 0.063518  1.0000   1.0000 #5TH HTD CORE
050231 0    0 2282.1963 593.4214 -1.000 0.063518  1.0000   1.0000 #6TH HTD CORE
C50241 0    0 2279.8950 605.3748 -1.000 0.063518  1.0200   1.0200 #7TH HTD CORE
C50251 0    0 2277.5598 615.4634 -1.000 0.063518  1.0000   1.0000 #8TH HTD CORE
050261 0    0 2275.3499 622.5461 -1.000 0.055578  0.8750   0.8750 #9TH HTD CORE
050271 0    0 2272.9883 627.6411 -1.000 0.071457  1.1250   1.1250 #10THHTD CORE
C50281 0    0 2269.8943 631.6531 -1.000 0.095276  1.5000   1.5000 #11THHTD CORE
C50291 0    0 2267.0774 633.5862 -1.000 0.039919  0.6875   0.6875 #UNHT T CORE
C50301 0    0 2267.4558 633.5886 -1.000 0.072500  0.2180   0.2180 #1ST UP PLEN
050311 0    0 2267.2222 633.5872 -1.000 0.144900  0.4360   0.4360 #2ND UP PLEN
C50321 0    0 2266.8999 633.5852 -1.000 0.354500  1.1700   1.1700 #3RD UP PLEN
050331 0    0 2264.8552 633.5725 -1.000 0.334300  0.8500   0.8500 #TS OUT
050341 0    0 2255.5483 633.5144 -1.000 0.200400  3.0000   3.0000 #VU SPOOL
050351 0    0 2266.8631 448.1497 -1.000 0.218700  2.3060   2.3060 #HOT BAFLE C
050361 0    0 2295.4536 545.7581 -1.000 0.052890  0.2917   0.2917 #IN DEAD LEG
*
*2-P FRIC FLOWA         DIAMV       ELEV    IAMBLO(VERT SLIP INDEX)
050012 0  0.0668100  0.2916999  927.1089  0                          #VERT INLET
050022 0  0.0668100  0.2916999  930.1050  0                          #TS INLET
050032 0  0.1884200  0.1791300  932.2610  0                          #TOP DWNCOM
050042 0  0.1884200  0.1791300  930.7620  0                          *  DWNCOM#1
050052 0  0.1884200  0.1791300  929.6377  0                          *  DWNCOM#2
C50062 0  0.1884200  0.1791300  928.7537  0                          *  DWNCOM#3
C50072 0  0.1884200  0.1791300  927.7649  0                          *  DWNCOM 4
050082 0  0.1884200  0.1791300  926.7458  0                          *  DWNCOM#5
C50092 0  0.1884200  0.1791300  925.7559  0                          *  DWNCOM#6
050102 0  0.1884200  0.1791300  924.7659  0                          *  DWNCOM#7
050112 0  0.1884200  0.1791300  923.7664  0                          *  DWNCOM#8
050122 0  0.1884200  0.1791300  922.8926  0                          *  DWNCOM#9
050132 0  0.1884200  0.1791300  921.7688  0                          *  DWNCOM#10
050142 0  0.1884200  0.1791300  920.2698  0                          *  DWNCOM#11
050152 0  0.1420600  0.1791300  919.5518  0                          #BOT DWNCOM
050162 0  0.3019000  0.1700000  919.3997  0                          #LOWER PLEN
050172 0  0.0635175  0.0205169  919.5518  0                          #UNHT L CORE
050182 0  0.0635175  0.0205169  920.2698  0                          #1ST HTD CORE
050192 0  0.0635175  0.0205169  921.7688  0                          #2ND HTD CORE
050202 0  0.0635175  0.0205169  922.8926  0                          #3RD HTD CORE
050212 0  0.0635175  0.0205169  923.7664  0                          #4TH HTD CORE
050222 0  0.0635175  0.0205169  924.7659  0                          #5TH HTD CORE
050232 0  0.0635175  0.0205169  925.7559  0                          #6TH HTD CORE
050242 0  0.0635175  0.0205169  926.7458  0                          #7TH HTD CORE
050252 0  0.0635175  0.0205169  927.7649  0                          #8TH HTD CORE
050262 0  0.0635175  0.0205169  928.7637  0                          #9TH HTD CORE
050272 0  0.0635175  0.0205169  929.6377  0                          #10THHTD CORE
C50282 0  0.0635175  0.0205169  930.7520  0                          #11THHTD CORE
050292 0  0.0580634  0.0214218  932.2610  0                          #UNHT T CORE
C50302 0  0.3699000  0.1914000  932.9468  0                          #1ST UP PLEN
050312 0  0.3699000  0.1914000  932.9639  0                          #2ND UP PLEN
050322 0  0.2609000  0.2693000  933.3799  0                          #3RD UP PLEN
C50332 0  0.0668100  0.2920000  933.7000  0                          #TS OUT
050342 0  0.0668100  0.2916999  930.7100  0                          #VU SPOOL
050352 0  0.0778400  0.0454000  933.300   0                         #HOT BAFLE C
050362 0  0.0668100  0.2916999  931.1533  0                          #IN DEAD LEG
```

```
* JUNCTION DATA CARDS:
*      JW1-2  IPMP  VALV   FLOW      AJUNC(FT2)    ZJUN(FT)   L/2A        FJUNF      FJUNR
080011   1   2    0    0 45.899994 0.0668100   930.10669   0.0         7.500      7.500
080021   2   4    0    0 45.899994 0.0668100   931.29932   0.0         0.0        0.0
080031   3   4    0    0   0.0     0.1884200   932.26099   0.0         0.0        0.0
080041   4   5    0    0 45.899994 0.1884200   930.76221   0.0         0.0        0.0
080051   5   6    0    0 45.899994 0.1884200   929.63843   0.0         0.0        0.0
080061   6   7    0    0 45.899994 0.1884200   928.76392   0.0         0.0        0.0
080071   7   8    0    0 45.899994 0.1884200   927.76514   0.0         0.0        0.0
080081   8   9    0    0 45.899994 0.1884200   926.75000   0.0         0.0        0.0
080091   9  10    0    0 45.899994 0.1884200   925.75977   0.0         0.0        0.0
080101  10  11    0    0 45.899994 0.1884200   924.76636   0.0         0.0        0.0
080111  11  12    0    0 45.899994 0.1884200   923.76709   0.0         0.0        0.0
080121  12  13    0    0 45.899994 0.1884200   922.89307   0.0         0.0        0.0
080131  13  14    0    0 45.899994 0.1884200   921.76929   0.0         0.0        0.0
080141  14  15    0    0 45.899994 0.1420600   920.27002   0.0         0.0        0.0
080151  15  16    0    0 45.899994 0.1420600   919.55225   0.0         0.300      0.300
080161  16  17    0    0 45.899994 0.0635180   919.55225   0.0         0.661      0.661
080171  17  18    0    0 45.899994 0.0635180   920.27002   0.0         0.772      0.772
080181  18  19    0    0 45.899994 0.0635180   921.76929   0.0         0.914      0.914
080191  19  20    0    0 45.899994 0.0635180   922.89307   0.0         0.696      0.696
080201  20  21    0    0 45.899994 0.0635180   923.76709   0.0         0.653      0.653
080211  21  22    0    0 45.899994 0.0635180   924.76636   0.0         0.696      0.696
080221  22  23    0    0 45.899994 0.0635180   925.75977   0.0         0.696      0.696
080231  23  24    0    0 45.899994 0.0635180   926.75000   0.0         0.696      0.696
080241  24  25    0    0 45.899994 0.0635180   927.76514   0.0         0.696      0.696
080251  25  26    0    0 45.899994 0.0635180   928.76392   0.0         0.653      0.653
080261  26  27    0    0 45.899994 0.0635180   929.63843   0.0         0.696      0.696
080271  27  28    0    0 45.899994 0.0635180   930.76221   0.0         0.914      0.914
080281  28  29    0    0 45.899994 0.0580634   932.26099   0.0         0.580      0.580
080291  29  30    0    0 45.899994 0.0580634   932.94727   0.0         0.411      0.411
080301  30  31    0    0 45.899994 0.1532200   933.00000   0.0         0.0        0.0
080311  31  32    0    0 45.899994 0.2609000   933.38989   0.0         0.0        0.0
080321  32  33    0    0 45.899994 0.0668100   934.50000   0.0         0.500      0.500
080331  33  34    0    0 45.899994 0.0668100   933.70459   0.0         7.500      7.500
080341  35  31    0    0   0.120000 0.0389000   933.38989   0.0         0.0        0.0
080351  36   4    0    0   0.0     0.0668100   931.29932   0.0         0.0        0.0
080361   0  34    1    0 -45.89999 0.0668100   930.71484   0.0         7.500      7.500
080371   0  35    2    0   0.1200  0.0004974   935.60000   0.0         0.0        0.0
*
*      JVERTL JCHOKE JCALCI MVMIX DIAMJ      CONCO  ICHOKE IHGCOR SRCOS IADJUN
080012  0   5   2   3 0.0      0.600   11 0 1.0      0
080022  0   5   3   0 0.0      1.000   11 2 1.0      0
080032  0   5   3   0 0.0      1.000   11 3 1.0      0
080042  0   5   3   0 0.0      1.000   11 3 1.0      0
080052  0   5   3   0 0.0      1.000   11 3 1.0      0
080062  0   5   3   0 0.0      1.000   11 3 1.0      0
080072  0   5   3   0 0.0      1.000   11 3 1.0      0
080082  0   5   3   0 0.0      1.000   11 3 1.0      0
080092  0   5   3   0 0.0      1.000   11 3 1.0      0
080102  0   5   3   0 0.0      1.000   11 3 1.0      0
080112  0   5   3   0 0.0      1.000   11 3 1.0      0
080122  0   5   3   0 0.0      1.000   11 3 1.0      0
080132  0   5   3   0 0.0      1.000   11 3 1.0      0
080142  0   5   3   0 0.0      1.000   11 3 1.0      0
080152  0   5   2   0 0.0      1.000   11 1 1.0      0
080162  0   5   2   0 0.0      1.000   11 2 0.0      0
080172  0   5   2   0 0.0      1.000   11 3 0.0      0
080182  0   5   2   0 0.0      1.000   11 3 0.0      0
080192  0   5   2   0 0.0      1.000   11 3 0.0      0
080202  0   5   2   0 0.0      1.000   11 3 0.0      0
080212  0   5   2   0 0.0      1.000   11 3 0.0      0
080222  0   5   2   0 0.0      1.000   11 3 0.0      0
080232  0   5   2   0 0.0      1.000   11 3 0.0      0
080242  0   5   2   0 0.0      1.000   11 3 0.0      0
```

```
080252 0  5  2  0 0.0      1.000  11 3 0.0      0
080262 0  5  2  0 0.0      1.000  11 3 0.0      0
080272 0  5  2  0 0.0      1.000  11 3 0.0      0
080282 0  5  2  0 0.0      1.000  11 1 0.0      0
080292 0  5  2  0 0.0      1.000  11 0 0.0      0
080302 0  5  3  0 0.0      1.000  11 0 0.0      0
080312 0  5  3  0 0.0      1.000  11 0 0.0      0
080322 0  5  2  0 0.0      1.000  11 0 0.0      0
080332 0  5  2  3 0.0      0.600  11 0 0.0      0
080342 0  5  3  0 0.0      1.000  11 0 0.0      0
080352 0  5  3  3 0.0      1.000  11 0 0.0      0
*
* MVMIX=-2 IMPLIES FILL WITH NEGATIVE FLOW REPRESENTING LEAK JUNCTION
*  USED IN J36 & J37
* CANNOT USE SLIP IN JUNCTIONS WITH FILL TABLES.
080362 0  5  2 -2 0.0      0.600  11 0 0.0      0
080372 0  5  3 -2 0.0      1.000  11 0 0.0      0
*
* FILL TABLE FOR JUNCTION FLOW INTO BAFFLE CAN FROM QUARTER INCH LINE
*  COMING TO TEST SECTION  (T105 TYPE FILL TABLE)
130200  2  4  10  1  LBS/SEC
130201  0.0  46.8  173.0
130202  0.5  46.8  192.0
130203  1.0  35.1  206.0
130204  2.0  27.3  227.0
130205  5.0  27.3  276.0
130206  7.5  23.4  299.0
130207 10.0  11.7  316.0
130208 12.5   7.8  326.0
130209 15.0   5.8   332.0
130210 20.0  2.34  338.0
*
* KINETIC CONSTANTS CARD
*
140000  0  0  0.  0.
*
* SCRAM POWER CARD
*
141001 20 2 0. 1.0  2.04 1.0  2.10 0.8247  2.15 0.7491  2.20 0.6804
141002  2.25 0.618  2.3  0.5614  2.40 0.4634  2.5 0.3827  2.65 0.2574
141003  2.8 0.2161  3.0 0.1482  3.25 0.0931  3.6 0.0495  4.0 0.0252
141004  4.35 0.0172  4.8 0.01031  5.8 0.00458  5.85 0.  50.  0.
*
* SLAB CARDS:
* THE TOP OF THE DOWNCOMER IS 2 INCHES FROM THE TOP OF THE UNHEATED PART
* OF THE CORE.  THEREFORE VOLUME 3 IS 2 INCHES SHORTER THEN VOLUME 29.
*  RATHER THAN USING ANOTHER SLAB FOR THE 2 INCH SECTION DUMPING HEAT INTO V29,
*  I WILL IGNORE IT.  (1/15/78)
*     ISVL-R IG ISB IXLO IMCL-R AHTXL     AHTXR      VOLS       HDML       HDMR
150011  0 18  1 0 0  2  2  0.0         8.1202488 0.07138985 0.0        0.03766000
150021  0 19  8 1 0  2  2  0.0         6.0901890 0.05354000 0.0        0.03766000
150031  0 20  9 1 0  2  2  0.0         4.7368088 0.04164000 0.0        0.03766000
150041  0 21  6 1 0  2  2  0.0         5.4134989 0.04759000 0.0        0.03766000
150051  0 22  7 1 0  2  2  0.0         5.4134989 0.04759000 0.0        0.03766000
150061  0 23  7 1 0  2  2  0.0         5.4134989 0.04759000 0.0        0.03766000
150071  0 24  7 1 0  2  2  0.0         5.4134989 0.04759000 0.0        0.03766000
150081  0 25 10 1 0  2  2  0.0         5.4134989 0.04759000 0.0        0.03766000
150091  0 26 11 1 0  2  2  0.0         4.7368088 0.04164000 0.0        0.03766000
150101  0 27 12 1 0  2  2  0.0         6.0901890 0.05354000 0.0        0.03766000
150111  0 28 13 1 0  2  2  0.0         8.1202488 0.07138985 0.0        0.03766000
150121  0 29 13 1 0  2  2  0.0         3.7217789 0.03272000 0.0        0.02626900
150131  0 17  1 0 0  2  2  0.0         3.8912182 0.03421000 0.0        0.03766000
150141 17 15  5 0 0  2  2  0.9584000  1.3776999 0.08485997 0.037xxJJJ  0.17912889
150151 18 14  5 1 0  2  2  2.0000000  2.8750000 0.17707998 0.037xxJJJ  0.17912889
150161 19 13  5 1 0  2  2  1.5000000  2.1562500 0.13281000 0.037xxJJJ  0.17912889
150171 20 12  5 1 0  2  2  1.1666689  1.5770773 0.10329998 0.037xxJJJ  0.17912889
```

```
150181 21 11  5 1 0  2  2  1.3332987  1.9166689 0.11805987 0.037ɔɔJOO 0.17912889
150191 22 10  5 1 0  2  2  1.3332987  1.9166689 0.11805987 0.037ɔɔJOO 0.17912889
150201 23  9  5 1 0  2  2  1.3332987  1.9166689 0.11805987 0.037ɔɔJOO 0.17912889
150211 24  8  5 1 0  2  2  1.3332987  1.9166689 0.11805987 0.037ɔɔJOO 0.17912889
150221 25  7  5 1 0  2  2  1.3332987  1.9166689 0.11805987 0.037ɔɔJOO 0.17912889
150231 26  6  5 1 0  2  2  1.1666689  1.6770773 0.10329998 0.037ɔɔJOO 0.17912889
150241 27  5  5 1 0  2  2  1.5000000  2.1562500 0.13281000 0.037ɔɔJOO 0.17912889
150251 28  4  5 1 0  2  2  2.0000000  2.8750000 0.17707998 0.037ɔɔJOO 0.17912889
150261 29  3  5 1 0  2  2  0.9166700  1.3177090 0.08115995 0.037ɔɔJOO 0.17912889
150271 15  0  3 0 0  2  2  1.5524893  0.0       0.52225387 0.0        0.0
150281 14  0  2 1 0  2  2  3.4361181  0.0       0.31907594 0.0        0.0
150291 13  0  2 1 0  2  2  2.5770884  0.0       0.23930699 0.0        0.0
150301 12  0  2 1 0  2  2  2.0044022  0.0       0.18612796 0.0        0.0
150311 11  0  2 1 0  2  2  2.2907457  0.0       0.21271700 0.0        0.0
150321 10  0  2 1 0  2  2  2.2907457  0.0       0.21271700 0.0        0.0
150331  9  0  2 1 0  2  2  2.2907457  0.0       0.21271700 0.0        0.0
150341  8  0  2 1 0  2  2  2.2907457  0.0       0.21271700 0.0        0.0
150351  7  0  2 1 0  2  2  2.2907457  0.0       0.21271700 0.0        0.0
150361  6  0  2 1 0  2  2  2.0044022  0.0       0.18612796 0.0        0.0
150371  5  0  2 1 0  2  2  2.5770884  0.0       0.23930699 0.0        0.0
150381  4  0  2 1 0  2  2  3.4361181  0.0       0.31907594 0.0        0.0
150391  3  0  2 1 0  2  2  1.1854610  0.0       0.11008108 0.0        0.0
150401  0 16  1 0 0  2  2  0.0        0.9022500 0.00793000 0.0        0.0
150411 16  0  3 0 0  2  2  0.9732700  0.0       1.84827900 0.0        0.0
150421 30  0  3 0 0  2  2  0.5771500  0.0       0.05358000 0.0        0.0
150431 31  0  3 1 0  2  2  1.1540890  0.0       0.10712987 0.0        0.0
150441 32  0  3 1 0  2  2  2.4387684  0.0       0.22638983 0.0        0.0
150451 33  0  4 0 0  2  2  3.2089987  0.0       0.15289986 0.0        0.0
150461 34  0  4 0 0  2  2  2.7500000  0.0       0.13089997 0.0        0.0
150471  2  0  4 0 0  2  2  2.3339987  0.0       0.11109996 0.0        0.0
150481  1  0  4 0 0  2  2  2.7500000  0.0       0.13089997 0.0        0.0
*
*        DHEL          DHER          CHNL          CHNR          XBOT          ZTOP
150012 0.0          0.0469300     0.0           0.0           0.0           0.0           .0          0.0
150022 0.0          0.0469300     0.0           0.0           0.0           0.0           .0          0.0
150032 0.0          0.0469300     0.0           0.0           0.0           0.0           .0          0.0
150042 0.0          0.0469300     0.0           0.0           0.0           0.0           .0          0.0
150052 0.0          0.0469300     0.0           0.0           0.0           0.0           .0          0.0
150062 0.0          0.0469300     0.0           0.0           0.0           0.0           .0          0.0
150072 0.0          0.0469300     0.0           0.0           0.0           0.0           .0          0.0
150082 0.0          0.0469300     0.0           0.0           0.0           0.0           .0          0.0
150092 0.0          0.0469300     0.0           0.0           0.0           0.0           .0          0.0
150102 0.0          0.0469300     0.0           0.0           0.0           0.0           .0          0.0
150112 0.0          0.0469300     0.0           0.0           0.0           0.0           .0          0.0
150122 0.0          0.0           0.0           0.0           0.0           0.0           .0          0.0
150132 0.0          0.0           0.0           0.0           0.0           0.0           .0          0.0
150142 0.0          0.0           0.0           0.0           0.0           0.0           .0          0.0
150152 0.0          0.0           0.0           0.0           0.0           0.0           .0          0.0
150162 0.0          0.0           0.0           0.0           0.0           0.0           .0          0.0
150172 0.0          0.0           0.0           0.0           0.0           0.0           .0          0.0
150182 0.0          0.0           0.0           0.0           0.0           0.0           .0          0.0
150192 0.0          0.0           0.0           0.0           0.0           0.0           .0          0.0
150202 0.0          0.0           0.0           0.0           0.0           0.0           .0          0.0
150212 0.0          0.0           0.0           0.0           0.0           0.0           .0          0.0
150222 0.0          0.0           0.0           0.0           0.0           0.0           .0          0.0
150232 0.0          0.0           0.0           0.0           0.0           0.0           .0          0.0
150242 0.0          0.0           0.0           0.0           0.0           0.0           .0          0.0
150252 0.0          0.0           0.0           0.0           0.0           0.0           .0          0.0
150262 0.0          0.0           0.0           0.0           0.0           0.0           .0          0.0
150272 0.0          0.0           0.0           0.0           0.0           0.0           .0          0.0
150282 0.0          0.0           0.0           0.0           0.0           0.0           .0          0.0
150292 0.0          0.0           0.0           0.0           0.0           0.0           .0          0.0
150302 0.0          0.0           0.0           0.0           0.0           0.0           .0          0.0
150312 0.0          0.0           0.0           0.0           0.0           0.0           .0          0.0
150322 0.0          0.0           0.0           0.0           0.0           0.0           .0          0.0
150332 0.0          0.0           0.0           0.0           0.0           0.0           .0          0.0
```

```
150342 0.0        0.0        0.0        0.0        0.0        0.0        .0        0.0
150352 0.0        0.0        0.0        0.0        0.0        0.0        .0        0.0
150362 0.0        0.0        0.0        0.0        0.0        0.0        .0        0.0
150372 0.0        0.0        0.0        0.0        0.0        0.0        .0        0.0
150382 0.0        0.0        0.0        0.0        0.0        0.0        .0        0.0
150392 0.0        0.0        0.0        0.0        0.0        0.0        .0        0.0
150402 0.0        0.0        0.0        0.0        0.0        0.0        .0        0.0
150412 0.0        0.0        0.0        0.0        0.0        0.0        .0        0.0
150422 0.0        0.0        0.0        0.0        0.0        0.0        .0        0.0
150432 0.0        0.0        0.0        0.0        0.0        0.0        .0        0.0
150442 0.0        0.0        0.0        0.0        0.0        0.0        .0        0.0
150452 0.0        0.0        4.000000   0.0        0.0        0.0        .0        0.0
150462 0.0        0.0        3.000000   0.0        0.0        0.0        .0        0.0
150472 0.0        0.0        2.549997   0.0        0.0        0.0        .0        0.0
150482 0.0        0.0        3.000000   0.0        0.0        0.0        .0        0.0
*
* CORE CARDS
160010  1  5  8  9 0.0     0.0540350 0.0        0.0   * -1
160020  2  5  8  9 0.0     0.0570030 0.0        0.0   * -2
160030  3  5 12 13 0.0     0.0767930 0.0        0.0   * -3
160040  4  5 12 13 0.0     0.1089540 0.0        0.0   * -4
160050  5  5 12 13 0.0     0.1378466 0.0        0.0   * -5
160060  6  5 12 13 0.0     0.1378466 0.0        0.0   * -5
160070  7  5 12 13 0.0     0.1378466 0.0        0.0   * -5
160080  8  5 12 13 0.0     0.1041970 0.0        0.0   * -6
160090  9  5 12 13 0.0     0.0757070 0.0        0.0   * -7
160100 10  5  8  9 0.0     0.0557380 0.0        0.0   * -8
160110 11  5  8  9 0.0     0.0540330 0.0        0.0   * -9
*
* SLAB GEOMETRY CARDS
*
170101  2  6  3  2  0.          7.467E-03  0.
170102     0  1  1              1.783E-03  0.402283
170103     0  5  1              9.170E-04  0.597717
170104     0  4  3              4.167E-03  0.
170105 0 6 1 1.6667E-6  0.
170106 0 2 5 3.333E-3 0.
170201 2 3 2 4 .36458 .02777 0.
170202 0 2 4 .02777  0.
170203 0 2 4 .02777  0.
170301 2 3 2 4 .34375 .02778 0.
170302 0 2 4 .02778 0.
170303 0 2 4 .02778 0.
170401 2 2 2 3 .1459 .01666 0.
170402 0 2 1 .025 0.
170501 1 3 2 4 0. .02431  0.0
170502 0 2 4 .02431  0.0
170503 0 2 4 .02431  0.0
170601  2  6  3  2  0.          8.725E-03  0.
170602     0  1  2              1.442E-03  1.0
170603     0  4  3              4.167E-03  0.
170604 0 2 4 2.49975E-3 0.
170605 0 6 1 4.1417E-6 0.
170606 0 2 2 8.3325E-4 0.
170701  2  6  3  2  0.          9.067E-03  0.
170702     0  1  2              1.100E-03  1.
170703     0  4  3              4.167E-03  0.
170704 0 2 4 2.49975E-3 0.
170705 0 6 1 5.489E-6 0.
170706 0 2 2 8.3325E-4 0.
170801  2  6  3  2  0.          7.925E-03  0.
170802     0  1  1              1.783E-03  0.573754
170803     0  5  1              4.580E-04  0.426246
170804     0  4  3              4.167E-03  0.
170805 0 6 1 1.6667E-6  0.
170806 0 2 5 3.333E-3 0.
```

```
170901  2  6  3  2  0.          8.408E-03  0.
170902     0  1  2              1.758E-03  1.0
170903     0  4  3              4.167E-03  0.
170904 0 2 4 2.49975E-3 0.
170905 0 6 1 3.262E-6 0.
170906 0 2 2 8.3325E-4 0.
171001  2  6  3  2  0.          8.725E-03  0.
171002     0  1  2              1.442E-03  1.0
171003     0  4  3              4.167E-03  0.
171004 0 2 4 2.49975E-3 0.
171005 0 6 1 5.422E-6 0.
171006 0 2 2 8.3325E-4 0.
171101  2  6  3  2  0.          8.408E-03  0.
171102     0  1  2              1.758E-03  1.0
171103     0  4  3              4.167E-03  0.
171104 0 2 4 2.49975E-3 0.
171105 0 6 1 4.987E-6 0.
171106 0 2 2 8.3325E-4 0.
171201  2  6  3  2  0.          7.925E-03  0.
171202     0  1  1              1.783E-03  0.573754
171203     0  5  1              4.580E-04  0.426246
171204     0  4  3              4.167E-03  0.
171205 0 6 1 3.24E-6 0.
171206 0 2 5 3.333E-3 0.
171301  2  6  3  2  0.          7.467E-03  0.
171302     0  1  1              1.783E-03  0.402283
171303     0  5  1              9.170E-04  0.597717
171304     0  4  3              4.167E-03  0.
171305 0 6 1 4.971E-6   0.
171306 0 2 5 3.333E-3 0.
*
*   VOLUMETRIC HEAT CAPACITY  BTU/F-FT**3  MATERIAL 1 - INCONNEL
*
190101 20        0.    51.41       200.    57.434      300.    59.527  * INCONNEL
190102         400.    61.167      500.    62.476      600.    63.872  * INCONNEL
190103         700.    64.578      800.    65.612      900.    66.795  * INCONNEL
190104        1000.    68.247     1100.    70.088     1200.    72.439  * INCONNEL
190105        1300.    75.420     1400.    79.150     1500.    83.750  * INCONNEL
190106        1600.    89.341     1700.    96.042     1800.   103.973  * INCONNEL
190107        1900.   113.255     2000.   124.008                      * INCONNEL
*
*   THERMAL CONDUCTIVITY BTU/FT-HR-F   MATERIAL 1 - INCONNEL
*
180101 20        0.     8.4294      200.     9.098      300.     9.495  *9INCONNEL
180102         400.     9.930       500.    10.398      600.    10.896  * INCONNEL
180103         700.    11.420       800.    11.967      900.    12.552  * INCONNEL
180104        1000.    13.113      1100.    13.704     1200.    14.303  * INCONNEL
180105        1300.    14.906      1400.    15.509     1500.    16.109  * INCONNEL
180106        1600.    16.701      1700.    17.282     1800.    17.849  * INCONNEL
180107        1900.    18.397      2000.    18.922                      * INCONNEL
*
*   LINEAR EXPANSION COEFFICIENT   1/F  MATERIAL 1 - INCONNEL
*
*
*   VOLUMETRIC HEAT CAPACITY  BTU/F-FT**3  MATERIAL 2 - 316 SS
*
190201 20        0.    51.68       200.    56.923      300.    59.020  * 316-STST
190202         400.    60.846      500.    62.447      600.    63.955  * 316-STST
190203         700.    65.141      800.    66.308      900.    67.490  * 316-STST
190204        1000.    68.444     1100.    69.463     1200.    70.430  * 316-STST
190205        1300.    71.508     1400.    72.563     1500.    73.552  * 316-STST
190206        1600.    74.782     1700.    75.952     1800.    77.162  * 316-STST
190207        1900.    78.406     2000.    79.672                      * 316-STST
*
```

```
*    THERMAL CONDUCTIVITY BTU/FT-HR-F    MATERIAL 2 - 316 SS
*
180201 20        0.      7.2458      200.      8.225       300.      8.991   * 316-STST
180202          400.      9.144      500.      9.586       600.     10.020   * 316-STST
180203          700.     10.448      800.     10.872       900.     11.294   * 316-STST
180204         1000.     11.718     1100.     12.145      1200.     12.577   * 316-STST
180205         1300.     13.017     1400.     13.467      1500.     13.929   * 316-STST
180206         1600.     14.406     1700.     14.900      1800.     15.414   * 316-STST
180207         1900.     15.948     2000.     16.507                         * 316-STST
*
*    LINEAR EXPANSION COEFFICIENT    1/F   MATERIAL 2 - 316 SS
*
*
*    VOLUMETRIC HEAT CAPACITY  BTU/F-FT**3   MATERIAL 3 - MGO
*
190301 20 0. 47.5516 200. 52.2156 300. 54.2084 400. 55.9468 500. 57.4944
190302 600. 58.8512 700. 60.0384 800. 61.0348 900. 61.9040 1000. 62.6460
190303 1100. 63.2608 1150. 63.5364 1200. 63.7908 1250. 64.0240 1300. 64.2360
190304 1400. 64.5964 1500. 64.9144 1600. 65.1900 1700. 65.4444 1800. 65.9776
*
*    THERMAL CONDUCTIVITY BTU/FT-HR-F    MATERIAL 3 - MGO
*
180301 20 0. 8.4435  200.  6.4805  300.  5.7049   400.  5.0470   500.  4.4937
180302  600.  4.0326   700.  3.6523   800.  3.3423   900.  3.0930
180303  1000.  2.8959   1100.  2.7431   1200.  2.6281  1300.  2.5450
180304  1400.  2.4888   1500.  2.4558   1600.  2.4428   1700.  2.4428
180305 1800.  2.4428  1900.  2.4428   2000.  2.4428
*
*    LINEAR EXPANSION COEFFICIENT    1/F   MATERIAL 3 - MGO
*
*
*    VOLUMETRIC HEAT CAPACITY  BTU/F-FT**3   MATERIAL 4 - BN
*
190401 20        0.     20.98       200.     29.896       300.     33.012   *        BN
190402          400.     36.265      500.     39.178       600.     41.775   *        BN
190403          700.     44.078      800.     46.112       900.     47.900   *        BN
190404         1000.     49.466     1100.     50.834      1200.     52.025   *        BN
190405         1300.     53.067     1400.     53.980      1500.     54.739   *        BN
190406         1600.     55.517     1700.     56.188      1800.     56.826   *        BN
190407         1900.     57.453     2000.     58.094                         *        BN
*
*    THERMAL CONDUCTIVITY BTU/FT-HR-F    MATERIAL 4 - BN
*
180401  20    0.      21.0962  300.    18.6490  500.    17.0927  600.    16.3442
180402        700.    15.6187  750.    15.2654  800.    14.9186  850.    14.5788
180403        900.    14.2463  950.    13.9212  1000.   13.6040  1050.   13.2950
180404        1100.   12.9944  1150.   12.7025  1200.   12.4196  1300.   11.8821
180405        1400.   11.3844  1500.   10.9287  1700.   10.1531  2000.    9.3650
*
*    LINEAR EXPANSION COEFFICIENT    1/F   MATERIAL 4 - BN
*
*
*    VOLUMETRIC HEAT CAPACITY  BTU/F-FT**3   MATERIAL 5 - 70CU30NI
*
190501 20        0.     52.55       200.     55.512       300.     56.317   * 70CU30NI
190502          400.     58.032      500.     59.179       600.     60.280   * 70CU30NI
190503          700.     61.358      800.     62.435       900.     63.532   * 70CU30NI
190504         1000.     64.672     1100.     65.876      1200.     67.157   * 70CU30NI
190505         1300.     68.567     1400.     70.098      1500.     71.732   * 70CU30NI
190506         1600.     73.641     1700.     75.697      1800.     77.973   * 70CU30NI
190507         1900.     80.489     2000.     83.269                         * 70CU30NI
*
*    THERMAL CONDUCTIVITY BTU/FT-HR-F    MATERIAL 5 - 70CU30NI
*
180501 20        0.     16.802      200.     17.972       300.     19.314   * 70CU30NI
180502          400.     20.960      500.     22.933       600.     24.919   * 70CU30NI
```

```
180503        700.    27.261      800.    29.964      900.    33.193  * 70CU30NI
180504       1000.    37.174     1100.    42.190     1200.    48.339  * 70CU30NI
180505       1300.    56.774     1400.    67.212     1500.    80.429  * 70CU30NI
180506       1600.    97.010     1700.   117.602     1800.   142.911  * 70CU30NI
180507       1900.   173.704     2000.   210.807                      * 70CU30NI
*
*
*   LINEAR EXPANSION COEFFICIENT   1/F  MATERIAL 5 - 70CU30NI
*
*
*   VOLUMETRIC HEAT CAPACITY  BTU/F-FT**3  MATERIAL 6 - AIR IN GAP
*
190601 20   25. .01973    68. .C1812     100. .01709   200. .01449
190602     300. .01258    400. .01111     500. .00995   600. .00901
190603     700. .00824    800. .C0758     900. .00702  1000. .00654
190604    1100. .00612   1200. .C0575    1300. .00543  1400. .00513
190605    1500. .00487   1600. .00463    1700. .00442  2000. .00385
*
*   THERMAL CONDUCTIVITY BTU/FT-HR-F   MATERIAL 6 - AIR IN GAP
*
180601 20   25. .01354    68. .0144688   100. .01516   200. .01732
180602     300. .01948    400. .02164     500. .02380   600. .02595
180603     700. .02812    800. .03028     900. .03244  1000. .03460
180604    1100. .03676   1200. .03892    1300. .04108  1400. .04324
180605    1500. .04540   1600. .04756    1700. .04972  2000. .05620
*
*   LINEAR EXPANSION COEFFICIENT   1/F  MATERIAL 6 - AIR IN GAP
* ///FILL TABLE TEST 105 VERT. OUT. GG1////
* OBTAINED FROM WGC. (2/6/78)
130100  2   4   297   1  LBS/SEC
130101  0.0  -668.26  660.64  0.05 -673.81  660.64  0.10 -789.50  666.34
130102  0.15 -561.84  658.80  0.20 -353.08  661.80  0.25 -224.95  661.86
130103  0.30 -159.32  664.50  0.35 -159.70  663.90  0.40 -182.94  664.03
130104  0.45 -196.19  663.55  0.50 -217.94  661.61  0.55 -205.56  659.06
130105  0.60 -181.57  657.14  0.65 -102.01  656.65  0.70  -56.68  656.00
130106  0.75  -31.98  655.99  0.80   15.17  656.15  0.85   47.49  656.16
130107  0.90   27.30  655.83  0.95   12.23  655.68  1.00    4.80  656.05
130108  1.05    2.33  656.98  1.10    1.13  658.19  1.15   40.33  657.17
130109  1.20   22.94  657.69  1.25  -17.26  657.26  1.30  -37.27  656.83
130110  1.35  -73.67  657.45  1.40  -73.18  658.96  1.45  -92.70  659.72
130111  1.50 -102.99  661.75  1.55 -108.61  663.40  1.60 -110.63  663.14
130112  1.65 -129.26  662.89  1.70 -130.71  664.77  1.75 -141.62  665.47
130113  1.80 -156.58  656.34  1.85 -145.45  665.12  1.90 -135.42  674.56
130114  1.95 -131.18  679.18  2.00 -130.94  677.95  2.05 -135.32  671.73
130115  2.10 -137.58  666.88  2.15 -127.55  672.55  2.20 -121.27  675.43
130116  2.25 -115.11  676.51  2.30 -102.80  682.88  2.35 -104.37  680.43
130117  2.40 -104.64  680.90  2.45 -115.25  671.09  2.50 -112.19  666.87
130118  2.55 -112.73  659.68  2.60  -97.69  664.00  2.65  -92.07  662.00
130119  2.70  -82.29  671.24  2.75  -77.91  690.21  2.80  -72.61  695.01
130120  2.85  -81.25  686.86  2.90  -78.90  701.62  2.95  -78.07  708.74
130121  3.00  -74.10  717.30  3.05  -75.70  713.96  3.10  -61.50  749.03
130122  3.15  -55.64  756.98  3.20  -53.67  758.37  3.25  -50.98  749.11
130123  3.30  -48.93  740.13  3.35  -40.53  765.46  3.40  -30.20  737.63
130124  3.45  -32.09  774.10  3.50  -30.09  760.26  3.55  -32.23  754.37
130125  3.60  -30.00  751.85  3.65  -32.14  750.39  3.70  -33.78  722.10
130126  3.75  -34.08  739.73  3.80  -28.92  741.29  3.85  -39.16  708.24
130127  3.90  -34.48  708.22  3.95  -32.07  738.04  4.00  -29.13  726.60
130128  4.05  -26.26  717.57  4.10  -29.36  728.62  4.15  -24.77  755.40
130129  4.20  -28.50  711.62  4.25   -3.52  710.94  4.30   -2.24  727.35
130130  4.35   -1.57  730.43  4.40   -1.00  780.95  4.45   -0.68  803.16
130131  4.50   -1.34  805.26  4.55  -21.92  750.20  4.60  -31.18  791.82
130132  4.65  -34.51  824.21  4.70  -40.17  859.85  4.75  -43.10  910.89
130133  4.80  -42.96  968.44  4.85  -43.96  991.52  4.90  -46.06 1017.66
130134  4.95  -46.33 1047.49  5.00  -49.40 1052.09  5.05  -53.27 1047.38
130135  5.10  -55.86 1044.22  5.15  -50.71 1089.09  5.20  -52.09 1073.20
```

130136	5.25	-70.81	958.57	5.30	-139.48	753.35	5.35	-187.76	597.51
130137	5.40	-216.62	669.22	5.45	-200.10	663.75	5.50	-162.88	675.94
130138	5.55	-131.63	689.96	5.60	-113.60	695.64	5.65	-107.08	691.97
130139	5.70	-109.10	685.67	5.75	-108.52	694.14	5.80	-93.30	729.06
130140	5.85	-90.09	741.99	5.90	-97.35	740.57	5.95	-107.77	727.20
130141	6.00	-88.84	776.94	6.05	-84.12	805.47	6.10	-76.29	845.99
130142	6.15	-67.23	892.40	6.20	-65.27	901.78	6.25	-66.96	888.95
130143	6.30	-69.69	880.06	6.35	-68.24	913.69	6.40	-73.23	917.93
130144	6.45	-72.21	943.49	6.50	-75.05	941.14	6.55	-76.79	947.04
130145	6.60	-83.69	930.78	6.65	-80.95	949.94	6.70	-92.32	912.49
130146	6.75	-94.43	930.91	6.80	-110.91	895.98	6.85	-116.20	895.98
130147	6.90	-124.03	881.83	6.95	-116.43	926.16	7.00	-109.63	971.42
130148	7.05	-100.88	1038.34	7.10	-108.47	1025.15	7.15	-105.71	1053.44
130149	7.20	-105.34	1069.17	7.25	-107.24	1066.09	7.30	-87.69	1195.18
130150	7.35	-86.53	1196.34	7.40	-87.17	1196.43	7.45	-82.89	1196.57
130151	7.50	-91.77	1195.28	7.55	-99.65	1137.69	7.60	-84.04	1196.93
130152	7.65	-84.88	1197.06	7.70	-83.34	1197.20	7.75	-86.81	1197.29
130153	7.80	-92.10	1195.62	7.85	-81.65	1197.38	7.90	-80.42	1197.51
130154	7.95	-90.89	1133.85	8.00	-87.49	1148.06	8.05	-71.65	1197.91
130155	8.10	-76.98	1198.00	8.15	-77.21	1198.14	8.20	-76.75	1198.23
130156	8.25	-84.13	1151.83	8.30	-79.55	1166.16	8.35	-79.11	1183.58
130157	8.40	-74.88	1198.72	8.45	-73.38	1198.77	8.50	-68.87	1198.95
130158	8.55	-65.81	1199.03	8.60	-66.83	1199.08	8.65	-62.95	1199.76
130159	8.70	-54.63	1199.12	8.75	-46.64	1199.17	8.80	-46.57	1199.26
130160	8.85	-44.71	1199.30	8.90	-36.47	1199.39	8.95	-37.68	1199.43
130161	9.00	-37.19	1199.63	9.05	-38.39	1199.67	9.10	-40.36	1199.74
130162	9.15	-33.17	1199.78	9.20	-42.99	1142.79	9.25	-35.39	1199.98
130163	9.30	-33.54	1200.17	9.35	-29.33	1200.25	9.40	-35.91	1200.37
130164	9.45	-31.77	1200.48	9.50	-32.22	1200.64	9.55	-23.23	1200.82
130165	9.60	-36.95	1200.82	9.65	-33.50	1200.89	9.70	-31.43	1201.03
130166	9.75	-31.10	1201.13	9.80	-29.86	1201.27	9.85	-32.45	1201.41
130167	9.95	-25.17	1201.65	10.05	-29.47	1202.00	10.15	-44.17	1202.39
130168	10.25	-45.08	1202.66	10.35	-60.13	1222.50	10.45	-67.38	1232.24
130169	10.55	-60.30	1232.11	10.65	-44.97	1229.08	10.75	-41.56	1229.91
130170	10.85	-42.23	1225.77	10.95	-31.74	1225.16	11.05	-29.23	1223.01
130171	11.15	-43.10	1229.66	11.25	-27.93	1231.60	11.35	-26.46	1234.17
130172	11.45	-23.63	1235.90	11.55	-23.03	1237.81	11.65	-16.57	1240.20
130173	11.75	-16.47	1240.01	11.85	-8.98	1204.50	11.95	-7.44	1204.49
130174	12.05	-4.02	1204.53	12.15	-3.75	665.84	12.25	98.65	472.44
130175	12.35	256.96	467.40	12.45	63.97	523.24	12.55	30.60	544.51
130176	12.65	25.50	536.51	12.75	12.36	577.44	12.85	17.51	552.64
130177	12.95	30.94	510.29	13.05	32.98	500.40	13.15	9.83	513.39
130178	13.25	12.22	505.31	13.35	2.50	510.38	13.45	0.32	535.42
130179	13.55	4.54	536.80	13.65	-2.88	492.92	13.75	-3.41	538.09
130180	13.85	-11.39	516.97	13.95	-10.30	605.53	14.05	-5.73	904.14
130181	14.15	-5.42	1204.65	14.25	-10.76	1126.15	14.35	-13.96	1204.52
130182	14.45	-42.04	958.18	14.55	-27.54	1204.23	14.65	-49.30	1204.22
130183	14.75	-29.36	1203.87	14.85	-47.51	1031.44	14.95	-33.15	1203.37
130184	15.05	-24.10	1203.17	15.15	-29.38	1202.97	15.25	-22.61	1202.75
130185	15.35	-20.93	1202.54	15.45	-19.64	1202.32	15.55	-23.78	1202.16
130186	15.65	-10.87	1202.11	15.75	-9.98	1202.16	15.85	-5.55	1202.32
130187	15.95	-9.33	623.07	16.05	-3.41	624.67	16.15	2.89	636.99
130188	16.25	5.29	626.58	16.35	28.69	471.24	16.45	58.76	441.21
130189	16.55	39.61	481.03	16.65	64.22	438.37	16.75	89.22	419.10
130190	16.85	52.41	445.63	16.95	45.72	442.11	17.05	41.84	434.67
130191	17.15	16.35	497.08	17.25	12.94	519.42	17.35	20.77	492.99
130192	17.45	15.20	464.66	17.55	5.10	518.84	17.65	3.51	454.57
130193	17.75	0.41	574.50	17.85	1.70	543.79	17.95	1.05	593.96
130194	18.05	1.63	502.07	18.15	0.38	497.84	18.25	2.05	573.12
130195	18.35	0.56	542.65	18.45	0.25	456.85	18.55	0.06	576.76
130196	18.65	0.05	588.48	18.75	0.09	487.41	18.85	0.03	747.70
130197	18.95	0.03	792.41	19.05	-0.74	809.98	19.15	-0.94	1202.08
130198	19.25	-1.63	1196.33	19.35	-2.26	1195.82	19.45	-6.43	1010.02
130199	19.55	-5.35	1194.92	19.65	-6.22	1194.54	19.75	-9.76	1038.35

Appendix E

RELAP VOLUMETRIC FLOW-DEPRESSURIZATION MODEL LISTING

```
=VF               VOLUMETRIC FLOW ON DEPRESSURIZATION - WATER LEAK
*
*
*
*    THIS IS A TEST OF THE RELATIVE EFFECTS OF VOLUMETRIC FLOW
*      ON DEPRESSURIZATION
*
*
*    WATER LEAK:  V1.V3.J1.J3 (LEAK = J3)
*
*    STEAM LEAK:  V2.V4.J2.J4 (LEAK = J4)
*
*
*
*
*
010001 -2 9 1 2 4 1 0 4 0 0 2 0 0 0 0 0 0 0
010002 0. 1.0
*
020000 AP 2 ML 2 JW 4 JF 4 JK 4 LM 0 LE 0 JC 4 AP 1
*
030010 10 100 10000 0 .01 .00001 210.
030002 2
*
040010 1 1 0 0 180.0 0.
040020 2 1 0 0 0.0 0.0
*
050011 1 0 2200. 0. 0. 20. 10. 5. 0 2. 0. 900. 0 *MAIN WATER
050021 1 0 2200. 0. 0. 20. 10. 5. 0 2. 0. 900. 4 *MAIN STEAM
050031 0 0 2200. 0. 0. .2 2.0 2.0 0 .1 0 898.1 1 *PIPE WATER
050041 0 0 2200. 0. 1.0 .2 2.0 2.0 0 .1 0 909.9 1 *PIPE STEAM
*
060011 .8 1.0E+06
*
080011 1 3 0 0 0. .1 900.05 0. 0. 0. 0 5 3 0 0. 1.0 11 0 1.0 0
080021 2 4 0 0 0. .1 909.95 0. 0. 0. 0 5 3 0 0. 1.0 11 0 1.0 0
080031 3 0 1 0 0. .005 898.15 0. 0. 0. 0 5 3 0 0. 1.0 11 0 0.0 0 *WAT
080041 4 0 2 0 0. .005 911.85 0. 0. 0. 0 5 3 0 0. 1.0 11 0 0.0 0 *STM
*
082003 .9 .8 .8 .01
*
120100 2 2 14.7 0.0 0.0 210.0 0.0 *WATER LEAK
120200 2 2 14.7 0.0 .1 210.0 .1 *STEAM LEAK
*
*
*
*
*
*
*
*
=VF               VOLUMETRIC FLOW ON DEPRESSURIZATION - WATER LEAK
*
*
*
*    THIS IS A TEST OF THE RELATIVE EFFECTS OF VOLUMETRIC FLOW
*      ON DEPRESSURIZATION
*
*
*    WATER LEAK:  V1.V3.J1.J3 (LEAK = J3)
*
*    STEAM LEAK:  V2.V4.J2.J4 (LEAK = J4)
*
*
*
```

```
*
*
010001 -2 9  1 2 4 1  0 4 0 0 2 0 0 0 0 0 0 0
C10002 0. 1.0
*
C20000 AP 1 ML 1 JW 3 JF 3 JK 3 LM 0 LE 0 JC 3 AP 2
*
030010 10 100 10000 0 .01 .00001 210.
C30002 2
*
040010 1 1 0 0 180.0 0.
040020 2 1 0 0 0.0 0.0
*
050011 1 0 2200. 0. C. 20. 10. 5. 0 2. 0. 900. 0 *MAIN WATER
050021 1 0 2200. 0. 0. 20. 10. 5. 0 2. 0. 900. 4 *MAIN STEAM
050031 0 0 2200. 0. 0. .2 2.C 2.0 0 .1 0 898.1 1 *PIPE WATER
050041 0 0 2200. 0. 1.0 .2 2.0 2.0 0 .1 0 909.9 1 *PIPE STEAM
*
060011 .8 1.0E+06
*
080011 1 3 0 0 0. .1 900.05 C. 0. 0. 0 5 3 0 0. 1.0 11 0 1.0 0
080021 2 4 0 0 0. .1 909.95 0. 0. 0. 0 5 3 0 0. 1.0 11 0 1.0 0
080031 3 0 1 0 0. .005 898.15 C. C. 0. 0 5 3 0 0. 1.0 11 0 0.0 0 *WAT
080041 4 0 2 0 0. .005 911.85 0. 0. 0. 0 5 3 0 0. 1.0 11 0 0.0 0 *STM
*
C82003 .9 .8 .8 .01
*
120100 2 2 14.7 0.0 .1 210.0 .1 *WATER LEAK
120200 2 2 14.7 0.0 0.0 210.C C.0 *STEAM LEAK
*
*
```

NUREG/CR-0105
ORNL/NUREG-45
Dist. Category R2

Internal Distribution

1. T. M. Anklam
2. R. E. Bohanan
3. S. B. Cliff
4-18. W. G. Craddick
19. R. M. Flanders
20. M. H. Fontana
21. R. H. Greene
22. R. C. Hagar
23. R. A. Hedrick
24. H. W. Hoffman
25. D. F. Hunt
26. C. R. Hyman
27. A. F. Johnson
28. C. B. Mullins
29. F. R. Mynatt
30. L. J. Ott
31. H. Postma
32. M. R. Sheldon
33. R. E. Textor
34. D. G. Thomas
35. H. E. Trammell
36. D. B. Trauger
37. K. G. Turnage
38. J. D. White
39. Patent Office
40-41. Central Research Library
42. Document Reference Section
43-44. Laboratory Records Department
45. Laboratory Records (RC)

External Distribution

46-49. Director, Division of Reactor Safety Research, Nuclear Regulatory Commission, Washington, D.C. 20555
50. Director, Research and Technical Support Division, DOE, ORO
51-410. Given distribution as shown under category R2 (25 copies — NTIS).